Rain Events and Recharge Processes in the San Luis Valley of Southern Colorado

Michelle Lanzoni

School of Geography and the Environment

University of Oxford

Doctoral Advisors:

Prof. W. Mike Edmunds

Prof. Heather Viles

Dr. Abi Stone

This work is submitted in partial fulfillment of the requirements for the degree of DPhil.

Contents

Chapter 1: Overview 1
1.1 Overarching Aim 1
1.2 Overarching Question 1
1.3 Sub-Questions of Individual Chapters 2
1.4 Primary Research Objectives 3
1.5 Study Rationale and Contributions 4
1.6 Why the San Luis Valley? 6
Chapter 2: Literature Review 9
2.1 Groundwater Recharge in Desert Basins 9
2.2 Introducing the San Luis Valley 11
2.2.1 Climate 11
2.2.2 Geology 13
2.2.3 Historic Mining 18
2.2.4 Hydrology 19
2.2.5 Water Quality 23
2.2.6 History of Water Use and Land Use Changes 28
2.2.7 Legal Battles and Water Law 33
2.3 Plants as Indicators of Water in Drylands 36
2.4 Groundwater Depletion, Dust Generation, and Mountain Block Recharge 43
2.5 Gaps in the Literature and What This Thesis Contributes 46
Chapter 3: Thesis Methods 48
3.1 Thesis Aims Revisited 48
3.2 Methods Overview 48
3.3 Methods Testing and Validation 52
3.4 Methods Details 56
3.4.1 Field Sampling and In Situ Measurements 56
3.4.2 Laboratory Analysis 61
3.4.3 Data Analysis and Visualization 64
3.4.4 Recharge Calculations 65

3.5 Limitations of the Techniques 66
Chapter 4: Precipitation Chemistry and Isotopic Baselines of Meteoric Waters 72
4.1 Chapter Questions, Aims, and Significance 73
4.2 Methods 74
4.3 Precipitation Patterns in the San Luis Valley 75
4.4 Precipitation Isotopes and a Local Meteoric Water Line for the San Luis Valley 80
4.5 Rain Chemistry 87
4.6 Discussion 94
Chapter 5: Pathways and Rates of Recharge in the San Luis Valley 97
5.1 Chapter Questions, Aims, and Significance 98
5.2 Introduction: Physical Setting and Hydrogeology 99
5.3 Methods 102
5.4 Location, Groundwater Layers and Depths 103
5.5 Groundwater Chemistry 107
5.5.1 Chemistry Overview 107
5.5.2 Water Chemistry at the Closed Basin Sump 113
5.6 Groundwater Isotopes in the San Luis Valley 117
5.6.1 Signatures by Aquifer Layer 117
5.6.2 Primary Pathways and Rates of Recharge in the Closed Basin Sump 120
5.7 Alternate Recharge Pathways: Sangre de Cristo Mountain Front and Fracture Flow, Ephemeral Creeks, and Aquifer Exchange 122
5.8 Snowmelt-driven Recharge at the Sump 127
5.8.1 Identification of an Unusual Pattern 127
5.8.2 Snowmelt-driven Recharge Through Time 131
5.9 Discussion and Conclusions 136
Chapter 6: Phreatophyte Shrubs as Indicators of Groundwater in the San Luis Valley 148
6.1 Chapter Questions, Aims, and Significance 149
6.2 Introduction and Past Work 149
6.3 Methods and Research Design 152
6.4 Site Descriptions 155
6.5 Comparison of Sites 164
6.6 Results of Phreatophyte Water Use 166
6.7: Discussion and Conclusions 170

Chapter 7: Moisture Movement in the Soil 173
7.1 Chapter Questions, Aims, and Significance 174
7.2 Introduction 174
7.3 Methods 175
7.4 Experimental Design at Study Site 177
7.5 Results 179
7.6 Discussion 187
7.7 Overall Conclusions 190
Chapter 8: Discussion of Results 192
8.1 Policy and Management Considerations 192
8.1.1 Rain Events and Dust Emissions 193
8.1.2 Toxic and Radiological Materials in the Air and in the Aquifer 197
8.1.3 Groundwater as Drinking Water 203
8.1.4 100 Years of Land-use Changes to the Valley's Hydrology 207
8.2 Policy and Management Recommendations 210
8.2.1 Mitigating Dust 210
8.2.2 Sustainable Groundwater Management 211
Conclusions 215
References 220
Appendices 235
Appendix 1: Precipitation Isotope Data 235
Appendix 2: Rainfall pH 236
Appendix 3: Isotope Data for Groundwater by Aquifer Layer and Surface Water Exposed to Evaporation 237
Appendix 4: Isotope Data used in Vegetation Study 240
Appendix 5: Summary Chemistry Data 242

Abstract

Many drylands around the world are dependent on high-elevation snowmelt for aquifer recharge. Much of the groundwater in the American West relies on precipitation formed in the Rocky Mountains. Understanding how snowmelt-driven recharge may change over time is an important component to sustainably managing these groundwater resources. The San Luis Valley of southern Colorado is the highest elevation area in the United States used for industrial agriculture. Precipitation on the valley floor is 200 mm/yr, but its water resources are sustained by precipitation > 1,000 m higher in the San Juan and the Sangre de Cristo Mountains, at the southern extent of the Rocky Mountains.

This study asks, what are the main pathways and rates of recharge? Using chemical and isotopic tracers, what can we learn about the water's source? To answer these questions, the following chapters examine 1) atmospheric source water 2) groundwater 3) plant-water, and 4) soil moisture. Chemical and isotopic tracers from >400 samples are used to follow water pathways from condensation, points of recharge, and along flowpaths. For near-surface moisture, chemical and isotopic tracers and electrical resistivity tomography are used to examine water-plant interactions and soil moisture movement in the unsaturated zone.

Over a three-year period from 2015 through 2017, >120 precipitation samples were collected and analyzed for chemistry and $\delta^2H/\delta^{18}O$ in order to produce a valley floor Local Meteoric Water Line (LMWL) and a mountain pass high-elevation MWL. Chemical analysis demonstrates a pattern of acid rainfall, reaching greatest acidity (pH 3.9) over a two-week period in late summer. Rain in the early summer of 2015 showed as much as 4.3 mg/L NO_3, 12 mg/L SO_4, 3.1 mg/L NH_4, and 4.6 mg/L K. Heavy metal analysis shows contaminants of health concern in rain, including Cr, Cd, As, Pd, W, Mo, and more than half the rainfall analyzed over three years shows the presence of uranium.

Recharge to the confined aquifer is snowmelt-driven. Mountain block recharge, where infiltration occurs at high elevations in the San Juan Mountains appears to contribute the most recharge to the upper confined aquifer. Of those wells sampled > 274 m deep in the eastern side of the valley, the mean isotopic signature is closer to the valley-floor LMWL, suggesting recharge primarily occurs through infiltration at the base of the mountains, as mountain front recharge and as fracture flow. The highest rates of recharge occur in long-screen wells in the deep, unconfined aquifer layer at the base of the Sangre de Cristo Mountains.

Old groundwater from the upper confined aquifer sampled within a 25km^2 area of the valley's sump shows a 2.5‰ ^{18}O spread and sits significantly above the LMWL and high-elevation MWL. This water shows a mean deuterium excess (d-xs) of 17.6 ‰, which is nearly double the d-xs of the LMWL. This study argues that in addition to other human alterations to recharge pathways (such as dust-on-snow albedo changes to snowpack, etc.) 20th Century draining of playa wetlands and diverting of surface water have altered a source of recharge not previously considered.

Most rain events in the San Luis Valley are < 2 mm and, based on time-lapse resistivity inversions, do not appear to penetrate to a depth sufficient to reach the water table. Soil profiles indicate most precipitation on the valley floor does not penetrate more than 25 cm. Two native phreatophyte plants of the San Luis Valley, *E. nauseosa* and *S. vermiculatus*, show distinct patterns of water use and seasonal shifts depending on water availability. Differences between the species are most apparent where groundwater is most accessible. However, where the water table has dropped 6 m over the last decade, both *E. nauseosa* and *S. vermiculatus* survive only on near-surface snowmelt and rain. At this site, shrub density is reduced by an order of magnitude, species diversity is lower, and the percentage of exposed, bare earth reaches 45%.

This work presents evidence that a primary pathway for aquifer recharge to the San Luis Valley occurs at high elevation, and the mechanism by which it occurs may be changing over time. This dissertation employs traditional and non-traditional hydrological techniques to follow water in the San Luis Valley watershed as it moves through its air-surface-ground water cycle, and by placing hydrological insight within a human context, offers suggestions for the future stewardship of these significant groundwater resources.

Terms and Abbreviations

Commonly Used Terms

CDWR	Colorado Division of Water Resources
RGWCD	Rio Grande Water Conservation District
CBC	Closed Basin Canal, sometimes Closed Basin Project
Closed basin	Hydrologic unit where groundwater flows toward an inland outlet (not to be confused with the Bureau of Reclamation's Closed Basin Project)
GMWL	Global Meteoric Water Line, international standard based on Craig, 1961
LMWL	Local Meteoric Water Line, determined by yearly precipitation in a given place

US Federal Agencies

BLM	Bureau of Land Management
USBR (BoR)	US Bureau of Reclamation
NPS	National Park Service
USFWS	US Fish and Wildlife Service
USGS	US Geological Survey
EPA	Environmental Protection Agency

Places

SLV	San Luis Valley
GRSA	Great Sand Dunes National Park and Preserve
ANWR	Alamosa National Wildlife Refuge
BNWR	Baca National Wildlife Refuge
MVNWR	Monte Vista National Wildlife Refuge
SLVWRC	San Luis Valley Wildlife Refuge Complex, refers to all three refuges

Notations, Standards, and Units of Measurement

δ	delta notation used to mark the ratio of two different isotopes of a single element with respect to an international standard of natural abundance
Δ	Delta used to compare two different δ isotopic ratios
VSMOW(2)	Vienna Standard Mean Ocean Water, standard set by the IAEA
SLAP(2)	Standard Light Antarctic Precipitation, standard set by the IAEA
IAEA	International Atomic Energy Agency
d-excess (d-xs)	Deuterium excess is the degree of movement away from the GMWL, defined as $d=d^2H-8\cdot\delta^{18}O$

g/L = grams per litre

mg/L = ppm, parts per million

µg/L = ppb, parts per billion

pg/L = ppt, parts per trillion

pCi/L = pico Curie, 1 pCi/L = 0.037 Bq/L

‰ = per mil (as opposed to per cent)

Cfs = cubic feet per second

Acre = 4,047 m^2 or 0.004 km^2

Acre feet	American hydrology unit used to measure large quantities of water in a visual manner. That is, the amount of water that would cover an acre of land with 1 foot of water.

Acknowledgements:

This work would not have been possible without the help of many people. I would like to thank John Sanderson, Suzanne Beauchaine, Rich Roberts, Andrew Valdez, Bob Trower, Jill Lucero, Negussie Tedela, Jenny Nehring, Cary Aloia, Pete Striffler, Laura Archuleta, Laura Bexfield, Mike Gibson, Bob Kirkham, Ben Drenth, and others from the NPS, USFWS, USGS, USBR, BLM, or "at large," who either frequent or base themselves in the San Luis Valley.

Thank you to Dave Williams, Craig Cook, Chandelle MacDonald, and others at the University of Wyoming's Stable Isotope Facility.

In Oxford, Manchester, and Wallingford, a special thank you to Heather Viles, Mike Edmunds, Abi Stone, and George Darling.

This work is dedicated to Wyndham Michael Edmunds.

Chapter 1: Overview

Rain Events and Recharge Processes in the San Luis Valley of Southern Colorado

1.1 Overarching Aim

The overall aim of this study is to better understand the timing and composition of rain events and rates and pathways of groundwater recharge in a high-elevation desert with complex hydrology and competing water needs. This interdisciplinary dryland hydrology study borrows techniques from ecology, biology, and geophysics. It investigates important questions based on the assertion that studies of groundwater recharge must be basin specific.

1.2 Overarching Question

What are the main pathways and rates of recharge in the San Luis Valley?

Using chemical and isotopic tracers, what can we learn about the water's source?

These overarching questions form the backbone of the dissertation, and each chapter builds on the previous to provide a complete picture of rain events and recharge processes in the high-elevation, 20,000 km^2 dryland San Luis Valley of southern Colorado. Answering this questions rests primarily on data collected from analyses of precipitation (individual rain and snow events collected from mountain pass and valley floor environments) and groundwater (from the shallow unconfined aquifer and the deeper, confined aquifer sampled at depths ranging from about 10 to more than 600 m below the surface) sampled year-round over three years. Chemical and isotopic tracers are used to follow water pathways from air mass condensation, points of recharge, water-rock interaction along flowpaths, and, for near-surface

moisture, chemical and isotopic tracers and electrical resistivity tomography are used to examine water-plant interactions and soil moisture movement in the unsaturated zone.

1.3 Sub-Questions of Individual Chapters

Chp 4: Precipitation Chemistry and Isotopic Baselines of Meteoric Waters

- What can precipitation isotope and chemistry data reveal about the sources of meteoric water?
- Do the isotope values and local meteoric water lines created from precipitation collected on the valley floor and on the San Juan mountain passes differ significantly in terms of slope, y-intercept, or deuterium excess?

Chp 5: Pathways and Rates of Recharge in the San Luis Valley

- What do isotopic and chemical analyses tell us about groundwater in the San Luis Valley?
- With a focus on the closed basin, what are the main pathways and rates of recharge in both the unconfined and confined aquifers?
- Is there any indication the rates and mechanisms of recharge have changed over time?

Chp 6: Phreatophyte Shrubs as Indicators of Groundwater in the San Luis Valley

- How does the area's dominant native vegetation (facultative phreatophytes *S. vermiculatus* and *E. nauseosa*) respond to a lowered water table?
- Are distinct patterns of water use and seasonal shifts between the phreatophytes visible?
- How might a lowering of the water table affect species richness and plant density?

Chp 7: Moisture Movement in the Soil

- Can movement of the zero flux plane be visualized using electrical resistivity tomography?

- In areas with shallow water tables, how do rain events influence soil moisture on the valley floor? Does this differ between vegetated and non-vegetated areas?

Chp 8: Discussion of Results

- After contextualizing the study's findings, are there important water and land management considerations for the San Luis Valley?
- What are the policy and management recommendations?
- What are the directions for further study?

1.4 Primary Research Objectives

The research objectives within this dissertation are summarized below by chapter:

Chapter 4: Characterize the chemical and isotopic signature of precipitation in the San Luis Valley and, using $\delta^{18}O$ and $\delta^{2}H$, develop a local meteoric water line.

Chapter 5: Determine different pathways and rates of recharge in the San Luis Valley using chemical and isotopic tracers, hydrographs, and groundwater fluctuations.

Chapter 6: Analyze stem water samples from the valley's two dominant facultative phreatophyte shrubs at three different study plots with increasing depth to groundwater in order to establish seasonal variation in their water use strategies.

Chapter 7: Apply time-lapse, near-surface electrical resistivity in order to characterize soil moisture movement between vegetated and non-vegetated areas under different wetting and drying conditions.

Chapter 8: Discuss, consider, and recommend water management strategies for the San Luis Valley based upon an increased understanding of the area's groundwater recharge and its air-surface-ground water

interactions. This chapter discusses implications of the study's findings and offers direction for future research.

1.5 Study Rationale and Contributions

Groundwater recharge studies often identify sources of recharge, flowpaths and rates of recharge by employing a variety of chemical and isotopic tracers. Chemical tracers may help identify water-rock interactions, flowpaths, redox conditions, and rates of recharge (Cook and Herczeg, 2000). Isotopic tracers may be used to identify modern water (e.g. $^{3}H/^{3}He$, ^{85}Kr, and CFCs broadly) for example Schlosser et al. (1989), Morris et al. (2005), Newman et al. (2010), Edmunds et al. (2014), submodern water (e.g. ^{210}Pb, ^{39}Ar, ^{32}Si, ^{4}He) for example Andrews et al. (1985), water > 10,000 years old (e.g. ^{14}C) for examples Gonfiantini et al. (1974), Plummer and Glynn (2013), and water > 50,000 years old (e.g. ^{40}Ar, ^{21}Ne, ^{81}Kr, ^{36}Cl) for example Phillips et al. (1986), Collon et al. (2000). However, when isotopic studies are limited by time, team (in this case, solo), and financial backing (such is the case with a doctoral study), innovations must be made in the quality and interpretation of data using only ^{2}H and ^{18}O as isotopic tracers. Fortunately, there are previous water-dating studies for this area (discussed in Chapter 2) that aid in the interpretation of flowpaths and groundwater recharge. The contribution of this doctoral study is to establish the first LMWL for this region of the southern Rocky Mountains (Lanzoni, 2017) and to use the high elevation and valley floor precipitation baselines to identify and infer how these sources, rates, and mechanisms of recharge may be changing over time (Lanzoni and Darling, 2019).

While several hydrological studies conducted in the San Luis Valley have examined surface and groundwater chemistry (Davis Engineering Service et al., 2012), and the isotopic composition of surface water and groundwater isotopes (Mayo et al., 2007, Rupert and Plummer, 2004), no study has examined the area's precipitation isotope signatures (which differ from Rocky Mountain-wide snow signatures at

high elevation, see Anderson et al., 2016) or the area's precipitation chemistry. Examining the isotope values of local meteoric waters and precipitation chemistry input are important components to any comprehensive study of groundwater recharge (Clark and Fritz, 1997, Kendall and McDonnell, 1998, Edmunds, 2008b). Chapter 5 accomplishes the analysis of groundwater recharge because it relies on local meteoric water lines established at more than one elevation as presented in Chapter 4.

Precipitation chemistry monitoring in the literature, and long-term regional monitoring of air quality in the Rocky Mountain West are usually confined to mineral dust emission migration and particle size analysis (e.g. Reynolds et al. 2016) or tracking basic chemical indicators of air pollution such as ammonia, nitrogen, sulfur, and mercury (as through the IMPROVE and NADP monitoring networks). By analyzing precipitation chemistry over a three-year period within the study site as presented in Chapter 4, this work identifies the heavy metal and actinide content of the valley's wet deposition (Lanzoni, 2017).

While the term "phreatophyte" was put into print by the hydrologist Meinzer (1927), it is the ecology community who have used xylem water $\delta^{2}H$ and $\delta^{18}O$ tracking of facultative phreatophytes for decades to inform facilitation-competition between plant species, adaptive water capture strategies, nitrogen-dominated rain pulse responses in soil, and vegetation patterning in deserts and desert margins. The San Luis Valley has experienced an unprecedented lowering of the unconfined aquifer, and some areas of greatest drawdown challenge the extent of phreatophyte taproots. Such a drop in aquifer levels allows another question then addressed in Chapter 6—in areas where the water table has dropped to 6 m below the surface, what water do these phreatophytes use?

This dissertation employs traditional hydrological techniques of chemical and isotopic tracers and measured groundwater fluctuations as well as techniques from other disciplines (cryogenic extraction of xylem water from ecology in Chapter 6 and electrical resistivity tomography from geophysics in Chapter 7) to follow water in the San Luis Valley watershed as it moves through its air-surface-ground water cycle, where water recharges the aquifers or becomes potential precipitation.

1.6 Why the San Luis Valley?

Many of the questions raised and answered in this dissertation are applicable to other high-elevation desert regions dependent on snowmelt as a primary mechanism of groundwater recharge, to other drained wetland playa systems in arid/semi-arid regions, and to global dryland areas more broadly, especially those dryland areas around that increasingly depend on groundwater for agricultural irrigation.

However, there are things that make the San Luis Valley a particularly interesting field site for academic research. The internal drainage system of the valley's closed basin sump houses groundwater that is >20,000 and 30,000 years old beneath organic-rich sediments deposited from the prehistoric Lake Alamosa. Today's playas are part of a diminishing landscape of wetlands that used to stretch across the northern part of the San Luis Valley.

Important to this study, meteoric water in the San Luis Valley offers a high degree of isotopic variation depending on its source. Precipitation in the San Luis Valley usually arrives from the Northwest in the autumn, winter, and spring, and from the Southwest in late summer. There is more than 1,000 m difference in elevation between the valley floor and the mountain ranges on either side of the valley. These are ideal conditions for a study using isotope hydrology.

The social, historical, and legal context of the San Luis Valley adds an additional element of interest. Water use, and groundwater abstraction, is regulated under the framework of western water law. The snowpack of the San Juan Mountains replenishes the valley's aquifer system as well as it contributes to the headwaters of the Rio Grande, a transboundary river whose waters must meet inter-state and international deliveries. Agricultural irrigation is the primary use of water in the valley, and this is at times at odds with the needs of other users.

While this study did sample water at high elevations in the mountains and at the valley's margins, it focuses its lens on the northeastern part of the valley, in the hydrologically closed basin. It sampled water, whenever possible, away from the Rio Grande and away from directly managed waters, because for this study, the chemical and isotopic tracers work better where they are not confused by anthropogenic influence. With regard to the vegetation plots used in this study, the priority was to choose three sites with native shrubs *E. nauseosa* and *S. vermiculatus* co-existing in areas with increasing depth to the water table. For the electrical resistivity experiments, the vegetation plot with the shallowest depth to groundwater was chosen.

The San Luis Valley was chosen as my study site in 2014 for reasons both academic and personal. This is the area of the country I currently call home. Among the more than 100 wells I sampled across the San Luis Valley floor, three of my own artesian wells, ranging in depth from 13 to 244 m, provide chemistry and isotope data used in this thesis. This is the water I drink.

While it is true aeolian forces are responsible for many of the landscape features in the valley—notably the tallest dune field in North America—and much of the observable landscape was formed from a combination of water, wind, and rifting, I am of the opinion that what has shaped the character of this high-elevation desert valley, more than anything else, is water. The San Luis Valley is a story about water. Where water is and where it was. Where that water came from, and where that water goes.

Conceptually:

Water = **$\delta^{2}H$** + **$\delta^{18}O$** + **Salts**

"All water is sweeter in winter, in summer less so, in autumn least and less during droughts. The taste of rivers is usually variable owing to the great difference in river beds. For waters vary with the land over which they flow and with the juices of the plants they wash… Waters take on the properties of the rocks through which they pass."

Pliny the Elder

Chapter 2: Literature Review

2.0 Overview

The following review discusses important topics in dryland hydrology related to groundwater recharge, mountain block recharge, movement of water in the unsaturated zone, the influence of dryland shrubs on soil stability and soil moisture, and the impacts dust emissions have on snowmelt recharge. The San Luis Valley is introduced, and a review of relevant literature is presented on the area's geology, hydrology, water quality, water use and land use changes over the past 100 years. By placing the San Luis Valley in a wider context of dryland hydrology, gaps in the literature and thesis contributions are considered.

2.1 Groundwater Recharge in Desert Basins

Excluding icecaps and glaciers, 97% of the world's fresh water is found in groundwater. 1.5 billion people depend on groundwater for potable water around the world, and as the population increases, so too does dependency on groundwater, most especially in arid and semi-arid regions (Stone et al., 2019). Drylands cover roughly 40% of the Earth's surface, and much of the groundwater in these regions was either formed during past-climate conditions (Edmunds, 2009, Taylor et al., 2012) or is dependent on highland hydrology to recharge the dryland aquifers. Mountainous areas offer significant recharge to inland deserts owing to higher precipitation at elevation and orographic effects (Hogan et al., 2004).

A significant portion of dryland regions depend on agriculture and utilize groundwater to meet agricultural needs. Drylands are characterized by sparse vegetation, and this vegetation may act as a buffer against land degradation. Changes in vegetation, along with slight shifts in climate, may alter the amount of groundwater recharge to the region (Phillips et al., 2004, Scanlon et al., 2006).

Determining the amount, timing, and chemistry of rain events, as well as the recharge processes past and present are critical to understanding groundwater resources in dryland areas. Much of the American Southwest comprises arid desert ecosystems whose aquifers are replenished through mountain snowmelt. These areas also appear to be subject to groundwater over-abstraction and drought (see Figure 2.1 (a)). Groundwater recharge through mountain block and mountain front pathways is expected to decline across much of the American Southwest due to decreased snowpack (Meixner et al., 2016, Rodell et al., 2018).

While it is clear human use and management of groundwater resources plays a role in their long term sustainability, groundwater systems are complex, and the most relevant insights will arise from basin-specific study. While many regional and global groundwater studies highlight the Southwestern aquifers of southern California, Arizona-Mexico, and the High Plains, a lesser-known aquifer system in the American Southwest dependent on mountain recharge offers a compelling case study based on its complex hydrology, changing land use, and importance to the region for both groundwater and surface water—the integration of which poses challenges to Western water law. This groundwater system is located in a high-elevation desert valley at the southern extent of the Rocky Mountains (Figure 2.1b, c).

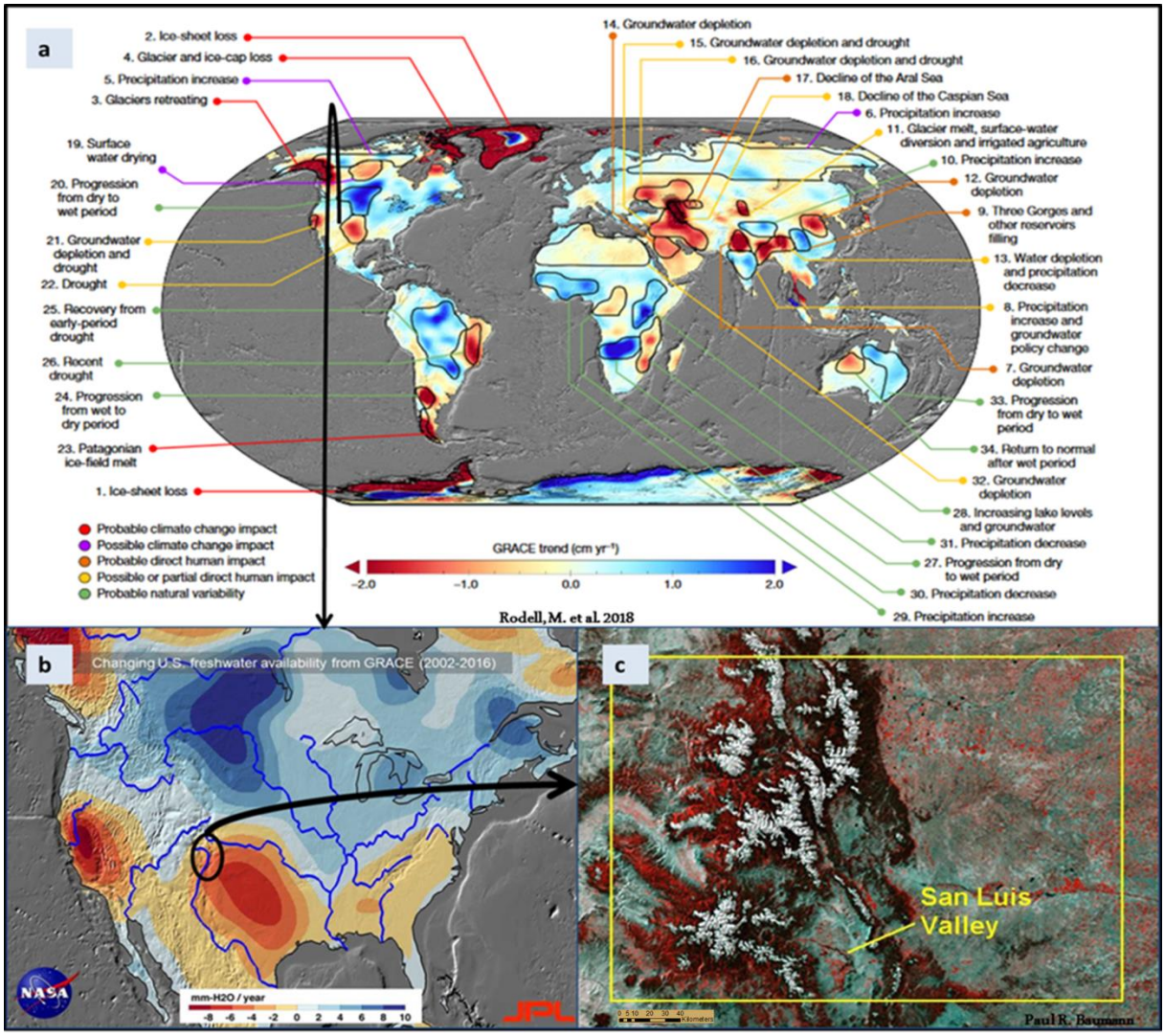


Figure 2.1: a) world map from Rodell et al., 2018, showing annotated water trends based on 2002-2016 GRACE satellite data. b) US water trends based on Rodell et al. 2018 that include precipitation, surface water, groundwater, soil water, and ice. c) Landsat Enhanced Thematic Mapper (ETM+) courtesy of Paul R. Baumann, 2001 showing southern Rocky Mountains and San Luis Valley.

2.2 Introducing the San Luis Valley

2.2.1 Climate

The climate of the San Luis Valley is characterized by warm summers, cold winters, and precipitation below 200 mm/yr. The region is arid to semi-arid; evaporation substantially exceeds precipitation (Bexfield and Anderholm, 2010). In the central part of the valley floor, annual precipitation is 170-200

mm, but at the valley margins closer to the mountain ranges, precipitation increases to just under 250 mm/yr. Precipitation in the mountains, mostly in the form of snowfall, averages 1,000 mm/yr. On the valley floor, most of the precipitation arrives in the afternoons during the late summer monsoon—part of the North American Monsoon system, which occurs in July, August, and the first few weeks of September. About 44% of precipitation arrives during the monsoonal season between July and September. In the higher elevation mountains precipitation, about 1,000 mm/yr, arrives predominantly in the form of snowfall in late winter and spring. Winter snowstorms originate from the Pacific Northwest. Summer monsoons originate from the Gulf of Mexico. Figure 2.2 shows patterns of moisture movement originating from the Pacific Northwest for most of the year, and the air mass movement from the North American Monsoon in the late summer, which originates in the Gulf of Mexico and Gulf of California.



Figure 2.2: Map showing SW monsoon (North American Monsoon) system with moisture originating in the Gulf of Mexico and Gulf of California. Dominant winter air masses move from the Pacific NW inward and south toward the San Luis Valley, shown here circled in yellow.

2.2.2 Geology

The total area of the San Luis Valley is sometimes reported as low as 8,288 km^2 (Emery, 1971a), if contributing watersheds are calculated separately, but the wider area of the San Luis Valley including surrounding mountain bases and contributing waters totals 21,217 km^2, inclusive of its southern tip in northern New Mexico. The valley, whose basin was in part formed by and encompasses the northern section of the Rio Grande Rift, is enclosed by mountain ranges to the east and west. Elevations of the tallest mountains on either side of the valley reach 4,270 m. The average elevation of the valley floor is 2,347 m above mean sea level, but the lowest elevation in the valley is 2,286 m in the closed drainage basin in the eastern part of the valley. The valley floor slopes downward to the east roughly 1 m every km, toward its low point known as the ancestral sump that once housed ancient Lake Alamosa more than half a million years ago, and which, as recent U-Th and ^{3}He age dating suggests, may have drained in stages and as late as 200,000 years ago (Machette, 2004, Machette et al., 2007, Machette et al., 2013, Ruleman et al., 2019). Overall, there is roughly a 1,000 m difference in elevation between the mountain passes of the San Juans and Sangre de Cristos and the valley floor.

The eastern side of the San Luis Valley is flanked by the Sangre de Cristo, or the "blood of Christ" mountains. This mountain range was named by 18th century Spanish explorers who, as the days ended, watched sunsets reflect a soft crimson glow off the mountains' rock faces. The "Ancestral Rockies"—replaced 80 to 40 Ma by the present Rockies—began to rise 320 Ma in Pennsylvanian time but were worn down by erosion 250 Ma. This erosion left coarse sediment fill (sand, pebbles, boulders) in the surrounding basins. Groundwater filled in the sediment of these basins. As the oxidizing water reacted with the gabbro, and the minerals hornblende and biotite, it pooled iron oxide into pore spaces that eventually formed hematite. Hematite may be responsible for augmenting the Sangre de Cristo's glow at sunset (Lindsey, 2010a).

The Sangre de Cristo Mountains are a long chain of fault block mountains at the southern extent of the Rockies to the east of the valley. They are sometimes subdivided into the northern Sangre, which most

notably include the Crestones (near to and north of Great Sand Dunes), a Permian-Pennsylvanian rock, and the picturesque Blanca massif, an older Precambrian section uplifted in the central part of the valley, and then to the south, the Culebra Range, that runs from Iron Mountain to Costilla Creek, concluded by the southern Sangre, which continue into New Mexico. Overall, the Sangre de Cristo Mountains are composed of Precambrian gneiss with large granite plutons, gabbro dikes (rich in Fe and Mg), and pegmatite (Lindsey, 2010a). Faults are found along the sides of the Sangre de Cristo Mountains, with research conducted on delineating the exact locations and extents of multiple minor faults in the San Luis Valley (Drenth et al., 2013, Grauch and Ruleman, 2013, Ball et al., 2015). These fault lines are shown in the San Luis Basin geologic map in Figure 2.3.

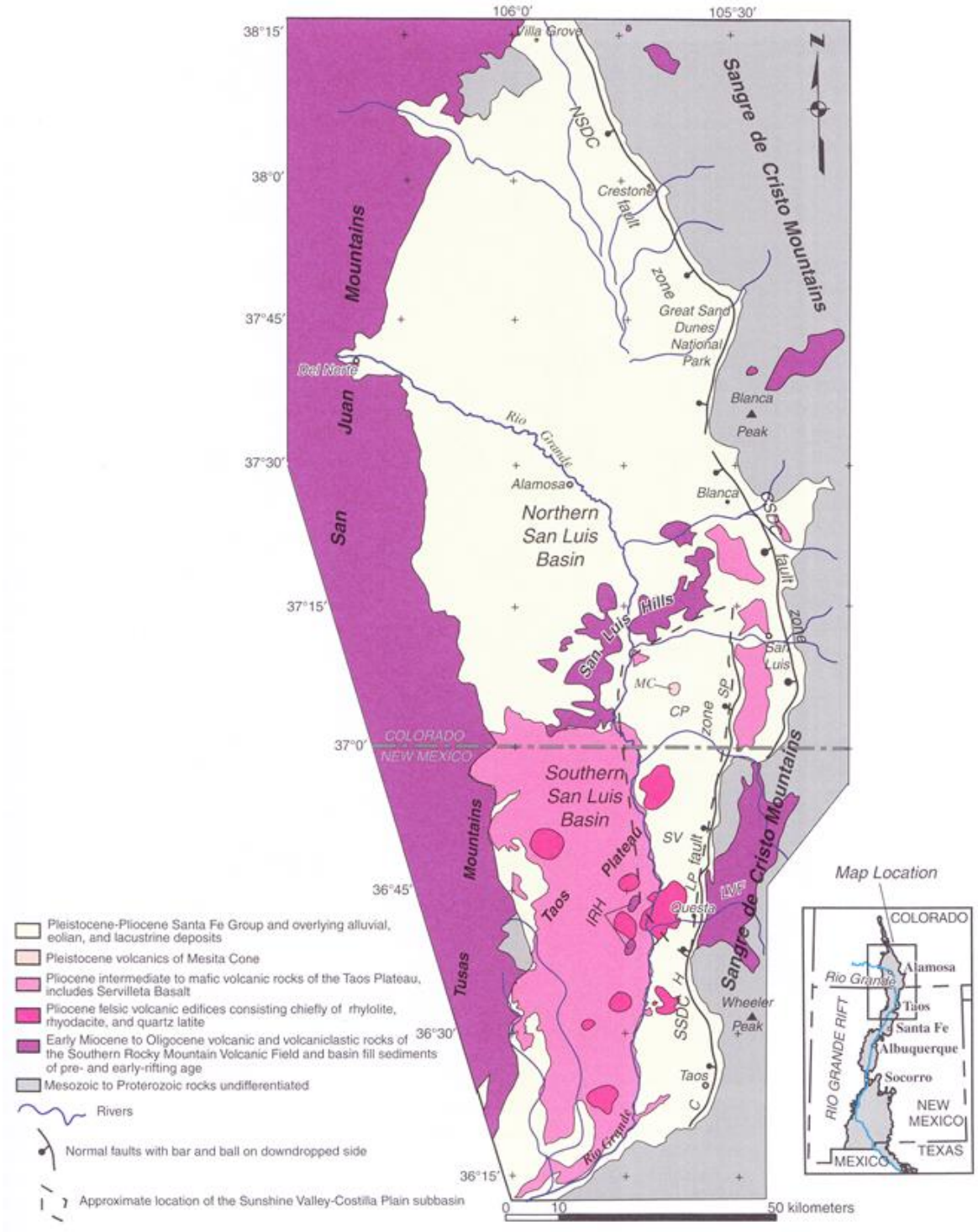


Figure 2.3: Summary geology of the San Luis Basin showing the San Luis Valley in southern Colorado extending to the Taos Plateau in northern New Mexico. Also shown on this map: the Rio Grande originates in the volcanic San Juan Mountains, and the creeks at and north of Great Sand Dunes originate from precipitation in the mostly granitic Sangre de Cristo Mountains. Source: Ruleman, et al. 2013.

One of the largest, most prominent peaks in the Sangre de Cristo is called Mount Blanca[1], named for what was, until recently, a year-round covering of snow. Mountain snowpack is vital to the valley's hydrology, and every year, hydrological forecasts and irrigation decisions are made based on predictions for the accumulation and timed melting of snow, especially snow in the San Juan Mountains. The large, rugged extension of the Rockies bordering the valley's western side is the San Juan Mountain Range. These mountains are composed of volcanic rock and sandstone. A series of volcanic eruptions created multiple layers to the San Juans beginning with lavas and breccias followed by silica ash-flow tuffs, ending with basalt flows and rhyolite (Lipman et al., 1970). The San Juan volcanic field includes over 25 extinct calderas including La Garita Caldera and Summitville Caldera (Valdez, 2017).

Water from the San Juan Mountains is important to people beyond the borders of Colorado. Snowmelt from these mountains drains to two international rivers: snowmelt from the western slopes drain into tributaries of the Colorado River; snowmelt from the eastern slopes forms the headwaters of the Rio Grande. The San Juan Mountains are responsible for the majority of aquifer recharge to the San Luis Valley, mainly through mountain block/underflow recharge (Mayo et al., 2007).

Figure 2.4 displays transects of the valley floor running west to east, with an orientation north. In these displays it is possible to imagine an eastward subsurface water flow direction. The valley floor is shown simply with the basin-fill Quaternary alluvium, primarily Tertiary sandstone and volcanic rock of the San Juans to the west, and the Paleozoic sediment and Precambrian crystalline basement of the Sangre de Cristos Mountains to the east. On the eastern side of the San Luis Valley, the Alamosa Formation overlies the Santa Fe Formation. Below this, in the centre-east section of the valley, is the raised Alamosa Horst. Fault lines are present, most notably along the base of the Sangre de Cristo Mountains.

[1] *Tsisnaasjini'* in Navajo marked the northeastern boundary of the Navajo ancestral homeland. In 2017 and 2018, the Navajo Nation purchased land on the eastern side of the Sangre de Cristos with views of *Tsisnaasjini'.*

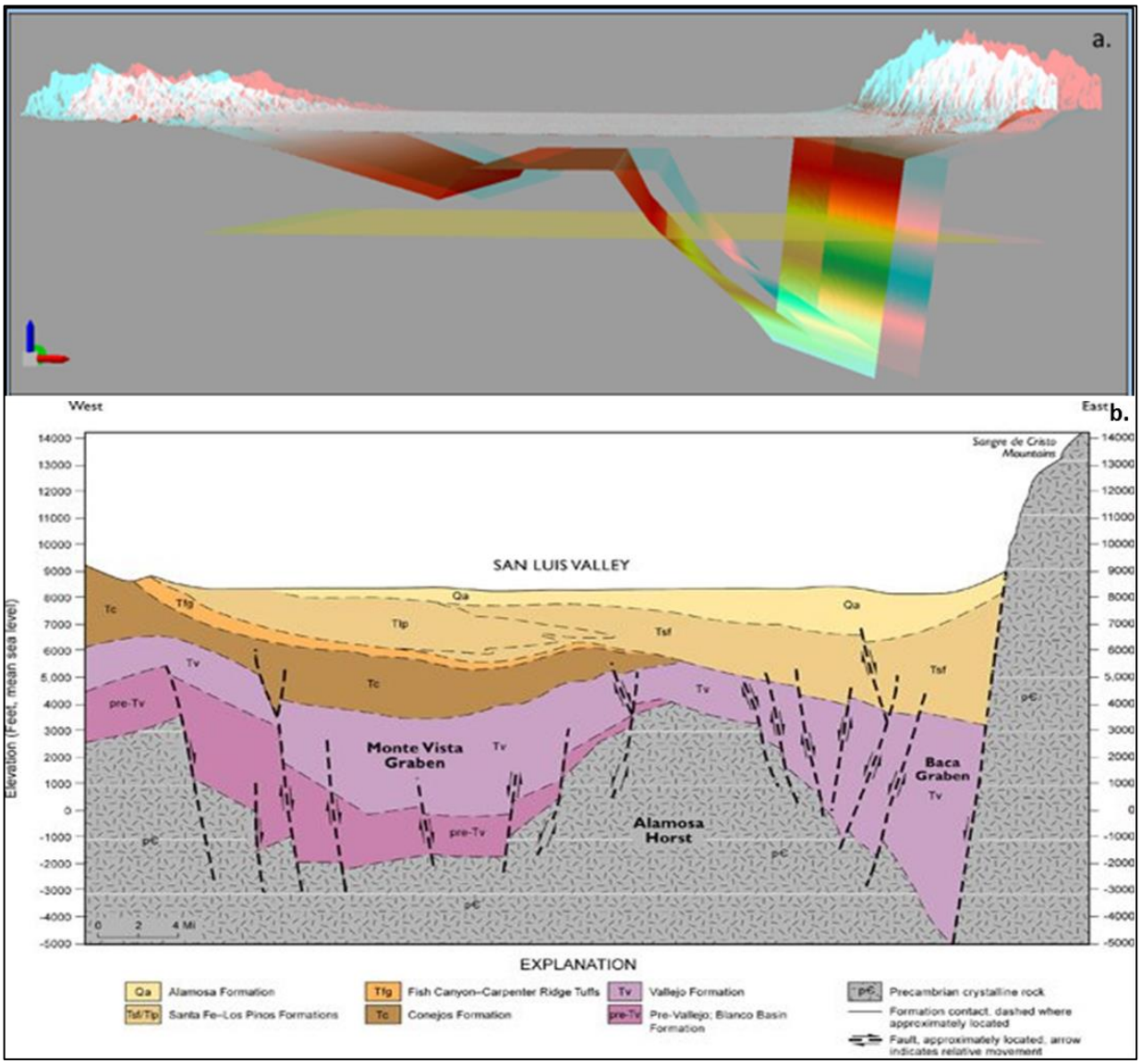


Figure 2.4: Geologic transects across the valley floor, looking north. (a) seismic survey results from Brister and Gries (1994) overlain with LiDAR-generated topography, courtesy of Valdez 2017. Yellow line represents sea level. Seismic layers color-coded by depth. (b) A—A' transect drawn in simplified geology, from Harmon, E. J., 1998, in Topper et al. (2003). For the location of the A—A' transect across the San Luis Valley, refer to Figure 2.5.

2.2.3 Historic Mining

The geology of the valley's surrounding mountains has enticed miners since the mid-1800s. Early gold prospecting brought miners to small mountain towns such as Liberty in the Sangre de Cristo and Creede in the San Juans. While Liberty was shortly abandoned, the town of Creede continues to grow. In both the Sangre de Cristo Mountains and the San Juan Mountains mining frequently produced gold, silver, lead, and copper. A century later on the valley floor (1970s) crystallized sodium carbonate (trona) was mined from dried playas near San Luis Lake. Other surface mining extracted sand and gravel from dried playas on the valley floor for commercial use (e.g. USGS MRDS ID DC04330 and DC04145).

In the late 1800s, the United States was the first country to mine for uranium (IAEA). The uranium ore from Pitch Mine[2] in Saguache County, CO, contained high grade U_3O_8 (averaging 0.5%) found predominantly in the Mississippian Leadville dolomite. It was noted, in addition, and in support of volcanogenic uranium deposits, that volcanic rocks within 10 km of the Pitch Mine showed higher radioactivity than other rocks including Precambrian granite. Sampled tuffs contained an average 10.5 mg/L U and 35 mg/L Th. Still, the most important source was the brecciated dolomite (dolomicrite), and from 1959-1962 the Pitch Mine produced 454 t of U_3O_8 (0.5%) through underground mining, after which time some of the deposit was recovered through solution mining. Later, a wider-defined zone was estimated at 3,245 t U_3O_8 at 0.17% (Nash, 2010, Ward, 1978). This high-grade uranium deposit is notable in contrast to the Precambrian Wet Mountains deposits east of the San Luis Valley (in Custer and Freemont Counties, CO) that are high in Th and low in U. Open pit mining occurred along a fault zone at the Pitch Mine site from the 1970s but stopped in 1982, in part due to protest and in part because of the high costs of transporting ore roughly 700 km from the northern extent of the San Luis Valley to the Homestake processing mill in Grants, NM (Nash, 1988).

[2] Though the IAEA does not list records on amounts extracted, the Pitch Mine is recorded as deposit 771 and the thorium extraction in the Wet Mountains Area is recorded with a Th to REE ratio of 2.2:1. In 1957, the Pitch Mine was called "Little Indian 36" due to its location at the headwaters of Indian Creek, which flows into Saguache Creek. In 1975 it became "Pinnacle Mine" when ownership changed from Homestake Mining Co to Pinnacle Exploration. A new processing mill was located in Rifle, Colorado.

Due to the general lack of heavy and trace metal water quality monitoring in the San Luis Valley, it is noted that geochemistry data from past geological explorations will help aid in the analysis and interpretation of this work's water chemistry and groundwater recharge objectives.

2.2.4 Hydrology

The San Luis Valley aquifers are replenished mainly through mountain block recharge (Wilson and Guan, 2004) as snow melts in the San Juan Mountains (Mayo et al., 2007). Greater recharge occurs through the San Juan Mountains owing to the permeability of the basalts and rhyolites of the Servilleta and Hinsdale Formations, volcanic tuff, and andesitic-quartz latite rock of the Conejos Formation (Lipman et al., 1970). The Sangre de Cristo's granitic complexes are less permeable and marked by dramatic, Precambrian uplift surrounded by alluvium, conglomerate imbedded sandstone, and thin layers of limestone and dolomite (Lindsey, 2010a, McCalpin, 1996). Recharge from the Sangre de Cristo Mountains occurs when snowmelt-fed streams infiltrate through rock fractures and faults, unconfined sandstones, and through alluvial fans along the mountain range's base.

The aquifer system of the San Luis Valley includes the shallow alluvial aquifer and the underlying confined aquifers. The unconfined and confined aquifers are separated, along the majority of the valley floor, by an Alamosa series "blue clay" layer. Yet, the aquifer system is recognized as a heterogeneous mixture of aquifers and leaky confining beds (Hearne and Dewey, 1988). The valley has two distinct groundwater flow systems—a closed basin to the north in the topographic low or sump, and the region to the south that is drained by the Rio Grande. The area of groundwater drainage that flows into the closed basin area of the valley is shown in Figure 2.5 with a dashed line, though Mayo et al. (2007) uses the term "ancestral sump" to mean a wider, organic-rich sump that marks the remains of the prehistoric Lake Alamosa. The sump is circled on this figure. To the east, Medano Creek forms in the Sangre de Cristo Mountains and moves across the Great Sand Dunes. Locally, it is an important source of groundwater

recharge, as are several other significant creeks originating the Sangres including Spring Creek, Sand Creek, and Deadman's Creek. Further south, the Trinchera, Culebra, and Costilla creeks offer local sources of recharge. On the western side of the valley, the Rio Grande originates in the San Juan Mountains and winds southeast across the southern half of the valley before entering New Mexico. In addition to the Rio Grande, which would overflow seasonally and restore wetlands and recharge large areas of the valley floor, the Conejos River, the Alamosa River, and La Jara, La Garita, and Saguache Creeks are water inputs from the San Juan Mountains. There are a number of smaller, ephemeral creeks that offer additional recharge locally.

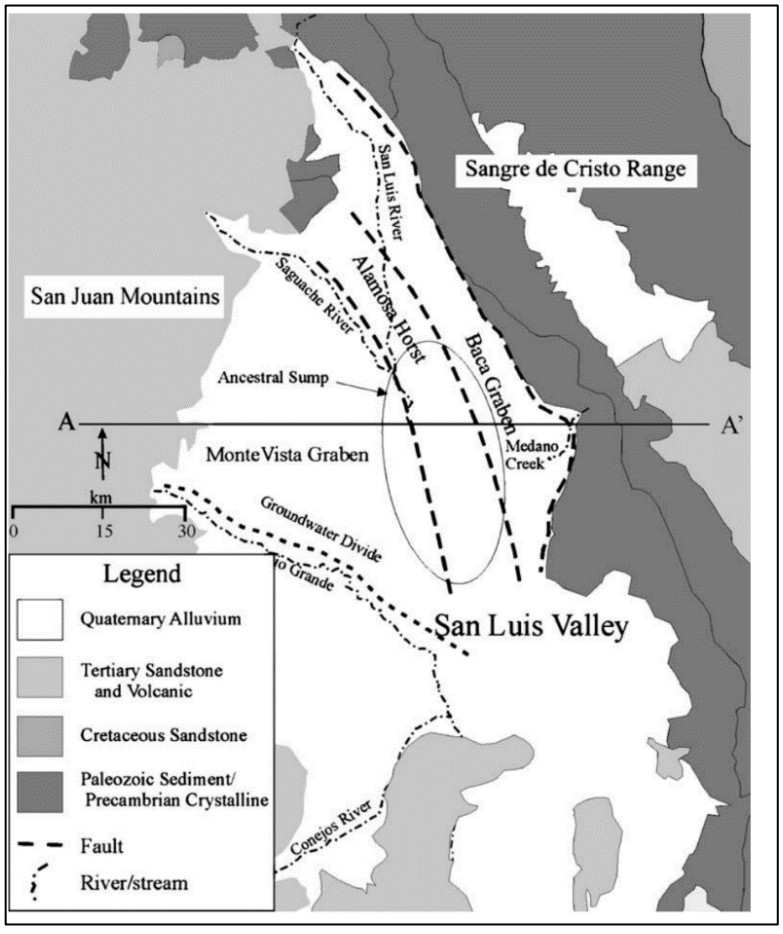


Figure 2.5: Simplified geologic map of the San Luis Valley. Taken from Mayo et al. 2007, who adapted from Johnson, 1969, Stevens et al. 1974, Tweto 1976.The A-A' transect is the location of the east-west transect depicted in Figure 2.4(b).

The largest source of natural recharge to the Alamosa Basin, for both the confined and unconfined aquifers, comes from subsurface inflow, or mountain block recharge, from the San Juan Mountains (Huntley, 1979, Hearne and Dewey, 1988, Huntley, 1976). Fractures and faults in the Sangre de Cristo Mountains is another source of recharge to the confined and unconfined aquifers. Mountain streams and creeks by the basin's margins provide some additional recharge. Diffuse recharge via precipitation to the valley floor offers a small contribution to total recharge and may be more significant in the wider dune field in the valley's northeast region. Both upward and downward movement of water between the confined and unconfined aquifers has been documented, and leakage upward from the confined aquifer to the unconfined aquifer was estimated by Emery and others (1971a, 1975) to be about 0.2 m/yr in the closed basin. Transmissivity estimates have ranged from approximately 65 m^2/day at the valley's margins to 2,800 m^2/day in the valley's western region, north of the Rio Grande. Age dating through ^{14}C analysis has estimated shallow groundwater in the San Luis Valley to be between 5,000 years old in margin areas of significant recharge to 20,000 years old in the valley's closed basin sump (Bexfield and Anderholm, 2010).

In recent times (post 1970), surface water irrigation, groundwater irrigation, and canals and lateral leakage provide an additional source of recharge to the unconfined aquifer. Of course, the disappearance of the valley's extensive, wetland playa complex, and the diversion of rivers so that they no longer overflow and replenish wetland areas is an unaccounted loss to unconfined (and confined) aquifer recharge. However, the Colorado Division of Water Resources has adopted a water budget for the San Luis Valley that separates water budget components into "predevelopment" and "modern (1970-2002)" for purposes of comparison. Modern recharge modelled from 1970 to 2002 estimates 1.275 million acre feet per year of total recharge to the Alamosa Basin. The model estimates recharge has tripled since pre-development times, though despite this, total discharge (particularly from irrigation wells) has more than tripled (CDWR, 2004).

Extensive and long-term hydrological monitoring has taken place in the San Luis Valley since the late 1970s, and the USGS lists 415 registered wells in Alamosa County that undergo some level of monitoring (USGS dataset 2014). The unconfined aquifer beneath Alamosa has experienced a 3.7 m (12 foot) drop in the last 35 years, and there is noticeable seasonal variation with March having the least and late September having the largest drawdown (Davey 2014). In the late 1940s, an early study of the San Luis Valley aquifers examined an inflow-outflow study area and found that unconfined aquifer pumping for irrigation went from 7,000 acre feet of water in 1949 to 280,000 acre feet of water in 1951. The average quantity of groundwater pumped per well went from 33 acre feet to 327 acre feet, and at that time in the San Luis Valley, there were 1,300 shallow irrigation wells. Figure 2.6 (a) suggests groundwater pumping increased in years when less snowmelt river water was available from the Rio Grande or when less surface water was available due to upstream or prior diversions. Agricultural dependence on groundwater only increased, and Figure 2.6 (b) offers a longer perspective of groundwater abstraction and aquifer drawdown in the west-central part of the valley, which most heavily utilizes pivot irrigation. Pivot irrigation is a modern method of irrigation where water is sprayed through a long set of sprayers which slowly rotate around a crop circle with a fixed point in the center of the circle. In the San Luis Valley, each crop circle is usually irrigated with a single well in the unconfined aquifer. It is noted the region of aquifer drawdown in Figure 2.6 (b) is located predominantly in the closed basin agricultural area where extensive pumping from the unconfined aquifer utilizes groundwater for irrigation. This area is west of the Closed Basin Project, a federal government pumping scheme that transfers water from the unconfined aquifer along an open canal to where it joins and augments surface water flow in the Rio Grande. A marked decline in groundwater level of the unconfined aquifer is observed in 2002. This sharp decline is attributed to over-abstraction and to a drought. Both the water level in the unconfined aquifer and groundwater pressure in the confined aquifer have fallen significantly since 2000. From 2000 to 2014, there has been a loss of over 1.2 million acre feet of stored water (Cooper et al., 2006). Groundwater drawdown in the valley threatens agricultural livelihoods, wetland habitat, and Rio Grande Compact deliveries.

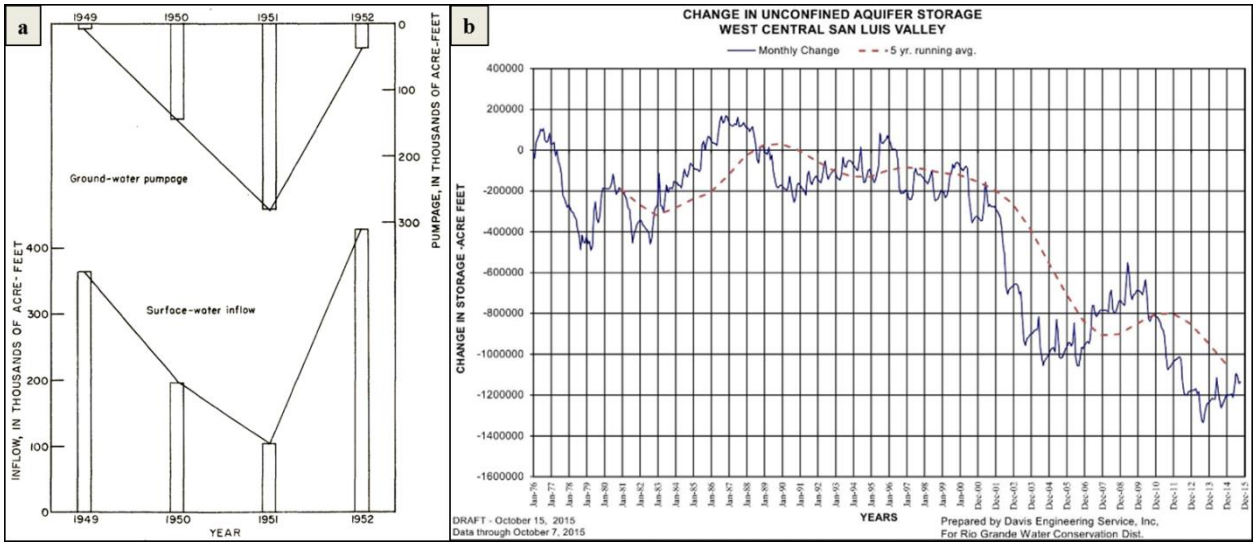


Figure 2.6: Historic groundwater abstraction a) Early groundwater abstraction from 1949-1952 indicates relationship between shallow pumped water in study area for irrigation versus the amount of surface water diverted to the study area for irrigation, from Powell et al. 1958 b) Sharp drawdown of the unconfined aquifer in the closed basin area of the valley post-2001, from Davey 2015.

2.2.5 Water Quality

Water quality has not been monitored routinely in the San Luis Valley, and compared to water quantity, it has received little attention. Groundwater on federal lands is more likely to have received some level of analysis (though this is usually done in response to specific agency objectives) and there have been a handful of published studies that characterize water parameters in isolated locations within the valley. The best source of water quality data for the entire valley is from several USGS studies examining groundwater in the region, and one such early study in the 1950s examined chemistry of the unconfined aquifer. Early on, the unconfined aquifer in the closed basin region of the valley was understood to be alkaline and high in salinity, which would vary by proximity to evaporite wetland playas. While groundwater from the unconfined aquifer may be an order of magnitude higher in salinity than groundwater from the confined aquifer, confined groundwater was found to be high in arsenic and

fluoride. Later water quality analysis would reveal groundwater deeper than 800 m is higher in salinity than the upper section of the confined aquifer.

In the 1950s Powell conducted a survey of water quality in the San Luis Valley analyzing 919 samples from 312 wells (Table 2.1). From the confined artesian aquifer Powell analyzed 64 samples ranging in depth from 18 m to 1300 m. He wrote, "It was not feasible to determine the quality of water in any particular artesian aquifer because the aquifers are discontinuous and leaky and because many of the wells obtain water from more than one aquifer"(Powell and Mutz, 1958). The chemical heterogeneity of water-bearing horizons within a single well has been evidenced in other studies (Mayo, 2010). Table 2.1 shows results from the valley's unconfined aquifer. The range in silica, calcium, and magnesium indicate variation in water-rock weathering in the valley. The range in total dissolved solids (TDS) and in chloride may indicate variation in well depth within the unconfined aquifer. A chloride concentration of 4,500 mg/L is too saline to drink and may represent groundwater subject to evaporation. Nitrate found at 120 mg/L in the unconfined aquifer is thought to originate, in part, from the over-application of fertilizers which were used in the 1950s in the San Luis Valley alongside flood and canal water irrigation practices.

Table 2.1: Water quality assessment of the unconfined aquifer in the 1950s from Powell et al., 1958.

Maximum and minimum concentrations of mineral constituents in unconfined ground water, in parts per million

Mineral constituent	Maximum	Minimum
Silica	66	2.5
Calcium	936	1.0
Magnesium	562	.24
Sodium[1] and potassium	3,100	.5
Bicarbonate	7,310	9.9
Sulfate	4,510	1
Chloride	4,510	.5
Fluoride	24	0
Nitrate (as NO_3)	120	0
Dissolved solids	13,800	52
Total hardness	5,060	10

[1] Percent sodium: maximum, 100; minimum, 1.

Surprisingly, nitrate concentrations in the unconfined aquifer are not routinely measured and reported from within the San Luis Valley despite the prevalence and heavy use of agricultural fertilizers. On the other hand, there has been some state and federal tracking of nitrate concentrations in the San Luis Valley groundwater. Application of commercial nitrogen fertilizer has increased substantially in the San Luis Valley over the last half century. Whereas in 1950 less than a couple of hundred tons of N fertilizer per year were used, in the 1980s, more than 12,000 tons of N fertilizer were applied annually. The increase in fertilizer use is paralleled by the explosion of pivot irrigation in the valley, which only began about 1965. In 1970 there were about 300 pivot irrigators in the valley, but by 1999 more than 2,200 were spraying groundwater for irrigation. Elevated nitrate concentrations have been documented in the unconfined aquifer of the San Luis Valley (Stogner, 2001), and this is thought to be a direct consequence of commercial fertilizer application[3]. Widespread areas exceeding 10 mg/L NO_3 as N are found in the northcentral/northwestern area of the closed basin region (see Figure 2.7). Later studies showed nitrogen leaching occurs in agricultural areas of the San Luis Valley (Eddy-Miller, 1993; LeStrange, 1995) at an estimated rate of -5.3 to 224 pounds of nitrogen as N per acre, and nitrate in the unsaturated zone was calculated to range from 21 to 267 pounds as N per acre (LeStrange, 1995).

In a 2012 USGS regional report, modeled conditions of aquifers across six Southwestern states predicted these basin-fill aquifers exceed the drinking water quality limit for nitrate: central Arizona basins near Phoenix; the San Joaquin, Inland, and San Jacinto basins of California; and the San Luis Valley of Colorado (Anning et al., 2012). The model also suggested it likely that higher nitrate concentrations in groundwater would be found in or migrate toward low-elevation sumps and wetland areas.

[3] The first nitrate analysis of unconfined groundwater quality in the San Luis Valley is from Scofield (1938), and 38 shallow wells showed $\leq$ 0.3 mg/L NO_3 as N. In the 1930s soil health was maintained through legumes and livestock manure only. In other studies at the valley's margins, 3 mg/L NO_3 has been recorded and may be considered a background concentration.

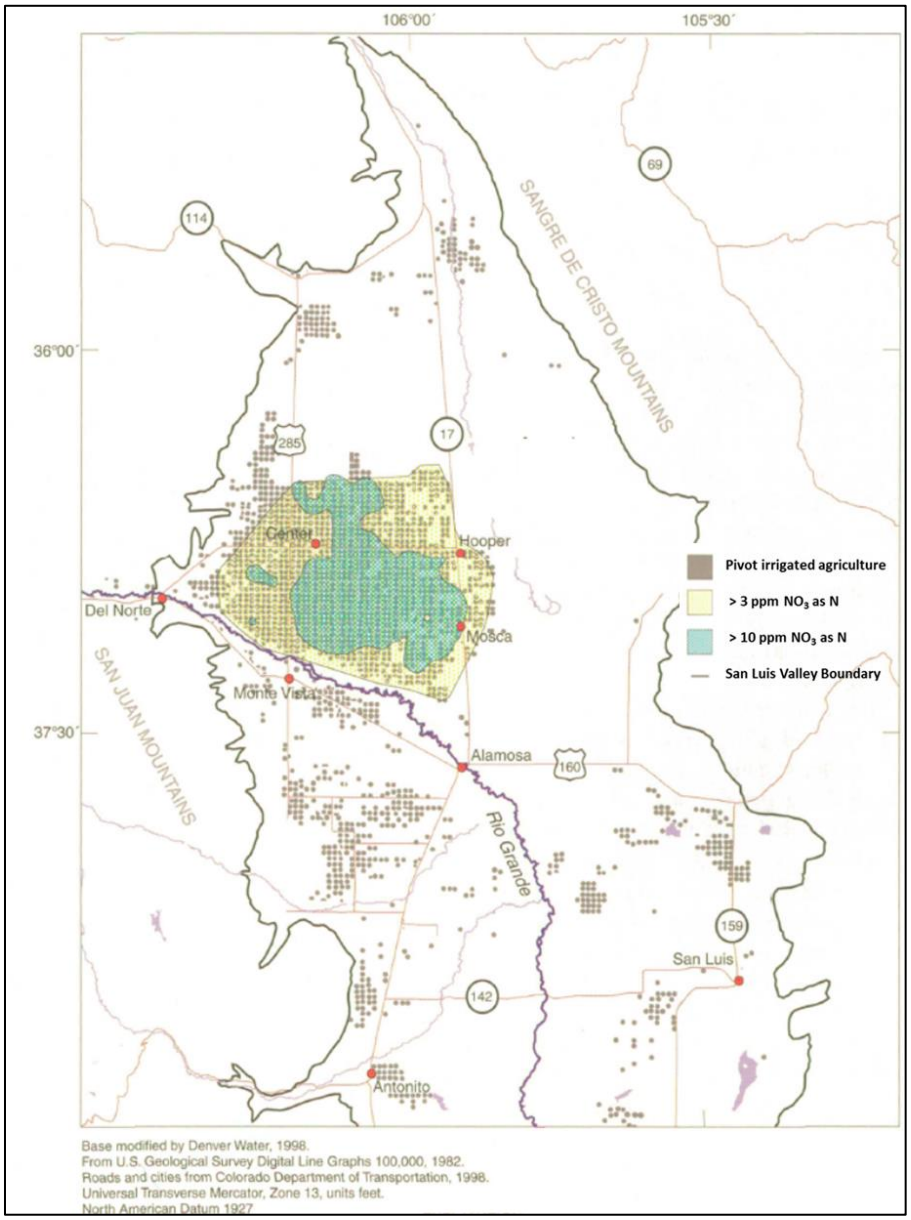


Figure 2.7: Nitrate concentrations found in the unconfined aquifer of the San Luis Valley, from Stogner 2001.

USGS trace element analysis in the San Luis Valley's shallow unconfined aquifer found elevated levels of uranium and radon that exceed drinking water guidelines. Two of the 35 drinking water wells sampled > 30 µg/L uranium with a maximum concentration of 84 µg/L, a mean of 10.4 µg/L, and 17% exceeding 20 µg/L (the then-provisional MCL). Eight of the drinking water wells sampled exceeded the gross alpha EPA standard, and while this normally prompts further analysis, none was conducted due to the limited

scope of this 1993 USGS study (published 1996). All of the shallow groundwater sampled exceed the EPA guideline for radon (300 pCi/L, or 11.1 Bq/L), nearly all exceed 1,000 pCi/L (37 Bq/L) radon-222, with a range of 700-1,900 pCi/L (25.9-70.3 Bq/L) (Anderholm, 1996, Bexfield and Anderholm, 2010). Additionally, gross beta radiation dissolved in shallow groundwater in the San Luis Valley ranged from 1.6-48 pCi/L (0.06-1.78 Bq/L) as Cs-137 equivalent (11 pCi/L mean) (Anderholm, 1996), and the EPA requires individual beta-emitting radionuclide testing when beta radiation exceeds 15 pCi/L (0.56 Bq/L).

When the Rio Grande aquifer system—which runs from the San Luis Valley through New Mexico—was viewed more widely as a whole, samples collected downstream of the San Luis Valley between 1991 and 2010 showed parts of the aquifer system used for public and domestic water supply exceed EPA maximum contaminant levels (MCL) and suggested contaminant levels in several parameters, notably arsenic (27%), uranium (3%), molybdenum (3%), and fluoride (3%), and 66% of these drinking water sources also exceeded a human health benchmark for radon with > 300 pCi/L (11.1 Bq/L). With regard to the shallow Rio Grande aquifer samples from monitoring wells beneath agricultural land, 28% exceeded the 10 mg/L $NO_3 + NO_2$ MCL, and 68% exceeded 300 pCi/L radon (DeSimone et al., 2015, Thiros et al., 2014).

In addition to water quality concerns owing to natural bedrock, heavy metal contaminants in the Rio Grande thought to originate through mining-related activities have been observed in creek headwaters and tributaries to the Rio Grande such as Willow Creek (Taylor et al., 2001) in the San Juans and the Alamosa River (Csiki and Martin, 2013, Kirkham et al., 1995). Pharmaceuticals and pesticides have been found in surface (Zenobia et al. 2015) and groundwater (Stogner 2001) samples within the San Luis Valley, and 160 km south of the San Luis Valley, research and development activities are responsible for radionuclide contamination of fluvial sediment in the Rio Grande (Gunderson et al., 1983, Graf, 1994, Graf, 1996).

2.2.6 History of Water Use and Land Use Changes

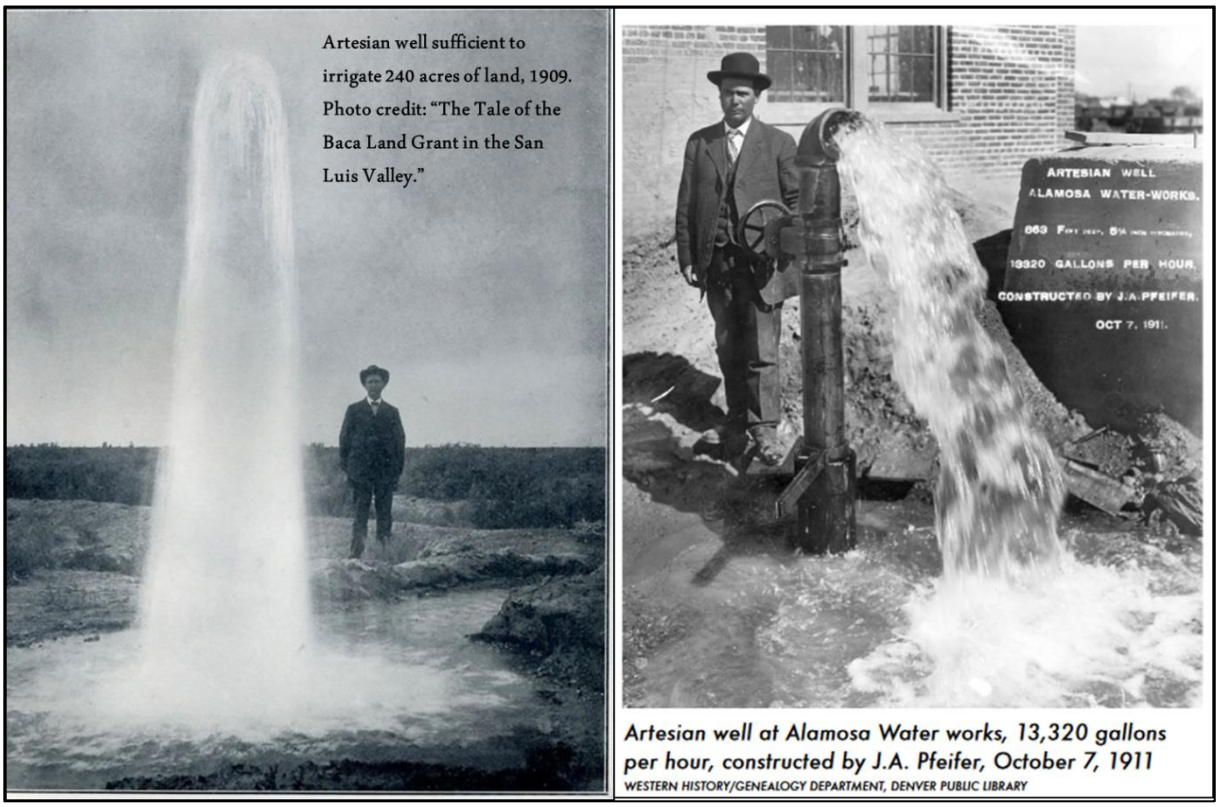


Figure 2.8: Newly discovered artesian groundwater produced excitement and a flurry of development at the turn of the 20th century in the San Luis Valley.

It is seen in many dryland areas of the world that when a river's water is over-allocated or inconsistent, the population turns increasingly to groundwater resources to meet its cultural, economic, and physical requirements (Figure 2.8 and 2.9). The San Luis Valley in southcentral Colorado is the highest-elevation agricultural area in the United States, and its economy as well as its cultural identity have relied on agricultural production—chiefly alfalfa, barley, and potato—and livestock production, most notably cattle. Because evaporation exceeds precipitation, crops must be irrigated, and cattle must be watered. The valley also provides important wetland habitat for birds and other wildlife, and this water use is at times at odds with agricultural and livestock water use (Rio Grande Roundtable, 2014). Agricultural diversions in the San Luis Valley have in part precipitated the water conflicts that lead to compacts for

international and interstate water deliveries (Mix et al., 2014). Agricultural production in the San Luis Valley brings in an estimated $220 to $357 million per year (SLVDRG, 2016).

The San Luis Valley has a long history of farming, from the Ute Native Americans to the Hispanic settlers and westward-moving homesteaders. Historically, agriculture was accomplished through flood irrigation. In the 1850s, irrigation water flowed through community ditches called *acequias*. By the end of the 1800s, nearly 400,000 acres were irrigated by canals, ditches, and nearly 2,000 newly-drilled artesian wells. By 1930, the irrigated land increased to 700,000 acres. Irrigation from the unconfined aquifer increased significantly in response to droughts in the 1930s and 1950s. By 1980, there were more than 2,300 irrigation wells drawing from the unconfined aquifer (Stogner, 2001). In 1989 it was estimated the valley had 750,000 irrigated acres consuming 1 million acre feet of water per year (Riverside Technology et al., 1998). By the early 21st Century, it was estimated 10,000 unmetered wells drew water from the confined and unconfined aquifers (Mix et al., 2014).

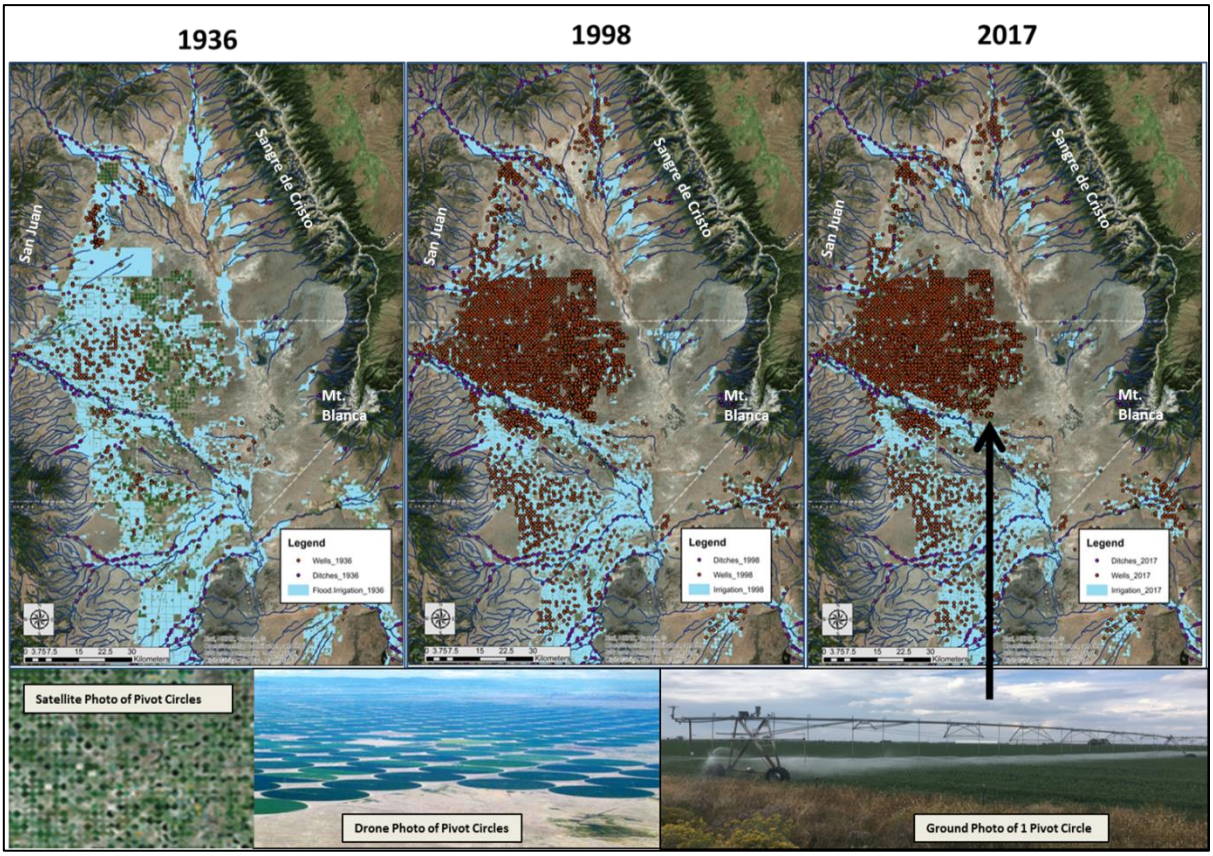


Figure 2.9: The increase in agricultural wells is shown for the San Luis Valley from 1936 to 2017 as flood irrigation is replaced by pivot irrigation. Each red circle represents a single well and one crop circle. These are visible from space.

In the decades leading up to the 1950s it was widely thought that shallow groundwater lost through evapotranspiration—termed "consumptive waste"—could be actively salvaged (Robinson, 1958, Lee, 1912). This could be engineered by one of two methods:

1) The water table could be lowered through pumping—as would happen with the US Bureau of Reclamation's 170-salvage well Closed Basin Project[4].

[4] One of the earliest examples of pumping to lower a water table in the American West also involved a water transfer scheme for the city of Los Angeles.

2) High value crops could be planted in the place of the "nonbeneficial phreatophytes"—as would happen through the valley's agricultural conversion[5].

Conceived during a period when the water table in the Alamosa Basin was very near the surface and groundwater was lost to evaporation, the US Bureau of Reclamation's Closed Basin Project, (which was only fully completed in 1993), sought to utilize shallow groundwater to replace surface water diverted for irrigation from the Rio Grande. The infrastructure was designed and built by the US Army Corps of Engineers and run through the US Bureau of Reclamation (USBR). Though run by and operationally overseen by the USBR (with an office in Alamosa, Colorado), the Closed Basin Project is administratively overseen by the Rio Grande Water Conservation District (RGWCD). In 1967 the Colorado General Assembly created seven basin-specific Water Conservation Districts within the state of Colorado. The RGWCD has jurisdiction over a 5-county region of the San Luis Valley and is headquartered in Alamosa, Colorado. The RGWCD is a corporate body and a political subdivision of the state that contracts the federal USBR to run the Closed Basin Project.

The Closed Basin Project draws groundwater from the unconfined alluvial aquifer in the northern closed drainage basin of the San Luis Valley through a network of salvage wells and transports this water along a 68 km open conveyance canal (1986) to augment the river's flow and fulfill Colorado's obligation under the 1906 Rio Grande Convention between the United States and Mexico and the 1938 Rio Grande Compact (Leonard and Watts, 1988, Paddock, 2001). However, due to a less transmissive aquifer than projected, biofouling with arsenic-dependent bacteria that clog the well screens, and evaporative loss/transport inefficiencies, the Closed Basin Project delivers less than 20% of the water it estimated it would (USBR, 2003). Because the Rio Grande Convention and Rio Grande Compact do not specify water delivery in time and place, there is currently no obligation to fulfil water delivery year-round or to keep a minimum baseflow in the river for sustaining water-dependent ecosystems. Instead, water delivery

[5] The classic phreatophyte replacement at the time was alfalfa, an early example of which came from Meinzer's 1927 observations in Escalante, Utah.

depends on projections made each year based on the previous winter's snowpack, and a priority system under western water law that delivers water first to those with the most senior water rights.

In order to mitigate potential damages caused by playa drainage and groundwater drawdown, Congress proposed and authorized the creation of the 14,000 acre Mishak National Wildlife Refuge, which was meant to be provided with 12,500 acre feet of mitigation water annually. The entire mitigation area, including the proposed Mishak Wildlife Refuge, would have totaled 139,000 acres (Radosevich and Rutz, 1979). This did not happen, due in part to the disappearance of available mitigation surface water and seasonal overflow. In 1972 the USBR's Project Authorization Act was amended in the early 1980s under H.R. 2823 and offered the Russell Lakes Wildlife (Waterfowl) Management Area instead. The proposed Russell Lakes Management Area would not have required locating external mitigation water, since the project planned to purchase 3,120 acres of private land and merging 1,520 acres of state-administered land with some existing water rights. It was thought that with these water rights, 1,100 acres of manufactured wetlands could augment the 1,900 acres of wetlands presently existing on the refuge area (1984).

The USBR was obligated to deliver annual mitigation water in the amount of 800 acre feet per annum to the Bureau of Land Management's (BLM) Blanca Wetlands, and 4,500 acre feet annually to the Alamosa National Wildlife Refuge, a 12,000 acre refuge that includes the Rio Grande river corridor as it progresses toward New Mexico. This wildlife refuge is part of the San Luis Valley Wildlife Refuge Complex, which also includes the 15,000 acre Monte Vista Wildlife Refuge with artificially created and managed wetlands meant to mimick those wetlands now extinct, and the 93,000 acre Baca National Wildlife Refuge on the eastern edge of the valley adjacent to Great Sand Dunes National Park and Preserve.

The vast majority of the Rio Grande's water—at times, upwards of 90%—is diverted for agricultural use in the San Luis Valley between the towns of Del Norte and Alamosa, and the irrigation season runs provisionally from April 1 through November 1 (see Figure 2.10 (a)). The river water is protected on

federal land, where it runs through the Alamosa Wildlife Refuge, and just before it flows into New Mexico, it is augmented by an open canal water shown in Figure 2.10 (b) from the Bureau of Reclamation's Closed Basin delivery of unconfined groundwater. In addition to the approximate 170 salvage wells[6] that extract unconfined groundwater for this delivery purpose, there is also a network of roughly 130 monitoring wells that record water and pressure levels for both the unconfined and confined aquifers. Though water samples are collected routinely from selected monitoring wells, only the parameters important for the Rio Grande Compact (%Na and TDS) are reported.

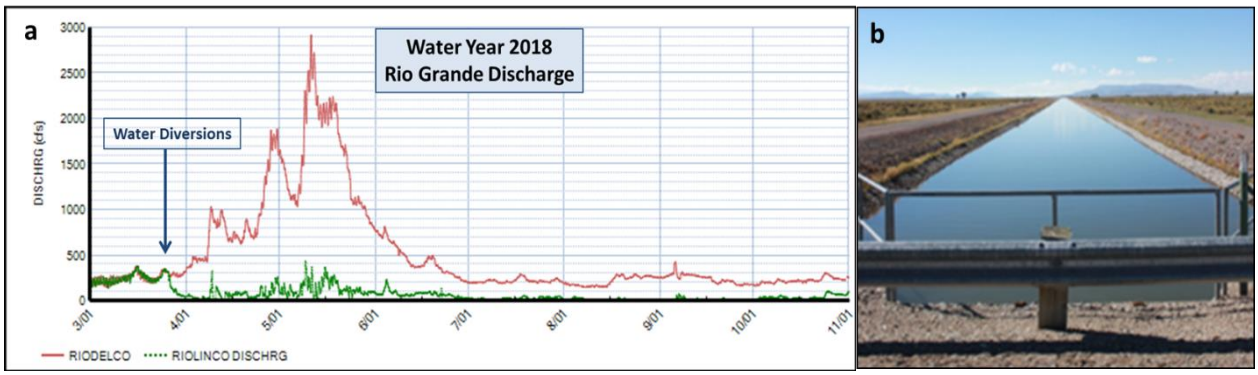


Figure 2.10: a) irrigation diversions cause a hydrograph separation between the gauge at Del Norte and the gauge in Alamosa using USGS water data. The Del Norte gauge, which is upstream of most agricultural abstraction, is shown in red. The Alamosa gauge, downstream of significant agricultural abstraction, is shown in green. b) this conveyance canal augments the Rio Grande with Closed Basin Project groundwater at Colorado's southern-most gauging station.

2.2.7 Legal Battles and Water Law

Water law in the American West was not developed through a sound understanding of hydrology. The doctrine of prior appropriation prioritizes surface water rights over groundwater rights so that when groundwater rights are discussed, they are most often understood in terms of injury to surface water rights (Johnson 2008). Therefore, the legal strategy of some cases has been to show evidence of a water channel, spring, or wetland that no longer exists due to groundwater drawdown. If it can be shown through models

[6] The number of salvage wells has changed slightly over time because well screens become clogged from biofouling or wells otherwise fail, and many of the original wells were re-drilled.

that heavy groundwater abstraction has reduced another's surface water rights, groundwater users must mitigate the amount of water affected or pay a mitigation fee to the Rio Grande Water Conservation District.

Early MODFLOW model work established simplified water budgets for the closed drainage basin that included recharge and evapotranspiration arrays (Williams, 1992, Leonard and Watts, 1988). Later model development most notably includes the Rio Grande Decision Support Model (RGDSM) used by the state of Colorado for estimating injury to surface water caused by groundwater abstraction (Riverside Technology et al., 1998). The RGDSM is used in Colorado Water Court (Division 3 being the Rio Grande) to account for surface water injury and to mandate water mitigation, whether in the form of water repayment or through monetary fines. Challenges to the decision support model usually rest on placement and thickness of the confined aquifer's boundary clay layers, an underestimation of recharge, an oversimplification of the model's response function, or a lack of data regarding water movement between the confined and unconfined aquifers.

Growing concern over the declining aquifers and the unchecked abstraction from roughly 10,000 unmetered wells, along with disappointment in the Closed Basin Project's water deliveries, prompted the passage of Colorado Senate Bill (SB) 04-222 in 2004. It requires restoring the confined and unconfined aquifers water levels and the confined aquifer pressure. It calls for sustainable use of the aquifers, and demands that groundwater irrigators replace or pay for water taken from the confined aquifer. The Rio Grande Water Conservation District (RGWCD) is the institution that currently manages efforts to restore the San Luis Valley's aquifer levels, and it works administratively by dividing the valley into six water user districts (shown in Figure 2.11). The closed basin sub-district (formerly sub-district 1) was the first formed sub-district and contains the greatest amount of groundwater withdrawal for agricultural use. If the RGWCD is unable to reduce pumping and restore the valley's aquifer levels to what they were in 2000, Colorado's State Engineer's Office will step in to regulate groundwater usage and force compliance

with SB-04-222, and this would cause many of the farms that rely on pivot irrigation to abandon irrigation.

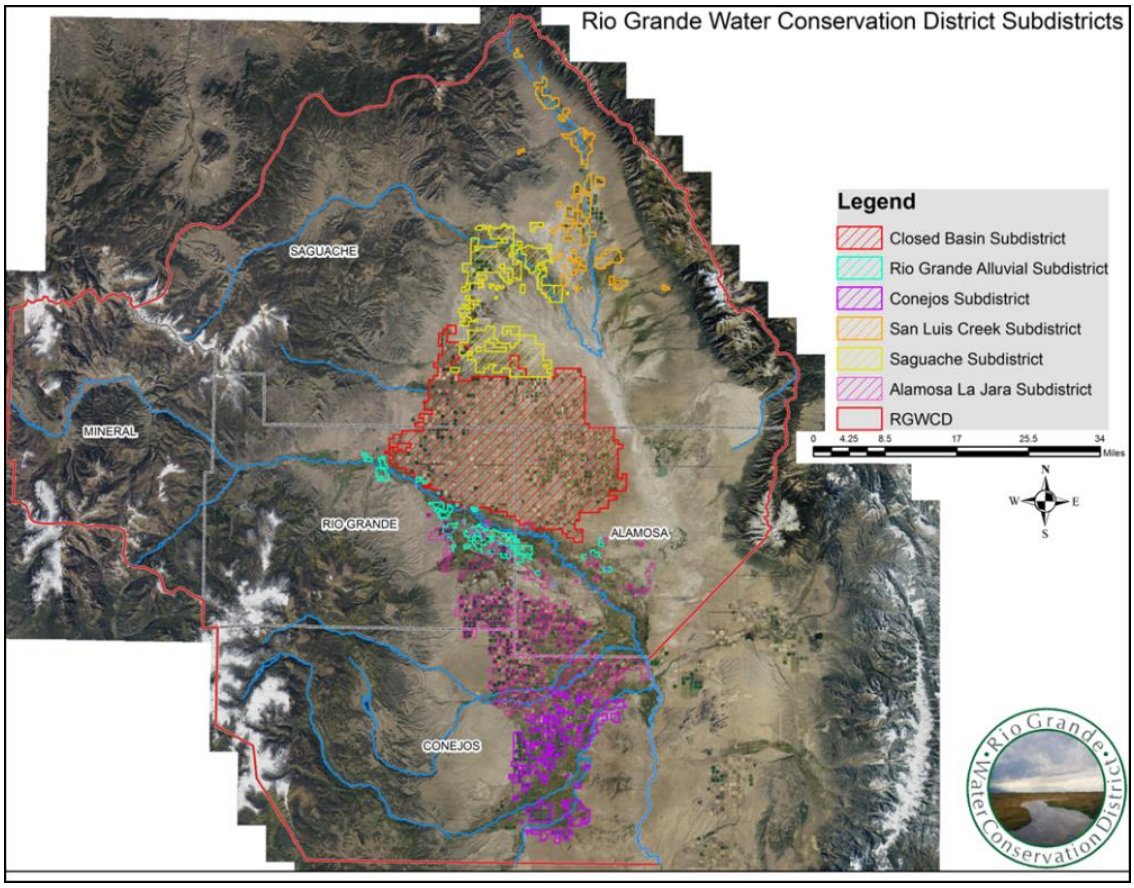


Figure 2.11: The San Luis Valley is divided into 6 sub-districts of water users governed by the Rio Grande Water Conservation District. For those water users who choose not to join a sub-district, they must develop their own water augmentation plan. Map source http://rgwcd.org.

As the Rio Grande Water Conservation District looks to control water use in the valley before the state of Colorado steps in and forces the closure of wells, legal challenges to the San Luis Valley groundwater have also arisen externally. On December 31, 1986, the American Water Development, Inc. (AWDI) made a court application to drill 112 wells 2,500 feet deep in the closed drainage basin of the valley for the purposes of abstracting 200,000 acre feet/yr (later amended to 60,000 acre feet/yr). They filed for the right to non-tributary water and claimed a right to the water under land they had acquired on the Baca

Land Grant No 4, based on Spanish and Mexican law and the 1848 Treaty of Guadalupe Hidalgo, signed between the United States and Mexico. In the original application, the company claimed its purpose was to sell water to the valley's agricultural industry and to apply it for other beneficial purposes. When AWDI amended its application in water court on August 31, 1990, it stated its intention was to transfer the water north via pipeline out of the valley and sell it to Denver and other cities along the Front Range. The AWDI application met strong opposition in multiple court cases and ultimately, the water transfer was unsuccessful (Miller et al., 1993).

A new water transfer proposal was announced in December, 2018, during a RGWCD meeting. The company is called Renewable Water Resources, and it's proposing to abstract 20,000 acre feet/yr for transfer to Denver and other cities along the Front Range. As the San Luis Valley comes to grips with threats to its water resources—both internal and external—it will struggle to understand its complex hydrology within the context of a changing climate.

2.3 Plants as Indicators of Water in Drylands

Recharge is generally defined as the downward flow of water reaching the water table and adding to water storage (Freeze and Cherry, 1979, Meinzer, 1923, Healy and Scanlon, 2018, Hogan et al., 2004, Hiscock, 2005) and is best understood by including an examination of the unsaturated zone (Stoertz et al., 1991). Water infiltration, movement, and retention change significantly between the unsaturated and saturated zones. Movement in the unsaturated zone is considered complex because there is an upward and downward movement of water, and the unsaturated zone faces complicating factors (such as hysteresis, air, and plant interactions). When not viewed from a microscopic lens, water movement into the soil may be described as a circular wetting front with horizontal and vertical movement. When the wetting front reaches a deeper soil layer, the textural stratification determines how and at what rate water moves beyond this soil layer barrier. If the next soil layer is coarser, the air space and lower matric potential will

cause a buildup of moisture. If the upper layer is loamy and the layer beneath is fine, the buildup of moisture will be due to lower hydraulic conductivity of the fine soil layer (Miyazaki, 2006).

Downward and upward movement of water through soil will vary between vegetated and non-vegetated areas (Noy-Meir, 1973), and plants may facilitate the distribution and conservation of moisture while at the same time they compete for water resources (Barbier et al., 2006). Soil layers in the unsaturated zone of drylands can be loosely divided into an upper layer, where evaporation is dominant over transpiration, and a lower layer in which only transpiration from plant roots occurs. Several models of soil moisture distribution incorporate a two-layer system to distinguish between types and rates of soil moisture distribution (Baudena and Provenzale, 2008, Tietjen et al., 2009) and plant water uptake (Schwinning, 2001). All of the processes modeled are strongly dependent on vegetation cover. Soil water content is influenced by a number of biotic (e.g. plant type and cover, evapotranspiration, water use efficiency and uptake, plant growth, microorganisms and biotic soil crusting, rooting architecture, etc.) and abiotic (e.g. topography, rainfall distribution, soil compaction, soil layering, porosity, hydraulic conductivity, clay content, etc.) factors (Wang et al., 2012). Depth to water table—notably where the water table and rates of evaporation are high—also has a significant impact on soil water content.

Because rain events in drylands are so significant in determining where and how vegetation can occur, understanding the importance of isolated rain events is critical, especially in areas where trends show decreasing rainfall. Additionally, predicted increases in aridity may threaten levels of biologically derived carbon and nitrogen and may negatively impact reactions controlling key ecosystem functions (Peñuelas et al., 2012, Delgado-Baquerizo et al., 2013). In drylands, there is a profound link between vegetation, soil moisture, and nutrient cycling. Water drives the biological activity of plants promoting mutualism, nitrogen cycling, and plant growth (Noy-Meir, 1973, Austin, 2004, Schwinning and Sala, 2004a, Collins et al., 2008). In turn, vegetation reduces wind erosion and evaporation, promotes cooling, and protects soil moisture (Barbier et al., 2008).

Desert rain events and the resulting 'pulse' of soil moisture and microbial activity are critical for plant life (Schwinning and Sala, 2004b, Austin et al., 2004). The term "rain pulse event" refers to these singular rain events which have the potential to provide extended periods of soil moisture for an area, which then promotes microbial activity, nutrient cycling, and plant growth (Loik et al., 2004). Nitrogen levels are governed mainly by soil moisture (Xie et al., 2001). Nitrogen (and carbon) dynamics in arid systems are frequently described by a pulse-reserve model where the first rain produces biological activity that generates biomass reserve, propagules, and organic matter that prime the ecosystem to respond quickly should more rain ensue (Collins et al., 2008). Frequent, small rain pulses are preferable to larger precipitation events. With existing climate change models, the ammonium: nitrate ratio will decrease because larger, more infrequent rain events produce nitrate losses but not ammonium losses. For this reason, it's predicted that deep-rooted plants that prefer nitrate to ammonia will have a competitive advantage (Yahdjian, 2010).

Vegetation in drylands directly corresponds to moisture availability, and may be tracked through seasonal variations and periods of drought. Dryland plants have adapted to extended periods of low moisture availability through, for instance, ways of retaining and redistributing water (Craine et al., 2013). Facilitation between plants in dryland areas may occur more readily in areas with high water stress (Belsky, 1993). Self-organized vegetation has been observed, primarily, in drylands where potential evaporation significantly exceeds mean annual precipitation (Lefever et al., 2009, Schlesinger, 1990, Ludwig et al., 2005). For plants, soil moisture is more important than precipitation. Due to high permeability, the soil moisture available to plants in sandy soils tends to be low at 3-9% (Noy-Meir, 1973, Brady, 1974). However, there is good moisture retention in desert sand below the upper 30-60 cm, and this zone is used by perennial mesophytic shrubs (Alizai and Hulbert, 1970, Chadwick, 1965). Models of plant competition and facilitation highlight the importance of conserving soil moisture and specifically near-surface soil moisture (Gilad et al., 2007). Some models more specifically refer to a "nurse plant" that provides protection for neighboring plants in terms of shading and moisture retention (Holmgren and

Scheffer, 2010, Peláez et al., 2019). The benefits of tree-grass or shrub-grass associations are well documented in terms of increased infiltration, canopy perimeter drip, and stemflow (Scholes and Archer, 1997, Callaway, 2007, Navar, 1993, Návar, 2011, Thurow et al., 1987). Root depth, density and spacing may affect facilitation and competition between plants. Deeply rooted trees and shrubs may increase soil moisture for shallow rooted plants through a process of hydraulic lift, where the deeper roots move water toward the surface both night and day (Saltz, 1999, Scholes and Archer, 1997, Caldwell et al., 1998, Richards and Caldwell, 1987, Dawson, 1993a). Kizito et al. (2012) measured field plots in the Sahel and found passive water release from shrub roots that rewetted the drier, upper soil layers during the night. The inverse movement has also been observed in sandy soils of the Kalahari (Schulze et al., 1998).

Dryland plants vary in their ability to utilize soil moisture and groundwater (Ehleringer et al., 1991). This is due primarily to different rooting systems. Many dryland plants have a dimorphic root system with a deeper tap root to access groundwater and branching surface roots that can utilize soil moisture in the upper layers. While plants can change their water capture strategy depending on seasonal water availability, plants may also change their rate of water uptake, which may increase as more water becomes available (Williams and Ehleringer, 2000).

Meinzer (1927) first coined the term “phreatophyte” to describe a plant with a dimorphic rooting system containing a central taproot that extended to the water table (depicted in Figure 2.12). Facultative phreatophytes, those plants which draw water from near-surface moisture as well as from groundwater, provide a lens through which to study water movement between the saturated and unsaturated zones in deserts with high water tables (Cooper et al., 2006, Froend and Sommer, 2010).

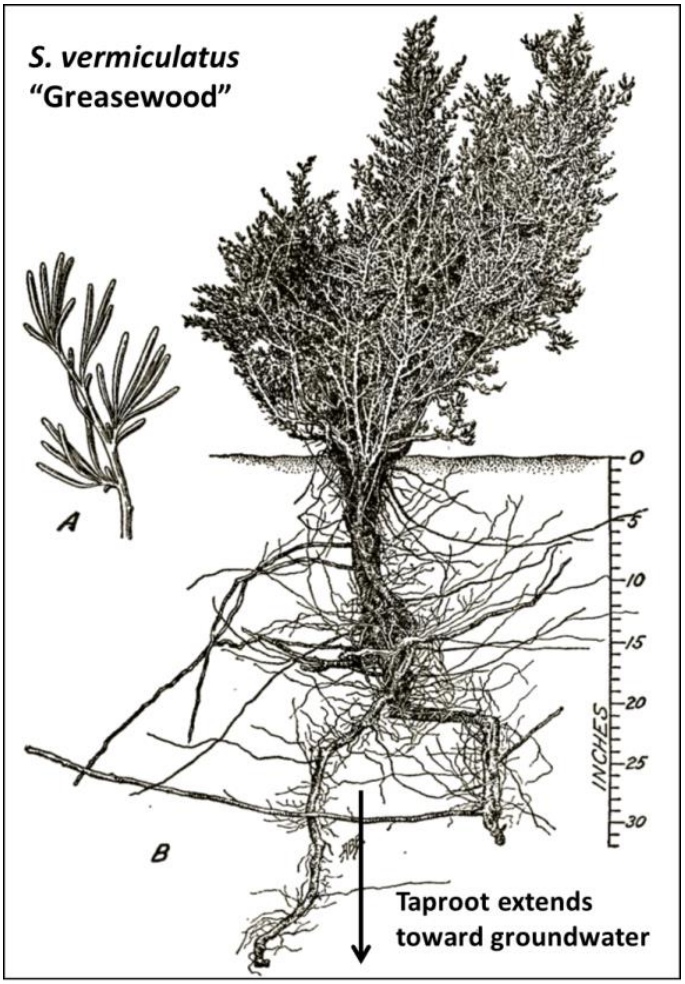


Figure 2.12: Modified early sketch of the phreatophyte *Sacrobatus vermiculatus* depicting an extended taproot.
From Meinzer, 1927.

In the 1950s it was thought phreatophytes such as *S. vermiculatus* would have a rooting depth sensitive to, and indicating the depth to, groundwater (Robinson 1958). While the roots of several subspecies of *E. nauseosa* have been excavated to a depth of 4.6 m, the roots of *S. vermiculatus* have been found to extend to even greater depths. Shantz and Piemeisel (1940) reported a large *S. vermiculatus* near Moab, Utah, had roots reaching 5.5 m deep with a taproot 7.6 cm in diameter. Previously, *S. vermiculatus* in Big Smoky Valley, Nevada, were found growing in an area where the depth to groundwater was 10.1 m (Meinzer, 1927), though, since the roots themselves were not excavated, it was not known if the *S. vermiculatus* roots reached the groundwater, and if they did, if the plant was utilizing the groundwater.

Both *E. nauseosa* (rabbitbrush) and *S. vermiculatus* (greasewood) have shown high tolerances for an elevated water table. Black *S. vermiculatus* tolerated surface flooding for 40 days without showing effects, and a water table 25-30 cm below the ground surface appeared to have no effect on *S. vermiculatus* (Ganskopp, 1986). Groeneveld and Crowley (1988) later extended flood inundation by a period of 6 months to show that *E. nauseosa* could not survive this length of flooding, and this is thought to be due, in part, to the plant's oxygen requirements for root morphology. Salt tolerance is the most important water quality parameter that differentiates phreatophytes and allows for or limits growth. Willow and cottonwood have low salt tolerances while *S. vermiculatus*, as a halophyte, has a high tolerance for salt. Additionally, *S. vermiculatus* also grows well in areas of high sodium carbonate groundwater, which in arid areas forms "black alkali" on the soil surface (Robinson, 1958). Both *E. nauseosa* and *S. vermiculatus* grow in light to moderately alkaline soil.

Much of the San Luis Valley is dominated by woody shrub-grassland, and the most common woody shrubs are the deeply rooted, phreatophytic, *Sarcobatus vermiculatus* and *Ericameria nauseosa* (see landscape photo Figure 2.13). Certain woody shrubs may encroach on grasslands because of higher water and light utilization efficiencies, while others, such as the common creosote bush, *Larrea tridentate*, survive higher oxidative damage (Liu and Guan, 2012). *S. vermiculatus* and *E. nauseosa* are facultative phreatophitic shrubs that may utilize groundwater in the early summer but can also draw precipitation water during the late summer monsoon (Chimner and Cooper, 2004). By altering soil moisture content and measuring xylem pressure potential, Kray et. al. (2012) found the xylem pressure potential of *S. vermiculatus* increased by 0.5 to 0.7 MPa once rains arrived but decreased across all plots by an average of 1.4 MPa as the volumetric water content of the 15—30 cm layer of soil declined. In contrast, they found *E. nauseosa* did not respond to an increase or decrease in surface soil moisture. Isotope analysis suggests that while *E. nauseosa* has a strong groundwater dependence, *S. vermiculatus* changes water capture strategies according to seasonal availability of precipitation recharge (Kray et al., 2012).



Figure 2.13: Landscape view of native shrubs *S. vermiculatus* and *E. nauseosa* in the San Luis Valley. Mount Blanca is visible on the right.

The zero flux plane is defined as a horizontal plane within the unsaturated zone where the hydraulic gradient in the vertical direction (dH/dz) is 0 (Richards et al., 1956). Above the zero flux plane, water moves upward in response to evapotranspiration. Below the zero flux plane, water moves downward and may contribute to recharge (Healy and Scanlon, 2018). Early work in the San Luis Valley often had difficulty distinguishing transpiration and evaporation and noted discrepancies in methods of evapotranspiration (ET) measurements. A 1987 report notes bare soil contributes a significant portion of ET measurements from *S. vermiculatus* and *E. nauseosa* where groundwater levels are shallow and depth to water < 1.25 m (Charles et al., 1987).

It can be argued after the discovery of water isotopes (Giauque and Johnston, 1929a, Giauque and Johnston, 1929c, Giauque and Johnston, 1929b, Urey et al., 1932, Dempster, 1918) their use as a tool to identify water's origin was first used in the disciplines of atmospheric science (Dansgaard, 1964, Dansgaard, 1953, Craig, 1961, Merlivat, 1978, Merlivat and Jouzel, 1979), oceanography (Craig and Gordon, 1965), and ecology (Gonfiantini et al., 1965) before gaining more widespread use in the discipline of water resource hydrology (Gat and Issar, 1974, Allison, 1982, Darling et al., 1987, Fritz and Fontes, 1980, IAEA, 1974, Fontes and Fritz, 1975). Stable isotopes have been used routinely to identify

source water for plants across growing seasons and years (Dawson, 1993b, Ehleringer et al., 1998, Williams et al., 2007, English et al., 2010) and for decades in the American Southwest.

Water resources and water movement (whether through soil, plants, or air) may be identified by measuring the relative abundance of hydrogen and oxygen isotopes (Charles et al., 1987). Water isotopes have been used to suggest seasonal and longterm variation in water capture strategy of the dominant phreatophytes of the San Luis Valley. However, never before has the water table dropped so low. It is not known if these dominant, native shrubs can reach groundwater under such conditions.

2.4 Groundwater Depletion, Dust Generation, and Mountain Block Recharge

While a lowered water table will significantly diminish water logging, capillary rise, and water loss due to evapotranspiration, the lack of soil moisture, the diminished movement of water between plants, the lack of soil structure plant roots provide, and the loss of protection from wind breaks, shading, and moisture retention will ultimately alter the near-surface soil environment.

Today in the San Luis Valley, irrigated agriculture is accomplished mainly through pivot irrigation (Figure 2.9) and accounts for the high majority, >90%, of water use (Hearne and Dewey, 1988). Intensive farming practices leave bare soils exposed throughout the winter and spring months (see time-lapse imagery in Figure 2.14) and susceptible to seasonal dust storms that occur in the spring. Agricultural practices such as tilling, crop extraction, and the driving of heavy machinery and trucks along dirt fields and roads also generate dust (for further visuals, please refer to Figure 8.1). When airborne dust lands on mountain snowpack in the fall, summer, and spring, these dust emissions lower the albedo of the mountain snow packs and hasten melting. Water for irrigation is derived from surface flow and groundwater from both the unconfined and confined aquifers.

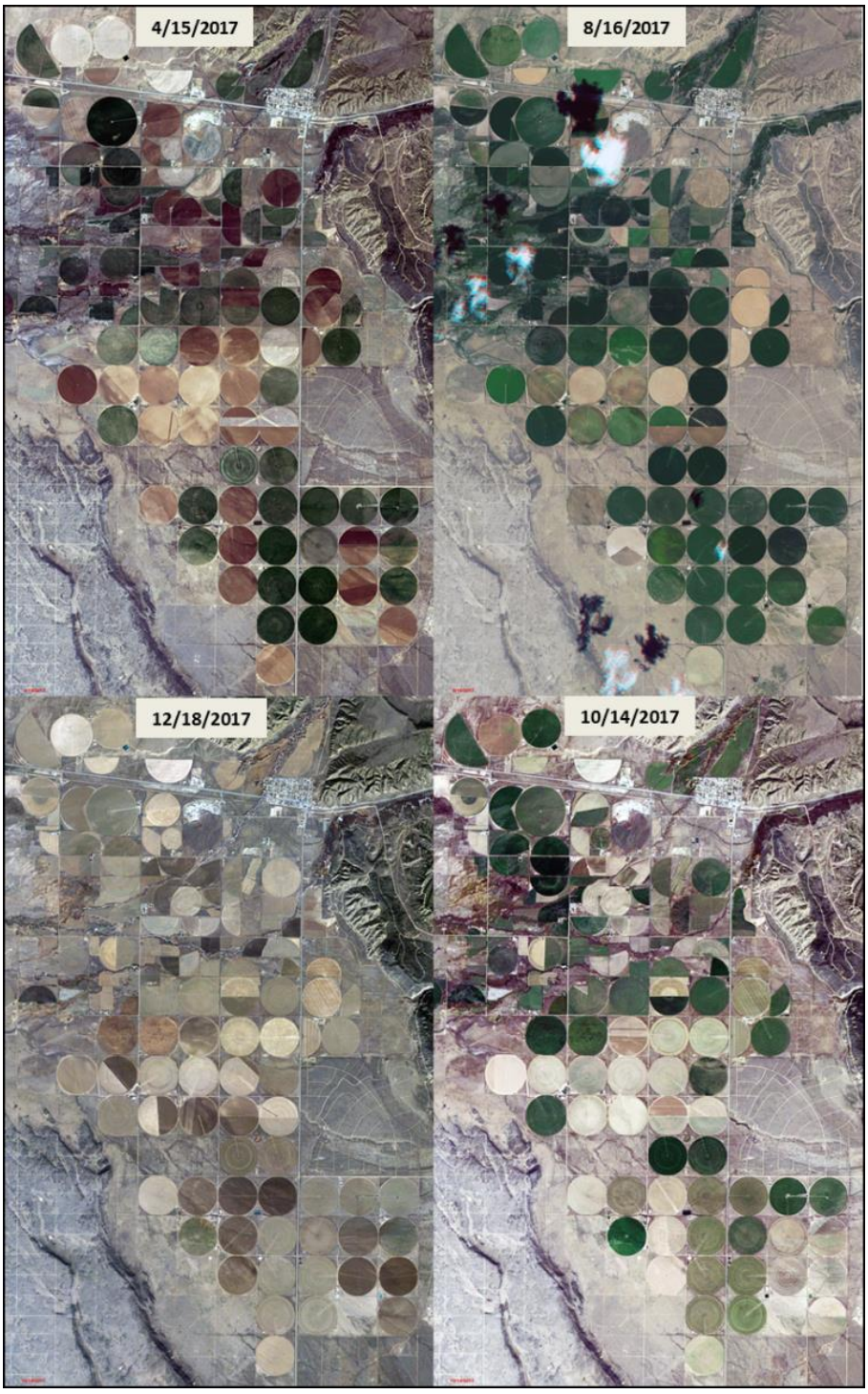


Figure 2.14: Farming in the San Luis Valley is only possible through irrigation. Aerial view of pivot irrigation circles in throughout and beyond the irrigation season, which typically runs April 1 through early October. In the winter and spring, many crop circles are left bare. Images from Apollo Mapping in Boulder, CO.

In some cases, long-range dust emissions originating from active sand dunes in the Sahara (Crouvi et al., 2012) and the Bodélé Depression (Washington et al., 2009), bring beneficial iron and phosphorus deposits to high-elevation areas where these minerals are scarce (Aciego et al., 2017). Other benefits include localized increases in precipitation. Mineral dust in the troposphere has been associated with increased cloud formation (Chaboureau et al., 2011, Wang et al., 2013), ice nucleation, and condensation (Weger et al., 2018, Bègue et al., 2015, Karydis et al., 2011). However, dust absorbs both solar and terrestrial radiation which it then scatters or re-emits (Muller et al., 2011, Köhler, 2017). Dust-on-snow events increase radiative forcing and hasten melting of mountain snowpack. Dust-on-snow events in the San Juan Mountains were found to decrease snow cover by 25—51 days in spring (Skiles, 2014). Much evidence exists linking the increase in dust-on-snow events in the San Juan to an increase in human land-use changes and disturbances to the soil (Painter et al., 2007, Skiles, 2014). Increased radiative forcing from dust emissions alters the timing and the amount of snowmelt, and this impacts surface water hydrographs as has been demonstrated with the Colorado River (Painter et al., 2017) and the Rio Grande. Changes to the timing and amount of snowmelt adversely affect mountain block recharge owing to frozen ground earlier in the spring and the diminished infiltration capacity from increased melt.

The San Luis Valley aquifers are replenished mainly through mountain block recharge as snow melts in the San Juan Mountains (Mayo et al., 2007, Wilson and Guan, 2004). Intensive farming practices leave bare soil exposed for many months and susceptible to dust storms, and these localized dust emissions, as well as dust emissions originating from the Colorado Plateau and elsewhere, have the potential to alter the way the snowmelt recharge in the San Juan Mountains (Mix et al., 2011, Painter et al., 2010) replenishes the San Luis Valley aquifers.

2.5 Gaps in the Literature and What This Thesis Contributes

Rain events—and precipitation chemistry—are an important component to understanding basin-specific hydrology and groundwater recharge. Yet, precipitation chemistry is rarely monitored in the detail it warrants. Precipitation chemistry monitoring in the literature, and long-term regional monitoring of air quality in the Rocky Mountain West are usually confined to mineral dust emission migration and particle size analysis (e.g. Reynolds, et al. 2016) or tracking basic chemical indicators of air pollution such as ammonia, nitrogen, sulfur, and mercury (as through the IMPROVE and NADP monitoring networks). More specific chemical analysis may be important in identifying recharge trends, changes, and future implications. Furthermore, while isotopic analysis of local precipitation in the Rocky Mountain West (Anderson, 2012, Anderson et al., 2016) offers region-specific local meteoric water lines (LMWL), none has been developed for the San Luis Valley, and this limits precision of water isotope interpretation.

While several hydrological studies conducted in the San Luis Valley have examined surface and groundwater chemistry (Davis Engineering Service et al., 2012), and the isotopic composition of surface water and groundwater isotopes (Mayo et al., 2007, Rupert and Plummer, 2004), no study has examined the area's precipitation isotope signatures (which differ from Rocky Mountain-wide snow signatures at high elevation) and therefore these studies have not analyzed nor interpreted groundwater chemistry with a full knowledge of recharge input. Examining the isotope values of local meteoric waters and precipitation chemistry is an important component to any comprehensive study of groundwater recharge (Edmunds, 1987a, Clark and Fritz, 1997, Kendall and McDonnell, 1998). Without reference to local isotopic signatures, it may be difficult to interpret groundwater isotopes correctly.

The contribution of this doctoral study is to establish the first LMWLs for this region of the southern Rocky Mountains (Lanzoni, 2017) at high elevation and on the valley floor. These isotope data may be used alongside precipitation chemistry to identify the sources of recharge and infer how these sources, rates, and mechanisms may be changing over time (Lanzoni and Darling, 2019).

The term “phreatophyte” was put into print in 1927, and early on, the connection between phreatophyte plants and the shallow water table was established. Phreatophytes may be used as a lens through which to view groundwater fluctuations, and the ability to use xylem water to isotopically differentiate near-surface and groundwater utilization is well established. The San Luis Valley has experienced an unprecedented lowering of the unconfined aquifer, and some areas of greatest drawdown challenge the extent of phreatophyte taproots. This thesis will investigate whether the native shrub vegetation still accesses groundwater despite significant drawdown.

This DPhil thesis employs traditional and non-traditional hydrological techniques to follow water in the San Luis Valley watershed as it moves through its air-surface-ground water cycle, and by placing hydrological insight within a human context, offers suggestions for the future stewardship of these significant groundwater resources.

Chapter 3: Thesis Methods

3.1 Thesis Aims Revisited

The overall aim of this study is to better understand precipitation events and recharge processes in the San Luis Valley. To this end, and based on gaps in the literature identified in Chapter 2, the primary study objectives throughout this study are to:

- Characterize the chemical and isotopic signature of precipitation in the San Luis Valley and, using ^{18}O and ^{2}H, develop a local meteoric water line.
- Determine different pathways and rates of recharge in the San Luis Valley using chemical and isotopic tracers, hydrographs, and groundwater fluctuations.
- Analyze stem water samples from the valley's two dominant facultative phreatophyte shrubs at three different study plots with increasing depth to groundwater in order to establish seasonal variation in their water use strategies.
- Apply time-lapse, near-surface electrical resistivity in order to characterize soil moisture movement between vegetated and non-vegetated areas under different wetting and drying conditions.
- Discuss, consider, and recommend water management strategies for the San Luis Valley within the context of this study's findings.

3.2 Methods Overview

This body of work is based primarily upon primary collection and analysis of water samples (year-round precipitation, groundwater, surface water, soil and plant water), analysis of vegetation plots, soil properties, rainfall amount, water elevation, and electrical resistivity. These data are augmented by

secondary data sets that include historical groundwater levels and precipitation records, past water chemistry results, past electrical resistivity surveys and GIS data layers, both ground-based and aerial. These quantitative data are complemented by a small amount of qualitative analyses generated by conducting informal interviews with water managers at the federal, state, and community levels, and attending water roundtable and groundwater district meetings in order to understand the wider context of water law, policy, and management in southern Colorado. Table 3.1 provides an overview of all of the primary data used throughout this thesis. Table 3.2 gives an overview of the secondary data used in this thesis, and Table 3.3 details the qualitative data used to help inform and provide context for this thesis.

Chapters 4—7 rest on primary data collection and physical analysis. From 2014 through 2018 I collected a total of 413 water samples from key source locations and groundwater depths in the San Luis Valley in southern Colorado (Fig. 2.1) across every season. This includes 121 precipitation (rain, hail, and snow), 31 surface (lakes, ponds, river, creeks), 109 groundwater (confined and unconfined), and 104 plant and soil water samples. Table 3.1 breaks down the number of samples by type and analysis employed per chapter. I conducted the physical analysis of samples in my field laboratory in Alamosa, Colorado, at a stable isotope laboratory in Laramie, Wyoming, and in the Earth Sciences and the Geography departments at the University of Oxford, UK.

Chapter 4 relies on 121 precipitation samples processed for basic chemistry, anion/cation, and heavy metal/trace element analysis. A subset of 55 precipitation samples, chosen to represent all seasons, and selected for least exposure to air, were analyzed for δD, $\delta^{18}O$ to establish local meteoric water lines and to provide data on baseline meteoric input. During April 2016, an unusual blizzard event moved into the San Luis Valley, and these blizzard samples were also collected and analyzed. Chapter 5 relies on 140 surface and groundwater samples analyzed for basic chemistry, anion/cation, and heavy metals/trace elements. 109 of these were analyzed on a Picarro cavity ring-down spectroscope (CRDS) for δD, $\delta^{18}O$ to establish water isotope signatures and identify sources of recharge. Chapter 6 relies on 83 cryogenically extracted plant and soil water samples analyzed on a temperature conversion/element analyzer, isotope-ratio mass

spectrometer (TC/EA IRMS) for δD and $\delta^{18}O$ owing to the preferred ability of the TC/EA IRMS to isolate isotopes from organic matter following cryogenic distillation. This analysis rested on a cooperative agreement with the University of Wyoming's Stable Isotope Facility where I worked. For chapter 7, soil properties were analyzed for particle size, and extracted moisture for chemical analysis (pH, anion/cation). Soil moisture contents were assessed both by measuring volumetric moisture content and through relative electrical resistivity tomography (ERT) readings (using GeoTom equipment) along transects of vegetated and non-vegetated areas. These measurements together facilitate an assessment of moisture movement in the soil of the shallow unsaturated zone layer.

Table 3.1: Overview of primary data collected and analyzed for Chapters 4-7.

Chapter 4	**Sample Type**	**N**	**Analysis**	**N**	**Analysis**
Precipitation Chemistry and Isotopic Baselines of Meteoric Waters	SLV Rain	33	δ^2H, $\delta^{18}O$	97	basic chemistry, anion/cation, ICP-MS
	SLV Snow	15	δ^2H, $\delta^{18}O$	17	basic chemistry, anion/cation, ICP-MS
	Valley floor precipitation	48	δ^2H, $\delta^{18}O$	114	basic chemistry, anion/cation, ICP-MS
	High elevation snow	7	δ^2H, $\delta^{18}O$	7	basic chemistry, anion/cation, ICP-MS
	Total snow	22	δ^2H, $\delta^{18}O$	24	basic chemistry, anion/cation, ICP-MS
	Total Precipitation	**55**	**δ^2H, $\delta^{18}O$**	**121**	**basic chemistry, anion/cation, ICP-MS**
Chapter 5	**Sample Type**	**N**	**Analysis**	**N**	**Analysis**
Pathways and Rates of Recharge	Surface Water	26	δ^2H, $\delta^{18}O$	31	basic chemistry, anion/cation, AAS, ICP-MS
	Unconfined GW	23	δ^2H, $\delta^{18}O$	40	basic chemistry, anion/cation, AAS, ICP-MS
	Upper confined GW	49	δ^2H, $\delta^{18}O$	58	basic chemistry, anion/cation, AAS, ICP-MS
	Active lower confined GW	11	δ^2H, $\delta^{18}O$	11	basic chemistry, anion/cation, AAS, ICP-MS
	Confined GW (total)	60	δ^2H, $\delta^{18}O$	69	basic chemistry, anion/cation, AAS, ICP-MS
	Artesian Sump Water	26	δ^2H, $\delta^{18}O$	26	basic chemistry, anion/cation, AAS, ICP-MS
	Total GW	83	δ^2H, $\delta^{18}O$	109	basic chemistry, anion/cation, AAS, ICP-MS
	Total Surface and GW	**109**	**δ^2H, $\delta^{18}O$**	**140**	**basic chemistry, anion/cation, AAS, ICP-MS**
Chapter 6	**Sample Type**	**N**	**Analysis**		
Phreatophyte Shrubs as Indicators of Groundwater	Xylem Water	76	cryogenic extraction, δ^2H, $\delta^{18}O$ (IRMS)		
	Soil Water	7	cryogenic extraction, δ^2H, $\delta^{18}O$ (IRMS)		
	GW Reference	12	δ^2H, $\delta^{18}O$ (IRMS)		
	Precipitation Reference	48	δ^2H, $\delta^{18}O$ (IRMS)		
	Total Plant and Soil Samples	**83**	**cryogenic extraction, δ^2H, $\delta^{18}O$ (IRMS)**		
Chapter 7	**Sample Type**	**N**	**Analysis**		
Moisture Movement in the Soil	Soil Profile	15	basic chemistry, anion/cation, particle size analysis		
	Soil Sample	6	basic chemistry, anion/cation		
	Soil Transect	> 30	electrical resistivity, inversion		
	Total Soil Samples/Readings	**> 51**	**chemistry, particle size, resistivity**		

Table 3.2: Overview of secondary data used in thesis.

Chapter	Data Type	Source	Use
4	GMWL	IAEA GNIP (Craig, 1961)	Reference and comparisons
4	Long-term precipitation record	NASA's Giovanni-derived based on Alamosa weather station records	Seasonal precipitation over time
5	LiDAR	NPS	Visualization of SLV topography
5	Well screen depths	BLM	Well depths in relation to aquifer boundary layers
5	Well logs, lithology, depth to water	Database of registered wells in the SLV	Analysis of specific areas
5	Water chemistry	BLM	water chemistry seasonal variations
5	Well logs, depth to water, lithology	NPS	Analysis of specific areas
5	Well logs, depth to water, lithology	BOR	Analysis of specific areas
6	Well logs	FWS	Historical data
6	Well logs	NPS	Historical data
6	Well logs	BOR	Historical data
6	Plant species identification	FWS	Assistance with plant IDs at study sites
7	Resistivity ground survey	USGS	Interpreted aquifer layers
7	Airborne resistivity data	USGS	Background
8	Water chemistry	EPA	Context and discussion

Table 3.3: Overview of qualitative data used to help inform context and discussion.

Data Type	Source	Use
Semi-structured interviews	managers as well as those with a long history in the SLV	Context and discussion
Public meetings	Water user association meetings, Rio Grande Roundtable meetings, Rio Grande Conservation	Context and discussion
Closed meetings	Inter-agency meetings on managing natural resources on public lands	Context and discussion
Alamosa water treatment plant tour	City of Alamosa	Context and discussion
Potato farm tour	Private owner	Context and discussion
Closed basin project tour	USBR	Context and discussion

The discussion of the scientific results in a wider context (Chapter 8) relies on the primary data collected and presented in Chapters 4—7. This chapter is augmented by secondary data sets, by additional sampling at the margins of the San Luis Valley, and through analysis of pivot spray samples from the valley's

agricultural water users. The discussion in this chapter is, in some part, informed by qualitative analysis of notes from 14 water conservation district roundtable and district groundwater meetings, all of which were open to the public and for which there are meeting agendas and minutes.

3.3 Methods Testing and Validation

Several experiments were conducted at an early stage of the thesis to verify the methods used in this thesis. For example, the method of collection for precipitation was investigated to determine the influence of dry deposition of Cl at/near the surface, which disrupts the assumption of meteoric source with chloride mass balance (e.g. Scanlon, 2006) and the method of sample filtration was investigated by comparing results from various filter pore sizes. Table 3.4 outlines these experiments, the method they investigate, and the thesis chapters that utilize these methods. Routine validation of analytical equipment was used to check pH values of rainwater, ^{2}H and ^{18}O isotope values from IRMS and Picarro (CRDS) machine outputs, Dionex ion calibrations and sample ion balances, ICP-MS values, and cryogenic extraction efficiency (results always > 99% extraction) of plant samples before isotope analysis.

Table 3.4: Methods Testing

Chapter Used	Method Tested	N	Analysis
4	Cl deposition wrt CMB	24	anion/cation, ICP-MS comparison between open and closed rain collection
4	pH testing	97	multiple pH meter use, calibration testing
4, 5, 6	filtration membrane pore size	18	ion, ICP-MS comparison of 0.8, 0.45, 0.2 µm filters
4, 5	anion and cation mEq balance	12	examination of unknown Dionex peaks
4, 5	anion peak match	83	element-specific AAS
6	soil water elution time	4	anion/cation comparison between timed intervals
4, 5, 6	IRMS and Picarro corrections	10	repeats and known standards (blind)
6	cryogenic extraction efficiency	76	oven dry weight comparison
7	soil water visibility on GeoTom	12	baseline artificial wetting experiments

Because precipitation chemistry is an important cornerstone of this research, and because it is not routine to analyze and report basic chemistry of rainfall, several steps were taken and tested to ensure accurate analysis of the water samples. First, an experiment was conducted to test if there is any discernable difference in basic chemistry, isotope values, and trace metals found in water samples passed through a 0.8 µm, 0.45 µm, and 0.2 µm filter. While 0.2 µm is the standard level of filtration applied in this thesis (it

is acknowledged that more stringent filtration is used for ^{15}N analysis, which was considered but not utilized for this thesis), it was important to show that larger, complex molecules weren't excluded in the 0.2μm filtered samples. For the analysis of heavy and trace metals, ions, and isotope ratios, 0.2 μm filters were determined to be the appropriate filtration with no discernable difference between 0.8 μm, 0.45 μm, and 0.2 μm filters.

The next test was whether there was a difference in chloride concentrations from collecting precipitation in an "open" versus a "closed" system, because the chloride mass balance (CMB) approach to estimate recharge is sensitive to variations in this input, and the inclusion of dry deposition distorts the meteoric input of chloride, on which the CMB approach is based (e.g. Scanlon, 2006*).* In addition, animal and plant matter can fall into the container, and may contain a source of chloride and other anions and cations. Throughout the 2015 spring, summer, and autumn field season, 39 rain samples collected in the "closed" system were compared to 17 rain samples collected in the "open" rain gauge system (sample numbers are determined by rain events registering > 0.2 mm for analysis).

Three large, sterilized glass bowls were placed outside on a raised surface three feet from the ground alongside a National Weather Service-issued plastic rain gauge with mm markings secured at the same height above the ground. Beginning in 2015, the glass bowls were placed outside just before or at the start of a rain event. They were taken into an on-site laboratory using plastic gloves immediately after the rain shower ended. Samples were filtered to 0.2 μm, aliquoted into 50 ml sterile containers, labelled, and frozen, ready for analysis on the Dionex (for ions), the ICP-MS (for heavy metals and trace elements), and the Picarro or IRMS (for δD, $\delta^{18}O$). The remaining water was tested for temperature, pH, EC, TDS. In between precipitation events the bowls were washed with distilled water, allowed to dry, and kept covered with a layer of plastic wrap in the lab until the next precipitation event (which should minimize or eliminate airborne deposition to which the open rain gauge was exposed). Samples from the open rain gauge were collected and stored in a similar fashion, but the rain gauge was not washed and was left outside to accumulate any dust deposition.

On a handful of instances over the sampling periods of 2015 and 2016, both the "closed" and the "open" rain collection systems were exposed to small leaf fragments, insects, and bird droppings. Trace amounts of bromide and nitrite were detected in only one open rain gauge sample. Nitrate and sulphate were detected repeatedly, sometimes in large concentrations, in open and closed rain samples—it is thought this entered through dissolved, wet deposition and not through contaminant debris while sampling. The most significant factor influencing whether and to what extent a sample was exposed to contaminants was the length of time the collection device was allowed to sit between collections. During frequent or long rain events, the open rain gauge was naturally flushed out as it was emptied between rain events.

The arithmetic mean for Cl concentrations from all 2015 open rain gauge samples is 0.59 mg/L, and the weighted mean Cl concentration (based on rainfall amount per event) is 0.41 mg/L. There was one outlier with respect to Cl concentration from the open rain gauge samples, and compared to the "closed" system of collection for that rain event. Without this outlier the arithmetic mean is 0.44 mg/L and weighted mean is 0.35mg/L. Chloride concentrations are slightly lower in the closed system of sampling, with an arithmetic mean of 0.44 mg/L and weighted mean of 0.26 mg/L. Figure 3.1 shows that the closed rain gauge method of sampling also contains one outlier (3.62 mg/l Cl), which if removed, reduces the weighted mean to 0.23 mg/L. Because there was no strong reason to omit this single datum point (as opposed to another), it was retained in the chloride mass balance calculation. CMB recharge estimation is based on 39 closed collection rain samples from 2015, because I achieved the lowest Cl calibration and best LOD for this analysis (LOD = 0.0702 and LOQ = 0.2340 with an R^2 of 0.9997). While the additional 2016 rain season brought the rain sample Cl analysis to N=73, the 2016 sample results were not used for CMB input or for ion chemistry analysis because the older Dionex equipment (since replaced) was not reliable during the period of analysis (summer 2017), with a poor limit of quantification (LOQ) for Cl of 1 mg/L.

The chloride concentrations found in San Luis Valley rainfall are not unusual for an inland dryland area that receives 200 mm/yr. Stone and Edmunds (2016), in reviewing literature on the use of chloride as a conservative tracer in the unsaturated zone, found that after a distance of 290 km inland from the coast and in areas with annual precipitation comparable to the 200 mm/y in the San Luis Valley, rainfall chloride concentrations fall between 0.2 and 0.3 mg/L (Figure 3.2).

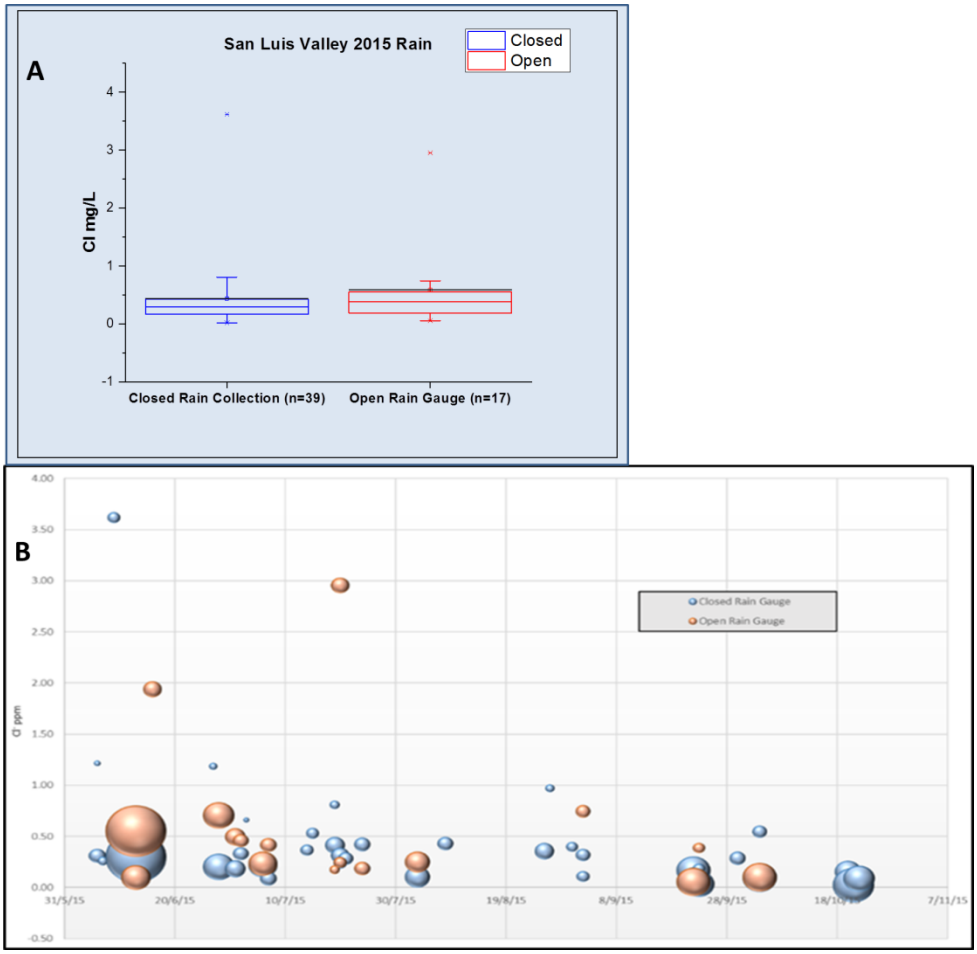


Figure 3.1: Cl concentrations in 2015 rainfall on the Alamosa Wildlife Refuge were analyzed, and rain collection methods were compared. A) The open and closed collection methods are compared, and B) the high chloride concentration outliers are found in small rain events. Circle sizes correspond to size of the rain event, which ranged from 0.2 to 18 mm in 2015. Note that rain events < 0.2 mm occur in the San Luis Valley, but this amount does not register on a tipping rain bucket and does not produce a volume sufficient for chemistry analysis.

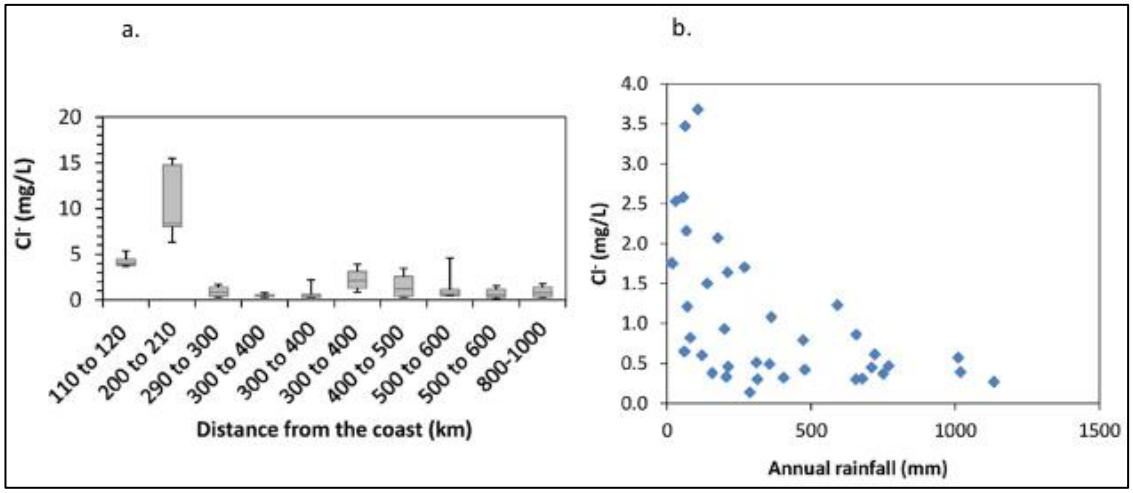


Figure 3.2: Cl concentrations in Australian rainfall (a) presented by distance from the coast and (b) plotted against annual rainfall totals (from Stone and Edmunds, 2016 using data from Crosbie et al. (2012))

3.4 Methods Details

The following is a description of the methods used throughout this entire thesis. An explanation of each chapter's experimental design and a summary review of methods and samples utilized will be presented at the start of each data-rich chapter that follows.

3.4.1 Field Sampling and In Situ Measurements

Field sampling took place throughout the San Luis Valley, but most of the groundwater sampled came from wells in the closed basin region and in the eastern half of the valley. Access to the wells for sampling was granted through federal agency permits and permissions. Figure 3.3 shows the locations of water sampling points overall, with surface water samples marked in green and groundwater samples marked in blue. The locations of three vegetation study sites used in Chapter 6 are marked on the map as white stars. Maps detailing precipitation sampling points and specific vegetation study locations are provided at the start of the appropriate chapters.

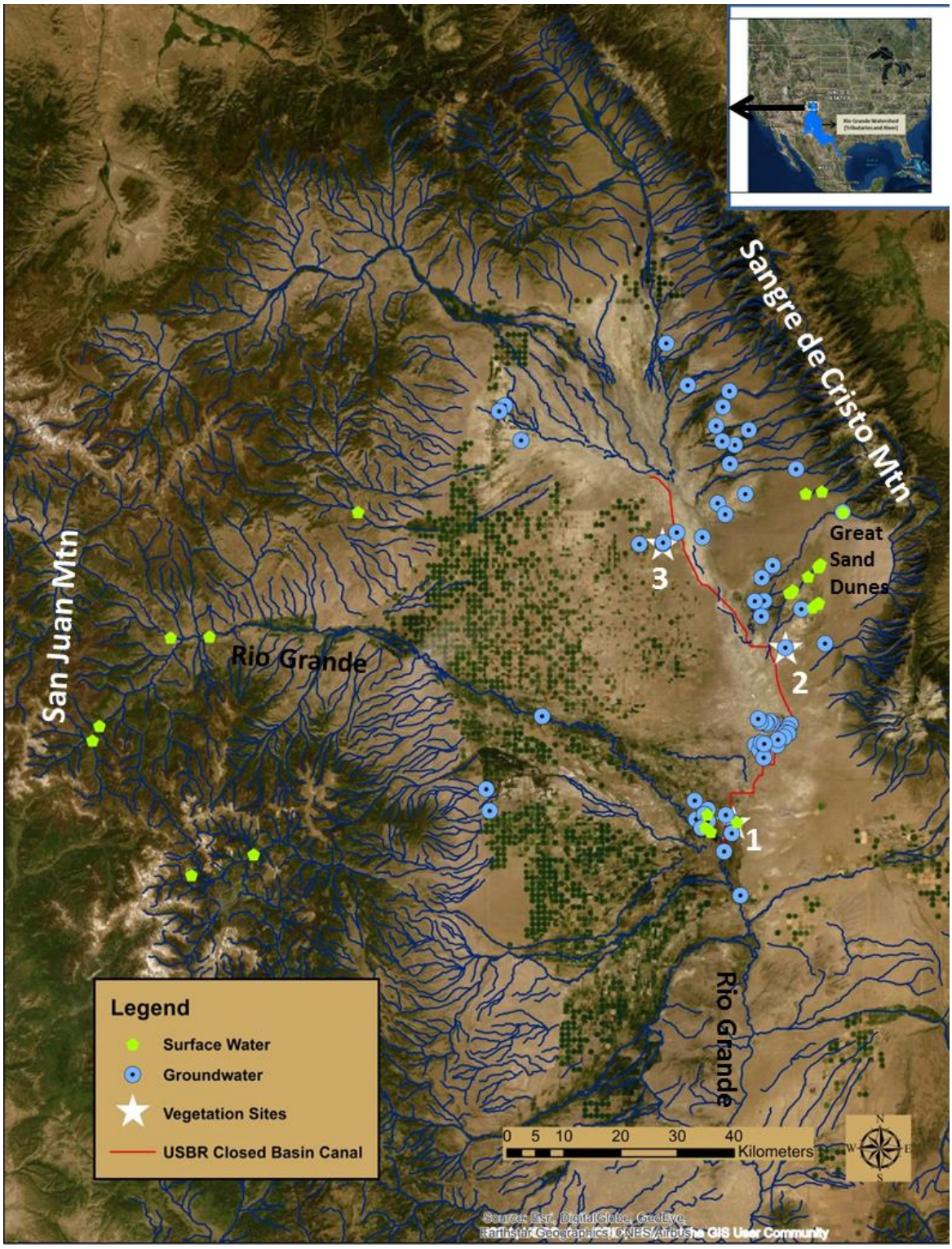


Figure 3.3: Map of San Luis Valley detailing surface water (green) and groundwater (blue) sampling locations. Surface water was sampled from the San Juan Mountains, the Sangre de Cristo Mountains, and the valley floor. The locations of vegetation sites 1, 2, 3 (Chapter 6) are shown with white stars. The extent of the Closed Basin Canal, which transfers groundwater to the Rio Grande, is shown in red for reference.

Groundwater samples were collected from wells ranging in depth from over 600 m in the active lower confined aquifer (Mayo and Christiansen, 1994) to 4 m in the unconfined aquifer. Confined aquifer wells with artesian flow were sampled directly. Unconfined aquifer wells and confined aquifer wells with lower hydraulic head were sampled using a generator-driven pump carried on the back of a pickup truck and attached to a sterile plastic sampling hose. The shallowest unconfined wells were sampled using a suction pump attached to a sterile plastic sampling hose. The wells were pumped for 20 minutes before sampling in order to sufficiently purge the static water volume sitting within the borehole, and sample from the aquifer (Hem, 1985, Hiscock, 2005). In most cases, a water table drawdown and recovery were recorded.



Figure 3.4: Wells from the unconfined aquifer were sampled using a generator-driven pump and a sterile tube for chemical sampling.

In situ measurements of pH, temperature, EC and TDS, were taken on nearly all groundwater, surface water, and rain samples. Results for rain sample pH in 2015 were compared, and averaged, from two different, calibrated Hanna pH/conductivity meters (HI991300). Due to consistently close results between

the two instruments, this approach was deemed unnecessary for the 2016 pH rain sampling. HCO_3^- measurements were taken after collection using a Hach digital titrator for measuring hydroxide alkalinity, calcium alkalinity, and total bicarbonate.

All samples were collected in sterile 50 ml containers, filtered in 0.2 µm, and transferred to new sterile 50 ml containers. These were kept on ice and then frozen until analysis in Wyoming for isotopes or analysis in Oxford for chemistry. Standard *in situ* chemical measurements (pH, EC, TDS, temp) were also taken at each well.

Snow samples were collected for both chemical and isotopic analysis. High-elevation snow sampling was conducted at the summit of Wolf Creek Pass (sample point 3 in Figure 4.1) during or immediately after a significant snow event, and isotope signatures of each snow event are an average of 6 and 12 samples of the fresh snow layer. Snow samples from the valley floor were collected each morning before 8am and/or near the conclusion of a snow storm from the 'closed' rain bowl collector. Snow samples for isotopic analysis were kept frozen with dry ice and in a freezer until they were ready for analysis at the Stable Isotope Facility at the University of Wyoming where 2.5 ml of each newly thawed and filtered (0.2 µm) sample was immediately transferred to an air-free vial for isotopic analysis. Samples for chemistry analysis were allowed to melt after collection, filtered to 0.2 µm, transferred into sterile 50 ml containers, and stored in a freezer before being transported to Oxford, where they are kept at 5^{o}C while awaiting anion and cation analysis via ion chromatography using the Dionex in the School of Geography and the Environment.

Plant stem samples (~ 5 cm in length) used in Chapter 6 were taken from marked *E. nauseosa* and *S. vermiculatus* shrubs within fenced study plot sites between the hours of 3-5 am to reduce the chances of stomatal opening and gas exchange (Kray et al., 2012). Samples were collected in replicates of three at each plant on July 15-16, 2015, October 15-16, 2015, April 15-17, 2015, and July 15-16, 2016. Stem samples were labelled in the field and immediately dropped into a 10 L canister of liquid nitrogen. These

samples were then driven to the University of Wyoming's Stable Isotope Facility and processed through the cryogenic extraction line.

The resistivity measurements of soil moisture content along transects (for Chapter 7) were measured using a GeoTom electrical resistivity tomography (ERT) unit connected to a cable transect using 25 metal electrodes with 0.2 m spacing along a vegetated and un-vegetated pathway (Figure 3.5). Dipole-dipole and Wenner arrays were used for gathering resistivity values and processed through inversion software, Res2Dinv, for 2-D relative resistivity displays. Transects placed along a semi-permanent pathway crossing vegetated and un-vegetated areas at each fenced study plot were exposed to artificial wetting experiments to establish baseline, time-lapse readings of near-surface resistivity and inferred water movement through the soil to a depth < 0.7 m. Between resistivity measurements, periodic coupling measurements were made to ensure all electrodes had proper contact and functioned correctly. Different array methods and calculation requirements produced different levels of uncertainty for each inverted resistivity output within a 2-D diagram, and any outliers had to be handled differently based on batch processing or individual processing within the inversion software. Processed resistivity values are interpreted as relative values, not absolute soil water concentrations.

A soil profile pit was dug > 0.5m deep at Site 1 following the electrical resistivity experiments. A measuring tape was used to mark depth, and a sterile laboratory spatula was used to extract soil samples at 5 cm increments that were weighed, bagged, and transported to Oxford for analysis. Soil water chemistry was determined through an elution method using deionized water analysed on a Dionex ion chromatography instrument. Particle size analysis was done using a wet method developed for the department's Malvern Mastersizer laser analyser.



Figure 3.5: ERT unit connected to a cable transect with metal electrodes in the San Luis Valley, CO. Artificial wetting experiments (shown on the right) were used to verify water movement can be tracked through time-lapse resistivity readings.

3.4.2 Laboratory Analysis

Isotopic analysis

This thesis relies on data generated from 247 water samples analysed for $\delta^{2}H$ and $\delta^{18}O$ through work conducted as a visiting researcher at the University of Wyoming's Stable Isotope Laboratory in the USA. 143 of these plant and soil water as well as precipitation and groundwater references were run on a temperature conversion elemental analyzer (TC/EA) connected to continuous flow isotope ratio mass spectrometry (IRMS), because this is a robust way to analyse samples potentially contaminated by carryover from the plant and soil water cryogenic extraction process (shown in Figure 3.6). After extraction, all stem samples were placed in an oven overnight and recorded weights showed > 99.8% extraction of fluid. 104 of these water samples (with a few precipitation repeats which were analysed on both the Picarro and IRMS), were run on a Picarro L2130-I cavity ring-down spectroscope (CRDS).

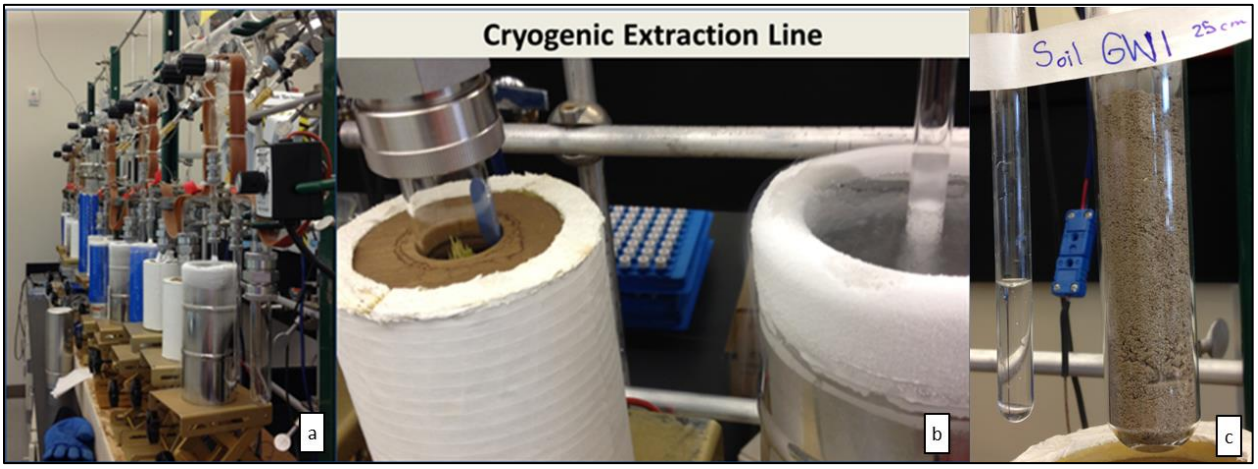


Figure 3.6: (a) Cryogenic distillation line at University of Wyoming (b) Plant stems stored in liquid nitrogen are placed under vacuum pressure before being lowered into a heating block where water vapour is pulled into a liquid nitrogen cooled glass tube (c) Despite no rain for the month preceding sampling, soil from 25-cm rooting depth produces ample distilled water for analysis.

Stable isotope analysis from plant and soil water samples through TC/EA IRMS operates on the following premise. The oxygen and hydrogen containing compounds that occur in both organic (e.g. plant stems) and inorganic (e.g. soil) systems have $\delta^{18}O$ and $\delta^{2}H$ ratios which can be determined by the analyzing the CO and H_2 generated by the pyrolysis of the material via temperature conversion elemental analysis (TC/EA). In this method, solid samples are placed into silver capsules and then dropped into a TC/EA generating the product gases. These gases (CO, H_2) are separated using a gas chromatograph, sent to an open split interface and then to the IRMS for analysis (TC/EA-IRMS on Thermo Scientific Delta V).

All isotope samples were run in triple injection mode; the last two values were averaged to produce the measured value of each sample. Four known, laboratory water references were run alongside the samples in each run as a quality control measure and used to correct for instrument drift. The first three references were generated by the University of Wyoming's Stable Isotope Facility—Evian water, UWSIF 302, UWSIF303, and the fourth I generated and incorporated into the run as a blind test (position in the run not disclosed to the Stable Isotope Facility). Quality assessment was conducted based on the standard

uncertainty of the known value of UWSIF reference materials, with an upper cut off of 0.3‰ for oxygen and 2.5‰ for hydrogen. No reanalysis was required. The accuracy and precision of isotope values analysed on the Picarro L2130-I Cavity Ring Down Spectroscope (CRDS) is greater than those run on the Thermo Scientific IRMS. The Picarro can achieve precision on the order of ±0.05 ‰ for $\delta^{18}O$ and ±0.3 ‰ for $\delta^{2}H$. The isotopic composition of oxygen is reported in per mil (‰) relative to VSMOW (Vienna Standard Mean Ocean Water) on a scale such that VSMOW and SLAP (Standard Light Antarctic Precipitation) water, respectively, are 0‰ and -55.5‰. The isotopic composition for hydrogen is reported in per mil relative to VSMOW water on a scale such that VSMOW and SLAP water, respectively, are 0‰ and -42.8‰ (Groning et al., 2006).

Anion and cation runs were performed in Oxford on a Dionex ion chromatography machine (DX500) in the School of Geography and the Environment using separate low concentration and standard concentration calibrations, with emphasis placed on the low concentration Cl^- calibrations for improved LOD and LOQ. Samples on the Dionex were run in double and triple injection mode between washes with deionized water. Additional measurements for Fe, Se, and Si were run on an Atomic Absorption Spectrometer (AAS), and the machine was re-calibrated after every ten water samples. These analyses were important, especially the Si analysis, because this is found in much of the groundwater across the SLV.

Inductively coupled plasma mass spectrometry (ICP-MS) on a Perkin Elmer NexION 350D ICP-MS in the Earth Sciences department was used to analyse water samples for heavy metals and trace elements. This was done in more than one batch, and the accuracy was at least 0.18% V, 0.67% Cr, 2.02% Mn, 0.51% Co, 0.43% Ni, 0.34% Cu, 0.56% Zn, 1.77% As, 1.04% Mo, 0.58% Ru, 0.63% Rh, 0.51% Pb, 0.33% Cd, 1.72% Tl, 1.78% Th, 1.16% U, 0.95% Hf, 0.67% W, 0.31% Re, 0.24% Hg using both high and low calibrations depending on water type. Dilutions were made using a 2% HNO_3 solution, prepared using in-house distilled nitric acid and 18.2 Mohm DI water. All blanks, standards and samples were also

spiked with 1ng/g In and Bi, so any general instrument drift could be normalised. These data are summarized with the method detection limits in Appendix 5.

3.4.3 Data Analysis and Visualization

GPS waypoints from a Garmin etrex were uploaded using ArcGIS 10.6.1 and visualized in ArcMap. Basemaps and riparian layers were taken from the ESRI database. Additional GIS monitoring-well waypoints and raster data sets were provided by the National Park Service and Colorado Division of Water Resources. LiDAR data for the San Luis Valley with 1 m resolution and 15 cm vertical accuracy was used to improve topography displays, and seismic data were used to display a transect of subsurface structures. Resistivity data were analysed and displayed using 2-D inversion software Res2Dinv (Loke, 2000, Cutler and Eklund, 2010).

Water geochemistry modelling was displayed using free versions of SigmaPlot and Origin software, though for inclusion of Si, which is a significant component of the San Luis Valley groundwater, Diagrammes software developed by Roland Simler at the Laboratoire d'Hydrologie d'Avignon in France was used. This free software produces data outputs compatible with USGS PHREEQC (version 3.3.10 and later) and Netpath XL (version 1.5.0 and later). Soil particle distribution data from the Malvern laser granulometer were processed using the Gradistat v. 8.0 program developed by Simon Blott using the Folk and Ward (1957) method. Analyses and visualization of modelled rainfall data by season presented in Chapter 4 were produced using the Giovanni online data system, developed and maintained by the NASA GES DISC (Acker and Leptoukh, 2007).

Secondary data including well logs, pump tests, and lithology reports were available for a series of wells across the San Luis Valley from the U. S. Bureau of Reclamation (USBR or BoR), Bureau of Land Management (BLM) and United States Geological Survey (USGS), as well as through the Colorado Division of Water Resources. Historical well log data (fluctuations, lithology, screening depths) are presented in Chapter 5 in order to discuss pathways and rates of recharge as well as in Chapter 6 to

discuss seasonal water fluctuations and long-term drawdown at selected study sites. Historical precipitation data were available from snow telemetry (SNOTEL) field stations as well as through rain gauges operated by National Park Service (NPS) and a local airport. Two Texas Electronics 0.254 mm-switch tipping rain buckets attached to two Campbell Scientific CR510 data loggers were set up for the duration of this study, and though they proved useful for limited, site-specific rainfall data, long-term analysis relies on the historical, secondary data.

3.4.4 Recharge Calculations

Chloride mass balance (CMB) is a method for estimating a conservative, long-term rate of recharge. The method used herein is expressed through equation 1:

$$Rd = P(Cp/Cs) \qquad \text{(Eq. 1)}$$

where Rd is diffuse recharge, P is the mean annual precipitation, Cp is the weighted Cl concentration of rainfall in mg/l, and Cs is the mean Cl concentration in groundwater samples.

This method is most often used on soil profiles in areas with deep unsaturated zones, but it is also used for estimating recharge of groundwater. This method has been used successfully in many dry parts across the world (Stone and Edmunds, 2016) including Northern Africa (Edmunds, 1987b, Gaye, 1996, Goni, 2001), Southern Africa (Stone, 2012, Sami, 1996), India (Rohde, 2009), China (Gates et al., 2008) and the American Southwest (Hogan, 2004, Scanlon et al., 2006, Walvoord et al., 2002). This method assumes a relatively homogenous, unconsolidated sediment, of the texture that piston-style flow, as opposed to finger-flow, is the dominant mode of water movement. It is a reliable method in porous lithologies where recharge is low. Therefore, this method is deemed more suitable for the Closed Basin region and the area in and around Great Sand Dunes National Park. It is less suited for the southern wetland areas with

significant, managed recharge, because the unsaturated zone is thin, to non-existent and the input of water is from managed recharge and not meteoric precipitation.

The CMB was complemented by the analysis of: (i) other tracers (anion/cation analysis and δ^2H, $\delta^{18}O$ in precipitation and groundwater) (ii) detection of silicate weathering or Ca^{2+}, HCO_3^- water types (which give information about water-rock interaction types and durations), (iii) physical fluctuations in historical groundwater data collected across the San Luis Valley and the Closed Basin region in particular. Together this facilitates an investigation of pathways and rates of recharge in the San Luis Valley.

3.5 Limitations of the Techniques

While nearly every single rain event during the 2015 and 2016 summers and falls were sampled, there were a few rain events that were missed due to physical absence. Most notably, during the first half of May 2016, there was a downpour that lasted several days. The amounts were recorded automatically, but no chemistry or isotope sample was taken during this time. In some instances, rainfall amounts were too low for measurements. Rainfall events of < 0.2 mm might be sufficient for anion analysis but no pH measurements could be taken.

Issues arose on the Dionex around low Cl^- confidence and Ca^{2+} carryover. The initial rain and water sample results collected in the summer 2014 and run over the winter of 2014/2015 had to be discarded due to a poor LOD of 1 mg/L and LOQ of 3 mg/L for Cl^-. During this time, construction work was occurring just outside the School of Geography and the Environment laboratory, and the drilling caused detectable shaking in the Dionex (even after anti-vibration mats were placed underneath), and this resulted in poor baselines between anion peaks. Water samples analysed over the winter and spring of 2015/2016 produced much better results, specifically for Cl^-, with an LOQ better than 0.2 mg/L. Unfortunately further Dionex issues arose in the summer of 2017 during analysis of the 2016 precipitation

samples and a select group of groundwater samples. The Dionex malfunctioned, beyond repair, near the end of the sample run, and this meant the calibration couldn't be improved beyond the 1 mg/L LOQ. Since an improved ion analysis of the select groundwater samples was more important for this thesis, the groundwater samples were re-run on the new Dionex machine in the spring of 2018.

With regard to cation analysis on the old Dionex, calcium carryover is thought to originate from highly alkaline source DI water as well as high concentrations of Ca^{2+} in water samples that aren't completely flushing out of the Dionex lines during washes. Running cation eluent (methane sulfonic acid) as a cleaning agent between every few water samples helped lower the calcium carryover effect. Calcium carryover was also addressed statistically when averaging the sample values.

Other Dionex issues that did not affect the majority of samples but did influence some of the ionic balances include a sulphate tail on some sample runs and an unidentified anion peak in several of the rain and near-surface soil water samples. Figure 3.7 shows a screenshot of a typical Dionex run that is problematic due to the sulphate tail and unknown anion peak. Initial investigation into the anion peak suggested Na_2SeO_3 may be the anion in question, but further analysis on the AAS proved that the dissolved element is not Se. After analysis on the ICP-MS, it is thought one of the frequent but unidentified Dionex peaks may be arsenate. Uncertainty in identifying the anion peak meant concentration could not be calculated, and this caused discrepancies in ionic balances.

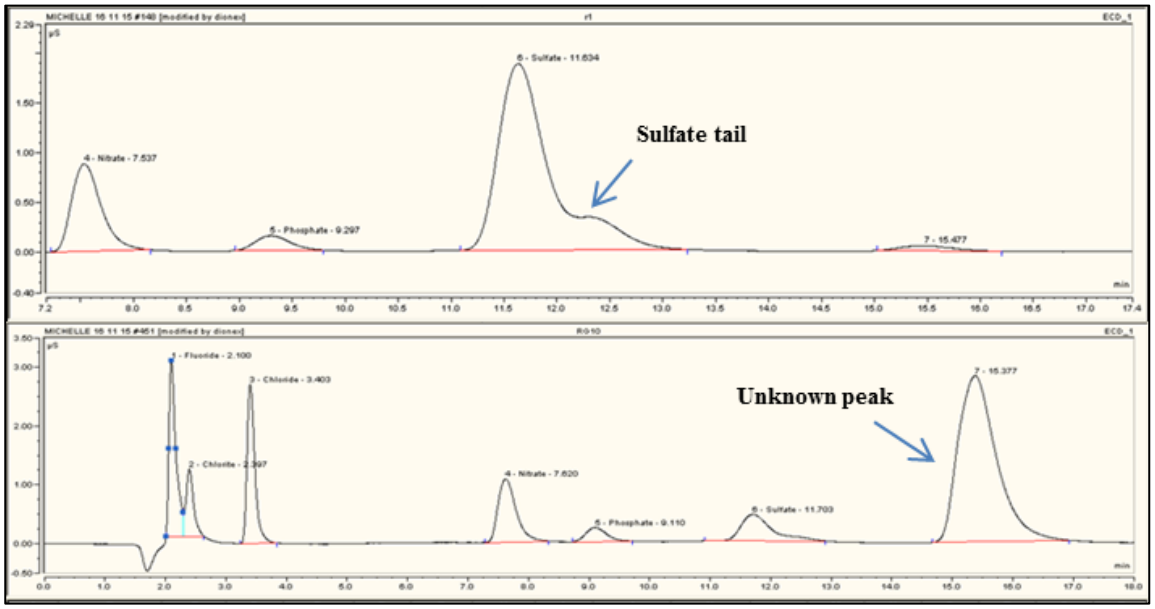


Figure 3.7: Rainfall analysis on the Dionex is limited, and there is uncertainty associated with sulfate tail masking and peaks lacking the correct ion standard.

Initially, suction lysimeters were buried at 20 cm and 50 cm depths around the phreatophyte study plants in an attempt to extract soil water during every seasonal stem water sampling. However, it frequently did not rain prior to a sampling period. The high aridity and low moisture content meant that water could not be extracted using this method. In the 2016 plant sampling season, soil samples collected at rooting depth (15 cm, 25 cm) were extracted, labelled, and frozen in liquid nitrogen. These soil samples (example shown in Figure 3.4c) produced ample water through a cryogenic distillation process for isotope analysis.

There are limitations of CMB as an approach for calculating recharge (critiques summarised clearly by Scanlon et al. (2006). These include assumptions about the origin of the Cl input into the (meteoric versus canopy interactions, dust deposition, rock weathering, and sources of artificial/recharge mixing). These factors were investigated and addressed by comparing open and closed methods of precipitation collection (see section 3.3, Figure 3.1). However, other techniques for estimating recharge face more insurmountable challenges in arid and semi-arid environments (de Vries and Simmers, 2002, Simmers, 1997). For example, applying a soil water budget method ($Q = P - E + \Delta S$), which is common in

temperate environments, is not practical for the semi-arid San Luis Valley, because accurate and precise data on change in soil water storage (ΔS) is unobtainable, and this does not allow the precision of resolution of E and ΔS relative to the small Q rate expected in (semi-) arid regions. Similar challenges arise when estimating arid-area water fluxes: $R = K(\theta)\ \Delta Ht$, where $K(\theta)$ is unsaturated zone hydraulic conductivity and Ht is total head gradient (gravity head + matric suction head), because the relationship between moisture content θ and hydraulic conductivity K gets more uncertain with soil dryness. This means that slight differences in measured moisture content (or moisture suction methods) translate into large differences in unsaturated hydraulic conductivity. Other considerations for CMB include potential uncertainty in the original input values, and instances where Cl deposition through rainfall may have changed over large time periods, such as in northern Africa (Lanzoni et al., 2018).

In addition to the wealth of primary data this study generates on hydrological processes in the San Luis Valley with implications for dryland areas beyond the Southwest USA, this study utilizes and discusses: (i) secondary physical data from previous studies, namely those using radioisotopes for dating residence and travel time of groundwater in the San Luis Valley, and (ii) incorporates primary qualitative data gathered from attending public water district meetings in Alamosa in order to inform discussion on how this work fits into water policy and management strategies (Chapter 8).

The use or consideration of secondary data carries its own set of uncertainties, such as missing periods of data recording and reliance on external analyses. Because it was beyond the scope of this study to perform ^{14}C analysis on water samples to date travel and residence time, secondary data were used from past, published studies to fill in these data gaps. It is therefore acknowledged as a study limitation that dating estimates are provided only on selected water samples (specifically in the San Luis Valley's ancestral sump and in the Eastern region of the valley) and rely on external analysis. In many instances of water depth logging, federal agencies such as the USGS, USBR, and NPS perform routine physical measurements to verify the accuracy of automated data loggers. I performed some of these physical checks alongside NPS and USBR staff. These routine visits and physical measurements increase the

reliability of the historical, automated logging. Both physical measurements and automated water depth readings are presented in Chapter 6. Secondary chemistry data provided by a US federal agency was used in one specific geographic location within the San Luis Valley (as presented in Chapter 5) to augment this study's analysis. To check the consistency of this secondary data, the data were ascertained more than once from different sources. Additional checks involved a comparison between ICP-MS results with those produced in Oxford analysing the same water samples. Data compiled on specific drinking water quality violations as presented in Chapter 8 (Discussion of Results in a Wider Context) were created by accessing the Environmental Protection Agency's (EPA) internal database of reported violations. Since the EPA sets the standards for drinking water quality, their database of reported violations is considered a reliable secondary source. Still, it is an acknowledged secondary source, and as such, a disclaimer is made for its completeness and accuracy.

The use of qualitative data from human subjects carries its own set of uncertainties and potential biases, many of which remain unknowable. This was, to the extent possible, mitigated by cross-checking and fact-checking. Water law, groundwater rules and regulations, active management of wetlands, irrigation season, the seniority of water rights, and ensuring water deliveries are met in compliance with the Rio Grande Compact all play an active part in everyday life and are crucial to understanding the context of water within the San Luis Valley. The Rio Grande Roundtable and Water District meetings attended were all open to the public. Published minutes and meeting agendas augment personal note-taking. Qualitative data are used only to help inform the discussion in Chapter 8. No finding in this thesis rests on qualitative or secondary data alone.

The following chapters may be thought of this way:

Chapter 4: *Atmospheric Source Water*

Chapter 5: *Ground Water*

Chapter 6: *Plant Water*

Chapter 7: *Soil Water*

Chapter 4: Precipitation Chemistry and Isotopic Baselines of Meteoric Waters

4.0 Summary

This chapter examines precipitation patterns in a 20,000 km^2 desert valley with over 1,000 m elevation difference between mountain pass and valley floor recharge pathways. This chapter uses basic chemistry, trace element analyses, and isotopic signatures from >100 samples collected over three years from the valley floor and from the mountain passes. This study establishes the first local meteoric water line (LMWL) for this area of the southern Rockies ($\delta D = 7.73\ \delta^{18}O + 5.8$ with an R^2 of 0.995) and notes δ^2H/ $\delta^{18}O$ differences in precipitation collected at mountain pass and valley floor elevations. A LMWL was also developed for high-elevation areas such as Wolf Creek Pass, ($\delta D = 7.82\ \delta^{18}O + 12.76$). These LMWLs and the precipitation chemistry (particularly Cl^-) help establish source water, pathways, and rates of recharge explored further within this thesis.

Source moisture baselines originating from the Pacific Northwest and from the monsoonal Southwest are identified. Isotopic signatures of an Arctic airmass blizzard which occurred in April 2016 were also identified at δ^2H -240.36, $\delta^{18}O$ -31.39. By examining long-term historical data, recent shifts in the timing of seasonal precipitation on the valley floor are detected. Chemical analysis demonstrates a repeating pattern of acid rainfall for the three years sampled, with highest acidity falling the last week of July and first week of August. Heavy metal analysis of rainfall shows contaminants of health concern in rain, and more than half the rainfall analyzed over three years shows the presence of uranium.

4.1 Chapter Questions, Aims, and Significance

This chapter focuses on addressing the following questions:

- What can isotope and chemistry data of precipitation reveal about the sources of moisture within this high-elevation valley?
- Do the isotope values and local meteoric water lines created from precipitation collected on the valley floor and on the San Juan mountain pass differ significantly in terms of slope, y-intercept, or deuterium excess?

To this end, the chapter aims to characterize the isotopic and chemical signature of precipitation in the San Luis Valley. This chapter also presents the development of a local meteoric water line, which will be used to analyze groundwater in Chapter 5.

While several hydrological studies conducted in the San Luis Valley have examined surface and groundwater chemistry, and the isotopic composition of surface water and groundwater isotopes (Mayo et al., 2007, Rupert and Plummer, 2004), no study has examined precipitation isotope signatures or chemistry. Examining the isotope values of local meteoric waters and precipitation chemistry is an important component to any comprehensive study of groundwater recharge (Edmunds, 1987a, Clark and Fritz, 1997, Kendall and McDonnell, 1998). Without reference to local isotopic signatures, it may be difficult to interpret groundwater isotopes correctly.

This study establishes the first valley-floor local meteoric water line (LMWL) for the Southern Rocky Mountains in addition to establishing a LMWL at mountain-pass elevation. These two LMWLs are important in determining recharge pathways, and the meteoric input of the conservative tracer Cl is important in determining recharge rates using a chloride mass balance approach. Chapters 5, 6, and 7 all rely on data presented here. In addition, this is the first study to highlight a repeating temporal pattern of

acid rainfall in the San Luis Valley and identify trace metal and actinide contaminants of concern in rain (Lanzoni, 2017).

4.2 Methods

Precipitation samples were collected year-round for three years from 2015-2017. Samples for isotopic and chemical analysis from the valley floor were obtained using a clean collection method (described in Chapter 3) whereby glass bowls rinsed with de-ionised water were placed outside at the beginning of a precipitation event and collected at the conclusion of the individual precipitation event. This method frequently produced more than one individual rain event per day during the monsoon season. Rain samples were tested for pH, temperature, electrical conductivity (EC) and total dissolved solid (TDS) content after each rain event using two different and freshly calibrated Hanna instruments. All rain samples were filtered to 0.2 µm, stored frozen in sterile, 50 ml containers, and carried to Oxford for chemical analysis. Samples analysed for heavy metals and trace elements were acidified using nitric acid prior to ICP-MS analysis. A subset of rain samples—selected for minimal exposure to evaporation—were carried to Wyoming for isotopic analysis (described in Chapter 3, Laboratory Analysis).

All of the snow samples were collected as freshly fallen snow except for one high-elevation sample from April 2015 that were collected the day after a snowstorm from snow that had accumulated on tree branches. Snow samples for isotopic analysis were kept frozen on dry ice and in a freezer until they were allowed to melt at room temperature immediately prior to isotopic analysis at the Stable Isotope Facility at the University of Wyoming. Snow samples for chemistry analysis were allowed to melt after collection, filtered to 0.2 µm, transferred into sterile 50 ml containers, and stored in a freezer before being transported to Oxford, where they are kept at 5˚C before analysis on an ion chromatography Dionex or acidified with nitric acid and run on an ICP-MS.

Figure 4.1 shows the locations of precipitation recording and physical sampling. At collection Site 1, precipitation was recorded using a 0.254 mm-switch tipping rain bucket attached to a Campbell Scientific data logger alongside a traditional, daily observation rain gauge on the valley floor. A similar 0.254 mm-switch tipping rain bucket recorded precipitation at Site 2. Snow telemetry (SNOTEL) monitoring sites in the Rocky Mountains and an airport weather station on the San Luis Valley floor provided data on long-term historical precipitation. Valley floor data were analysed using NASA's Giovani software (Acker and Leptoukh, 2007).

Isotopic analysis of 50 precipitation samples from Site 1 and Site 2 was used to create a linear regression event-based LMWL. Because this line will (and does) show a slight bias toward smaller rain events with greater exposure to evaporative fractionation, a weighted monthly mean LMWL was developed using 15 weighted monthly mean values. High-elevation snow was collected at Site 3 (Wolf Creek Summit Pass) in the San Juan Mountains. Isotopic values averaged from 6 and 12 individual samples per snow event were used to create the high-elevation LMWL.

4.3 Precipitation Patterns in the San Luis Valley

The San Luis Valley is a high elevation desert located in southcentral Colorado and northern New Mexico. It is nestled between two mountain ranges—the San Juan Mountains to the west and the Sangre de Cristo Mountains to the east. As detailed more fully in Chapter 2 the majority of the valley's aquifer system is recharged through snowmelt, primarily in the San Juans, which are composed of basalts and rhyolites of the Servilleta and Hinsdale Formations, volcanic tuff, and andesitic-quartz latite rock of the Conejos Formation (Lipman et al., 1970). The Sangre de Cristo's granitic complexes are less permeable and marked by dramatic, Precambrian uplift surrounded by alluvium, conglomerate imbedded sandstone, and thin layers of limestone and dolomite (Lindsey, 2010a, McCalpin, 1996). Recharge from the Sangre de Cristo occurs when snowmelt streams infiltrate through rock fractures and faults, unconfined

sandstones, and through alluvial fans at the mountain range's base. Since the majority of aquifer recharge originates from snowmelt in the San Juan Mountains, it is important to examine precipitation in the San Juan Mountains as well as on the valley floor.

The Rocky Mountain region (which includes the San Juan Mountains) is monitored by automated snow telemetry (SNOTEL) sites in high-elevation, remote locations that record snowfall, precipitation, and temperature, all of which are important for forecasting streamflow. One of these SNOTEL sites is located at the summit of Wolf Creek in the San Juan Mountains. San Juan snowpack provides significant replenishment to the San Luis Valley's aquifers through mountain block recharge. When this snowpack melts in the spring, it also provides significant tributary water to the Rio Grande, which flows through the San Luis Valley. Wolf Creek Pass Summit, at an elevation of 3,309 m, is more than 1,000 m above San Luis Valley mean floor elevation. Surrounding mountain summits and SNOTEL sites are located at similar elevations (±200 m). The elevation difference between mountain passes in the Sangre de Cristo mountain range and the valley floor is also roughly 1,000 m. The average elevation of the valley floor is 2,347 m, and the lowest point on the valley floor is 2,286 m in the area known as the ancestral sump, which once housed ancient Lake Alamosa 450,000 years ago (Machette, 2004, Machette et al., 2007).

As in many arid and semi-arid environments, the rainfall in the San Luis Valley is highly variable in space and time. Summer rain storms in the valley can follow isolated pathways; rainfall amounts in one location will not be consistent with rainfall amounts less than one kilometre away. Isolated rainfall events can be observed moving across the valley floor. Virga is a frequent phenomenon. Typically, the windward side of the Sangre de Cristos receives an inch of rainfall annually more than the dry centre of the valley. Measured precipitation (logged from a tipping rain bucket located at Site 1 in Figure 4.1) for the 2015-2016 year was 200.13 mm and is close to the long-term historical average for the valley floor. Measured mean precipitation at collection Site 2 (Figure 4.1) at the base of the Sangre de Cristos from 2010 to 2015 was 271 mm/year.

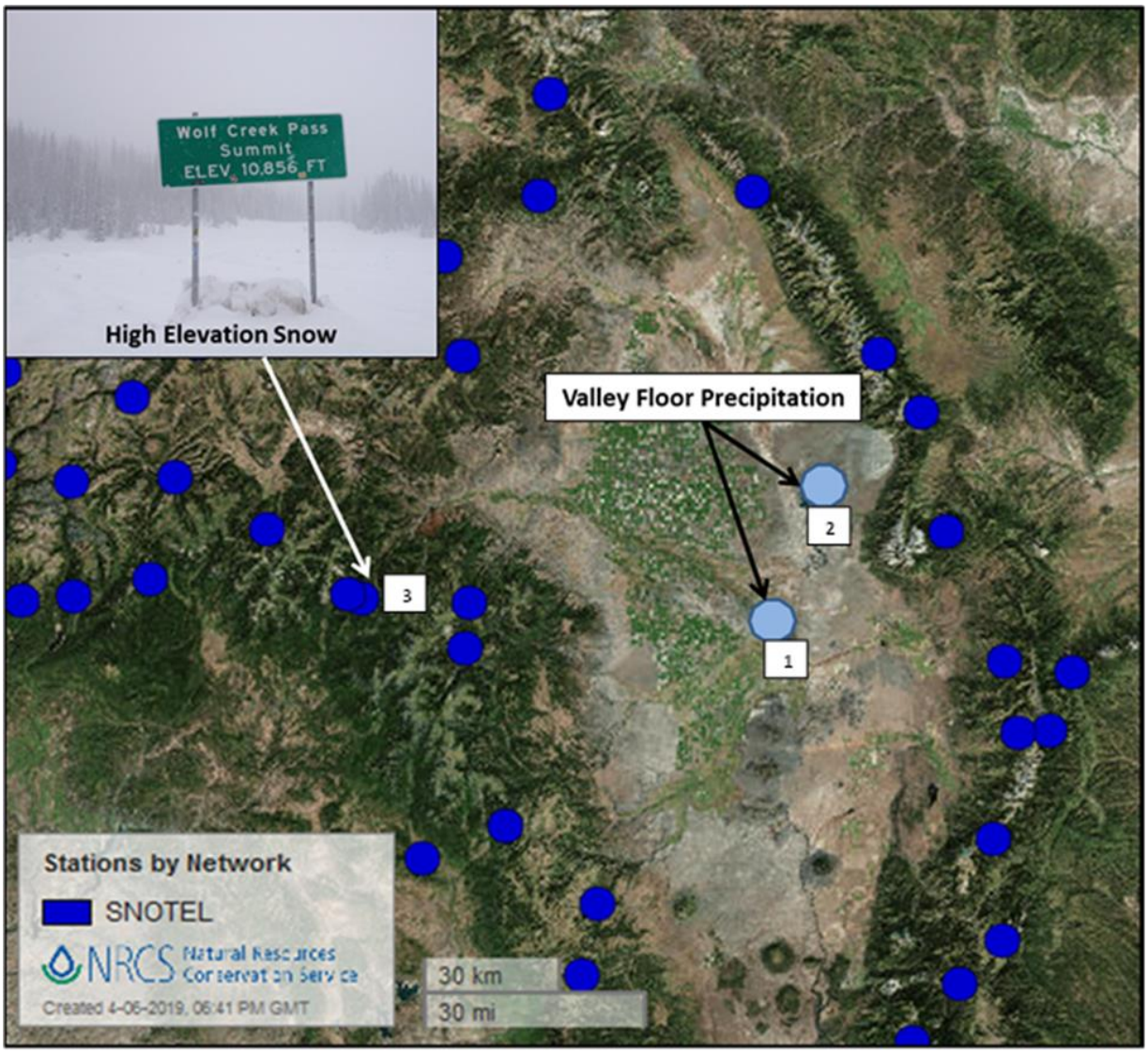


Figure 4.1: San Luis Valley map showing area topography and precipitation collection points. Light blue circles 1 and 2 are valley floor collection points for rain and snow. Dark blue circles are SNOWTEL stations throughout the Rocky Mountains. Dark blue circle 3 is the collection point for high-elevation snow.

On the valley floor, most of the precipitation arrives in the afternoons during the late summer monsoon—part of the North American Monsoon system, which occurs in July, August, and the first few weeks of September. In the higher elevation mountains precipitation, about 1,000 mm/yr, arrives predominantly in the form of snowfall in late winter and spring. Winter snowstorms originate from the Pacific Northwest. Summer monsoons originate from the Gulf of Mexico.

Most of the snow in the San Juan Mountains arrives in February, March, and April. While the Wolf Creek Summit Pass SNOTEL site was established in 1985, precipitation records are available since 1981. The mountain pass precipitation recorded over a 30-year period from 1981-2010, shows mean snow-water-equivalent accumulation reaches 858 mm by May 1. By June 1, mean snowpack has melted to 40 mm, and by August 1, no snow remains. The mountain pass historically has no snow cover from Aug 1 through late September. Figure 4.2 (a) presents yearly SNOTEL data at Wolf Creek Pass from 1986 to 2019. While mean yearly snowfall is > 800 mm/yr, there is significant yearly variability. A record low for snowpack in 2002 preceded the San Luis Valley's steepest decline in unconfined aquifer levels (RGWCD, 2017).

Long-term historical precipitation data collected at the airport weather station on the valley floor (with data from nearby stations for reference) were used to model valley floor-wide precipitation from 1979-2019 by season. Figure 4.2 (b) shows NLDAS Fora (0.124 degree resolution) modelled mean monthly precipitation presented by season. Winter months includes December, January, February, spring consists of Mar, Apr, May, summer is Jun, Jul, Aug, and autumn is Sep, Oct, Nov. Historically, most of the valley's precipitation arrives in summer (JJA) as a result of the North American monsoon, and the highest summer rainfall years occurred in 2013, 2015, and 2017. The summer monsoon precipitation has been variable in recent years. June, July, August (prior and during monsoon season) was > 40 mm/month average in 2017, but precipitation amounts fell to nearly half this amount the following year. In recent years, seasonal precipitation has reached its record high for the 40-year record. December, January, February reached its record high in 2017. Autumn precipitation reached its record high in 2013. March, April, May reached its record high in 2015 and produced spring flooding along several creeks. Spring precipitation on the valley floor then dropped close to its lowest amount in 2018 (following a record low for DJF winter season).

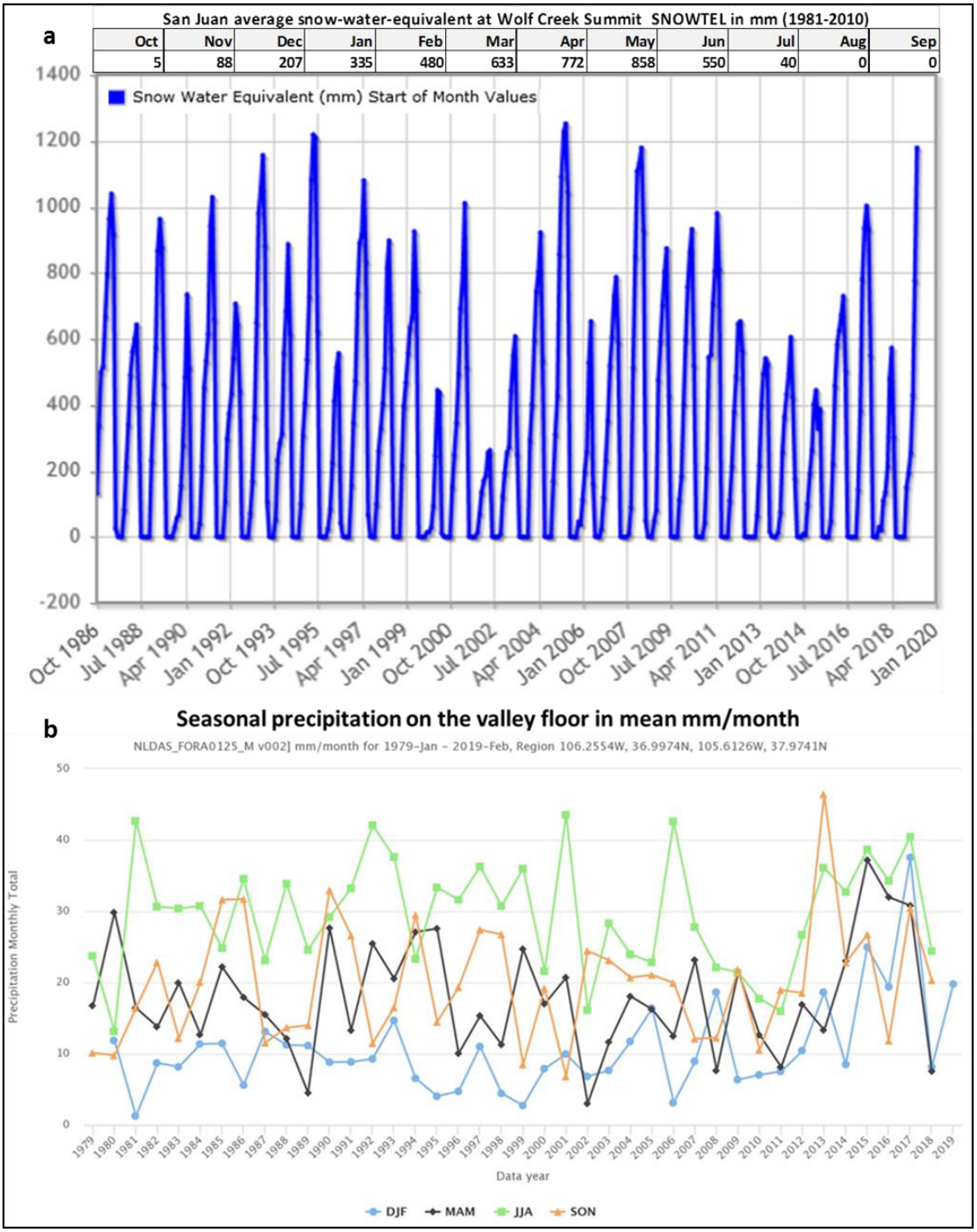


Figure 4.2: Precipitation patterns in the San Juan Mountains and on the valley floor at (a) Wolf Creek Summit Pass and (b) by season using the NASA's Giovani database and visualization tools.

4.4 Precipitation Isotopes and a Local Meteoric Water Line for the San Luis Valley

This study uses the isotope signatures of 50 rain and snow events collected for every month from 2015-17 across the eastern valley floor (Site 1 and 2 in Figure 4.1) to produce the first Local Meteoric Water Line (LMWL) for the San Luis Valley. The event-based LMWL, which is based on values from 50 precipitation events is presented in equation Eq. 4.1, with an $R^2 = 0.9857$. Using 15 weighted monthly means spanning the same 3-year period, the equation is presented in Eq. 4.2, with an R^2 of 0.9954.

$$\delta D = 7.3606\ \delta^{18}O - 0.8626 \qquad \text{[Eq. 4.1]}$$

$$\delta D = 7.7274\ \delta^{18}O + 5.7974 \qquad \text{[Eq. 4.2]}$$

In 1981, Yurtsever and Gat developed a reference meteoric water line for North America using all the North American International Atomic Energy Agency (IAEA) network stations (Eq 4.3):

$$\delta D = 7.95\ \delta^{18}O + 6.03 \qquad \text{[Eq. 4.3]}$$

This was thought to be a more specific reference for North American meteoric waters than the Global Meteoric Water Line (GMWL) (Eq. 4.4):

$$\delta D = 8\ \delta^{18}O + 10 \qquad \text{[Eq. 4.4]}$$

While the difference between the two equations' slopes is insignificant, the intercept or 'd' parameter may show less kinetic fractionation during evaporation of ocean water around North America than that of the global average (Gat and Gonfiantini, 1981). In 1992, Rozanski et al. produced a weighted annual average of global precipitation collected from all IAEA network stations worldwide (Eq. 4.5):

$$\delta D = 8.13\ \delta^{18}O + 10.8 \qquad \text{[Eq. 4.5]}$$

Because this equation was produced using weighted precipitation samples, it is sometimes referred to as the real GMWL. For the purposes of this chapter and for the entirety of this thesis, the term GMWL shall refer to the standard Eq. 4.4 by Craig (1961), and all isotope work (except otherwise noted) is expressed in per mil (‰) in relation to Vienna Standard Mean Ocean Water (VSMOW).

Figure 4.3 presents this study's event-based LMWL as a black dotted line and the weighted monthly LMWL as a blue dashed line in relation to the global standard GMWL (shown as a solid red line) for reference. The event-based LMWL was created using 50 precipitation samples that were selected for minimal exposure to evaporative loss from the subset of > 100 precipitation samples collected. However, the event-based LMWL will still show bias through small-size rain events more prone to evaporative loss and fractionation. The slope of the event-based LMWL is 7.36, whereas the slope of the weighted monthly LMWL (dark blue dashed line, fitted through dark grey circles) is 7.73. Arid environments with high rates of evaporation will produce open surface waters with a slope < 8 on a meteoric plot, and meteoric water lines may face similar challenges associated with evaporative fractionation. The weighted monthly meteoric water line guards against amount effect and evaporative enrichment. The weighting of the LMWL helps correct for amount effect in arid regions where very small amounts of rainfall may evaporate below the cloud base and enrich the $\delta^{18}O$ (Dansgaard, 1964, Clark, 2015b). This weighted monthly LMWL for the San Luis Valley is closer to the GMWL. The weighted monthly LMWL is used as the reference LMWL in this and in following chapters.

Snow samples from the valley floor at Site 1 and at Site 2 (Figure 4.1) were included in the monthly weighted LMWL. Including winter precipitation events is important for a more representative LMWL, since precipitation on the valley floor is a combination of colder precipitation arriving from the northwest and summer monsoons arriving from the southwest. Snow storms generally move eastward across the valley before hitting the windward side of the Sangre de Cristo mountain range. Snow samples collected

on the same day (April 18, 2016) at Site 1 and Site 2 have very similar isotope signatures, and this repetition acts to validate the unusually depleted isotope values found during the April blizzard of 2016.

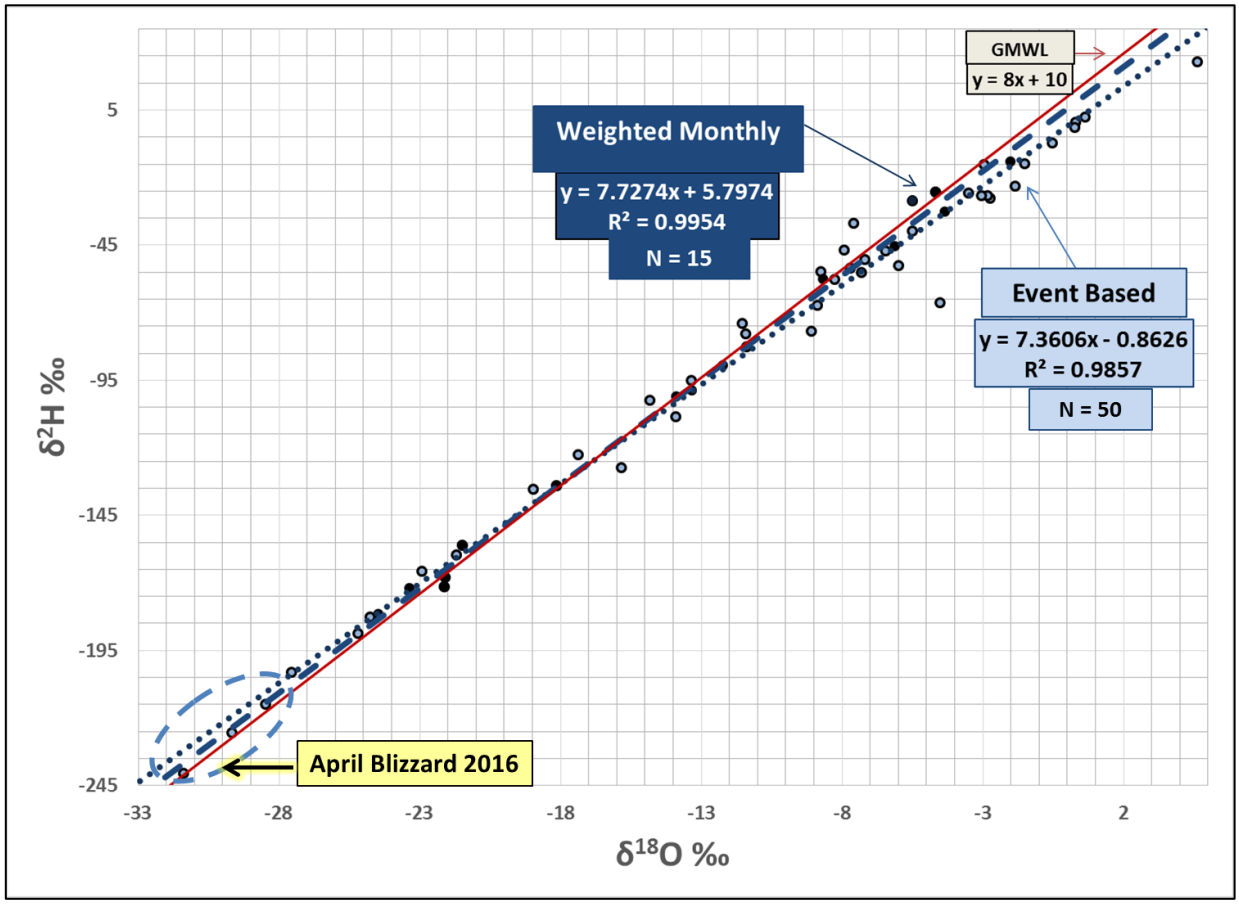


Figure 4.3: Local Meteoric Water Lines for the San Luis Valley floor, expressed through monthly weighted means (dark blue, long dashed line) and the individual precipitation events (black dotted line). The GMWL is shown in red for reference.

It is worth noting the snow event that appears in the bottom-left corner of Figure 4.3 with -214.79 δ^2H, and -28.47 $\delta^{18}O$. On April 16, 2016, a blizzard swept through Colorado. The blizzard affected the southern Rocky Mountains and adjacent High Plains. The storm disrupted airports and appeared on national news. Snow samples were collected at the Alamosa Wildlife Refuge on April 16 (02.00 am) and again at the end of this blizzard, during another and much larger snowstorm on April 18 (9:30 am). At the same time, snow samples were collected at Great Sand Dunes National Park and Preserve on April 18 (before 10.00 am) and April 19 (before 10.00 am). While the initial storm of April 16 (4.06 mm melted

precipitation) produced the heaviest, or most positive value of all snow samples, δ^2H -73.79, $\delta^{18}O$ -11.56, (which falls within the normal range for snow), the much larger snow storm that followed on April 18 (13.46 mm precipitation) produced the δ^2H -214.79, $\delta^{18}O$ -28.47 signature. The snow sample collected the same day at Great Sand Dunes National Park had a value of δ^2H -240.36, $\delta^{18}O$ -31.39. The following day at Great Sand Dunes another fresh snow sample was collected, and this produced an isotope signature of δ^2H -225.33, $\delta^{18}O$ -29.68. This means that in April, 2016, fresh snow was collected on the floor of the San Luis Valley in Colorado with an isotopic value of δ^2H -240.36, $\delta^{18}O$ -31.39. Similar (slightly less negative δD values) were ascertained from other samples collected that same day and the next. Snow this light does not normally fall in Colorado. Anderson et al. (2016) conducted a study on the isotopic signatures of North American Rocky Mountain Snow using 1345 snow pack samples collected over a 21-year period, and their most negative values were δD -189.7 and $\delta^{18}O$ -24.7. Gooseff et al. (2006) report isotope signatures in this range of δ^2H -240, $\delta^{18}O$ -30 for their fresh snow and ice core samples—from McMurdo Valley, Antarctica. Isotope signatures this depleted are also found in the Arctic.

The mid-April blizzard of 2016 occurred at the end of what was one of the strongest El Nino seasons ever observed (Nino 3.4 index) and has been compared to years 1982/3 and 1997/8. El Nino has been shown to influence ^2H and ^{18}O depletion in Rocky Mountain precipitation (Welker, 2012). At the same time, the polar vortex in April 2016 forced arctic air southward, and as water vapor condensed and re-circulated through these conditions over the continent, the isotope signature became increasingly depleted. It may be that the initial 2:00 am sample taken on April 16 was from water vapor originating in another air mass and had begun to fall briefly over the San Luis Valley before the cold front and its blizzard set in. The snow that descended on the San Luis Valley is a striking example of how isotope signatures in precipitation record the many different influences exerted on their abundance and fractionation. This unusual storm event highlights how extreme variations in weather could produce signature pulses that, if taken out of context, might be misinterpreted as having paleoclimatic origins if the events were not

averaged out in a long-term record. Reading isotope signatures in meteoric waters may be similar to reading them in ground waters; care must be taken to place the sample in context.

The coldest snow samples from the North are the most negative in value and so make up the lower left-hand end of the LMWL. Their ^{18}O values tend to be depleted in relation to their ^{16}O, which are enriched, so the resulting $\delta^{18}O$ is more negative. The warmer monsoons of late summer, which originate off the Gulf of Mexico, are isotopically heavier or more positive in values and appear in the upper right-hand portion of the LMWL. The $\delta^{18}O$ of different precipitation samples reflects differences in temperature, elevation, and latitude of the storm's origin. When the $\delta^{18}O$ of precipitation samples are plotted over time, as shown in Figure 4.4, a history of winter snow, spring blizzards, cold spring rain, early summer rain (still from the Northwest), late summer monsoons (from the Southwest), and autumn rain that transitions into snow can all be identified. This LMWL for the San Luis Valley creates a precipitation reference line to assist in the analysis of all groundwater, soil water, and plant water discussed in the proceeding chapters of this thesis. Seasonal precipitation values are important for tracing storms, understanding the timing of recharge, and identifying input to soil water.

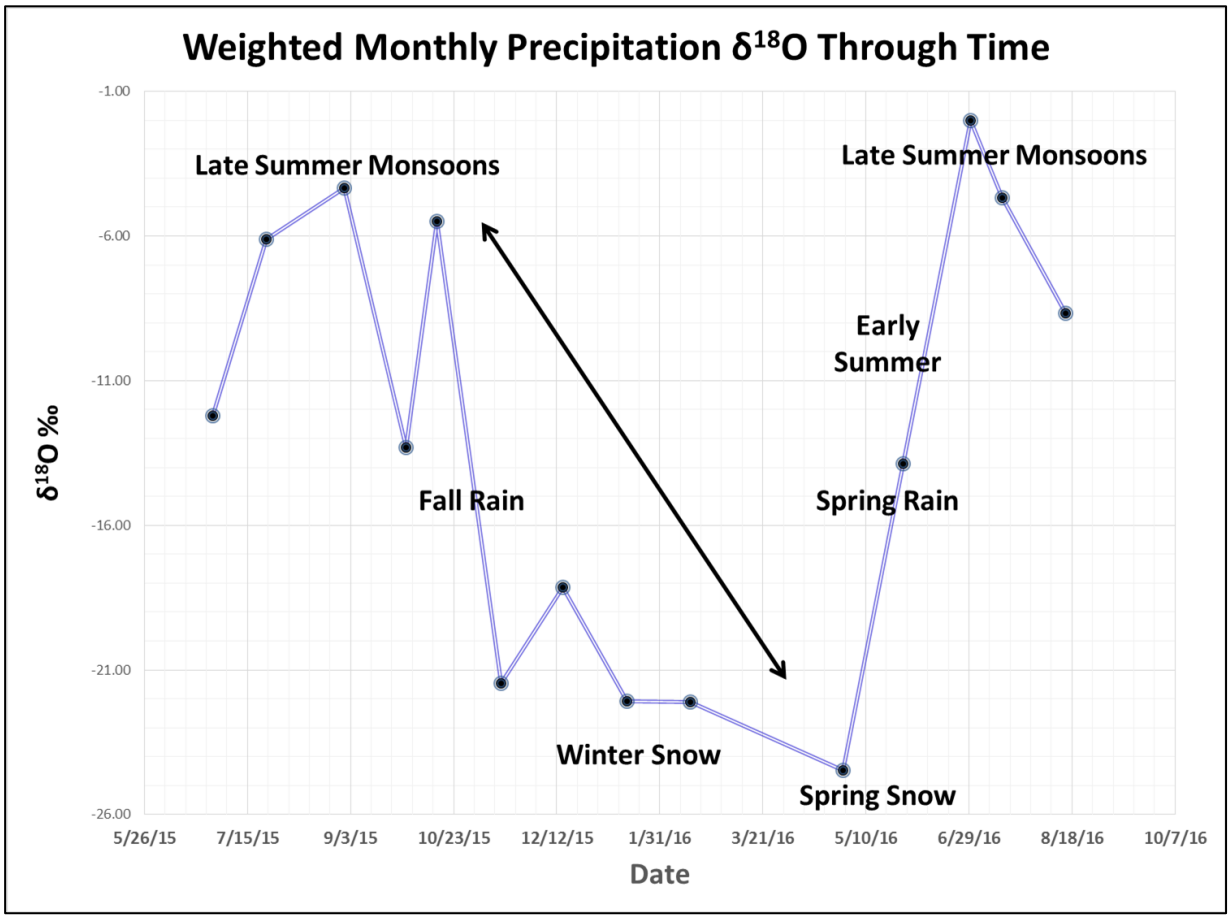


Figure 4.4: The $\delta^{18}O$ of weighted monthly precipitation through time. Isotopic signatures of $\delta^{18}O$ in precipitation show seasonal trends.

Isotopic elevation effects are well defined on the windward side of a mountain range, because condensation increases with cooling according to an adiabatic lapse rate. Isotopic elevation effects are more difficult to track on the leeward side of a mountain range because the leeward precipitation may include spillover from precipitation formed above the mountain top elevation. From the valley floor to the mountain passes in the San Juan Mountains there is > 1000 m difference in elevation. Since much of the valley's aquifer system is recharged through snowmelt in the San Juan Mountains, it is important to investigate potential differences between meteoric waters deposited on high-elevation mountain passes (3309 m) and meteoric waters deposited on the valley floor (2286 m). To this end, a meteoric water line

was also developed using snowfall collected at 3309 m mountain passes in the San Juan Mountains during storms in the months of February, March, April, and June. The San Juan high elevation snow line has a slope similar to that on the valley floor, but the 'd' parameter is 12.8 versus the valley floor's 'd' parameter of 5.8. The San Juan Snow Line, shown in Figure 4.5 (a) sits above the valley floor's LMWL and the GMWL. The San Juan snow in Figure 4.5 (b) shows greater deuterium excess than valley floor samples collected at similar times.

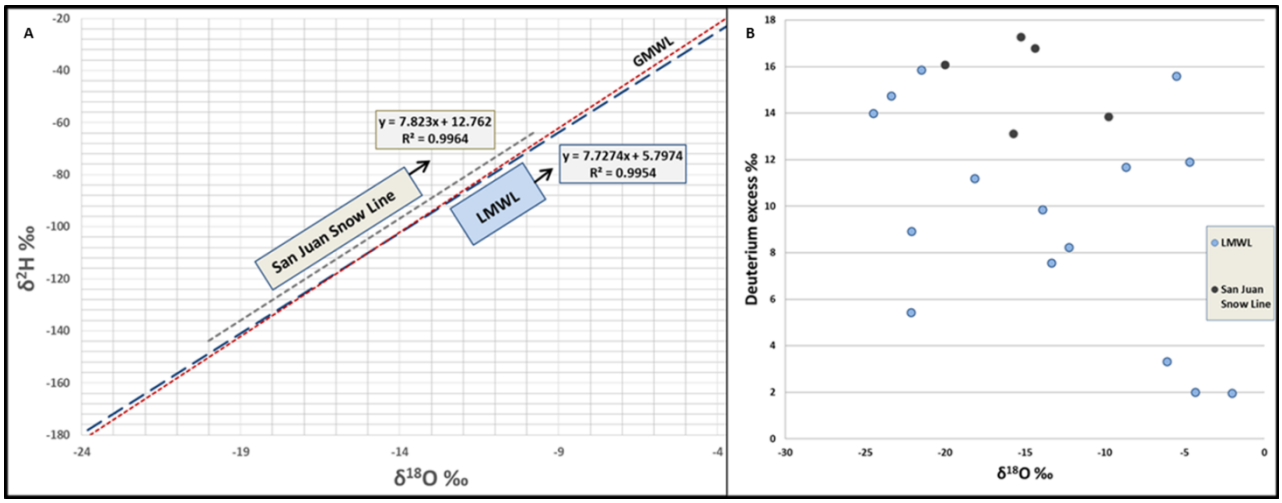


Figure 4.5: (a) San Juan snow line from high elevation samples collected during storm events in Feb, Mar, Apr, Jun in relation to the LMWL from the valley floor. (b) Deuterium excess of both lines plotted against $\delta^{18}O$.

If only the event-based snowfall is examined, valley floor snow collected at Site 1 (Figure 4.1) just east of the San Juan mountain range has a 'd' parameter higher than that of the San Juan snow line, and a linear regression line formed from this Site 1 valley floor snow sits above the LMWL, much closer to the San Juan high elevation snow line. This may be due, in part, to carryover of snowfall formed at mountain-pass elevation as the storms typically move NW to SE, depositing snow in the San Juans before the Sangre de Cristos. On the eastern side of the valley, snowfall was collected near the base of the Sangre de Cristo mountain range (collection Site 2). A trendline formed from these snowfall samples is closer to the valley's year-round LMWL. It is important to note that the bulk of precipitation on the valley floor arrives in the form of rain, and mainly through the southwest monsoon. The vast majority of the precipitation in

the San Juan Mountains arrives in the form of snow. In Figure 4.5b deuterium excess from San Juan snow samples is more pronounced than d-excess from valley floor samples, even when comparing only those snow samples collected at similar times.

4.5 Rain Chemistry

In order to understand meteoric input and assess precipitation chemistry in the San Luis Valley, more than 110 precipitation samples (in the form of individual rain events and fresh snow) were collected across 2015, 2016, and 2017. A few gaps in data exist: while nearly all rain events during the 2015 and 2016, and half of 2017 rain seasons were sampled, rain events < 0.2 mm did not always leave enough sample remaining to ascertain a pH measurement. A few rain events in the first half of May 2016 (including a large downpour) were missed due to physical absence.

4.5.1 Cl and Ion Chemistry

It was important to establish chloride concentrations in rainfall since chloride is used as a conservative tracer for rates of recharge calculations (Chapter 5). Chloride Mass Balance (CMB) calculations are based on weighted mean 0.26 mg/L Cl input (arithmetic mean is 0.44 mg/L) using a 39-sample subset from 2015 because the best low-Cl calibration (R^2=0.9997) and lowest LOD (LOD=0.07 and LOQ=0.2 was achieved for this period on the School of Geography and the Environment's old ion chromatography Dionex machine (since retired). The arithmetic mean for conservative tracer Cl^- concentrations from all 'open' rain gauge samples is 0.59 mg/L, whilst the weighted mean Cl^- concentration (based on rainfall amount) is 0.41mg/L. For the 'closed' system of sampling, the chloride concentrations in rain were slightly less. The arithmetic mean is 0.44 mg/L; the Cl^- concentration weighted mean is 0.26 mg/L. The methods used, the validation of these methods, and more detailed Cl results are presented in Chapter 3 (see Figure 3.1). The most significant factor influencing whether and to what extent a sample was exposed to external contaminants was the length of time the collection device was allowed to sit between collections, and, owing to the variability of rain event length, the time of day and length/intensity of the

storm. During frequent and heavy rain events, the open rain gauge was naturally flushed out as it was emptied between readings and rain events.

A potential signature of acidified rainfall may be found in high concentrations of dissolved nitrate and sulphate. Results from ion chromatography analysis show concentrations up to 4.3 mg/L NO_3 and 12 mg/L SO_4 in the Alamosa 2015 rainfall. Nitrate concentrations were as high as 4.3 mg/L in the 'closed' method of collection and 5.4 mg/L in the 'open' rain gauge collections. Phosphate concentrations were as high as 1.9 mg/L in the closed collection and 2.7 mg/L in the open collection. Sulphate concentrations were as high as 12 mg/L in the closed collection and 2.8 mg/L in the open collection, but this is thought to be due to higher concentrations of dissolved sulphate on the particular day of June 5, 2015, in which a small, overnight rainfall produced only enough rain for the 'closed' method of collection. One potential uncertainty and particular bias of ion chromatography analysis on the Dionex is that sulphate peaks sometimes produce 'tails' that mask sulphate compounds or closely related anions, producing artificially high concentrations. In any event, SO_4 found in Alamosa rainfall is significantly higher than historical records of sulphate would suggest for this region of the southern Rocky Mountains. For rainfall in this region, 1 mg/L SO_4 is typical (Drever, 1988). Of the cations, NH_4 was found as high as 3.1 mg/L in the closed collection and 1.8 mg/L in the open rain collection. Potassium was also found at concentrations up to 4.6 mg/L K. Ion chromatography analysis also showed appreciable dissolved F and an unconfirmed anion peak thought to be arsenate. (Later analysis on ICP-MS shows high concentrations of dissolved arsenic in rainfall.)

In situ measurements of rainfall revealed certain rainfall events in the San Luis Valley are acidified. Figure 4.6 presents summary comparisons of rainfall by comparing ions in mEq/L. Rainfall samples for the 2015 year are divided into those < pH 5, those > pH 5, and those ascertained from the open rain gauge method of collection.

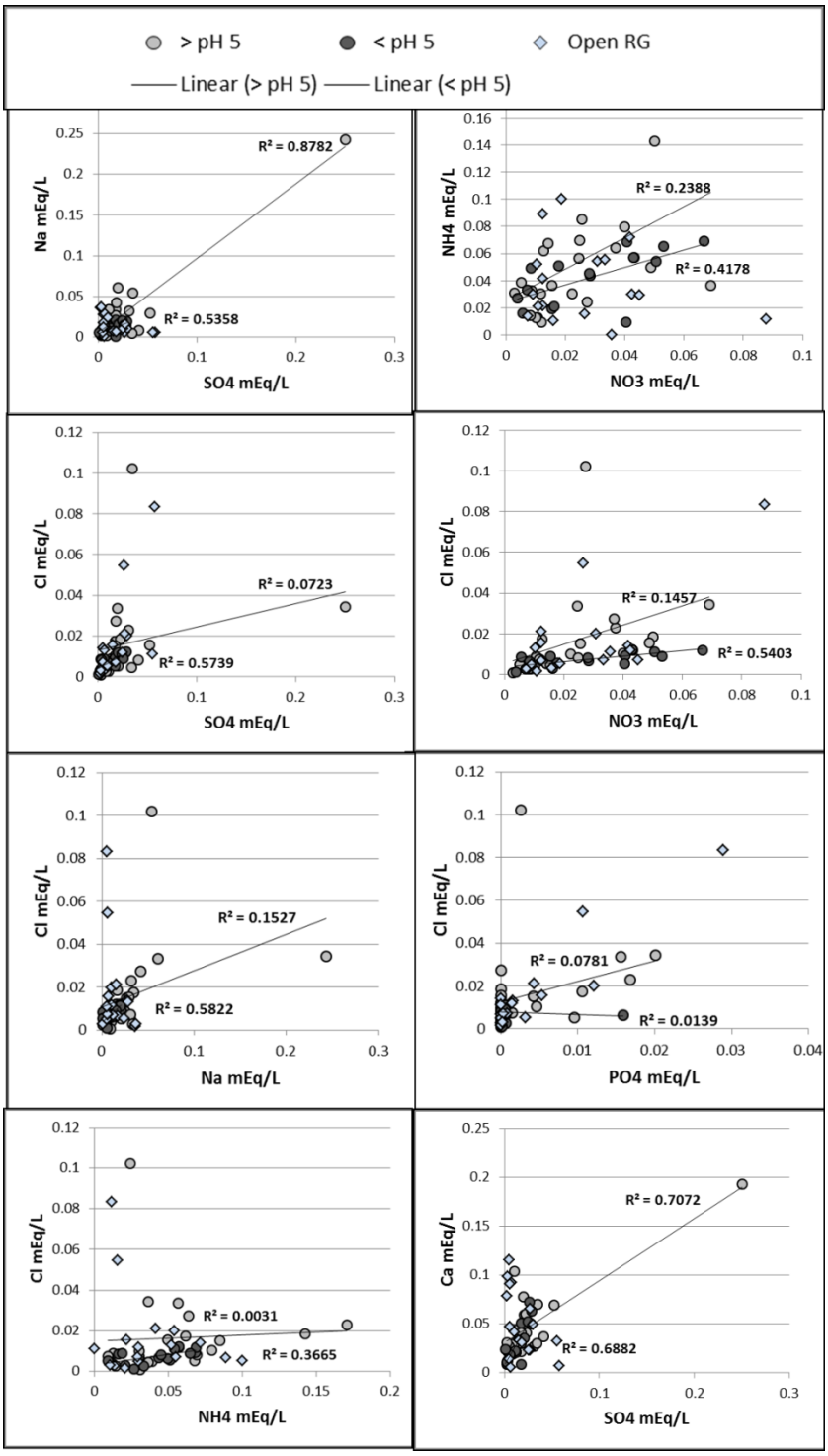


Figure 4.6: Summary rainfall chemistry comparing ions in mEq/L units.

4.5.2 Rainfall Acidity and Heavy Metal Contaminants

Rainfall acidity is usually reported in annual weighted means. However, because the San Luis Valley has distinct precipitation patterns, it is more informative to track patterns through individual rain event measurements and weighted monthly means. Over a three-year period of in situ measurement, a pattern of acid rainfall was detected in the San Luis Valley. Data from the years 2015 and 2016 show better temporal coverage and are herein discussed. For the 2015 season, the rain sample weighted mean is pH 5.06. The 2016 rain sample weighted mean is pH 4.80. The lowest weighted monthly means for 2015 occurred in July, August, and September at pH 4.79, 4.80, and 4.96 respectively. The following year, the lowest weighted monthly means occurred in June, July, and August at pH 4.95, 4.8, and 4.57 respectively. As shown in the graph, the most acidic rain arrived during the last week of July and the first week of August. The lowest pH value recorded in 2015 occurred as a 1.25 mm event at the end of July and registered pH 3.98. In 2016 the lowest value was pH 4.09 and occurred as a 10.4 mm downpour during the first week of August. Rainfall acidity does not correlate to the size of the rain event.

Figure 4.7 shows rainfall acidity through time for the 2015 and 2016 years. Rainfall acidity data from 2017 were not included in this graph because records began too late in the season. However, the abridged 2017 data also show lowest pH values during the same two-week period at the end of July and beginning of August. Figure 4.7 shows rainfall classified as acid rain (pH < 5) in red, with the size of the rain event labeled in mm within each sphere. Raw data on rainfall amounts and pH values are found in Appendix 2.

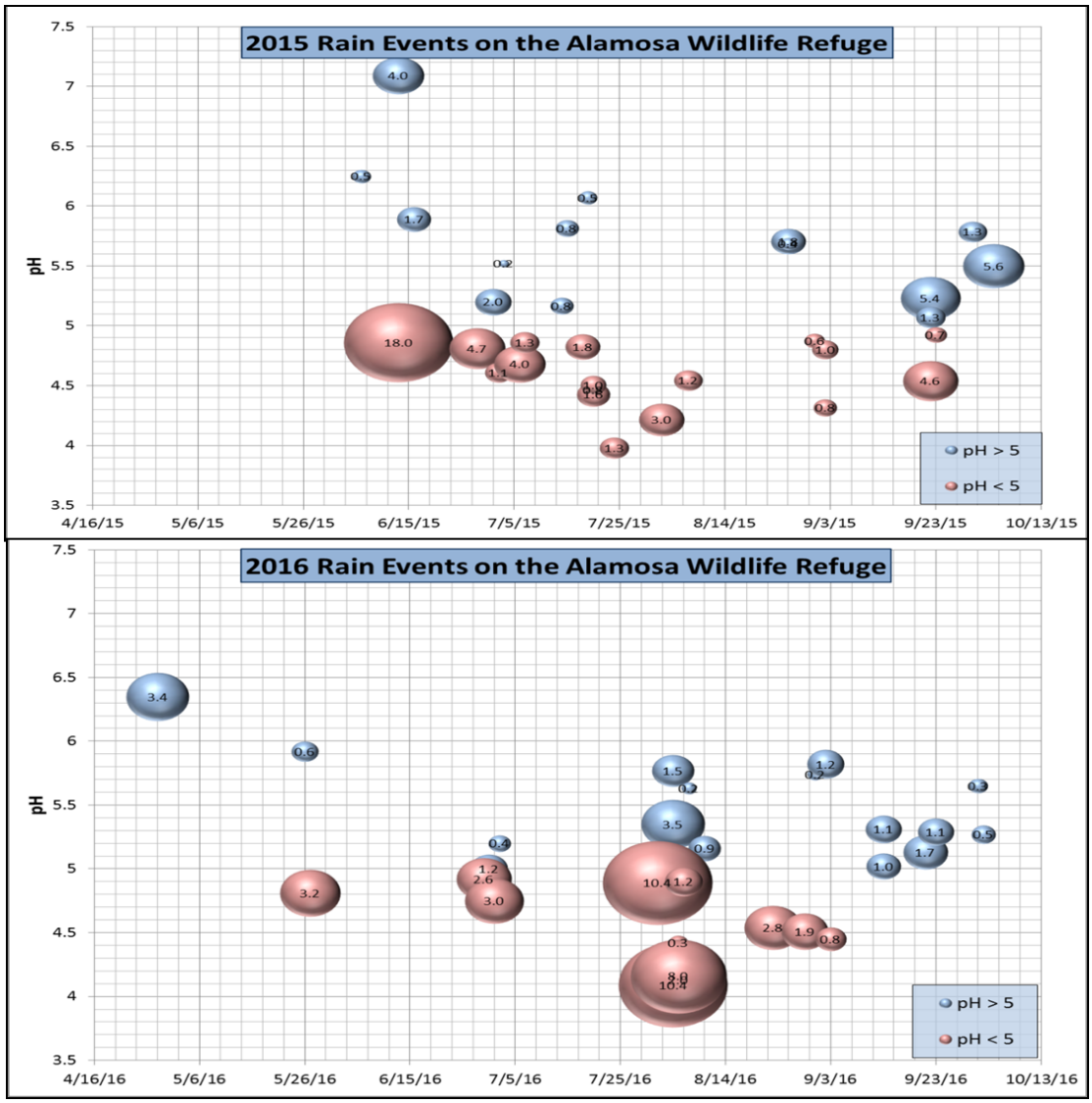


Figure 4.7: Rainfall acidity in the San Luis Valley throughout 2015 and 2016. Circle sizes correspond to size of the rain event, with the rain amount in mm superimposed on each sphere. Although most rain events in the San Luis Valley are < 3 mm, the rain event of 18 mm in 2015 and the two 10 mm rain events in 2016 suggest acidity is not linked to the size of the rain event.

Heavy and trace metal analyses were conducted on 64 precipitation samples collected throughout 2015-2017. These included 11 snow samples (from Wolf Creek Summit Pass and from the valley floor) and 53 rain samples. All precipitation samples had iron, manganese, zinc, zircon, hafnium, copper, and lead. Most rain had cobalt, nickel, vanadium, chromium, cadmium, and arsenic. None had detectable levels of mercury. One had ruthenium (^{99}Ru). Rain samples had detectable quantities up to 143.3 µg/L manganese

(^{55}Mn), 104.7 µg/L zinc (^{66}Zn), 40 µg/L iron (^{156}Fe), 7.4 µg/L copper (^{65}Cu), 2.2 µg/L lead (^{208}Pb), 1.26 µg/L arsenic (^{75}As), 1.13 µg/L vanadium (^{51}V), 0.6 µg/L chromium (^{52}Cr), 0.16 µg/L cadmium (^{111}Cd), 0.64 µg/L tungsten (^{183}W), 0.19 µg/L thorium (^{232}Th), 0.1 µg/L uranium (^{238}U), and—because it's more pleasant to think of gold dust than uranium in rainfall—0.024 µg/L gold (^{197}Au). Six of the 11 snow samples show the presence of ^{238}U in the range of 0.001 to 0.007 µg/L, with the greatest concentrations occurring in February and late March (rather than January).

Trace metals found in dust particles deposited on mountain snowpack may be removed during sample filtration < 0.45 µm (Carling et al., 2012), so it is not presumed this study's heavy metal concentrations in snow are directly comparable or represent the total (undissolved) concentrations. As a test of the methods (presented in Chapter 3), this study compared rain and groundwater samples filtered through 0.8 µm, 0.45 µm, and 0.2 µm membranes with similar ICP-MS concentrations. It is therefore considered that heavy metal concentrations in rainfall are derived from the dissolved, wet deposition. While some of the heavy metals associated with Southwest dust emissions and mining activity in the San Juan Mountains have been previously reported in snowpack (Lawrence et al., 2010, Carling et al., 2012), this is the first time ^{238}U and ^{232}Th are reported in this region's rain. In general, very few studies collect and analyze the chemistry of individual rain events, so a baseline of rainfall chemistry is lacking. Uranium was present (above the detection limit of 0.001 µg/L) in 37 of the 64 precipitation samples; these samples ranged from 0.001 µg/L to 0.1 µg/L of ^{238}U. There were 6 rain events with higher ^{238}U concentrations that fell between 0.03 µg/L and 0.1 µg/L. These rain events occurred on June 5, 2015, in the early morning of April 28, 2016, June 1, 2016, June 5, 2016, June 31, 2016, and August 29, 2017. Most of these rain events were recorded at only 0.2 mm, but as much as 1.2 mm. Most of the ^{238}U was detected in small, low-intensity rain events (as shown in Figure 4.8b). The first rain of the season (as happened on April 28, 2016) or the first, light rain after a long dry spell held higher ^{238}U. ^{232}Th was present in 12 of the 64 samples ranging from 0.1 µg/L (just above the method LOD) to 0.19 µg/L. Figure 4.8 shows some heavy metal contaminants of concern found in rainfall across the years 2015-2017. The graph charts concentrations of

heavy metals Cr, Cd, As, Pb, W, Mo in rainfall as well as the radioactive actinides U and Th. While it appears U correlates inversely with rainfall amount, this does not appear to be the case with Mo and W.

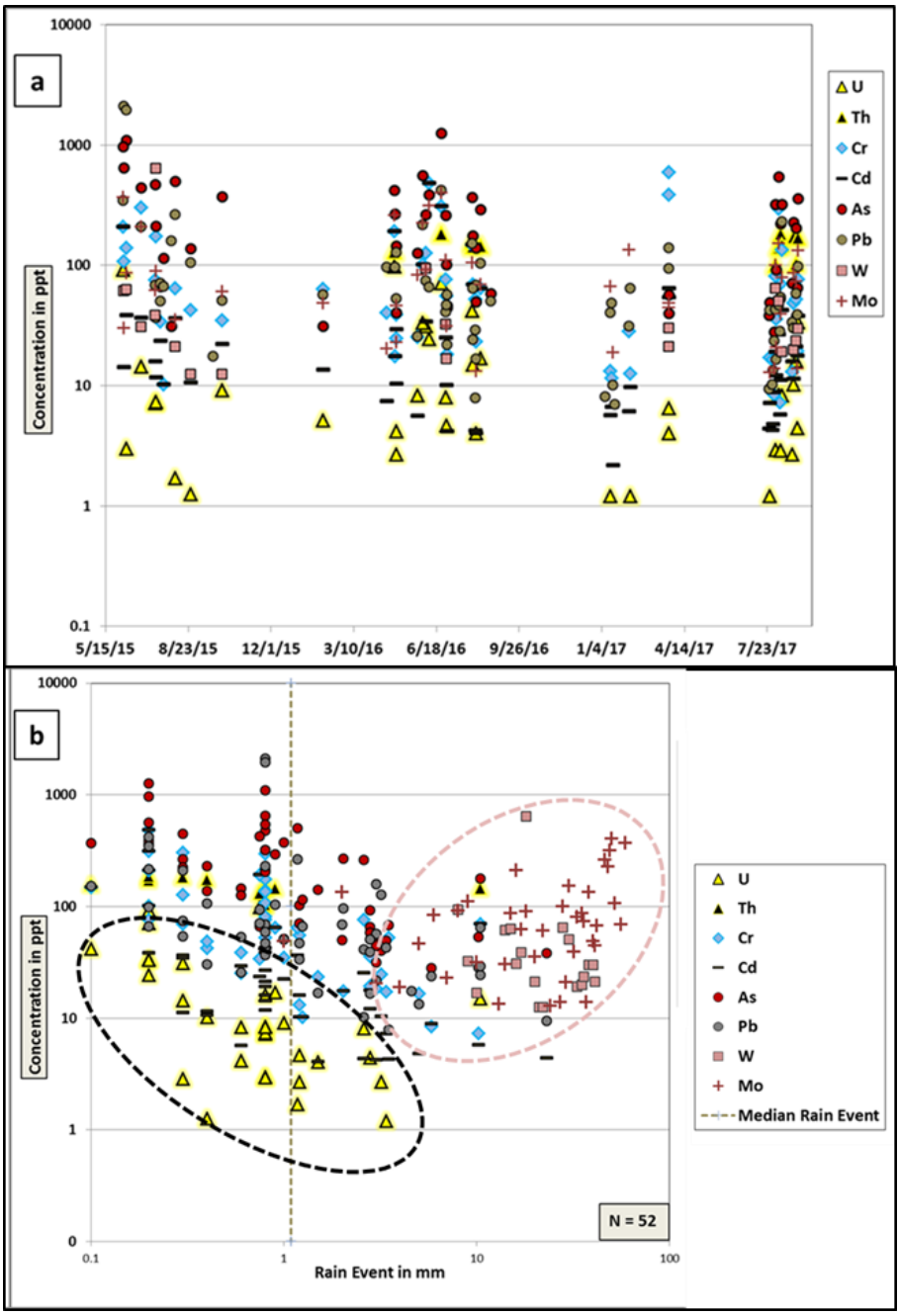


Figure 4.8: Trace contaminants detected in rainfall (a) plotted across three years (b) and by rainfall amount. While the detection limit will vary by element, the circled groups in 4.8 (b) show opposing trends with respect to rainfall amount.

4.6 Discussion

By examining long-term historical precipitation data by season for the San Luis Valley, we can detect recent shifts in seasonal precipitation patterns. Low snowfall years see low surface water availability, curtailment of surface water rights for irrigation, and an increased reliance on groundwater abstraction. While aquifer drawdown for human consumption increases, snowmelt-driven recharge decreases for those same low-snowfall years. The diminished snowpack in 2002 marked an unprecedented drawdown in the San Luis Valley unconfined aquifer levels (RGWCD, 2017). Winter precipitation on the valley floor reached its record high in 2017. While the 2017 surrounding mountain snowpack was credited with replenishing some of the valley's aquifer deficit (Cotten, 2017), it should be noted with caution that this amount of winter precipitation on the valley floor was the greatest amount recorded in a 40-year record. San Juan snowpack was significantly higher-than-average for the 2017 and 2019 water years.

A LMWL for the San Luis Valley floor was developed from year-round precipitation over three years with a slope of 7.73 and a 'd' parameter of 5.8. This weighted monthly meteoric line corrects against event-based amount effect and evaporative loss. There is more than 1000 m difference between the mountain passes of the surrounding mountains and the valley floor. The San Luis Valley is on the leeward side of the San Juan Mountain Range. Precipitation in the San Juans is dominated by snowfall whose moisture originates from the NW while precipitation on the valley floor is dominated by the late summer SW monsoon. A high elevation LMWL created using snowfall from the San Juan Mountains sits above the GMWL and San Luis Valley LMWL. This is expected, because as the air mass travels upward in altitude, the heavier ^{18}O isotopes of water will precipitate preferentially, leaving the higher-elevation precipitation with a relatively depleted signature (Kendall and McDonnell, 1998). While the San Juan snow line has a very similar slope to the San Luis Valley LMWL, the 'd' parameter is 12.76. The average deuterium excess for the San Luis Valley LMWL is 9.47, whereas the average deuterium excess for the

San Juan snow line is 15.42. This suggests additional fractionation processes may be taking place, and this will be explored further in the following chapter.

Over the period of this study, it was observed the San Luis Valley experiences a pattern of acid rainfall in the late summer. Rainfall acidity does not correlate to the size of the rain event. The lowest pH of 3.98 in 2015 occurred during a 1.25 mm monsoon rain event. In 2016 the lowest pH of 4.09 occurred during a 10.4 mm monsoon downpour. It was observed the most acidic rain occurs during the last week in July and first week of August. Consistent with acid rainfall chemistry, the rain samples were found to have high concentrations of nitrate and sulphate. Appreciable concentrations of phosphate, ammonium, and potassium were also present. The potential agricultural origins of some of these dissolved ions will be discussed in Chapter 8. The uncertainty present with ion chromatography analysis will be addressed in Chapter 5, in particular with respect to recharge calculations.

Perhaps more concerning than acid rain is the presence of heavy and trace metal contaminants in rainfall deposition. These heavy metal contaminants of concern include Mo, Cr, Cd, As, Pb, and the actinides U and Th. Certain elements, such as U and Th are detected at greater concentrations in lighter, dustier rain events under 1.5 mm. Small, light rains are the most frequent form of precipitation in the summer, and these are punctuated by the occasional > 10 mm downpour. While U and Th were below the limit of detection in the larger downpours, other elements, such as Mo and W were found at higher concentrations. This suggests Mo and W originate from a different source than the U and Th. More than half of the rainfall samples tested over a three-year period from 2015-2017 show the presence of U, and this represents a potential exposure pathway not previously accounted for in this area.

Examining a basin's precipitation patterns and chemistry inputs as well as establishing a reference line for meteoric water isotope signatures is an important first step in a comprehensive investigation of groundwater recharge. The following chapters of this thesis use this chapter's isotopic baselines for meteoric water as a critical reference to identify pathways of groundwater recharge, sources and shifts in

plant water use, and water movement in the unsaturated zone. Precipitation chemistry established in this chapter informs discussion on recharge pathways and is used to calculate rates of recharge in Chapter 5. Chapter 8, which discusses this study's results in a wider context, returns to the significance of a high-elevation LMWL and considers human health concerns regarding aerosolized uranium. Trace elements may also contribute to our understanding of groundwater recharge pathways, and this is considered further in the following chapters.

Chapter 5: Pathways and Rates of Recharge in the San Luis Valley

5.0 Summary

Many dryland regions around the world depend on snowmelt from surrounding mountains for aquifer recharge. Understanding how this mechanism of snowmelt-driven recharge may change over time is an important component to sustainably managing these groundwater resources. This isotope hydrology study examines precipitation, surface and groundwater in order to trace recharge pathways and estimate rates of recharge in a 21,000 km^2 high-elevation valley with > 1,000 m elevation difference between mountain pass and valley floor. 237 ground, surface, and precipitation water samples were analysed for chemistry and a subset of 127 water samples were analysed for δ^2H/ $\delta^{18}O$.

This chapter examines groundwater recharge in the San Luis Valley by selecting examples of and discussing four different recharge pathways. The most significant recharge pathway is mountain block recharge from the melting and infiltration of snow in the volcanic San Juan Mountains. This study examines San Juan mountain block recharge that replenishes confined aquifer layers in the eastern region of the San Luis Valley. Beyond this primary recharge pathway, this chapter also investigates mountain front and fractured flow from the Sangre de Cristo Mountains, lateral recharge from ephemeral creeks originating in the Sangre de Cristo Mountains, and a degree of groundwater exchange between the upper confined and unconfined aquifer layers.

This study identifies an isotopically unusual area of upper confined artesian water in the valley's sump. Though these confined aquifer wells were sampled within a 25 km^2 area, they show a 2.5 ‰ $\delta^{18}O$ spread. This old water in the valley's sump forms a distinct δ^2H/ $\delta^{18}O$ line that sits significantly above the LMWL and even above the high-elevation snow line with a mean deuterium excess of 17.59. This study presents these physical data in line with a conceptual graph and, when understood in the context of previous water

dating studies and the history of land use changes, these data suggest that a primary mechanism of groundwater recharge in the San Luis Valley may be altered through recent land use changes in the 20th century.

5.1 Chapter Questions, Aims, and Significance

The aim of this chapter is to investigate a central overarching question—what are the main pathways and rates of recharge in the San Luis Valley?

To this end, the chapter asks:

1) What do chemical and isotopic analyses tell us about groundwater in the San Luis Valley?
2) With a focus on the closed basin, what are the main pathways and rates of recharge in both the unconfined and confined aquifers?
3) Is there any indication the rates and mechanisms of recharge have changed over time?

The objectives of this chapter are to determine pathways and rates of recharge in the San Luis Valley. Because the San Luis Valley is roughly the size of Wales, specific areas were selected on which to focus, and these are considered representative of generalized pathways of recharge in the valley. This assessment is based on chemical (e.g. ions, in particular Cl^-, Na^+, Ca^{2+}, dissolved uncharged compounds such as silica, and trace metals) and isotopic (δ^2H, $\delta^{18}O$) analyses, which provide insight into recharge processes given the surrounding geology and the elevation differences between mountain pass and valley floor. Secondary data including historical groundwater fluctuations and stream flow records, nested well pump tests, and previously published chemical and isotopic studies will be used to compare, augment and support this chapter's primary data, which include 237 ground, surface, and precipitation water samples

analysed for chemistry, and 88 ground/surface water and 39 precipitation samples analysed for δ^2H and $\delta^{18}O$.

After presenting a generalized overview of chemical and isotopic signatures of groundwater in the valley, the chapter presents and discusses specific examples of different recharge mechanisms. While it has been established that the primary recharge input is from mountain block recharge in the San Juan Mountains, other recharge pathways provide significant or localized recharge, and these are important to consider. Four generalized mechanisms of recharge for the San Luis Valley are investigated using the following examples:

1. San Juan snowmelt-driven subsurface recharge to the eastern region of the valley
   (e.g. as seen through analysis of the valley's sump)
2. Sangre de Cristo mountain-front and fracture flow
   (e.g. as seen through analysis of BP-7 boundary monitoring wells at Great Sand Dunes)
3. Surface water overflow and lateral recharge from ephemeral creeks
   (e.g. as seen through BP-3 monitoring well next to Sand Creek in Great Sand Dunes)
4. Groundwater exchange between the unconfined and upper confined aquifers
   (e.g. as seen through the Closed Basin Project's nested monitoring wells)

After reviewing these main pathways and presenting rates of recharge, this chapter returns to isotopic analysis of the valley's sump. This study identifies a highly unusual pattern of isotope signatures from the upper confined aquifer at the valley's sump that plots significantly above the meteoric water line. Examples of this nature with sufficient explanation are rare to find in the literature. This study provides physical data in line with a conceptual diagram to help explain why there is isotopic depletion of this magnitude and how these results may indicate the primary recharge pathway for the San Luis Valley is changing over time.

5.2 Introduction: Physical Setting and Hydrogeology

The San Luis Valley is a 21,000 km^2 high elevation desert located in southcentral Colorado. In the central part of the valley floor, annual precipitation is 170-200 mm, but at the valley margins, closer to the

mountain ranges, precipitation increases to just under 250 mm/yr. Precipitation in the mountains, mostly in the form of snowfall, averages 1,000 mm/yr. The average elevation of the valley floor is 2,347 m above mean sea level, and natural flow direction is from west to east. While surface runoff and baseflow in the southern part of the valley drain into the Rio Grande, surface and groundwater in the northcentral and northeastern part of the valley drain into a closed basin. The valley, whose basin was in part formed by and encompasses the northern section of the Rio Grande Rift, is enclosed by mountain ranges to the east and west. Elevations of the tallest mountain peaks on either side of the valley reach 4,270 m.

The Sangre de Cristo Mountains to the east are a long chain of fault block mountains at the southern extent of the Rockies. Overall, the Sangre de Cristo Mountains are composed of Precambrian gneiss with large granite plutons, gabbro dikes (rich in Fe and Mg), and pegmatite (Lindsey, 2010b). Faults are found along the western front of the Sangre, notably through the western portion of Great Sand Dunes National Park and Preserve, and south along the Rio Grande Rift. On the valley's western side is the San Juan Mountain Range. These mountains are composed of volcanic rock and sandstone. A series of volcanic eruptions created multiple layers to the San Juans beginning with lavas and breccias followed by silica ash-flow tuffs, ending with basalt flows and rhyolite (Lipman et al., 1970). The San Juan volcanic field includes over 25 extinct calderas (Valdez, 2017).

Snowmelt from the San Juan Mountains contribute to two international rivers; snowmelt from the western slopes drain into tributaries of the Colorado River; snowmelt from the eastern slopes form the Rio Grande. The San Juan Mountains are responsible for the majority of aquifer recharge to the San Luis Valley, mainly through mountain block/underflow recharge (Mayo et al., 2007). Mountain snowpack is vital to the valley's hydrology, and every year, hydrological forecasts and irrigation decisions are made based on predictions for the accumulation and timed melting of snow, especially snow in the San Juan Mountains. One of the largest, most prominent peaks in the Sangre de Cristo Mountains is called Mount Blanca, named for what was, until recently, a year-round covering of snow.

Groundwater flowpaths and chemistry in the San Luis Valley may be understood by examining the predominantly volcanic/volcanoclastic rocks of the San Juans, the less permeable Paleozoic sediment and Precambrian crystalline basement of the Sangre de Cristos, and the Quaternary alluvium of the valley floor. It is also necessary to understand baseflow from the San Juans, and mountain front flow from the Sangre de Cristo drain in the northern part of the valley toward a depression known as the sump. This part of the valley is a hydrologically closed basin because this groundwater does not drain toward the river to the south. Historically, groundwater from the closed basin provided water for surface wetland playas that appeared across the entire northern/northeastern valley landscape. The sump, which is outlined in Figure 5.1, includes the valley's water-elevation low. The mostly volcanic San Juan Mountain range is shown in the west, the valley floor is basin-fill, and the mostly granitic Sangre de Cristo Mountains are shown as metamorphic or intrusive igneous. For a more detailed geologic map, please refer to Figure 2.3.

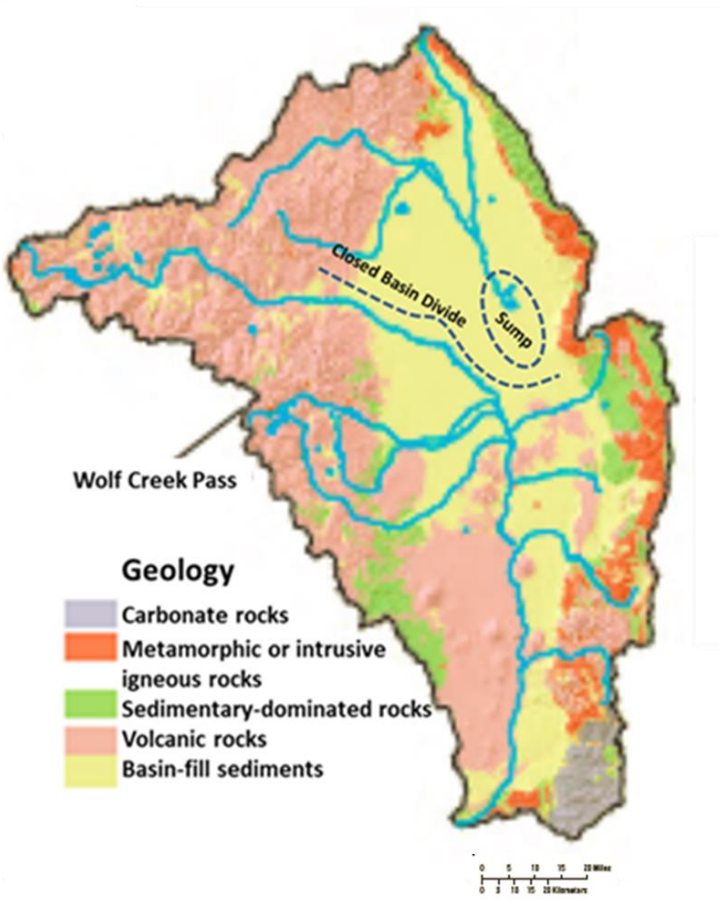


Figure 5.1: Simplified geologic map of the San Luis Valley. Modified from Bexfield and Anderholm 2010.

5.3 Methods

The majority of groundwater samples were collected from the northern half of the valley's closed basin watershed, which does not drain into the Rio Grande. Groundwater boundary distinctions are made between the unconfined and the confined aquifer, which exists below an Alamosa series clay layer. Samples from the confined aquifer were further divided by depth: the shallow layer is defined as < 274 m and called the upper active confined; the layer below 274 m is called the lower active confined. Most of the sampling took place on federal as opposed to privately-owned land owing to private property restrictions and the ease of using established, pre-existing monitoring networks.

This chapter relies on 237 water samples collected at key source locations and groundwater depths across every season between summer 2014 and winter 2017 in the San Luis Valley, an area just over 20,000 km^2. The analysis in this chapter utilizes analysis from the previous chapter of 117 precipitation samples from 2015, 2016, and 2017 for both a chemical input baseline and for a LMWL reference. A subset of 39 rain samples from the best-precision ion chromatography Dionex run (LOQ = 0.07 mg/L Cl) was used for the weighted precipitation value (0.26 mg/L Cl input) to calculate rates of recharge based on the Chloride Mass Balance (CMB) technique. Over 120 surface and groundwater samples collected from major creeks and rivers arising in both the San Juan Mountains and the Sangre de Cristo mountains and from the confined and unconfined aquifers from locations across the valley floor were analysed for basic chemistry, and a subset of 88 groundwater and surface water references were analysed using the University of Wyoming's Picarro L2130-I Cavity Ring Down Spectroscopy (CRDS) for δ^2H and $\delta^{18}O$ ‰ relative to VSMOW. *In situ* measurements included temperature, pH, EC, TDS. HCO_3 was calculated using a Hach digital titrator while Fe, Se, and Si were analysed using an Atomic Absorption Spectrometer (AAS). Sampling locations were marked using a Garmin GPS, and all non-artesian groundwater was purged for roughly 20 minutes before sampling.

Chloride mass balance was used alongside anion/cation analysis, detection of silicate weathering or Ca^{2+}, HCO_3^- water types, physical fluctuations in historical groundwater data collected across the San Luis

Valley and the closed basin region in particular, and δ^2H, $\delta^{18}O$ analysis of water samples to investigate pathways and rates of recharge in the San Luis Valley. Care was taken to avoid recharge estimates using CMB in areas deemed inappropriate for the method, and artificially managed areas were avoided or noted as such and used only for reference.

For further detail on the methodology of this chapter, the field and laboratory methods used herein, and the method limitations and uncertainties present, please refer to Chapter 3.

5.4 Location, Groundwater Layers and Depths

Because the San Luis Valley includes a large area, sampling focussed on key locations. Source waters from the margins of the San Luis Valley were sampled and serve as important chemical and isotopic references, but most of the groundwater sampling occurred in the closed basin area, outlined for reference in Figure 5.2. This is the northern section of the San Luis Valley where groundwater flows away from the Rio Grande and toward a terminal sump. Focusing on this region of the valley's groundwater served two purposes. The primary purpose was to examine groundwater flowpaths to the older water in the sump. The other reason to concentrate sampling away from the Rio Grande was to avoid artificial input from irrigation. It was also easier to sample on federal lands rather than on private property such as the agricultural areas in the western part of the valley. Figure 5.2 illustrates the direction of groundwater flow toward the ancestral sump. Sampling locations are indicated on the map, and they are divided into surface water samples and groundwater samples from the unconfined and confined aquifers. Surface water samples include Rio Grande water in the San Juan Mountains and the valley floor and many of the smaller mountain creeks originating from the Sangre de Cristo Mountain Range. These include Sand Creek, Medano Creek, Big Spring, Little Spring, and Crestone creeks within and north of Great Sand Dunes National Park. Sampling covered a large area. Samples were taken from within 5 of the 6 counties of Colorado that form the San Luis Valley.

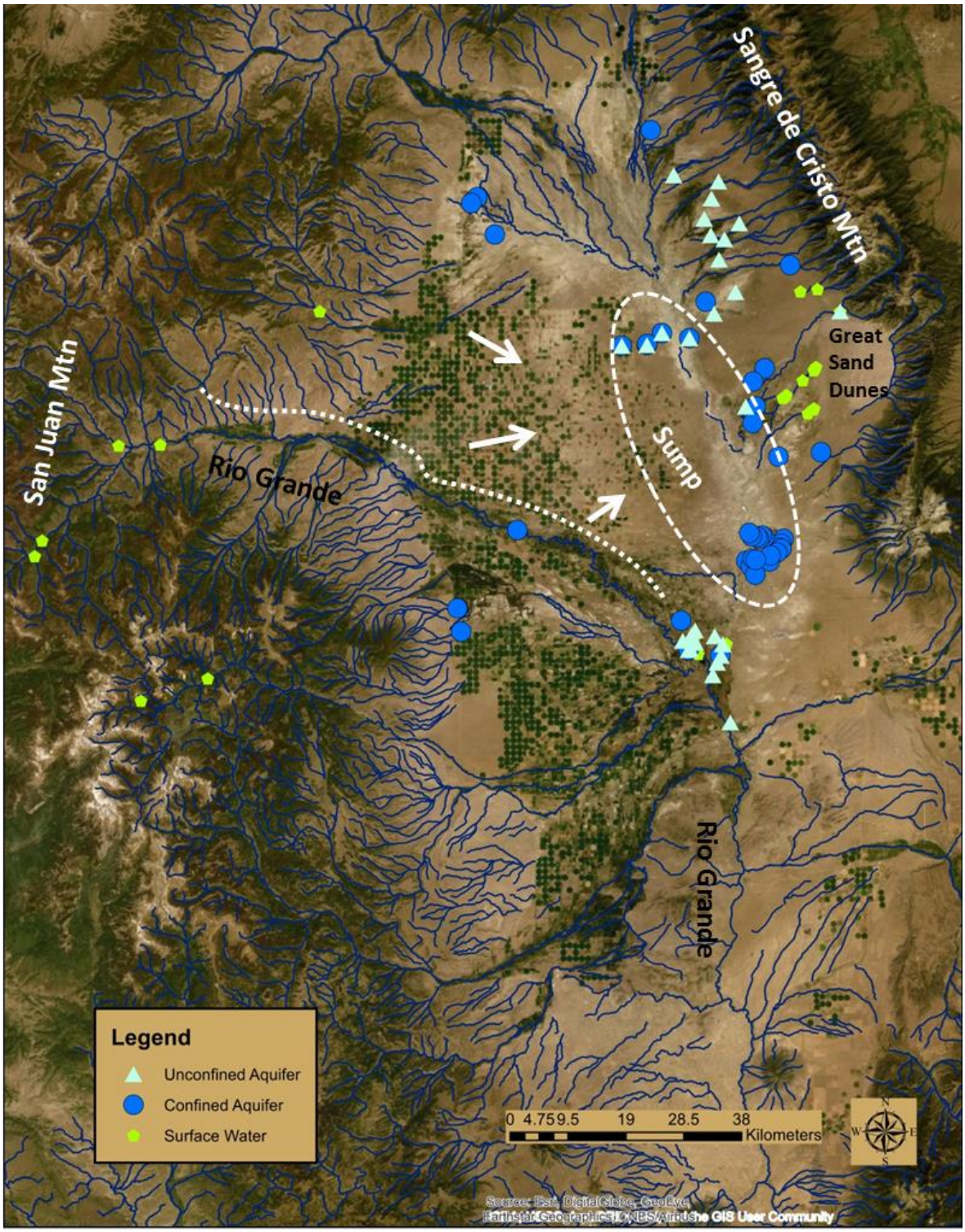


Figure 5.2: Surface water (green hexagon) and groundwater sampled from the unconfined aquifer (light blue triangle) and confined aquifer (blue circle) are shown. Multiple samples in close proximity may be obscured by a single marker. Confined aquifer samples are both upper and lower active confined. Groundwater flow direction is indicated with white arrows and the ancestral sump is circled in white.

Groundwater sampled from the San Luis Valley may be grouped into water taken from the unconfined, upper confined, and lower active confined regions of the aquifer system. The groundwater analyzed in this study was sampled at a depth range of 5-610 m. Water sampled from the valley's margins may, in areas close to the mountain base, extend 100 m or more in depth (McCalpin, 2018). While water from these regions may be on a flowpath leading toward saturated parts of the upper confined aquifer, if this groundwater is not saturated, under pressure, or exposed to reducing conditions, it is classified as unconfined (Hiscock, 2005, Robinson and Ward, 2017, Simmers, 1997). Samples taken from beneath the Alamosa series clay layer are classified as confined. Samples taken from within a pressurized aquiclude are also called confined. The confined aquifer in the San Luis Valley can be further subdivided. Confined aquifer distinctions reflect an evolving study of the San Luis Valley Basin's lithology, hydrology, and geochemistry from early USGS studies (Siebenthal, 1910, Emery, 1971b) and others (Huntley, 1979) that made no distinction between confined waters, to confined aquifer distinctions of active and passive (Hanna and Harmon, 1989) to upper and lower active versus passive (Mayo and Christiansen, 2004). All studies place the confined aquifer layers at depths of roughly 60 m to 4500 m, and an important distinction between active and the inactive/passive is located at roughly 1200 m. None of this study's samples were taken at depths exceeding 1200 m. Previous chemical and isotopic work (Mayo et al., 2007) has placed the upper and lower active boundary distinction at 300 m. However, if chemical and isotope analysis is used to distinguish differences in these boundary layers, the "upper active confined" (sometimes referred to simply as the "upper confined") and "lower active confined" (shortened herein as "lower confined") distinctions would vary based on site-specific hydrogeochemistry. After analyzing the groundwater collected for this study, and noting the severe depletion of a sample drawing from a depth of 244 m and noting this sample has more in common—chemically and isotopically—with other lower active groundwater samples, the author has decided to adjust the theoretical boundary between upper and

lower active confined. In an effort to balance the need for consistency with the spread of groundwater sampled for this study, this author designates the upper/lower active divide at 274 m.

A series of Colorado Water Court rulings (2008) and rising tensions around the appropriation of water resources in the San Luis Valley have prompted further classification of the valley's aquifer systems. Colorado State's Rio Grande Decision Support System (RGDSS), developed for water managers and the State to measure and reduce or mitigate negative impacts to surface water rights holders according to Western US water law, to help fulfill southern Colorado's surface water obligations under the Rio Grande Compact (Riverside Technology et al., 1998), and to maintain hydraulic head in the confined aquifer within the range measured between the years 1978-2000 (Reeves et al., 2014, Chen et al., 2017), relies on 5 MODFLOW boundary layers. These layers divide the valley into a 15-30 m unconfined layer 1, an aquitard layer 2, and a depth-divided confined layers 3-5. Aware that these distinctions exist, but also aware that these model distinctions were created to define boundaries of influence with legal implications, this study will refer to groundwater simply as unconfined, upper confined, and lower (active) confined, sampled at depths > 274 m. When chemistry and isotopic analysis includes groundwater sampled from depths including the upper and lower confined aquifer layers, a distinction may only be drawn between the unconfined and confined (upper and lower active) aquifers. Figure 5.3 shows wells sampled in the valley's ancestral sump that draw water from a wide range of depths. The state's groundwater model distinctions are shown labeled as Layer 1 through 4. Also shown are depths for the Alamosa series clay layer beneath the unconfined aquifer boundary, and the depth distinction between the upper and lower (active) confined layers.

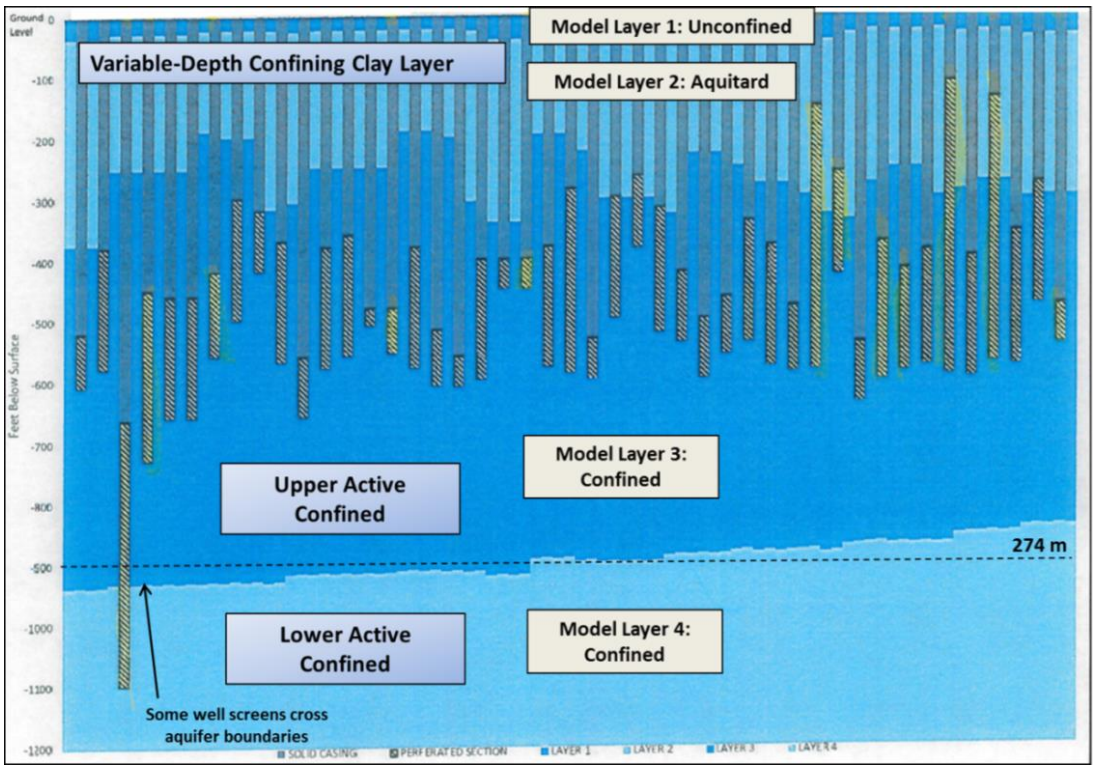


Figure 5.3: Groundwater layer distinctions and depths used by the state groundwater model versus those used in this and previous studies based on general chemistry distinctions.

5.5 Groundwater Chemistry

5.5.1 Chemistry Overview

Water chemistry is useful in understanding flowpaths, residence time, sources and rates of recharge. Major ion and trace element chemistry was analysed for snowmelt-fed creeks and rivers in the mountains, from surface water playas and irrigation canals, and from groundwater sampled at depths ranging from 5 to 610 m. Early studies on groundwater in the San Luis Valley have found that both unconfined and confined aquifer water as type Ca—HCO_3 at the valley's margins evolves toward the valley's closed basin as type Na⁻HCO_3, Na—SO_4, and Na—Cl for unconfined water and toward type Na—HCO_3 in the confined aquifer (Huntley, 1976, Huntley, 1979). While these water types are still found to be dominant

and the flow direction the same, newer ideas have developed (and continue to do so) about how the valley's old water has evolved into what it is given potential influence from ancient Lake Alamosa's organic-rich sediment (Mayo et al., 2007), potential interaction with gases from methanogenesis, and the extent and movement of the clay layers.

Figure 5.4 presents an overview of this study's groundwater chemistry results from the San Luis Valley. These results are derived from 57 groundwater samples from different layers of the aquifer. The San Luis Valley's groundwater samples have been divided into unconfined, upper (active) confined, and lower (active) confined. The orange triangles show the unconfined aquifer samples. The green boxes display samples from the upper confined aquifer, and the yellow circles represent the deepest samples from the lower active confined. This graph shows a clear separation between the unconfined and the confined aquifer chemistry, with some notable exceptions, especially from unconfined aquifer samples taken at the valley's eastern margin, at the base of the Sangre de Cristos. Samples from the upper confined typically cluster in different water facies as do those from the lower confined. On the cation plot, all of the samples are lower in magnesium and high in calcium or sodium/potassium. Only three of the unconfined samples (and the majority of upper confined samples) fall within the latter affiliation. On the anion plot, only a few unconfined aquifer samples contain high concentrations of sulphate. Samples are generally low in nitrate and chloride, but the unconfined aquifer samples have higher concentrations of these anions. While some of the unconfined aquifer samples are lower in bicarbonate than in sulphate, the majority of samples are dominated by bicarbonate anions. Overall, these results show Ca^{2+}/Mg^{2+}-HCO_3^- to Ca^{2+}-HCO_3^- water types for lower confined and unconfined groundwater. Upper confined samples appear predominantly in the Na^+/K^+--HCO_3^- water type. Roughly 1/3 of the unconfined samples appear to be Ca^{2+}/Mg^{2+}--Cl^-/SO_4^{2-} water type. As expected, the samples with the highest TDS concentrations are in the unconfined aquifer.

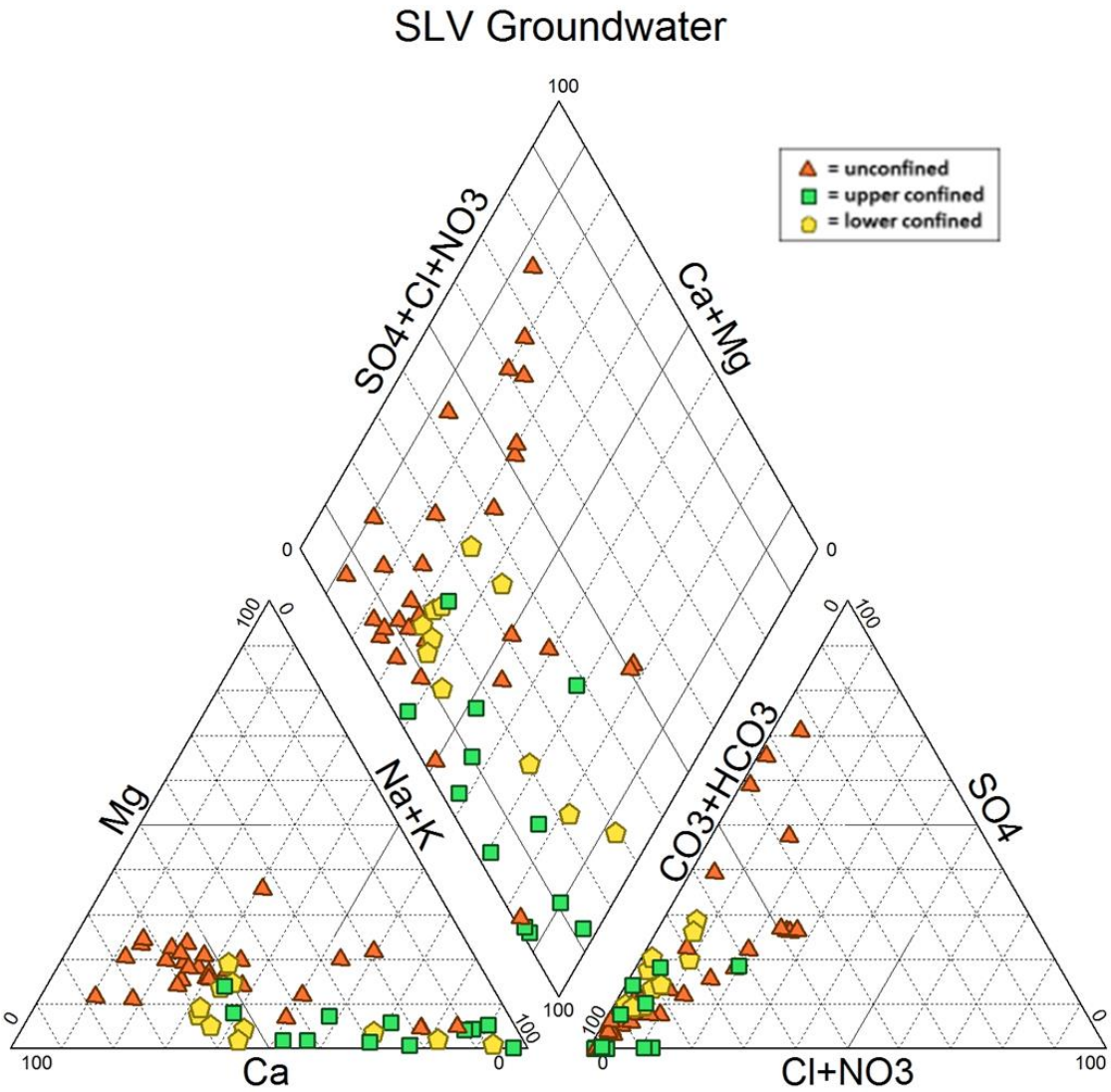


Figure 5.4: Chemical facies of 57 groundwater samples from across the San Luis Valley (excluding the closed basin, low-elevation sump). Unconfined samples are shown as orange triangles while samples from the upper confined and lower confined are shown in green and yellow respectively.

Because mountain block recharge (note, mountain block and mountain front recharge are lumped together here for practical purposes, with an argument similar to that of Wilson and Guan (2004)) from the San Juan Mountains is understood to be the primary source of recharge to the unconfined aquifer—even in the eastern region of the valley, it was considered advantageous to examine silicate weathering of volcanic

rocks in an attempt to differentiate groundwater flowing through the San Juans versus the Sangre de Cristo. Figure 5.5 shows a chemical grouping and separation of wells by aquifer layer—unconfined, upper confined, and lower active confined using sulphate, silicate, and bicarbonate as axis. As expected, only unconfined water samples show a high percent SO_4. The upper confined samples showing the greatest concentrations of silicate also show a high percent bicarbonate. On the other hand, the grouping of deeper wells in the lower active confined layer show a lower concentration of bicarbonate.

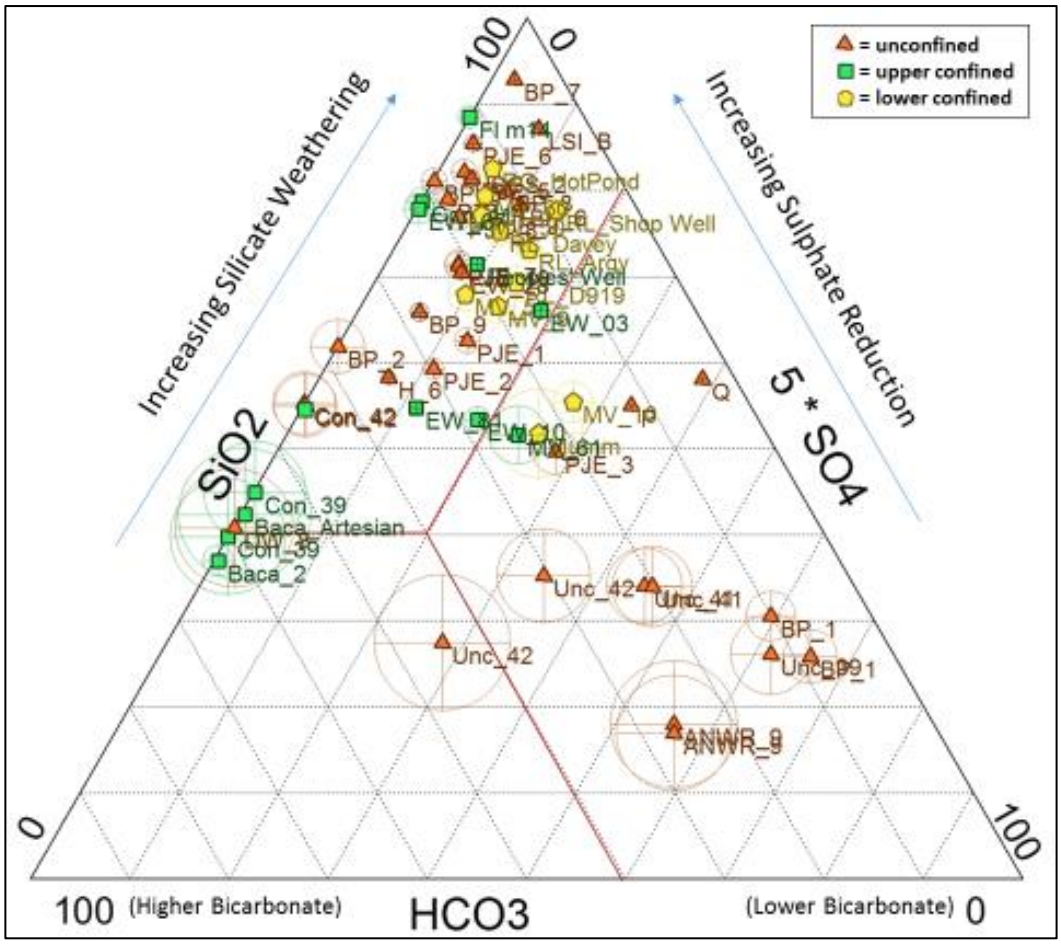


Figure 5.5: Tertiary diagram showing silicate weathering in 57 groundwater samples from across the valley. Relative TDS concentrations shown as crosshair circles, with a 34—608 mg/L range and a mean of 155 mg/L. Summaries of all chemistry data are provided in Appendix 5.

Figure 5.5 differentiates groundwater samples based on their concentration of silicate (SiO_2). When dissolved silica is found in water with HCO_3 as is the case with Ca^{2+}--HCO_3^- to Na^+--HCO_3^- facies, this likely occurs from weathering of feldspar in silicate landscapes as anorthite and alkali feldspars produce clay. Figure 5.6 shows chemical reactions and pH-dependent processes of anorthite feldspar weathering. Feldspar is found throughout the San Juan Mountains but has also been spread through erosion and fluvial/aeolian deposits across the valley floor.

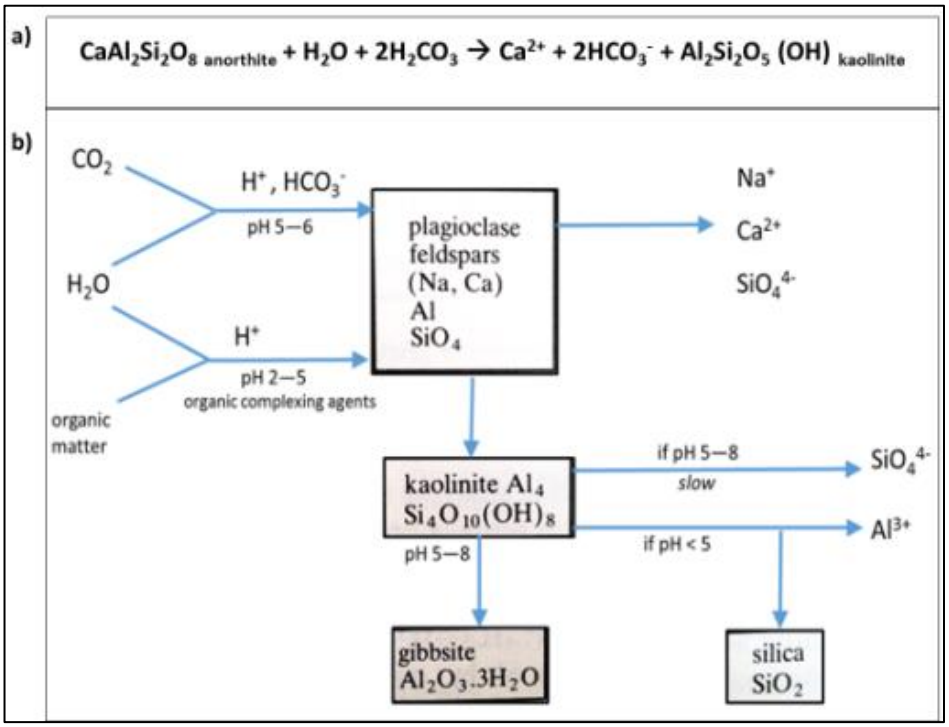


Figure 5.6: Example silicate weathering reactions. Diagram from Mayo et al. 2007.

There are many silicate weathering reactions. In some silicate weathering reactions, weathering of ferromagnesian minerals (e.g. pyroxene) produces iron hydroxide. While a couple of groundwater samples were found to have Fe from AAS analysis, with some Fe concentrations (DW8 well) as high as 1.2 mg/l, not all samples were acidified and run on AAS (discussed in Chapter 3 limitations). Additionally, Fe precipitated out of some of the samples run on AAS, reducing confidence that the AAS

readings were properly quantifying Fe. Fe and Al hydroxides have very low solubilities, so it's not expected these elements appear in drainage water samples. Silica does have high solubility, so dissolved Si is the primary indication of silicate weathering reactions (The AAS does not distinguish between H_2SiO_4, SiO_2, etc. The pH of the tested water samples suggests SiO_4^{-4} is likely). Acid rain (see Chapter 4) plays a strong role in silicate weathering, and the degree of weathering can be evidenced, in part, by the transition of pH in snow, rain, and soil water to an alkaline groundwater solution. Between pH 5-9, silicon is more soluble in water and will leave behind Al and Fe oxides. This changes at pH < 5, where the Al (and Fe) become more soluble.

The right-hand axis of the ternary diagram in Figure 5.5 shows sulphate ranges. The lower confined samples are more likely to be in reducing conditions, and as this water is sourced from the San Juan Mountains, it shows signs of silicate weathering. An anomaly to the assumption that deep, closed system wells experience sulphate reduction is the Great Sand Dunes Park boundary well, BP-7. BP-7 is an unconfined well located in the northern third of the park's western boundary (discussed later in this chapter). Water from this well is extracted from a screen placed at about 90 m deep.

Many of the San Luis Valley samples have high HCO_3^-. While bicarbonate is most readily associated with carbonate aquifers such as limestone and chalk, high bicarbonate concentrations may be produced in open system weathering of basalt where carbonic acid is also present. The chemistry of confined well 42 (Con_42) shows a greater concentration of Si, which indicates its source of water undergoes increased silicate weathering. These data, in combination with this well's isotope signature, indicate this well is recharged predominantly through snowmelt in the San Juan Mountains. Because this well is located in the eastern half of the valley and is surrounded by wells whose isotope and chemical signatures more closely resemble snowmelt streams from the Sangre de Cristo Mountains, it is reasonable to consider an underflow pathway of San Juan mountain block recharge.

In addition to examining the major ion chemistry of waters, trace element analysis was also conducted on a subset of water samples. Trace elements may, in some cases, be used to identify potential water sources and areas of water-rock interaction. Analysis results from a limited number of deep groundwater samples show distinct heavy metal profiles. Mercury was only found at one site, from thermal groundwater extracted at a depth of 610 m. Samples from this source averaged 0.6 μg/L Hg, 1 μg/L Pb, 56 μg/L As, 38 μg/L Mo, 83 μg/L W, 3 μg/L U, 2 μg/L Th, and 0.1 μg/L Tl.

Because they serve as useful reference points, surface water from the San Juan Mountains was analysed. Winter samples from the Rio Grande upstream of Del Norte show low levels (~0.2 μg/L) of lead, cadmium, molybdenum, and cobalt, as well as 0.4 μg/L arsenic, 0.04 μg/L uranium, and 4 pg/L rhenium. No tungsten or thorium was found. Similar results were found for La Garita Creek with the exception of high (~200 μg/L) iron in La Garita and high (~150 μg/L) manganese and zinc in the Rio Grande. While both sources showed 0.1 μg/L chromium, only the Rio Grande samples had cadmium. During the same winter days, samples from the Closed Basin Canal sampled prior to its joining of the Rio Grande averaged 1μg/L tungsten, 0.02 μg/L rhenium, 0.05 μg/L lead, 0.07 μg/L cadmium, 0.35 μg/L chromium, 1.5 μg/L uranium, 6 μg/L molybdenum, 4.5 μg/L vanadium and manganese, 8 μg/L iron, and 1.7 μg/L arsenic. Despite the existence of legacy mines in the San Juan Mountains, the higher concentrations of tungsten, uranium, and molybdenum sampled from the Closed Basin Canal are consistent with this surface water being sourced from a spread of unconfined aquifer wells in the closed basin region of the valley that includes the sump.

5.5.2 Water Chemistry at the Closed Basin Sump

The playa wetlands in the valley's ancestral sump serve as the outlet for regional baseflow, for natural springs and artesian wells. The wetland playas would, historically, also receive seasonal input from the surrounding snow-fed creeks, namely Saguache Creek to the northwest and Sand Creek, Big Spring

Creek, and Little Spring Creek to the east when these creeks flushed the playas or flooded San Luis Lake, which in turn overflowed and supplied the playas. However, due to agricultural diversions and increased water use, this network of creeks no longer overflow to replenish the valley's playa system (Valdez, 2016). As a result, many of the playas have dried up. This explains why those that remain have highly concentrated nutrients, heavy metals, and salinity high enough to be considered saline. The sump area is also highly alkaline, as is much of the surrounding groundwater. The playas in the valley's sump have a mean pH 9, with total alkalinity averaging 4.2 g/L. Playa water sampled in 2011 (Lucero, 2016b, Tedela, 2019) show mean concentrations of 35 g/L Cl, 28 g/L SO_4, 32 g/L Na, 2 g/L K, 76 mg/L Ca, 34 mg/L F, and 240 μg/L U. In contrast, this study found the artesian wells located within the playa system of the sump (many of these wells now provide water for the managed playas), to contain mean concentrations of only 1 mg/L Cl, 6.5 mg/L SO_4, 331 mg/L Na, 0.13 mg/L NO_3, 11.5 mg/L Ca, and 0.9 mg/L F. Artesian wells sampled in the sump show no phosphate or magnesium. Potassium < 2 mg/L.

The Closed Basin Canal (marked in red in Figure 5.2, refer to Chapter 2 for detail) draws groundwater from ~170 unconfined wells in the closed basin to augment Colorado's annual water deliveries on the Rio Grande. Along the way, it delivers augmentation water in the spring to a portion of the BLM's federally managed wetland playas in the sump. Some of the playa wetlands therefore now reflect the chemistry of combined unconfined aquifer pumping from the closed basin (rather than baseflow and mountain creek overflow) and artesian input from long-screen wells (Figure 5.3) beneath the playas. Under past, natural conditions, the playas would have been flushed every year from seasonal creek flooding and overflow, and they would have remained wet year-round. Secondary data of seasonal sampling of the playas in May and August (not shown) shows the concentration of major ions and heavy metals within a single season due to surface water evaporation. The TDS of surface playas reaches brine water concentrations.

Figure 5.7 shows major ion chemistry of sampled playas (marked in red) versus the confined groundwater beneath these playas (marked in blue). Figure 5.7 shows trace element analysis of the (a) same playa surface water versus the (b) confined water beneath. In Figure 5.7, the upper confined groundwater shows

an evolution of Ca^{2+}--HCO_3^-- to Na^+/K^+--HCO_3^-. The confined aquifer sample that extends into the lower active confined layer is type Na^+/K^+--HCO_3^-. The playa surface water becomes more saline in late summer, reflected in the Na^+--SO_4^-/Na^+--Cl^- type.

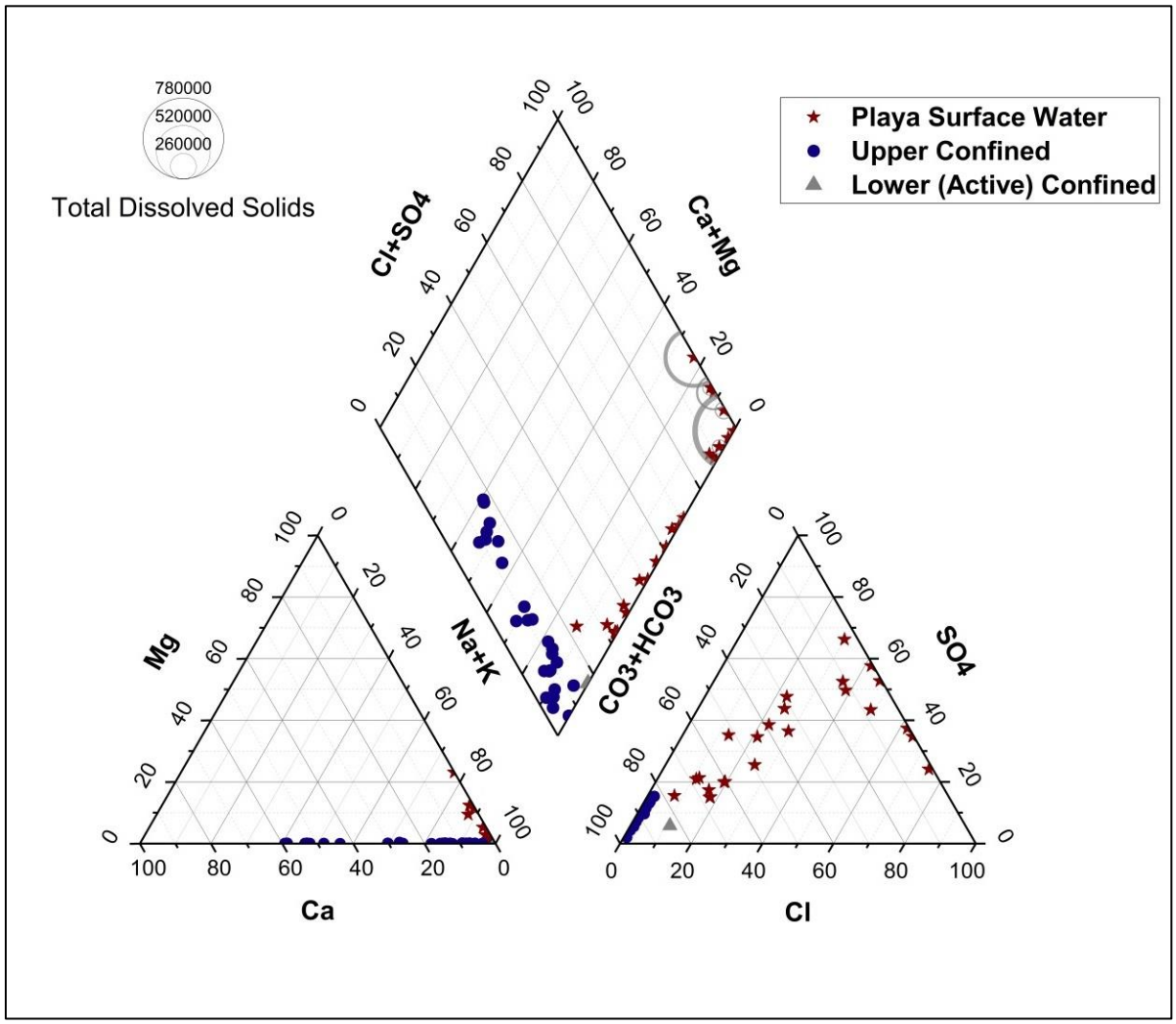


Figure 5.7: Chemical facies of water sampled in the closed basin ancestral sump with surface playa water in red and confined water beneath the playa in blue and grey.

Chemistry analysis of trace elements and heavy metals in the sump's surface water playas versus the artesian groundwater immediately beneath the playas is shown in Figure 5.8. While many of the elements are highly concentrated in the playas, it is worth drawing attention to the high levels of selenium, reaching 3 g/L in one playa, and uranium, reaching 3.5 mg/L. Other concentration highs include 4.4 mg/L Mo, 2.1 mg/L Cr, 39 ug/L Cd, 43 ug/L Be.

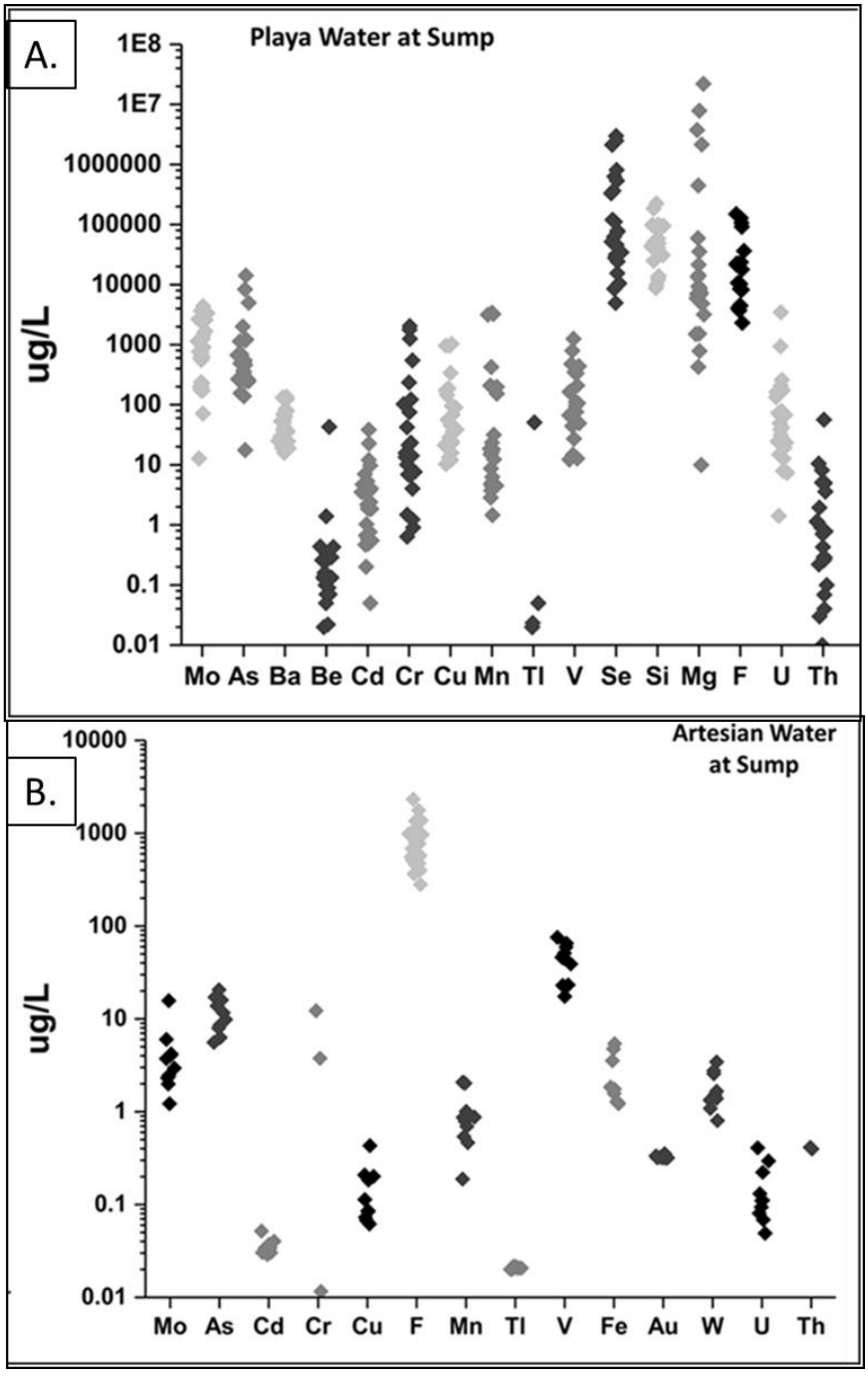


Figure 5.8: Heavy metal analysis of sump water. (A) surface playa water, raw data curtesy of Tedela, 2019. (B) Confined groundwater sampled from directly beneath the playas and analyzed as part of this study.

5.6 Groundwater Isotopes in the San Luis Valley

5.6.1 Signatures by Aquifer Layer

Groundwater isotope analysis (δ^2H, $\delta^{18}O$) was conducted on a subset of groundwater sampled from the San Luis Valley. These include 23 unconfined, 48 upper confined, and 11 lower active confined aquifer samples. The δ^2H range for all groundwater samples is -87.57 to -123.32 ‰, and the $\delta^{18}O$ range is -12.83 -17.38 ‰ if the one outlier from the unconfined aquifer (-84.38, -10.40) receiving significant recharge from a surface water playa and shown in Figure 5.9(b) along the evaporation trajectory is not considered. This study found the greatest $\delta^{18}O$ range occurs in the upper confined aquifer. The upper confined aquifer samples reveal a 4.55 ‰ range in $\delta^{18}O$, and this is an even greater range than the unconfined aquifer group if it retained the evaporated outlier.

Figure 5.9 shows groundwater samples from the San Luis Valley plotted for comparison between a 2007 study (Mayo et al. 2007) that examined isotope values from the unconfined, upper confined, and lower active confined aquifers using the Global Meteoric Water Line (GMWL) and this study of groundwater samples using the newly established LMWL and a San Juan high elevation snow line for comparison. This study's findings differ from the Mayo et al. study findings on two important counts. The first, as mentioned earlier, is that this study found the greatest $\delta^{18}O$ variation in the upper confined aquifer samples. This analysis would change, however, if the boundary between the upper confined aquifer and the lower active confined were shifted slightly. Regardless of where this depth boundary lies in the confined aquifer, in the unconfined aquifer, this study did not find such a dramatic spread of isotope values. Another significant difference between these studies is the mean value for the upper confined aquifer samples. Despite the range of unconfined aquifer values in Figure 5.9(a), both studies show similarity in the mean unconfined aquifer value. The difference in mean values for the lower active confined aquifer may owe to some extent to differences in the geographic areas sampled (closed basin or not, influence from San Juan versus Sangre de Cristo recharge), different recharge mixing ratios, and the slight difference in boundary designation (300 versus 274 m). The most striking difference between the

results of this study and of Mayo et al. 2007 study is that in Figure 5.8(b), the upper confined samples average a value that sits above the LMWL and GMWL. Because a high-elevation snow line was also established as part of this study, it's clear the primary recharge mechanism and pathway for these samples is mountain block recharge at high elevation.

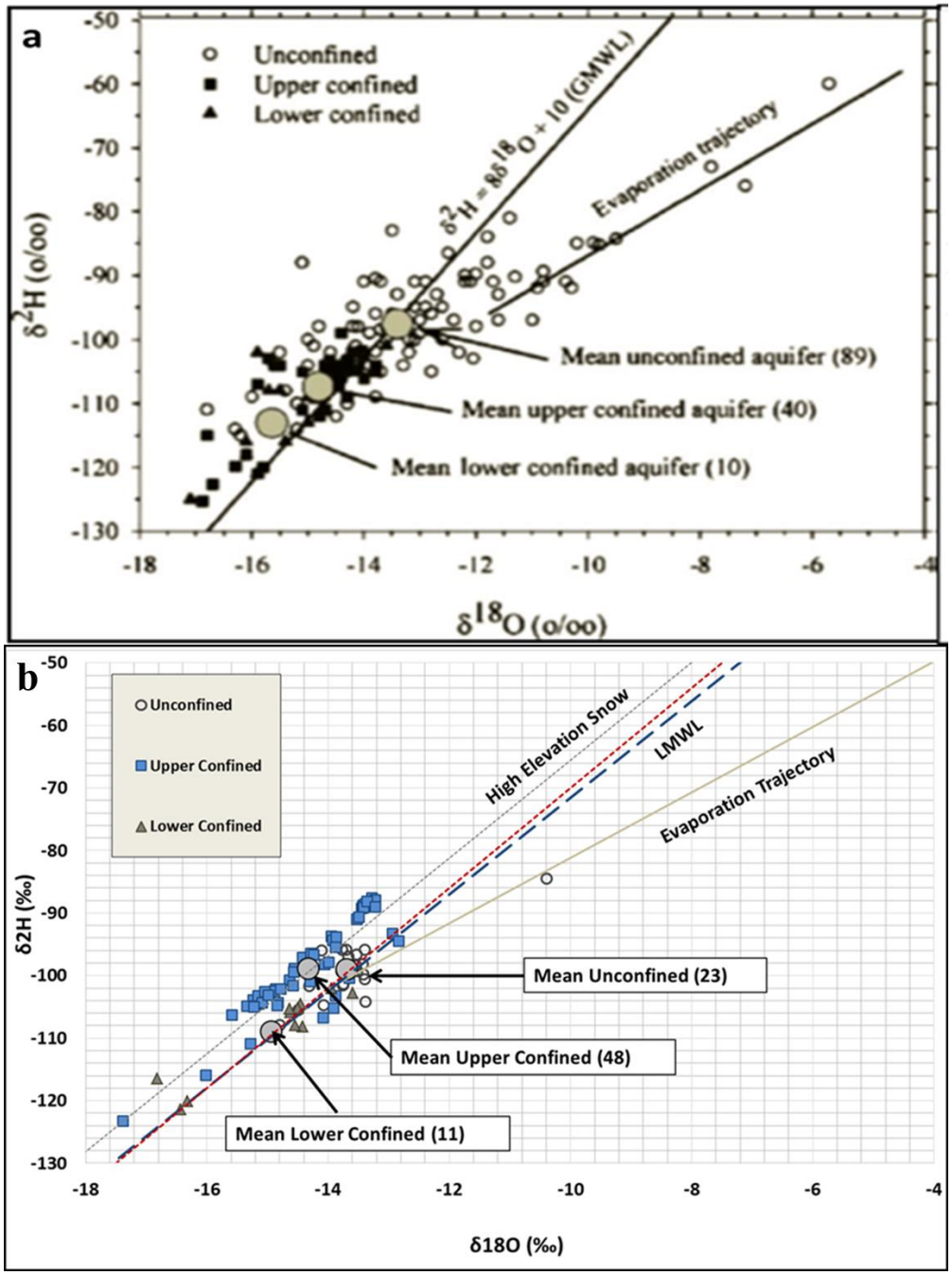


Figure 5.9: A. Previous work from Mayo et al. (2006) shows groundwater isotope signatures for unconfined, upper confined, and lower active confined aquifers in the San Luis Valley (using the GMWL for reference). B. This study analyzed groundwater in similar groupings and applied a valley-floor LMWL and high-elevation LMWL for reference. (GMWL shown in red for reference.) These lines indicate mechanism and elevation of groundwater recharge.

When analyzing isotope values for all unconfined, upper confined, and lower active confined wells in the San Luis Valley, broad generalizations can be drawn about each aquifer layer by examining differences in the linear regression lines formed on a $\delta^2H/\delta^{18}O$ plot. Although the linear regressions for each groundwater classification (unconfined, upper confined, and lower active confined) are not displayed in Figure 5.9(b), their equations are presented below as Eq. 5.1, Eq. 5.2, and Eq. 5.3. And, though the unconfined samples vary considerably, the linear regression (read with a note of caution—R^2=0.61) shown in Equation 5.1 has a slope and intercept suggesting a high degree of fractionation from evaporation. A high rate of evaporation in the unconfined layers sampled is consistent with a high water table in some areas that lose water through capillary fringe, and in a few cases, groundwater that is recharged by playa lakes (as is thought to be the case with the outlier in Figure 5.9), by small discharge creeks, and by diverted surface irrigation water that is exposed to evaporative loss along canals. For example, the unconfined sample outlier positioned on the evaporation trajectory in Figure 5.9(b) is from a shallow unconfined well drilled next to a surface water playa. The electrical conductivity and Cl^- concentrations can be an order of magnitude higher in the unconfined aquifer than in the confined aquifer. The difference between equations for the upper confined (shown as Equation 5.2, R^2 = 0.80) and lower active confined layers (Equation 5.3, R^2 = 0.89) suggest differences in recharge pathways, and this, alongside chemistry differences suggests different avenues of mountain front recharge in the San Juan Mountains versus the Sangre de Cristo Mountains. The mean upper confined aquifer value shown in Figure 5.9(b) sits near the high-elevation San Juan snow line, suggesting the San Juan contributes significant water which infiltrates directly at a high elevation. The slope (Eq. 5.2) for this same group of upper confined samples is closer to the LMWL while the d-parameter is closer to that of high-elevation snow. This suggests that water in the upper confined aquifer is not subjected to evaporation the way that water in the lower active confined aquifer (Eq. 5.3) might have been as it traveled along a recharge pathway. Less exposure to evaporation would be consistent with immediate recharge occurring at high

elevations. Of course, generalizations about the aquifer layers are limited by and biased toward the geographic sampling areas. For example, on the eastern margin of the valley, close to where some of these wells were sampled, mountain front recharge at the base of the Sangre de Cristo Mountains may travel from the unconfined aquifer (absent a confining clay layer) to depths > 274 m where it travels toward and joins the lower active confined layer.

$$\delta D = 4.4384\ ^{18}O - 38.407 \quad \text{[Eq. 5.1]}$$

$$\delta D = 7.6794\ ^{18}O + 10.965 \quad \text{[Eq. 5.2]}$$

$$\delta D = 6.0599\ ^{18}O - 18.599 \quad \text{[Eq. 5.3]}$$

5.6.2 Primary Pathways and Rates of Recharge in the Closed Basin Sump

Isotopic data, when combined with basic chemistry, reveal more than sources of recharge. Information on the groundwater's source can be examined alongside the groundwater's long-term mean rate of recharge. This study suggests the majority of upper confined water samples taken from the valley's sump are recharged through a high-elevation pathway in the San Juan Mountains. Their mean rate of recharge, based on chloride mass balance estimates, is 35 mm/yr.

It is sometimes informative to examine the spread of $\delta^{18}O$ by Cl concentration or EC. It may also be valuable to investigate if there is any impact from temperature variation on $\delta^{18}O$ since temperature exerts a control on ^{18}O fractionation. The $\delta^{18}O$ spread of the 26 confined groundwater samples from the valley's sump is shown in these manners in Figure 5.9. The figure shows end members clustering at -13.2 to -13.6 and -15.1 to -15.5 ‰. The less negative $\delta^{18}O$ end members cluster around a low electrical conductivity value, seen in Figure 5.9(a). These values sit closer to the San Juan Creek isotope signals that were sampled summer and winter 2015-2017. It should be noted that Figure 5.10(a) shows the range and mean isotope signals for creeks that originate in each of the mountain ranges but that isotope signals from individual snow storms offer a much broader range of $\delta^{18}O$ signals based strongly on source vapor

temperature. One significant difficulty in analyzing sump groundwater samples for correlations between chemistry, temperature, and $\delta^{18}O$ range is that most of these wells were drilled with long screen openings and draw from groundwater at more than one depth of the confined aquifer (see Figure 5.3). Although water temperature generally increases with depth, the $\delta^{18}O$ signals of sump groundwater and San Luis Valley confined aquifer samples shown in Figure 5.9(b) do not correlate well to changes in temperature.

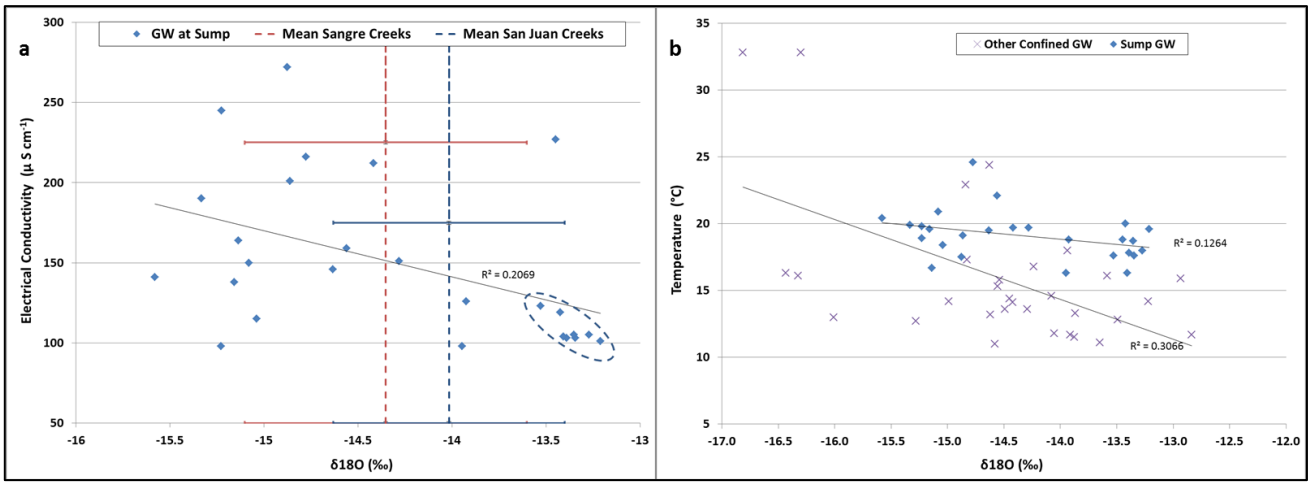


Figure 5.10: (a) Range of $\delta^{18}O$ of sump groundwater is shown plotted against EC. Mountain creek water is shown for reference. There is a cluster of low-EC water samples between -13.2 and -13.6. (b) Range of $\delta^{18}O$ for sump groundwater and other San Luis Valley groundwater plotted by temperature.

By examining chloride concentration by rough category of well screen depth (as could be roughly identified in Figure 5.3 and approximated from long screen openings, and from GIS attribute tables), differences in aquifer boundary can be seen. For those artesian wells in the ancestral sump that could be identified with known screen depth, groundwater from wells covering 300 feet below ground had an mean 0.57 mg/L Cl, those groundwater samples averaging 500 feet below ground were 0.65 mg/L Cl, and, most notably, the one artesian well in the ancestral sump that moves below the upper confined aquifer boundary into the lower active confined aquifer has a Cl concentration of 8.22 mg/L. This is consistent with other studies that have reported increased salinity at greater depths, and Mayo et al. estimated travel

times for the upper and lower active confined aquifer as 10,000 and 20,000 years respectively. This stratification in Cl concentration based on aquifer boundary layer also suggests different rates of recharge are occurring in each of these different layers.

5.7 Alternate Recharge Pathways: Sangre de Cristo Mountain Front and Fracture Flow, Ephemeral Creeks, and Aquifer Exchange

In order to discuss other significant but less dominant recharge pathways in the San Luis Valley, three specific examples of recharge pathways away from the San Juan Mountains will be considered. Good examples to illustrate fast recharge from Sangre de Cristo mountain front (and) fracture flow and seasonal recharge from ephemeral creeks come from the Great Sand Dunes boundary wells (labelled BP wells), which are monitored and provide historical data. The example of limited water exchange between the clay layer boundary is illustrated using historical data from the Bureau of Reclamation and chemistry data analysed in Oxford.

In general, rates of recharge for groundwater in the San Luis Valley ranged from 345.5 mm/yr in deep unconfined sandy soil near fractured rock to 0.8 mm/yr in shallow, unconfined but clayey soil. The deepest well, pulling geothermal water at 612 m below ground, has a low recharge rate of 3.9 mm/yr. Those wells with the greatest recharge were firstly those situated in fractured rock and receiving mountain front recharge. An example of this form of recharge is seen in the eastern edge of the San Luis Valley at the base of the Sangre de Cristo Mountains.

On the eastern margin of the San Luis Valley, near the extent of what was Ancient Lake Alamosa up until >200,000 years ago (Machette, 2004, Machette et al., 2013), the sand/sedimentary layers extend to much greater depths before encountering Quaternary Alamosa Formation clay layers, or in some cases Tertiary Sante Fe Formation clay layers (the latter are often interfingered with units of sand and gravel). Further

east, and near the base of the Sangre de Cristo Mountains, these clay layers are absent. Mountain front recharge in these regions can reach greater depths. Great Sand Dunes National Park and Preserve has a series of monitoring wells at its perimeter. BP-7, starred in Figure 5.11, is not located next to any surface water or ephemeral creek. BP-7 is a long-screen well with screen length running from 5-85 m deep. Its depth-to-water range is 3-5 m. Of all the unconfined wells tested, this well receives the greatest amount of yearly recharge. For a generalized, subsurface examination of BP-7, please consult Chapter 7, Figure 7.7. Those unconfined wells situated near or next to ephemeral mountain creeks and bodies of surface water receive the next greatest annual recharge. An example of this form of recharge is seen in boundary park well BP-3 (also starred in Figure 5.11, and for a more detailed description and geophysical report on BP-3, see Grauch et al., 2015). The next greatest rates of recharge were seen in upper confined aquifer wells receiving water from snowmelt-driven, underflow pathways. In some cases, as is possible with monitoring wells in the eastern half of the San Luis Valley, these aquifer layers can be understood by examining same-location (or nested) wells drilled into the unconfined and upper confined layers.

Nearly all of the federal agency wells in the San Luis Valley have historical groundwater fluctuation data available online (Davis Engineering Service and Principia Mathematica, 2019). For the most part, downward trends in the unconfined groundwater level are quickly detected, but the well data usually offer more minor, seasonal fluctuations too. Where drawdown is steep, this seasonal fluctuation may not be so perceptible. In the central part of the valley, drawdown is related to agricultural pumping, which, during the agricultural season, significantly impacts the valley's groundwater. Once pumping stops, the groundwater level will recover. This groundwater recovery does not result from an increase in recharge; it is recovery from abstraction. Some of the valley's historical well data show a steep downward trend after the year 2000, precipitated by a diminished snowpack and significantly increased abstraction. Some of the unconfined agricultural wells used for pivot irrigation in and around Center, Colorado, dropped 12 m (40 feet) between 1968-2016. The winters of 2014, 2015, and 2016 have received above average snowpack,

and this (in combination with some fallowed agricultural land) has caused as much as a 1.52 m increase in the last two years (RGWCD, 2017).

In cases where surrounding abstraction has ceased or slowed, the downward trend may be mild enough to again see a seasonal fluctuation of recharge. A good example of this seasonal pattern of recharge can be seen in two of the boundary wells at Great Sand Dunes National Park and Preserve (GRSA) that are located near creeks whose maximum discharge comes in the late spring, when snowmelt from the Sangre de Cristo sometimes causes the creek banks to overflow. BP-3 is the only one of all the BP wells that actually shows an increasing trend. Many of the GRSA wells that show seasonal fluctuation peak between late April to early June, when Sangre de Cristo snowmelt-fed creeks have their highest discharges. BP-3 is a shallow well very near Sand Creek (Figure 5.11). Depending on the winter snowpack, Sand Creek can overflow as late as early July. When this happens, Sand Creek recharges BP-3. Annual mean discharge of Sand Creek between the years 1994 through 2016 is 13.8 million m^3 (11,198 acre feet). The mean peak flow is 5.9 m^3/s. Discharge is variable and depends on snowpack. In 2000 and 2002, the annual discharge at Sand Creek was only 4.4 million m^3 (3567 acre feet) and 0.3 million m^3 (237 acre feet) respectively. 2012 was also a below-average discharge year, and the banks of Sand Creek did not overflow. Total discharge in that year was below-average at 6.7 million m^3 (5441 acre feet) and peak flow only reached 2.2 m^3/s. 2015 and 2016 were good years for snowpack. In 2015 Sand Creek total annual discharge was 20.7 million m^3 (6.4 m^3/s peak flow) and in 2016 the annual discharge was 14.6 million m^3 (5.7 m^3/s peak flow).

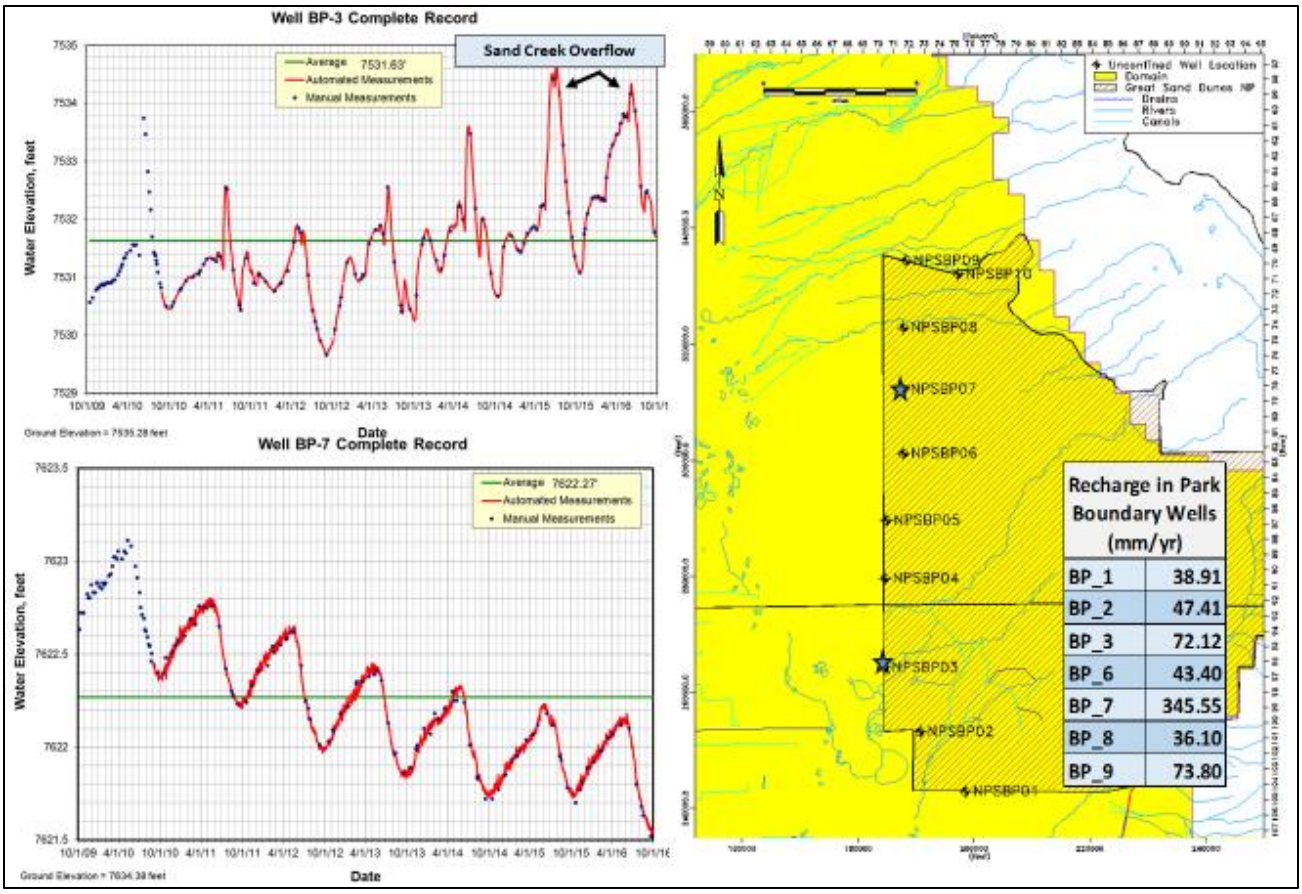


Figure 5.11: Location and rates of recharge for Great Sand Dunes National Park boundary wells. BP-3 recharge (alternate label NPSBP03 on map) coincides with overflow periods from Sand Creek. Hydrograph shown for the years 2009 through 2016. BP-7 receives the greatest annual recharge in a deep area with no confining clay.

Nested wells 41 and 42 have been monitored by USBR from 1983-2019. Nested well 39 has been monitored from 1982-2019. In each of the nested wells, confined wells have total depths between 36.58 and 42.67 m, with screen placement about 3 m from bottom. The unconfined wells stop just above the clay layer, at about 12.19 m. Confined well 39 (red star on Figure 5.12), when first drilled in 1982, had a depth to water of just 0.61 m. Its static water level has since dropped to 6.22 m, with a 0.91-1.22 m seasonal fluctuation between 2006 and 2012, and a 0.3 m seasonal fluctuation between 2013 and 2016. This well is located on the southern edge of the Baca Wildlife Refuge. The 41 wells (yellow star) are located just west of the Baca Wildlife Refuge in a residential agricultural area that uses unconfined water

(and to a lesser extent, surface water canals) for crop irrigation. Depth to water measurements at 41 have gone from 1.22 m to water to 11.28 m to water—they also have the greatest rates of recharge as compared to the other nested wells. The unconfined well of this nesting pair shows the presence of agricultural contaminants. As shown on the aerial map, wells 41 are located between two pivot circles. The unconfined aquifer sample shows Ca^{2+}, Mg^{2+}, SO_4^{2-} and NO_3^- concentrations that are an order of magnitude higher than the corresponding confined aquifer sample. In addition, the unconfined sample shows double the concentration HCO_3^- . Still, there is some level of interaction observed between the confined and unconfined wells at 39 and 41.

On the other hand, the nested wells at site 42 are a good example of clear separation between the unconfined and upper confined aquifer layers. The hydrographs in Figure 5.11 show the clay layer boundary between these two well layers is more intact at this location. The unconfined well has dropped significantly in water level since 1992, recovered some, and now fluctuates seasonally. While 42 confined has lost hydraulic head and its depth to water has increased (from 1983 to 2016 it went from 1.83 m above ground to 3.66 m below ground), it began with artesian flow, and its fluctuations are independent of its unconfined well. Interestingly, 42 is located on the Baca Wildlife Refuge close to an ephemeral wetland. While this surface water is present only some of the time, it plays a role in recharging 42 unconfined. In contrast, the chemical and isotopic data for 42 confined suggest it is recharged primarily through snowmelt from the San Juan Mountains.

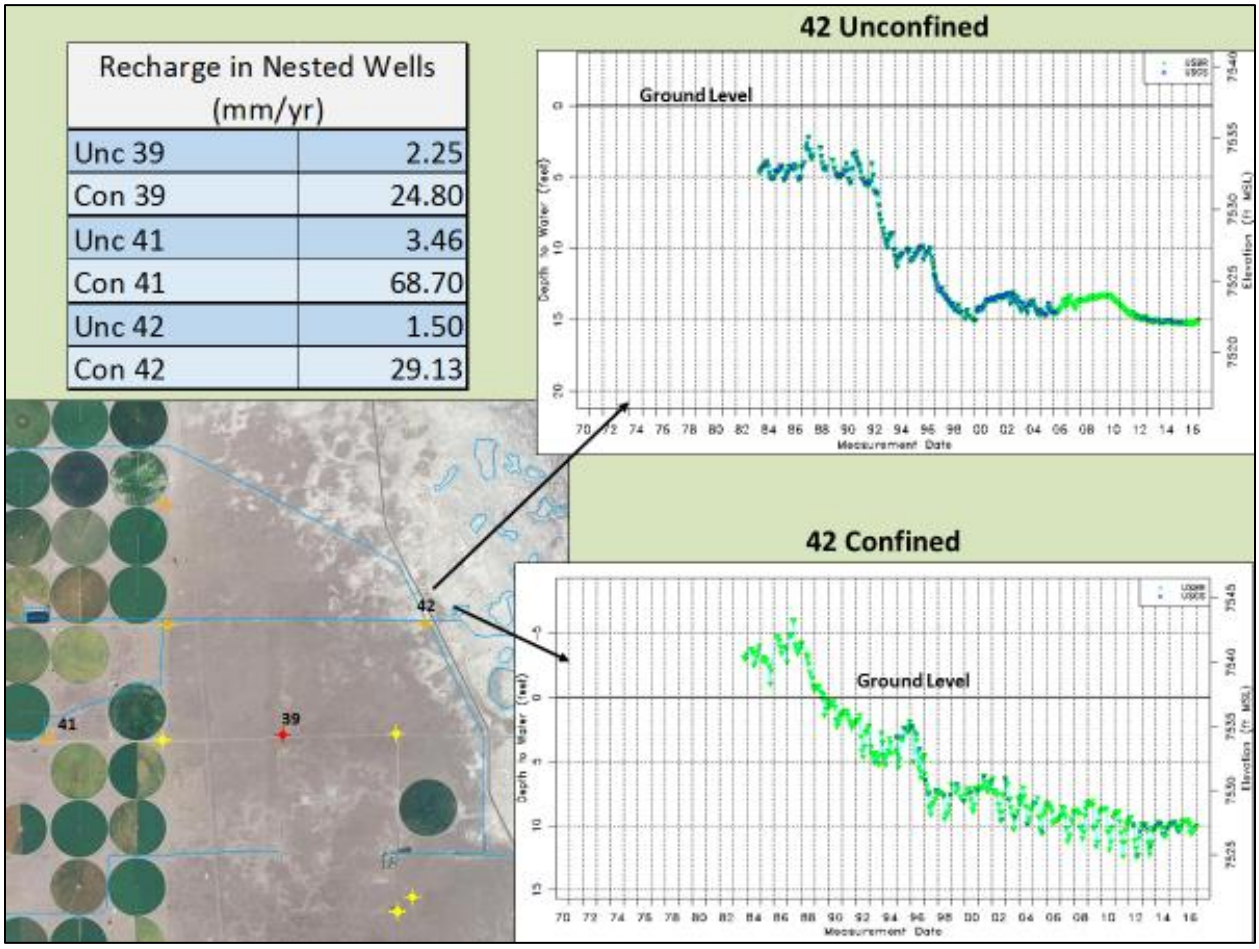


Figure 5.12: Rates of recharge in nested wells. Nested wells 41 and 42 marked with yellow stars. Nested well 39 marked with red star. The confined and unconfined well 42 logs show they are accessing different aquifer layers.

5.8 Snowmelt-driven Recharge at the Sump

5.8.1 Identification of an Unusual Pattern

The benefit of sampling water within a basin at various depths, areas, phases, and elevations, is a more complete picture of the hydrological processes at work. Before the establishment of a LMWL for the San Luis Valley, it would have been difficult to identify trends away from meteoric waters on the valley floor, and before identifying the difference between isotope values at mountain pass elevation and valley floor elevation, it would have been difficult to identify at what elevation the recharge occurs. Over 1000 m elevation difference exists between valley floor and mountain pass, so it is expected that an elevation

effect induced by orographic lift will appear in the precipitation values as the heavier ^{18}O isotopes are precipitated first and the lighter ^{16}O isotopes remain. Another reason for isotopic depletion is through local, thermal convective storms common to desert regions when the sun heats the valley floor and causes air masses to rise. Isotopic fractionation will cause the remaining water vapor to show depleted $\delta^{18}O$ values. A reciprocal phenomenon occurs when water is exposed to evaporation, and this form of isotopic fractionation is especially pronounced in arid regions. The water that remains in the soil, lake, or playa after evaporation is enriched, and because this enrichment occurs through an equilibrium fractionation ratio less than described by the GMWL or LMWL ($\alpha D/\alpha^{18}O$) this water will plot below (and intersecting) the meteoric water line. Surface waters undergoing evaporation typically will plot with a slope between 4 and 7 (Kendall and McDonnell, 1998). In some hyperarid regions, precipitation may undergo such significant evaporation before ground collection that even the LMWL, such as in southern Nevada, shows a slope of 6.87 (Ingraham et al. 1991). Figure 5.13 shows an evaporation trajectory constructed using surface playa water with a slope of 5.24 and a deuterium parameter (d-parameter) of -29 (equation 5.3). In centuries past, the playa wetland system in the San Luis Valley was fed predominantly through overflowing creeks originating in the mountains. Today they are fed through artesian wells and augmented with pumped water from the unconfined aquifer. Also shown in Figure 5.14 are the equations associated with the LMWL and high-elevation snow line of the San Juan Mountains. The weighted monthly LMWL, established in Chapter 4 in the equation 4.4, and shown again here in equation 5.4, reveals only a slight difference in slope and a much greater difference in intercept with the high-elevation snow line established from snow samples in the San Juan Mountains, equation 5.5.

A significant finding from this study is an isotopically depleted trendline, equation 5.7 ($R^2 = 0.99$), that sits above the LMWL and above the high-elevation snow line. These depleted waters were found at various depths of the upper confined aquifer in a 25 km^2 area of the closed basin, in the northern region of the San Luis Valley at the elevation low-point, owing to a prehistoric lakebed. The slope, intercept, and mean deuterium excess (d-xs) of these sump groundwater samples reveal differences in fractionation

pressures that suggest unique isotopic influences and recharge processes. This sump groundwater line is shown in Figure 5.13 and 5.14.

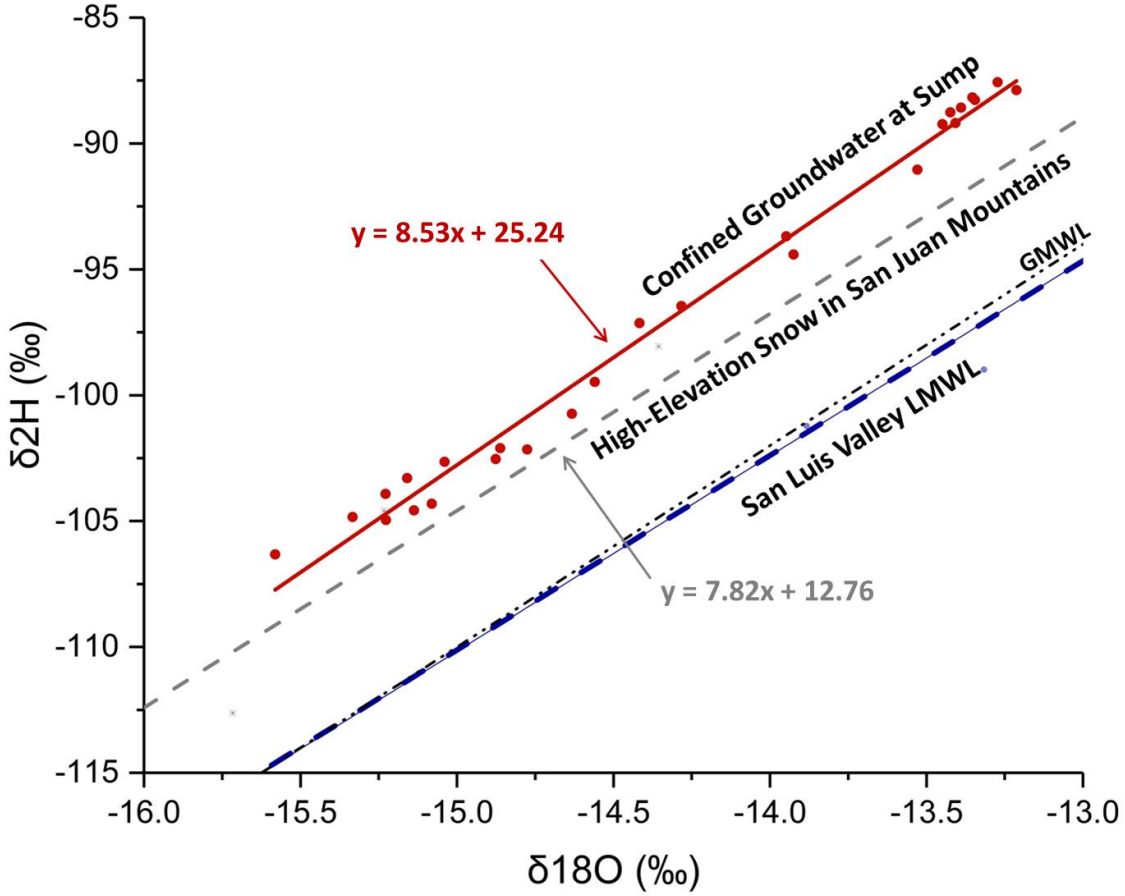


Figure 5.13: Focus on 26 isotope signatures from the confined water at the ancestral sump. These samples form their own depleted trendline that sits above the high-elevation MWL and the valley-floor LMWL.

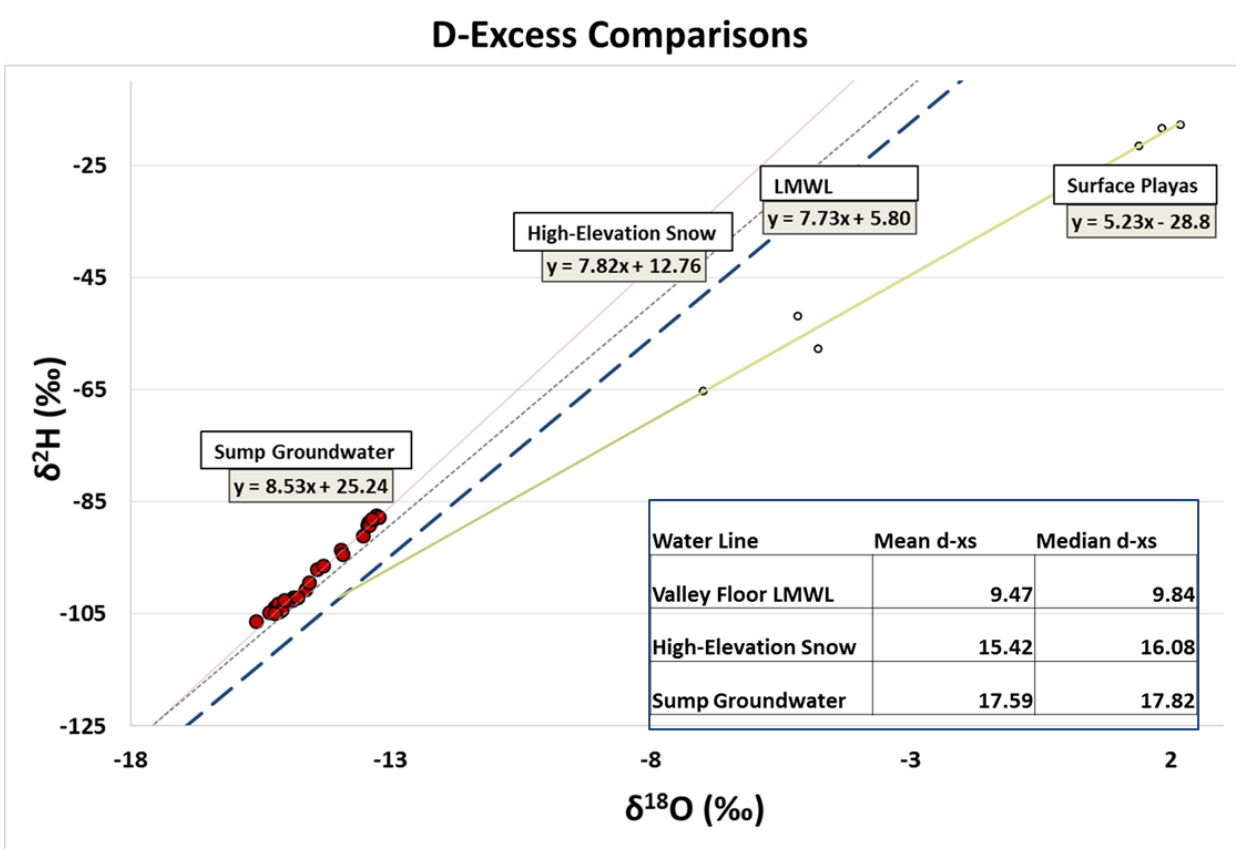


Figure 5.14: The sump groundwater line, created from 26 artesian groundwater samples within a 25 km^2 area of the valley's sump shows the highest deuterium excess at nearly twice that of the LMWL

$$y = 7.727x + 5.797 \quad \text{[Eq. 5.4]}$$

$$y = 7.823x + 12.762 \quad \text{[Eq. 5.5]}$$

$$y = 5.236x - 28.749 \quad \text{[Eq. 5.6]}$$

$$y = 8.534x + 25.242 \quad \text{[Eq. 5.7]}$$

5.8.2 Snowmelt-driven Recharge Through Time

Travel times from snowmelt recharge in the San Juan Mountains to the upper confined and lower active confined aquifer layers beneath the San Luis Valley sump area have been suggested at 20,000 and 30,000 years respectively (Mayo et al., 2007). These artesian waters were sampled below the confining clay layer at a low point in the ancestral sump that once housed the freshwater Lake Alamosa for 3 million years before it was released to join the Rio Grande 440 ka (Machette et al., 2007). The 26 samples used to construct this ancestral sump line ranged in depth from about 10 to 300 m, and some of the wells drew water from more than one depth. The pH was alkaline—8.97 to 9.30, and the EC and TDS were low, ranging from 68 to 124 mg/L TDS. This suggests there is little to no mixing from the unconfined aquifer, which in this area has high salinity (Kappen et al., 2004).

It was important to establish that the ancestral sump groundwater line sits above a high-elevation snow line constructed from San Juan snow samples collected over 2016 and 2017 from December to April from > 3200 m elevation. The April snow samples were taken before the April 2016 blizzard, so these samples do not reflect the deep depletion along the LMWL seen in snow samples on the valley floor (illustrated in Chapter 4). In regions where snow is a significant contributor to recharge water (Benjamin et al., 2004, Earman et al., 2006), the elevation where recharge occurs can be inferred from $\delta^{18}O$ depletion (Blasch and Bryson, 2007) if enough fresh snow samples are collected across different elevations and seasons (Gustafson, 2007).

This combination of long travel time through volcanic rock and residence time below clay layers where methanogenesis exposes water to gas interactions allows the possibility of water-rock-air reactions to influence δD and $\delta^{18}O$ values. While movement above meteoric water lines has been ascribed to mineral hydration and silicate weathering reactions (Clark, 2015a), and some studies have undergone controlled, laboratory experiments to show this movement in isolated samples, it is a very difficult to prove this mechanism is responsible for the isotope depletion in groundwater. Finding examples of where this groundwater depletion occurs in nature is rare in the literature, and in the event such groundwater

examples do plot above a global or local meteoric water line, authors typically do not attempt to explain this isotopic deviation. There is, however, another possible explanation.

One way to analyze the difference between the LMWL, the high-elevation snow line, and the confined, sump groundwater line is to examine differences in deuterium excess and d-parameter because these indicate different levels and types of isotopic fractionation. Kinetic fractionation controls deuterium excess and plays a significant role in evaporation into unsaturated air and condensation of ice from water vapor (Cappa, 2003). Sub-cloud evaporation alters the isotopic composition of precipitation (Ren et al., 2017). Both evaporation and sublimation play a significant role in the isotopic composition of high-elevation precipitation in the San Luis Basin. Assuming the confined groundwater at the sump was recharged primarily through San Juan high-elevation snowmelt at least 20,000 years ago, the sump water samples and high-elevation snow samples may undergo similar types of fractionation.

If water vapor is sourced from an arid, inland sea, deuterium excess may be > 20 ‰. This has been shown in the Persian Gulf, Red Sea, Black Sea, and the Mediterranean Sea (Gat and Gonfiantini, 1981). The mean d-xs of the sump groundwater is 17.6 ‰. While the high-elevation snow samples also have a high mean d-xs of 15.4 ‰, the confined sump water d-xs is greater and nearly double that of the LMWL. This suggests a significant degree of water recycling whereby sub-cloud evaporation or evaporation from surface water on the valley floor rises in vapor form until the most depleted molecules freeze at high-elevation as snow. The intercept, or the d-parameter, may indicate how evaporation affects the water source. For instance, the d-parameter of playa surface water is -29. This suggests a significant amount of water evaporates from the surface playas, and the surface water becomes isotopically enriched. The confined groundwater located at the valley's sump shows a d-parameter of +25 and this suggests a complementary process whereby water vapor evaporated from the surface playas may travel across the valley, rise in elevation, and fall as snow crystals on the San Juan Mountains. This snowmelt, and recharge from this snowmelt, would be isotopically depleted.

Snow is subject to sublimation after leaving the cloud and before reaching the ground (Moser and Stichler, 1980, Peng et al., 2017) but it is also subjected to sublimation as evaporating snowpack in mountains and as freezing water vapor when new crystals form from this snowpack vapor. Timing of recycled snow formation and timing of snowmelt-driven recharge (Taylor, 2001) are important factors determining level of ^{18}O depletion. Friedman et al. (1991) used controlled snowmelt experiments to show how the isotopic composition of snowpack may become more varied within the snowpack's stratigraphy and how upper layers within the snowpack may become more depleted over time. Their work suggests that as the bottom layers of snow warm up, there is an upward migration of isotopically lighter water vapor, and when this water vapor freezes, it produces snow that is further depleted isotopically. The San Luis Valley experiences wide fluctuations in temperature throughout the day due to high elevation, low latitude, and clear skies. This allows mid-day and early afternoon evaporate to rise through heat convection on the valley floor and freeze after adiabatic cooling (whether through vertical or orographic lift) and accumulate as isotopically depleted snow. Late season snowmelt may contain snow deposits that experience sublimation of recycled water more than once. However, by mid to late May in most years, evenings in the mountains no longer experience freezing temperatures, and once snow stops falling or forming, evaporation will enrich the remaining piles of snow.

While these explanations of how recycling of evaporated water, sublimation, and the timing of snowmelt-driven recharge isotopically deplete water satisfies isotope results for the high-elevation snow line and high-elevation creek water, these explanations don't satisfy why the old groundwater in the valley's closed basin sump shows a greater level of deuterium excess. Why do these groundwater samples sit so perfectly above the high-elevation snow line?

In the 1870s, surveyors of the San Luis Valley mapped an extensive wetland complex that traversed the width of the closed basin section of the valley and extended for 100 km (Wheeler and Humphreys, 1878). These wetlands, then termed collectively the San Luis Marshes or Swamp, consisted of a subsection of wetlands that came to be known as the Mishak Lakes complex. They were fed primarily through

mountain streams, though some wetlands received groundwater inflow. Shortly after 1878, most stream inflows were diverted and appropriated for agricultural use. In the decades following, extensive agricultural stream diversions and pumping schemes for both agriculture and the US Closed Basin Reclamation Project (beginning in the 1970) further reduced any inflow to the wetlands, and many of the wetlands dried or became ephemeral (Sanderson, 2006). To mitigate the effects of this human-altered hydrology in the early 1980s, a Mishak National Wildlife Refuge was proposed and authorized by Congress, but a revised decision (H.R. 2823) which amended the 1972 Reclamation Project Authorization Act reduced the total 560 km^2 project area requiring > 15.4 million m^3 annually of mitigation water to a 12 km^2 Russell Lakes Waterfowl Management Area receiving no additional water rights other than those included with private land purchases and already existing to the State of Colorado on bordering lands (Udall et al., 1984). A 2008 study sought to reconstruct a natural hydrologic regime for the Mishak Lakes complex and test how stream diversions and pumping have altered these patterns. Sanderson et al. (2008) compared observed water budget calculations over a four year period (1998-2002) to modelled simulated natural conditions over nearly a century (1915-2002) for the playa wetland system in the San Luis Valley. Present-day observations placed stream inflow at 80% of total playa wetland inputs and ET accounted for nearly 70% of losses. Every year of observation the playas dried completely. This study found natural simulated conditions to be quite different in terms of greater water depth and frequency of flooding, and it found playas retained water year-round in three out of five years, with the longest simulated stretch of inundation running nearly 17 years.

Past water resources in the San Luis Valley were more plentiful—not only in terms of aquifer storage but also in terms of mountain stream flow, Rio Grande flooding, and consistent surface wetlands. It was found in a recent study on wetlands in the San Luis Valley the valley's wet acreage has declined by 50% since the 1980s (2019). Public lands have had the greatest decline, and, because much of the northwestern portion of the valley is privately owned and irrigated throughout the irrigation season (running April through October) humans are changing the season the wet acres are available (and this doesn't always

accommodate migrating birds, for instance (2019). Travel time for groundwater in the upper confined aquifer near the valley's sump is roughly 20,000 years. The surface water resources available year-round for evaporate recycling on the valley floor would have been greater than those recorded in the late 1800s. The mechanisms of isotopic depletion through evaporate water recycling and sublimation have not changed over the centuries. However, the amount of water available to recycle through this process has decreased, and the timing of snowmelt in the San Juan Mountains is shifting. Results from this study suggest that due to a decrease in recycled-water precipitation, the isotopic signatures of confined groundwater recharged at high-elevation from San Juan snow may have been more depleted in the past (and currently show greater depletion) than present-day high-elevation snowfall.

In the conceptual diagram shown in Figure 5.15 we see water vapor sourced from playa wetlands, shown on the surface water evaporation line with double arrows, provides depleted water for condensation or sublimation in the San Juan Mountains. The confined aquifer sump line shows 26 upper confined groundwater samples plotting above the LMWL and above the high-elevation San Juan snow line. This confined groundwater line runs nearly parallel to the LMWL but represents a mixing of ultra-depleted vapor and high-elevation San Juan snow water.

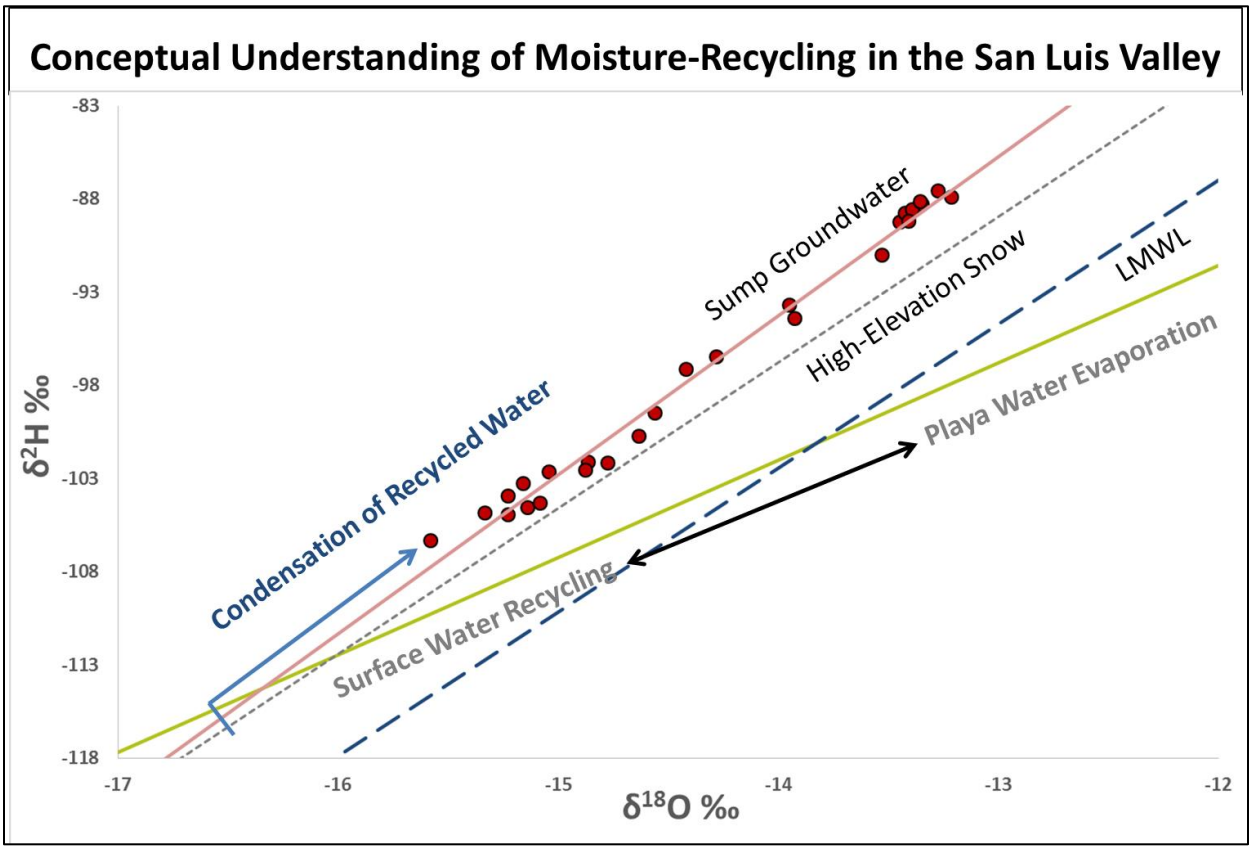


Figure 5.15: This conceptual diagram offers an explanation for old groundwater depletion in the valley's sump by showing how the groundwater may have been sourced from recycled surface water vapour and high-elevation snow in the San Juans (Lanzoni and Darling, 2019).

5.9 Discussion and Conclusions

5.9.1 What does chemistry tell us about pathways and rates of recharge?

Water across the San Luis Valley differs chemically depending on source of recharge, recharge pathway, and rate of recharge. Whether or not an aquifer layer receives input from water containing agricultural fertilizers and pesticides, from ponds and canals subject to evaporative loss, from precipitation on the valley floor or mountain front, or from high-elevation snow that infiltrates directly and travels along flowpaths where water-rock interactions alter the water's dissolved constituents, all of this potentially changes the groundwater's chemistry. Overall, results from this study show some similarities between

water in the unconfined aquifer and water in the lower (active) confined aquifer on the eastern side of the valley in that both are Ca^{2+}/Mg^{2+}-HCO_3^- to Ca^{2+}-HCO_3^- water types and show, to a greater or lesser extent, recharge originating from the valley floor. (There are of course some notable exceptions for the deeper wells, but this is the case if their mean values are discussed. Greater variability in the lower active confined aquifer is seen closer to the upper and lower active confined boundary, and it is thought that this boundary shifts slightly depending on location.) Roughly 1/3 of the unconfined samples appear to be Ca^{2+}/Mg^{2+}--Cl^- /SO_4^{2-} water type. Upper confined samples appear predominantly in the Na^+/K^+--HCO_3^- water type.

As expected, the samples with the highest TDS concentrations are in the unconfined aquifer. In the unconfined aquifer, rates of recharge are orders of magnitude higher for select areas lacking confining clay at the valley's margins that receive mountain front/fracture flow. An example of this is on the eastern margin of the valley at Great Sand Dunes BP-7, where a deep, unconfined well is located at the base of the Sangre de Cristo Mountains. The group of wells that receives the second greatest recharge (seasonally) are those unconfined areas that receive recharge from creek overflow and ephemeral surface water. An example of creek overflow recharge comes from BP-3 at Great Sand Dunes, which is located next to and displays similar water level fluctuations to Sand Creek. Aside from these areas of fracture-flow /mountain front and surface water/ephemeral creek recharge, confined wells generally receive greater recharge than unconfined wells in the valley's central region—especially for those wells receiving significant recharge from snowmelt underflow.

This study found the fastest flowpath (greatest rate of recharge) of the wells sampled to be fracture/mountain front flow at the base of the Sangre de Cristos, yet the dominant recharge pathway overall to the upper confined aquifer is from high-elevation infiltration in the San Juan Mountains, which recharges groundwater on the eastern part of the valley. Water movement between the unconfined and confined aquifers is limited but noticeably as seen through monitoring nested wells. Mostly, the nested wells in the closed basin are useful to compare pathways and rates of recharge. CMB estimates should be

regarded with caution with respect to fissure/fracture flow, and the predominant underflow originating from a higher precipitation region of the San Juan Mountains. Yet, for purposes of comparison, let us entertain a slight CMB estimate modification. The CMB method for this chapter assumes a long term mean 200 mm/yr precipitation, and the chloride input associated with this amount of precipitation is used to estimate long term, mean recharge. While the weighted chloride input may not change significantly the mean annual precipitation increase to 800 mm/yr (at the point of infiltration) would cause long term mean estimates of recharge in the upper confined sample areas to jump to 141 mm/yr. If we look at the three nested wells to illustrate this point, with estimates relying on valley floor precipitation, the upper confined wells 39, 41, and 42 have a rate of recharge that is 11, 20, and 19 times greater than their adjacent unconfined wells. However, if recharge estimates to the upper confined are calculated using annual precipitation in the San Juans, then recharge to the upper confined aquifer in the eastern region of the closed basin at these well sites is 44, 79, 78 times greater than recharge to the nested unconfined aquifer wells (see Table 5.1, and refer to the table embedded in Figure 5.12). This may be important to consider given that unconfined well 42 is near an ephemeral wetland, and unconfined well 41 is located at the edge of an agricultural pivot circle. Both of these wells are therefore exposed to a small degree of increased potential recharge from surface water infiltration. Despite this, the rate of recharge to these unconfined wells is 19 to 79 times less than the rate of recharge to the adjacent upper confined wells.

Table 5.1: Rates of recharge depending on recharge source.

Different Rates of Recharge in mm/yr		
Nested Well	**Valley Floor Input**	**San Juan Input**
Upper Confined 39	**25**	**100**
Upper Confined 41	**69**	**275**
Upper Confined 42	**29**	**117**

Another uncertainty with the application of CMB in this thesis is that (described in greater detail in Chapter 2) the weighted mean precipitation Cl concentration was ascertained by running and re-running ion chromatography analysis with the purpose of achieving a good low-concentration calibration and a LOD better than 0.1 mg/L. Not all sample analysis achieved this level (on the department's old Dionex). Therefore, the Cl concentration measured in groundwater samples is not as accurate as those concentrations measured in the 2015 precipitation. It is reasonable to argue better precision is necessary for rainfall (and snowmelt) versus groundwater due to the expected lower Cl concentrations, but this is, nevertheless, an uncertainty inherent in this analysis that may pose a challenge for reproducibility and consistency.

Previous studies have estimated that the upper confined aquifer contributes no more than 20% to the unconfined aquifer. Drilling, pumping, and other anthropogenic manipulation of the valley's hydrology has significantly impacted the integrity of the clay barrier and movement between the confined and unconfined layers. Pumping from multiple-screen and long-screen wells also offers the opportunity to move water from one aquifer layer to another (Mayo, 2010) Though this study took every effort to avoid sampling areas with expected influence from anthropogenic alterations, the nested monitoring wells provide a window into the agricultural contaminants now found in the unconfined aquifer as well as some movement between the unconfined and upper confined layers when the unconfined aquifer is severely depleted and when the upper confined loses hydraulic head.

5.9.2 What do isotopes tell us about pathways and rates of recharge?

Isotope values (δ^2H and $\delta^{18}O$) of groundwater in the San Luis Valley will differ depending on elevation, latitude, temperature, and continental depletion of the source water. Precipitation isotopes from recharge source waters are an important component to understanding the story of groundwater recharge and flowpaths in the San Luis Valley. Since groundwater in the San Luis Valley may be loosely divided into

unconfined water, based on the absence of a confining clay layer, and into upper or lower active confined water based on depth of the active confined aquifer, grouping groundwater samples in this way and analysing mean isotope values gives insight into major recharge pathways for groundwater at these three aquifer levels. Groundwater in the unconfined aquifer shows the most variation and is subjected to the most evaporation as soil water infiltrates and evaporates from shallow depths. Along the valley's margins, at the base of the San Juan Mountains and the Sangre de Cristo Mountains, the unconfined aquifer may be deep, and along the Sangre de Cristo base, fault lines and fissures provide swift access for mountain front recharge. By looking at the overall mean isotope values, we can say the unconfined aquifer and the lower active confined aquifer reflect present-day meteoric water recharge from mountain base and valley floor elevations, even if the travel time for the lower active confined layer is estimated to be 30,000 years (Mayo et al., 2007). The mean isotope value for the upper confined aquifer clearly shows a high-elevation recharge pathway, predominantly from the San Juan Mountains. These values, which differ slightly from previous studies, are biased toward the specific geographic locations of the sample bulk, which is highly influenced by the northern closed basin region of the valley's sump. This study's analysis is enhanced from previous studies due to the establishment of meteoric input baselines at valley floor and mountain pass elevations.

Mountain block recharge, where infiltration occurs at high elevations in the San Juan Mountains (with some of this also potentially categorized as mountain front recharge—see Wilson and Guan, 2004), appears to contribute the most recharge to the upper confined aquifer in the San Luis Valley. The amount of mountain block recharge to the unconfined aquifer is more variable and will depend on what region of the valley the groundwater is located. Concerning recharge to the lower confined aquifer, of those wells sampled below 274 m, the mean isotopic values lie closer to the valley-floor meteoric water line, suggesting that, at least on the eastern side of the valley, recharge primarily occurs through infiltration at the base of the Sangre de Cristo Mountains where there is no confining clay layer before moving slowly to greater depths. Confined aquifer recharge is primarily snowmelt-driven, with sources of moisture

originating from the NW. Some of the unconfined aquifer areas show isotopic values with more similarity to warm, monsoonal rains.

Some of the uncertainties present in this study have much to do with limited coverage. The San Luis Valley is a very large and hydrologically complex area, and therefore this study attempts to illustrate major and minor pathways for recharge and their associated rates of recharge by using specific examples drawn from the predominantly eastern side of the closed basin area. However, even within this area of coverage, only a limited number of short-screen wells were known to exceed 274 m in depth (N=11). Another limitation of this study is the use of only $\delta^{2}H$ and $\delta^{18}O$ for isotopic tracers. While it is indeed preferable to include dating isotopes to help identify flowpaths and residence time, this study had to make due with its examination and use of the stable isotopes of water. It is fortunate that previous work has been done dating travel times to the sump, and this information helps inform this study.

When we examine specific areas of the San Luis Valley more closely, we see interesting patterns emerge. Isotope values for artesian upper confined groundwater from a 25 km^2 area of the valley's low-point sump show an unusual and well-defined movement above both the valley floor and high-elevation meteoric water lines. An example such as this, where 26 samples plot so perfectly above the meteoric water lines, is difficult to find in the literature. In those rare cases when isotope samples do plot above the meteoric water line—such as in past isotopic studies of the San Luis Valley—these samples are often overlooked, not identified due to lacking local meteoric water lines, or perhaps thought to be the result of water-rock-gas interaction over long periods of time.

This thesis devoted time to understanding isotope signals of groundwater in the San Luis Valley. It was fortunate, over the years of sampling, to capture 'heavy' and 'light' water isotopes from precipitation events originating through the North American Monsoon system and those originating from cold air masses in the North. The blizzard event of 2016 that originated from an Arctic "polar vortex" highlights how even these severely depleted signatures fall along the LMWL. Seeing these latitude and temperature

extremes when creating a LMWL was useful then in identifying when water sample—as occurred with old groundwater from the valley's sump—strayed.

The high-elevation snow line was constructed from San Juan snow samples collected over 2016 and 2017 from December to April from > 3200 m elevation. The April snow samples were taken before the April 2016 blizzard, so these samples do not reflect the deep depletion along the LMWL seen in snow samples on the valley floor. In regions where snow is a significant contributor to recharge water (Benjamin et al., 2004, Earman et al., 2006), the elevation where recharge occurs can be inferred from $\delta^{18}O$ depletion (Blasch and Bryson, 2007) if enough fresh snow samples are collected across different elevations and seasons (Gustafson, 2007).

Groundwater samples were used to construct the ancestral sump line. It was important to establish that the ancestral sump line sits above the high-elevation snow line. The 26 samples used to construct this ancestral sump line ranged in depth from about 10 to 300 m, and some of the wells drew water from more than one depth. The pH was alkaline—8.97 to 9.30, and the EC and TDS were low, ranging from 68 to 124 mg/L TDS. This suggests there is little to no mixing from the unconfined aquifer, which in this area has high salinity (Kappen et al., 2004).

Old groundwater clusters showing significant deviation from a present-day MWL are sometimes assumed to suggest paleo-recharge. In North African cases where paleo groundwater is thought to have been recharged during past climatic conditions, the $\delta^{18}O$ values are depleted due to a well-documented shift in source water origin from the Atlantic (Edmunds, 2008a, Stone et al., 2019). A previous study conducted in the closed basin sump area of the San Luis Valley did find sediment core evidence to support the idea that a recent climatic shift has enriched $\delta^{18}O$ signatures (Yuan et al., 2013). However, analysis of present-day precipitation and creek water collected at high elevation in the San Juan Mountains indicates this study's $\delta^{18}O$ depletion of groundwater is less likely to do with a major climatic shift and more likely driven by a mechanisms still occurring.

Mineral hydration and silicate weathering were considered as potential mechanisms for movement above the LMWL (Clark, 2015a), but these mechanisms were ruled out in favour of surface water recycling and sublimation of high-elevation snow. Initially, it was considered the ancestral sump groundwater line may pertain to silicate weathering reactions in the San Juan Mountain volcanic rocks and biogeochemical reactions that may affect the isotopic composition of groundwater in closed conditions over tens of thousands of years. Travel times from snowmelt recharge in the San Juan Mountains to the upper confined and lower active confined aquifer layers beneath the San Luis Valley sump area have been suggested at 20,000 and 30,000 years respectively (Mayo et al., 2007). These artesian waters were sampled below the confining clay layer that formed hundreds of thousands of years ago from organic-rich deposits left behind by the ancient, freshwater Lake Alamosa (Machette et al., 2007). This combination of long travel time through volcanic rock and residence time below clay layers where methanogenesis exposes water to gas interactions allows the possibility of water-rock-air reactions to influence δD and $\delta^{18}O$ values.

When gas production takes place in the subsurface, the gas can cause an enrichment of the residual water phase. For example, an enrichment in $\delta^{2}H$ may occur with exposure to large quantities of H gas, in the form of H_2, H_2S, or CH_4–particularly through methanogenesis. While methane was present in specific areas of the closed basin, the only well sampled with concentrations of CH_4 sufficient to ignite (estimate 5-15% in atmosphere for igniting) was not found in the 25 km^2 area used to construct the sump line. It is noted that some secondary data on methane concentrations in wells exists in the literature, and Mayo et al. (2007) report a limited number of upper confined well samples from the closed basin with up to 89% CH_4. Gas sampling was not conducted as part of this thesis, so primary data on methane is not available. Still, it was considered that methane may have an enrichment factor on $\delta^{2}H$ groundwater signatures in the sump.

Hydration of primary silicates is another example of rock-water interaction influencing isotope signature, and this would affect ^{18}O and ^{2}H differently. As water-silicate reactions produce kaolinite, the water $\delta^{18}O$

becomes more negative but the δ^2H becomes more positive, moving it along an angled trajectory toward the upper left. There is a similar effect for rock-water isotope enrichment with gypsum and occurs through hydration of anhydrite (Clark, 2015a).

Water recycling has been shown to occur through various mechanisms including ET from oasis crops, sub-cloud evaporation, convective storms, snow sublimation, and vapour recycling of surface water (Bershaw et al., 2016, Froehlich et al., 2008, Liu, 2011, Zhu et al., 2019). Collecting snowfall samples—and creek samples—at high elevation in the San Juan Mountains helped show the elevation effect in meteoric water signatures. This then led to the comparison between the old groundwater at the sump and the high-elevation MWL. The d-excess helped identify the mechanism of vapour recycling of surface water, and an understanding of land-use changes in the San Luis Valley helps explain why the water recycling signal of today is not as depleted at it was, even 100 years ago.

The present-day, high-elevation San Juan snowline and high-elevation creek water from summer and winter 2015, 2016, 2017 offer good isotopic references by which to examine the upper confined sump water. Important differences in deuterium-excess, slope, and d-parameter offer insight into how the fractionation mechanism and fractionation amount separates the valley's sump groundwater from present-day, high-elevation precipitation and creek water. These key differences, along with documented differences in the amount and consistency of surface water present in the San Luis Valley over the last century and over the last 20,000 years suggest that groundwater in the valley's sump was recharged during a time when a greater amount of surface playa water was recycled and sublimated over the San Juan Mountains, in turn feeding this depleted isotope signal through mountain block and underflow recharge to the valley's sump. While water management considerations have gone into changing snowpack conditions with regard to dust-on-snow events and a change in timing of seasonal snowmelt (Lawrence et al., 2010, Painter et al., 2007, Painter et al., 2017), no one has considered that the type of snow, isotopically speaking, may also be changing, and this may point to the importance of local sources of water vapour for generating precipitation, especially high-elevation snow in dryland areas.

An important contribution of this doctoral work then is the consideration of source water for the high-elevation snow that contributes substantially to the valley's aquifer recharge. This study examines the mechanism by which recycled water from the valley floor condenses at high elevation and infiltrates at high elevation in the San Juan Mountains. Old water from the upper confined aquifer sampled within a 25km^2 area of the valley's sump have a 2.5‰ ^{18}O spread and sit significantly above the LMWL and high-elevation MWL. This water shows a mean d-xs of 17.6 ‰, which is greater than d-xs of the high-elevation snow line, and nearly double the d-xs of the LMWL. This study argues that in addition to changes such as lowered albedo of mountain snowpack and reduced baseflow recharge from the San Juans, humans have altered a mechanism (and rate) of recharge not previously considered through the draining of playas and surface water diversions in the 20th Century.

5.9.3 Are there indications these pathways and rates of recharge have changed over time?

In a high desert valley in southern Colorado, land use changes have drained wetland playas and enabled windstorms to deposit valley soil on surrounding mountain snowpack. Dust-on-snow accelerates snowmelt, changing the patterns of seasonal melt. This reduces infiltration and aquifer recharge. Additionally, long-term historical precipitation data for the valley floor show recent, unprecedented seasonal shifts. Environmental changes and significant agricultural abstraction have caused a sharp decline in the valley's aquifer levels.

In the 1800s, a complex of wetland playas populated the valley floor, some more than 3.7 m deep, and this wetland complex known as Mishak Lakes and San Luis Lakes spanned 100 km across the valley from the north to the east (Wheeler and Humphreys, 1878). These wetlands received water input from baseflow, from artesian springs, and—to the largest extent—surface water overflow from Saguache Creek, Alamosa Creek, Sand Creek, and Big Spring and Little Spring Creek (Valdez, 2016). These creeks no longer provide water to the wetlands. Due to groundwater abstraction and agricultural diversion, the

playas became dry by the 1950s and were known as the "dry lakes." Federal efforts to restore some of the wetlands were successful, but the wetlands' area and volume of water was much reduced. In early 2000 it was estimated that while the former wetland playa complex remained wet year-round for multiple years at a stretch—the longest being 17 years—current conditions for the federal wetlands caused them to go dry every year (Sanderson et al., 2008). A 2019 study of the valley's wetlands found that across the valley, wet acreage has decreased by 50% since the 1980s (with federal lands experiencing the greatest declines). Additionally, private land irrigation is changing the season this acreage is wet, with state-run irrigation season beginning in April and ending in October. If water vapour from the valley floor is no longer available or is limited in colder months, this may mean significantly less water is recycled as isotopically depleted, high-elevation snow.

The state decision support model, relying on water budget components from previous studies, draws distinctions that highlight how humans have altered the water budget by diverting river and creek water (which now no longer overflow where heavily diverted—this includes the entire Rio Grande, which historically flooded great distances every spring) and by lowering the aquifer tables/pressure through groundwater pumping. The model credits irrigation ponds and irrigation ditches/canals with increasing recharge to parts of the unconfined aquifer. However, human alterations have significantly decreased baseflow recharge from the San Juans (CDWR, 2004, Bexfield and Anderholm, 2010).

By examining old water (20,000 yrs or older) in the valley's sump (Mayo et al., 2007) that was sourced from snowmelt and high-elevation recharge in the San Juan Mountains, and by comparing this water isotopically with present-day high-elevation snowmelt in the San Juans, this study presents evidence that old water was significantly more depleted, shows greater d-excess, and has a d-parameter that suggests greater isotopic fractionation consistent with that which occurs through water recycling. Figure 5.13 shows how this study's physical data points align with a conceptual understanding of past water recycling in the San Luis Valley. It is long held that this mechanism of water recycling occurs in arid environments with playa systems in closed basins, but it is unusual to find physical data points taken from a 25 km^2 area

that show such a wide $\delta^{18}O$ spread and form their own ultra-depleted water line. These findings support the idea that greater condensation of recycled water occurred at high elevations in the San Juans in the past. Given the 20th Century land use changes and the ways in which these human changes have altered the hydrology of the San Luis Valley, this study argues that in addition to changes such as lowered albedo of mountain snowpack and reduced baseflow recharge from the San Juans, humans have altered a mechanism (and rate) of recharge not previously considered—that of condensed recycled water in the San Juan Mountains.

This chapter illustrates primary pathways and rates of recharge in the San Luis Valley. The shift in seasonal precipitation trends (discussed in Chapter 4) significant groundwater drawdown (discussed further using specific site examples in Chapter 6) give every indication that groundwater recharge in the San Luis Valley does not exceed groundwater abstraction.

Chapter 6: Phreatophyte Shrubs as Indicators of Groundwater in the San Luis Valley

6.0 Summary

In southern Colorado where phreatophyte shrubs *E. nauseosa* and *S. vermiculatus* are the valley's dominant vegetation, these plants play an important role in fostering biodiversity, stabilizing soil and facilitating recharge. For centuries, wetland playas populated the valley providing habitat for permanent and migratory wildlife. Now dust storms strip away the valley's topsoil, and dust deposited on surrounding mountain snow increases radiative forcing, which in turn lowers infiltration and recharge from seasonal snowmelt. Since the 1990s, this area has experienced a sharp decline in aquifer levels. Where agricultural abstraction is significant, the unconfined aquifer has experienced a 9 m drop.

To better understand how the area's dominant vegetation responds to a lowered water table, 76 stem water samples were cryogenically extracted from the facultative phreatophyte shrubs *E. nauseosa* and *S. vermiculatus* over the summer, fall, spring, and summer of 2015 and 2016 from study plots chosen for increasing depths to groundwater. Stable isotopes $\delta^{2}H$ and $\delta^{18}O$ were analyzed to determine the plant's water source. Distinct patterns of water capture strategy and seasonal shifts are visible, and these species differences are most apparent where groundwater is most accessible. However, where the water table has dropped 6 m over the last decade, both *E. nauseosa* and *S. vermiculatus* survive only on near-surface snowmelt and rain. At this vegetation plot, shrub density is reduced by an order of magnitude, species diversity drops, and the percentage of exposed, bare earth reaches 45%. The broader implications of this work point to a potential feedback loop perpetuating a reduction in groundwater, vegetation, ground cover, and snowmelt-driven recharge. These are important considerations beyond transpiration losses for managing shallow groundwater systems in arid environments dependent on mountain-front recharge.

6.1 Chapter Questions, Aims, and Significance

- How does the area's dominant native vegetation—facultative phreatophytes *Sarcobatus vermiculatus* (greasewood) and *Ericameria nauseosa* (rabbitbrush)—respond to a lowered water table?
- Are distinct patterns of water use and seasonal shifts between the phreatophytes visible?
- How might a lowering of the water table affect species richness and plant density?

To this end, this chapter analyzes stem water samples from the valley's two dominant facultative phreatophyte shrubs at three different study plots with increasing depth to groundwater in order to establish seasonal shifts in water use and to examine if the phreatophytes utilize groundwater from the unconfined aquifer where there have been significant declines.

6.2 Introduction and Past Work

Dryland plants vary in their ability to utilize soil moisture and groundwater (Ehleringer et al., 1991). This is due primarily to different rooting systems. Many dryland plants have a dimorphic root system with a deeper tap root to access groundwater and branching surface roots that can utilize soil moisture in the upper layers (refer to Chapter 2, Figure 2.7 for a diagram of *S. vermiculatus*'s root system). While plants can change their water capture strategy depending on seasonal water availability, plants may also change their rate of water uptake, which may increase as more water becomes available (Williams and Ehleringer, 2000). Meinzer (1927) described plants with a dimorphic rooting system containing a central taproot that extended to the water table. Facultative phreatophytes, those plants which draw water from near-surface moisture as well as from groundwater, provide a lens through which to study water

movement between the saturated and unsaturated zones in deserts with high water tables (Cooper et al., 2006, Froend and Sommer, 2010).

In the 1950s it was thought phreatophytes such as *S. vermiculatus* would have a rooting depth sensitive to and indicating the depth to groundwater (Robinson 1958). While the roots of several subspecies of *E. nauseosa* have been excavated to a depth of 15 feet, the roots of *S. vermiculatus* have been found to extend to even greater depths. Shantz and Piemeisel (1940) reported a large S. vermiculatus near Moab, Utah, had roots reaching 5.5 m deep with a taproot 7.6 cm in diameter. Previously, *S. vermiculatus* in Big Smoky Valley, Nevada, were found growing in an area where the depth to groundwater was 10.1 m (Meinzer, 1927), though, since the roots themselves were not excavated, it was not known if the *S. vermiculatus* roots reached the groundwater, and if they did, if the plant was utilizing the groundwater.

Both *E. nauseosa* and *S. vermiculatus* have shown high tolerances for an elevated water table. Black greasewood tolerated surface flooding for 40 days without showing effects, and a water table 25-30 cm below the ground surface appeared to have no effect on *S. vermiculatus* (Ganskopp, 1986). Groeneveld and Crowley (1988) later extended flood inundation by a period of 6 months to show that *E. nauseosa* could not survive this length of flooding, and this is thought to be due, in part, to the plant's oxygen requirements for root morphology. Salt is the most important water quality parameter that differentiates where and how well different phreatophytes live. Willow and cottonwood have low salt tolerances while *S. vermiculatus*, as a halophyte, has a high tolerance for salt. Additionally, *S. vermiculatus* also grows well in areas of high sodium carbonate groundwater, which in arid areas forms "black alkali" on the soil surface (Robinson, 1958). Both *E. nauseosa* and *S. vermiculatus* grow in light to moderately alkaline soil.

Much of the San Luis Valley is dominated by woody shrub-grassland, and the most common native shrubs are the deeply rooted, phreatophytes *Sarcobatus vermiculatus* (greasewood) and *Ericameria nauseosa* (rabbitbrush). *S. vermiculatus* and *E. nauseosa* are facultative phreatophytes that may utilize groundwater in the early summer but can also draw precipitation water during the late summer monsoon

(Chimner and Cooper, 2004). By altering soil moisture content and measuring xylem pressure potential, Kray et. al. (2012) found the xylem pressure potential of *S. vermiculatus* increased by 0.5 to 0.7 MPa once rains arrived but decreased across all plots by an average of 1.4 MPa as the volumetric water content of the 15—30 cm layer of soil declined. In contrast, they found *E. nauseosa* did not respond to an increase or decrease in surface soil moisture. Isotope analysis suggests that while *E. nauseosa* has a strong groundwater dependence, *S. vermiculatus* changes water capture strategies according to seasonal availability of precipitation recharge (Kray et al., 2012).

These native shrubs were dominant on the valley floor when the groundwater in the valley was very shallow and, in some places, even water logged seasonally. In the mid-20th Century, native phreatophytes were removed to clear land for agriculture and to salvage the water table from unnecessary transpiration loss. In the 1970s, the Closed Basin Project began pumping groundwater from 170 unconfined "salvage" wells in the closed basin to lower the water table, avoid further ET loses, and to augment water deliveries on the Rio Grande, which were in danger of not being met due to upstream river diversion for agriculture. Subsequently, flood irrigation has been replaced by pivot irrigation. Both significant agricultural withdrawals and U.S. Bureau of Reclamation (herein USBR) salvage well pumping have impacted the valley's water table. Since the 1990s, the San Luis Valley has experienced a sharp decline in the unconfined aquifer. On one of the federal wildlife refuges where *S. vermiculatus* and *E. nauseosa* dominate, the groundwater table has dropped more than 4 m (13 feet) during this 25-year period (Site 3).

Phreatophyte shrubs often exist in communities with facultative phreatophyte grasses. These plant networks are important in keeping the dry soils of the San Luis valley floor in place, especially during the wind storms in the spring, which can, at their worst, darken the landscape and make driving on roads hazardous. Such windstorms strip away the valley's topsoil and deposit dust on the Sangre de Cristo and San Juan mountain snow. Dust-on-snow lowers the snow's albedo and hastens melting. This increases runoff and lowers infiltration and aquifer recharge.

In an effort to better understand what may be happening to the native phreatophytes as the groundwater table drops, and with an intention to view the facultative phreatophytes as a way to examine groundwater, this study asks, do the water capture strategies of these phreatophytes change as the depth to groundwater increases? Are shrubs in areas with the greatest drop in water levels able to access the groundwater? What level of groundwater depletion lowers phreatophyte productivity?

6.3 Methods and Research Design

The source of a plant's water, and any seasonal variation, can be determined by comparing stable isotope signatures ($\delta^{18}O$ and $\delta\ ^{2}H$) from the plant's xylem tissues (shrub stem sections) with those of water reference points such as rain water samples from preceding months, ground water samples from adjacent wells, and upper horizon soil samples (Ehleringer and Osmond, 1989, Kray et al., 2012).

Three sites were chosen in the San Luis Valley. Sites were chosen in dry chaparral areas where both *S. vermiculatus* and *E. nauseosa* dominate. All sites are located on federal land away from visitors and accessed through special research permits. The sites are fenced and are situated next to monitoring wells that offer historical and current data. Two of the sites have tipping-bucket rain gauges attached to data loggers that record precipitation in 0.254 mm increments. No site receives or is near artificial irrigation. Sites were chosen for varying depth to groundwater. Site 1 has shallow groundwater that fluctuated seasonally during the sampling periods of 2015-2016 from 1.7 to 2.16 meters (5.6 to 7.1 feet) to water. Site 2 depth to groundwater fluctuated less but ranged from 4.5 to 4.6 meters (14.8 to 15.1 feet). Site 3 has the deepest wells; depth from ground to water in the unconfined aquifer is about 6 meters, ranging from 5.92 to 6.01 m (20 feet).

Groundwater monitoring at Site 1 began in 1994 with the installation of 17 shallow piezometers. Data were collected manually at these piezometers at routine intervals from 1994 to 1998 by the USGS. Beginning in 2000, manual readings were taken sporadically by the FWS until, in 2015, submersible transducers were installed to record groundwater fluctuations several times daily. Groundwater at Site 2 is

monitored by both the NPS and the USBR. Manual measurements began in 2009 and continue to present day; automated measurements began in 2010. The data logger equipment is maintained by the USBR and data are transmitted to the NPS, which also conducts routine manual measurements to verify the accuracy of the data loggers. Monitoring of groundwater at Site 3 began in 1982 by the USBR.

Groundwater samples were collected in the summer and fall seasons from each of the study site wells. Groundwater at Site 1 was extracted using an external suction pump and a sterile sampling hose. Groundwater at Sites 2 and 3 (being deeper) were sampled using a generator-powered external suction pump with sterile sampling hose. All water samples were collected in sterile 50 ml containers and transported on frozen ice. Once in the lab, samples were filtered using 0.2 μm filters into new, sterile 50 ml containers. Samples were transported on dry ice to the laboratory in Laramie, Wyoming, where 200 μl aliquots were placed in air-free vials for IRMS analysis.

Stem samples were collected between 3-5 am in the pre-dawn mornings in mid-April, mid-July, and mid-October of 2015 and 2016 (Table 1). Care was taken to sample the phreatophytes before dawn, when the plant stomata would open and allow for air exchange. Because the three sites are roughly 40-minutes driving distance apart, and one of the sites requires a short hike, not all three sites could be sampled on a single day. Therefore, Site 1 was sampled on the 15th of these sampling months while Site 2 and 3 were sampled the following day, on the 16th. One exception occurred in April 2016 when a blizzard, which began in the early hours of the 16th, forced sampling of Site 2 and 3 to be delayed by one day.

Table 6.1: Plot Site locations, depths to water, and sampling periods.

Name	DTW in Meters	Point Location	Spring Sampling	Summer Sampling	Fall Sampling
Site 1 (ANWR)	**1.7-2.2**	37.44426, -105.76111	Apr 15, 2016	Jul 15, 2015 and 2016	Oct 15, 2015
Site 2 (GRSA)	**4.5-4.6**	37.66370, -105.67832	Apr 17, 2016	Jul 16, 2015 and 2016	Oct 16, 2015
Site 3 (BNWR)	**5.9-6.0**	37.79483, -105.87277	Apr 17, 2016	Jul 16, 2015 and 2016	Oct 16, 2015

Liquid nitrogen was provided by a local supplier and was carried into the field using a 10 L cryogenic tank with color-coded sample dippers. In order to clip and drop the sample efficiently into the tank of

liquid nitrogen and minimize any contact with air, samples were pre-labeled, clipped, wrapped in tinfoil, and lowered into the tank of liquid nitrogen. Three stem samples were taken per shrub per site. Stem samples were taken as near to the ground as possible, well below any foliage, and were roughly three centimeters in length. Samples were kept frozen in liquid nitrogen and transferred to the University of Wyoming's Stable Isotope Facility in Laramie, Wyoming, where they were removed, one by one, and placed on a cryogenic vacuum line. Transfer from the liquid nitrogen tank to the sample tubes was done swiftly, and samples were kept frozen on liquid nitrogen until a clean vacuum line was established and heat began the distillation process. Soil water samples were cryogenically extracted using a method similar to that used for the stem water samples. Roughly 5 gram soil samples collected at 15 cm and 25 cm depths which had been wrapped in aluminum foil and stored in liquid nitrogen, were transferred to frozen sample vials on the extraction line, and a thick layer of sterile, glass wool was placed over the soil to ensure the soil stayed in place as vacuum pressure was adjusted.

The distillation process took two to three hours per sample to ensure 100% of the stem water condensed into the sample vial. Samples were weighed before and after distillation and compared to weights after 24 hours at 95°C to ensure the water extraction was complete. Since cryogenic plant extraction also transfers alcohols and may, in some cases, contain oil contamination from the o-ring linings, all of these samples were run through an elemental analyzer and placed on an IRMS machine for analysis. In this manner, condensed stem water was pipetted into air-free vials and run on IRMS machines, where oxygen and hydrogen molecules were separated into individual columns and the isotope fractionation was counted using isotope ration mass spectrometry (IRMS).

Temperature conversion elemental analysis (TC/EA) was used to convert compounds containing oxygen and hydrogen into the gases CO and H_2 for separation using gas chromatography. Oxygen and hydrogen were then analyzed separately using continuous flow isotope ratio mass spectrometry (IRMS) via a ConFlo IV. This method is known as TC/EA-IRMS. Plant samples were run on a Thermo Scientific TC/EA and Thermo Scientific Delta V Plus IRMS. The IRMS was run in three injection mode; the last

two values were averaged to produce the measured ratio of each sample. Four known, laboratory water references were run alongside the samples in each IRMS run as a quality control measure and used to slightly correct the isotope signals. The first three references were generated by the University of Wyoming's Stable Isotope Facility—Evian water, UWSIF 302, UWSIF303. The fourth reference material I generated and did not disclose to others working in the Stable Isotope Facility, either in content or sample loading position. Quality assessment was conducted based on the standard uncertainty of the known value of UWSIF reference materials. If the standard uncertainty was larger than 0.3 ‰ for oxygen or 2.5‰ for hydrogen, the samples would have been re-analyzed. The isotopic composition of oxygen is reported in per mil relative to VSMOW water on a scale such that VSMOW and SLAP water, respectively, are 0 ‰ and -55.5 ‰. The isotopic composition for hydrogen is reported in per mil relative to VSMOW water on a scale such that VSMOW and SLAP water, respectively, are 0 ‰ and -428 ‰.

Each IRMS run contained precipitation (snow and rain events from the previous two months), nearby surface water, and groundwater from each of the three sites alongside the season's plant water samples. Isotope signatures (specifically $\delta^{18}O$) of precipitation were enriched or depleted based on air temperature, saturation, and storm direction, so it is important to use precipitation from the current and preceding month(s) as reference points. While groundwater chemistry changed slightly (e.g. Cl^-, NO_3^-) across seasons, the $\delta^{18}O$ and $\delta^{2}H$ signatures of groundwater remained constant over the testing period. The well water from each site was sampled in different seasons, and the isotope signatures were averaged to give a groundwater signature value for each site.

6.4 Site Descriptions

The growing season in the high-elevation valley begins in May and continues through September. State-regulated irrigation season begins in April and continues through the first week of October. In April and May there is also increased runoff from nearby snowmelt.

6.4.1 Site 1

Site 1 is a 5m x 4m plot located at 37.44426, -105.76111, beside a shallow piezometer (ANWR-9) on the Alamosa National Wildlife Area. The ANWR is an 11000 square acre chaparral and grassland area punctuated by irrigated wetlands and the winding path of the Rio Grande as the river heads south toward New Mexico. The wildlife refuge is home to wildlife, notably elk and migratory birds including the Sandhill crane. While cattle and sheep grazing is allowed under permit, Site 1 is fenced. Within Site 1, pictured in Figure 6.1, there are six small *Sarcobatus vermiculatus*—greasewood shrubs. Five of these are connected under an earthen mound on the western side of the plot. The other, a very small shrub, is isolated on the eastern side of the plot. There are five distinct *Ericameria nauseosa*—rabbitbrush shrubs, though they are close enough to retain association. Besides these phreatophytes, the plot contains other facultative phreatophyes. These consist of 40 *Sporobolus airoides*, or alkali sacatone tufts, a handful of these creating a ring shape, and 29 *Distichlis spicata*, or salt grass. In addition, there are 30 native purple aster plants. The largest *E. nauseosa* and largest *S. vermiculatus* were chosen for sampling. Each was marked within the plot, and during each sampling period (Summer ’15, Autumn ’15, Spring ’16, Summer ’16) three stem samples were taken per plant. The sampled *E. nauseosa* has a canopy height of 1.2 m. Its gnarled base consists of 8 woody stems, each about 0.07 m. The sampled *S. vermiculatus* measures 0.5 m high from a slightly raised earthen mound. This mound covers where two of the S. vermiculatus shrubs are entangled. The remaining *S. vermiculatus* plants covering this mound are offsprings.

Groundwater is the most accessible at Site 1 due to the high water levels. Groundwater on the Alamosa Wildlife Refuge was first monitored by the USGS and then by the US Fish and Wildlife Service, so the history of this well is stitched together between the two data sets. While these data span a twenty-year period, the consistency and quality of these data are less reliable than at the other two sites—in part, because the priorities of the US Fish and Wildlife Service are on wildlife monitoring and not on natural resource monitoring. (A more reliable system of data logging has since been established at Site 1.) The first data series depicted in Figure 6.2 is from the periodic USGS readings. The second data series is from

the sporadic manual monitoring over a fourteen-year period by USFWS. Although not every year is represented in this data series, and the readings are irregular, the groundwater levels clearly show a distinct seasonal pattern as well as a generally downward trend. Beginning in February of 2015, automatically recorded transducer data establish a well-marked up and down seasonal fluctuation as well as a general downward trend. In 2015 the highest spring groundwater levels were recorded at 1.98 m in the first week of April. In the first half of August, groundwater levels dropped to 2.16 m but recovered to 1.58 m in mid-November. In 2016, the highest groundwater levels were recorded in the second half of May at 1.27 m and the lowest groundwater levels were recorded late August through early October at 2.18 m. During the plant sampling periods in 2015 and 2016 overall, groundwater fluctuated between 1.7 and 2.16 m deep.

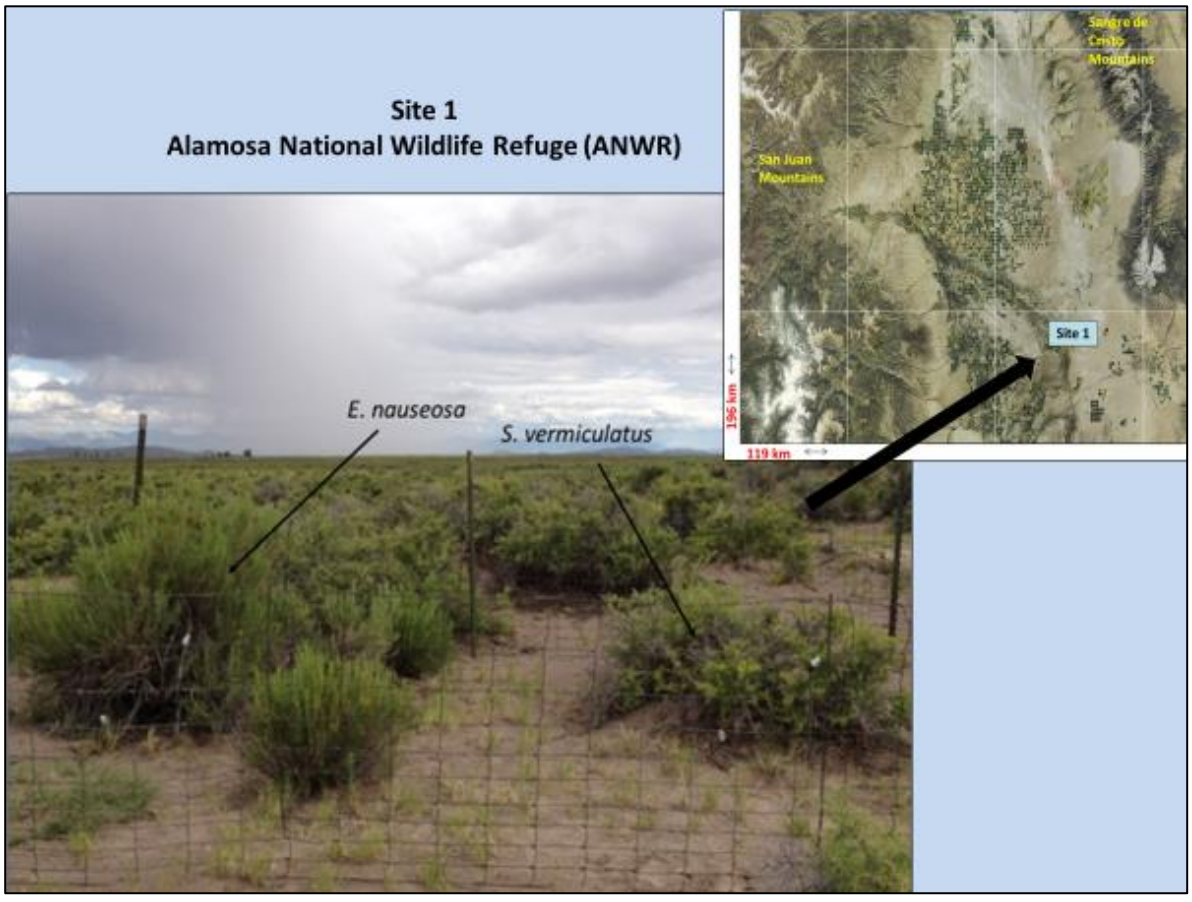


Figure 6.1: Site 1 location on the Alamosa Wildlife Refuge has the highest groundwater table.

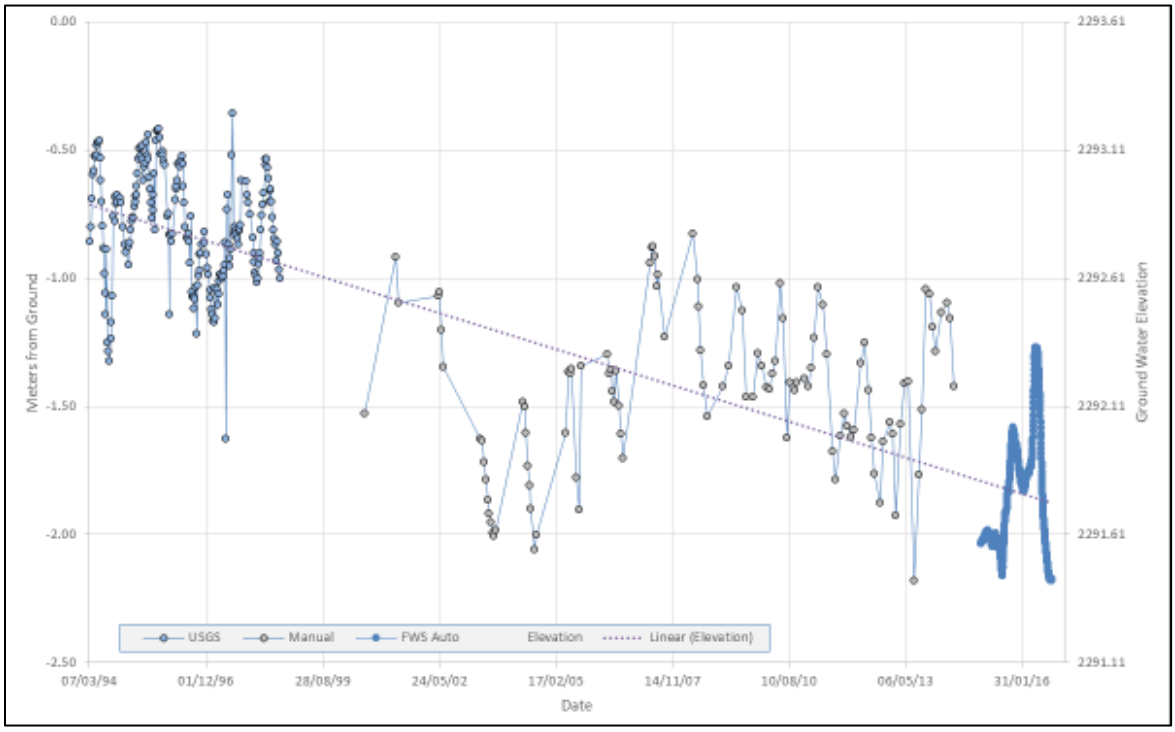


Figure 6.2: Seasonal and yearly fluctuations of groundwater at Site 1 shallow well.

6.4.2 Site 2

Site 2 is a 5m x 5m fenced plot located at 37.66370, -105.67832, on the southern sand sheet transition zone of Great Sand Dunes National Park and Preserve. It is located 56 kilometers (35 miles) north of Site 1. Site 2 is nearer the main recharge areas of the Sangre de Cristo Mountain Range, where a minor fault runs north-south along National Park Service land nearer the mountain base. Site 2 is accessed via a Park Service dirt road. There are no creeks near this site, but rainfall quickly infiltrates the sand sheet. Site 2 is located next to a monitored boundary well (BP-1) 14 m deep, and records show water table fluctuations of 4.5 to 4.6 m throughout the sampling period. Great Sand Dunes National Park is home to large and small

mammals. Before erecting the study plot barrier, evidence of elk grazing was found near the selected shrubs. As opposed to some other areas of the San Luis Valley, S. vermiculatus and especially *E. nauseosa* here appear large and healthy.

Within Site 2, shown in Figure 6.3, there are 4 *S. vermiculatus* shrubs and 5 *E. nauseosa* shrubs. There are 4 prickly pear cactus colonies. There are 38 *Sporobolus airoides* grass clumps and 11 *Distichlis spicata* grass tufts. There is one native purple aster. The largest *E. nauseosa* and *S. vermiculatus* shrubs were selected and marked for sampling. They stand 1.3 m apart. The *E. nauseosa* measures 1.1 m and 1.23 m high, 1.82 m and 0.83 m across the canopy, and 1.76 m across the mid-section foliage at its thickest points. Diagonally, it measures 1.8 m and 1.63 m across. The base of the shrub is split into two thick gnarled sections which measure 0.06 m and 0.08 m across. The *S. vermiculatus* shrub measures 1.09 m and 0.93 m high, 0.87 m and 1.08 m across the canopy, and 1.26 m across its foliage mid-section. Diagonally, it measures 1.1 m and 1.32 m across. Its base is made up of about 40 thin stems and measures 0.24 m and 0.16 m across.

Figure 6.4 shows Site 2 has a depth to groundwater of 4-4.5 m. Groundwater fluctuations and overall drawdown at Site two are less distinct than at Site 1. The groundwater fluctuation during sampling seasons in 2015 and 2016 was 4.5 to 4.6 m.

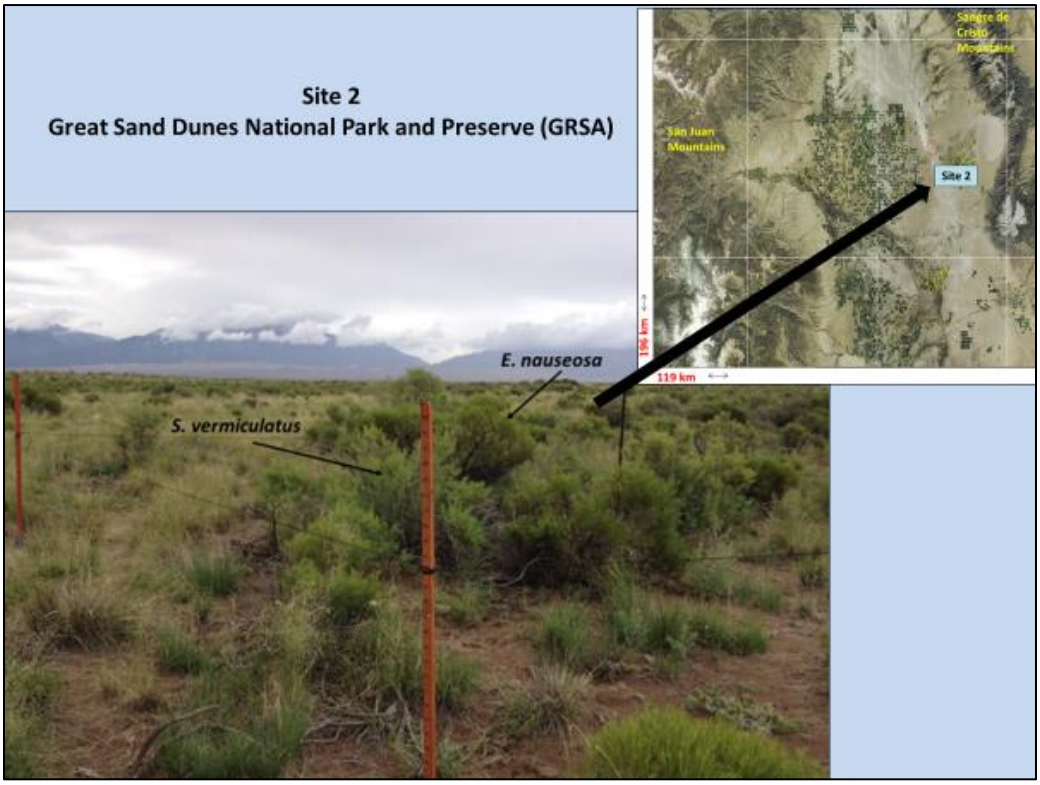


Figure 6.3: Site 2 located in Great Sand Dunes National Park and Preserve.

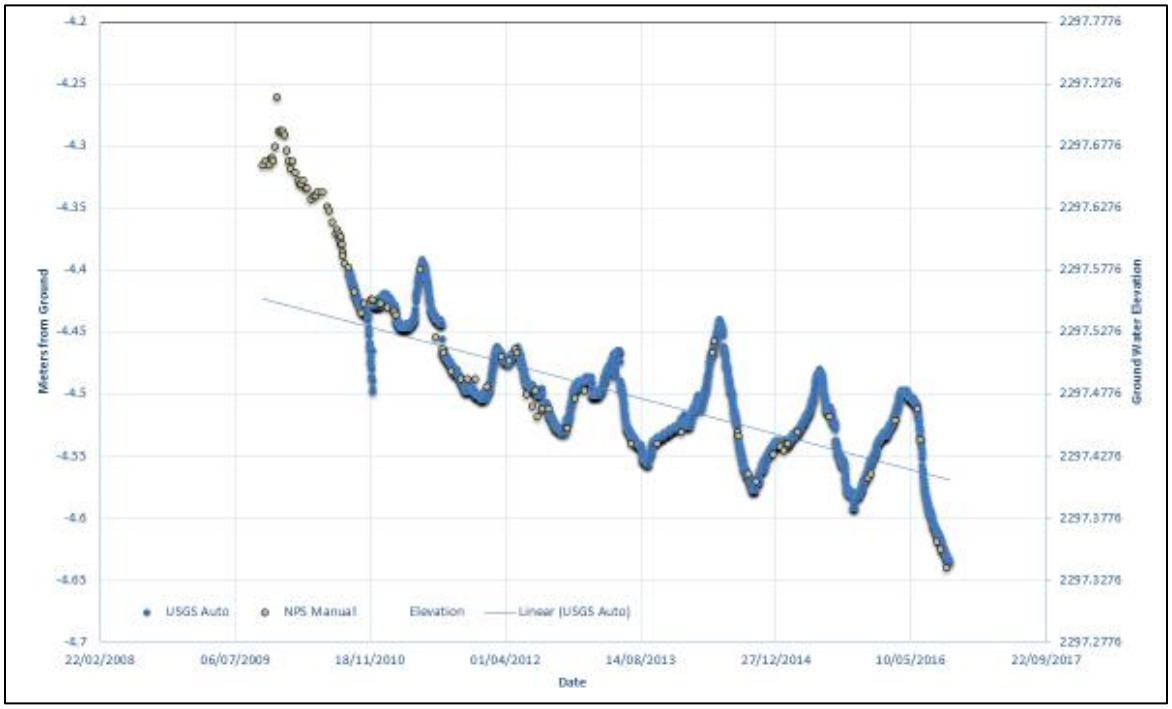


Figure 6.4: Groundwater fluctuations at Site 2 unconfined boundary well.

6.4.3 Site 3

Site 3 is located at point 37.79483, -105.87277, in the northern valley floor of the San Luis Valley, but on the southern edge of the Baca National Wildlife Refuge (BNWR). This area of the BNWR sits between production salvage wells supplying water to the Closed Basin Project to the east, and agricultural pivot irrigation wells to the west. Due to lower species abundance, and due to difficulties in identifying an *E. nauseosa* shrub large enough for seasonal sampling, it was necessary for this site to encompass a greater area (seen in Figure 6.5). It is also further away from a monitoring well. US Bureau of Reclamation (USBR) monitoring well EW-39 is located 160 paces from Site 3, but this well is understood to be a good indicator of the lowered groundwater table underneath Site 3. The plot size at Site 3 is 5m x 10m, and the two facultative phreatophyte shrubs selected for sampling are 6.6 m apart. There are two *E. nauseosa* and four *S. vermiculatus* plants. The bare earth exposed within this plot is about 45%. Besides the *E. nauseosa* and *S. vermiculatus* shrubs, there are 12 *S. airoides* grass rings. The largest *E. nauseosa* canopy measures 0.8 m high and 1.02 m across the thickest midsection area of foliage. The base of the shrub consists of a single stem measuring 0.07 m across. The canopy cover has about 70% foliage with branches radiating outward from the center. The largest *S. vermiculatus* canopy measures 1.03 m high and 1.87 m across the thickest midsection with foliage. The canopy has about 50% foliage cover. The shrub's base comprises about 20 individual stems, and these measure 0.17 m across. There is evidence of cattle grazing near the *S. vermiculatus* shrub, and there is evidence that prairie dogs have made tunnels under the *S. vermiculatus*.

The groundwater at Site 3 has been remotely monitored and physically measured since 1982. EW-39 is part of a nested well system (which was discussed in Chapter 5). The monitoring wells consist of two upper confined aquifer wells and one unconfined aquifer well. The groundwater table has declined sharply in this area over the past few decades. This is shown in Figure 6.6. The longterm history of the

monitored well at Site 3 shows that in the early 1980s, when the depth to water table hovered near 1.6 m, seasonal fluctuations of drawdown and recharge appear consistently every year. Every year, the drawdown is replaced by recharge. The late 1980s see an increase in water and a higher water table. In 1986 and 1987, the depth to water is 1.37 m. After 1988, there is a significant decline in the water table with little yearly recovery. The graph shows a groundwater drawdown of roughly 5 m. The depth to groundwater at time of sampling was roughly 6 m.

This area of the valley's closed basin is marked by significant groundwater abstraction. Although this monitoring well was instituted to monitor drawdown caused by CBC pumping, the network of monitoring wells show significant drawdown from the agricultural fields to the west. Just to the west of Site 3 is the beginning of a vast expanse of privately owned pivot circles, each pumping groundwater from the unconfined aquifer for agricultural use. These pivot circles are easily identified in satellite photos of the San Luis Valley and can be seen in the aerial image of Figure 6.5. Site 3 is situated on the southern extent of a national wildlife refuge—this southern portion of the BNWR has experienced a dramatic drawdown of water over the last twenty years. This has left the landscape—which at one time supported wetlands and playas—more dependent on ephemeral surface waters (those not diverted) and on the summer monsoons.

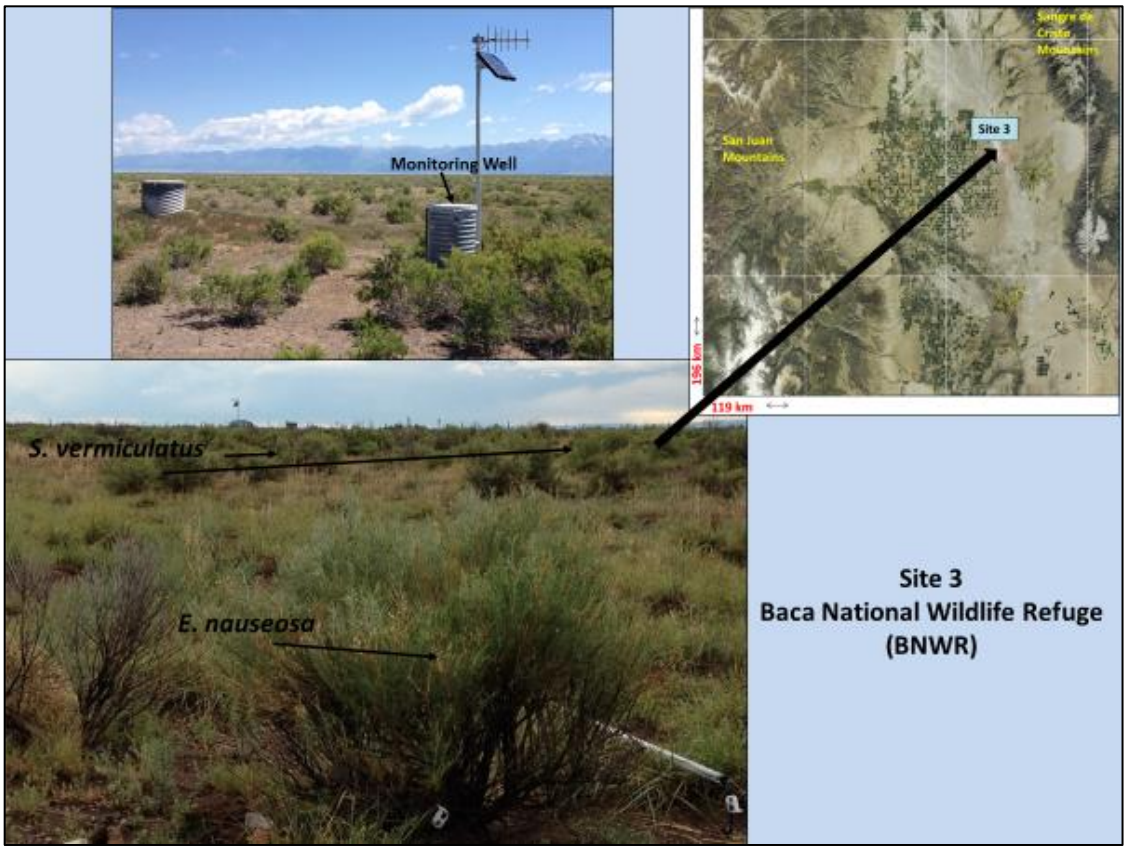


Figure 6.5: Site 3 located at the southern end of the Baca National Wildlife Refuge.

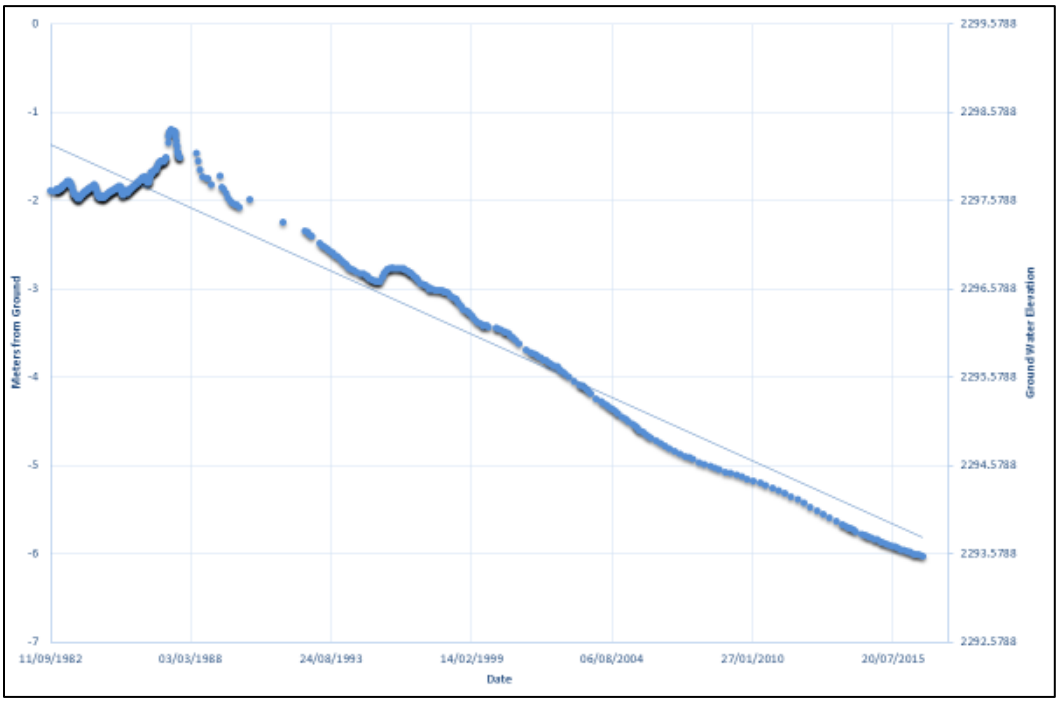


Figure 6.6: Groundwater levels measured in the unconfined aquifer at well EW-39. Linear line is trend in drawdown.

6.5 Comparison of Sites

The three vegetation sites were chosen primarily for increasing depth to water. Barring slight seasonal variation, the sites have depths to groundwater as follows: Site 1 is 1.7 m, Site 2 is 4.5 m, Site 3 is 6 m. In some ways, Site 1 and Site 3 are more similar in soil compaction, though Site 1 had more clay content beginning at about 15 cm depth. Both may be categorized as medium sandy silt. For a detailed soil profile of Site 1, please refer to Chapter 7, Figure 7.2. The soil at Site 2 is sandy and unconsolidated. The pH of groundwater at all three sites was comparable (ranging from pH 6.9 at Site 1 to 7.05 at Site 3). The TDS of groundwater sampled at Site 1 was roughly twice as high as the other two sites at 510 mg/L for Site 1, 208 mg/L for Site 2, and 280 mg/L for Site 3. There were some significant differences between the sites in plant traits and the makeup of the vegetation community. A summary comparison of vegetation metrics can be seen in Table 6.2.

Table 6.2: Summary comparison of plant metrics.

Metric	Site 1	Site 2	Site 3
Depth to groundwater (m)	**1.7**	**4.5**	**6**
Site area (m^2)	20	25	50
Distance between sampled plants (m)	2	1.3	6.6
% of site that is exposed, bare earth	~10	~20	~45
Density *E. nauseosa* (n/m^2)	0.25	0.2	0.04
Density *S. vermiculatus* (n/m^2)	0.3	0.16	0.08
Species richness (ni/m^2)	0.25	0.28	0.06
*Shannon Diversity Index	1.373	1.223	0.849
*Evenness	0.853	0.628	0.773
E. nauseosa canopy height (m)	1.2	1.23	0.71
E. nauseosa maximum crown Ø (m)	1.36	1.82	1.02
E. nauseosa # of stems on sampled plant	8	2	1
E. nauseosa largest stem Ø (m)	0.07	0.04	0.07
S. vermiculatus canopy height (m)	0.5	1.09	1.03
S. vermiculatus maximum crown Ø (m)	1.36	1.26	1.87
S. vermiculatus # of stems on sampled plant	~32	~40	~20
S. vermiculatus largest stem Ø (m)	0.01	0.01	0.01

*Note: Diversity index and evenness are not directly comparable between sites because site area varies.

Since it is necessary to compare stable isotope signatures from plant stems to stable isotope references for groundwater and precipitation water, reference values were established for unconfined groundwater at each site, and a seasonal, weighted precipitation value was used for all sites. Near-surface soil water references were established for each site. As opposed to major ion and trace metal chemistry, which could at times shift widely based on the season, stable isotope values did not shift perceptibly in groundwater at these three sites sampled through different seasons. In Figure 6.7, the Site 1-3 groundwater references can be seen as shaded circles. The weighted seasonal precipitation references are pictured as shaded diamonds. Note that the spring 2016 weighted sample appears at the depleted edge of the graph owing to the severely depleted snow signature of the 2016 blizzard event, which occurred just days before the spring 2016 plant sampling.

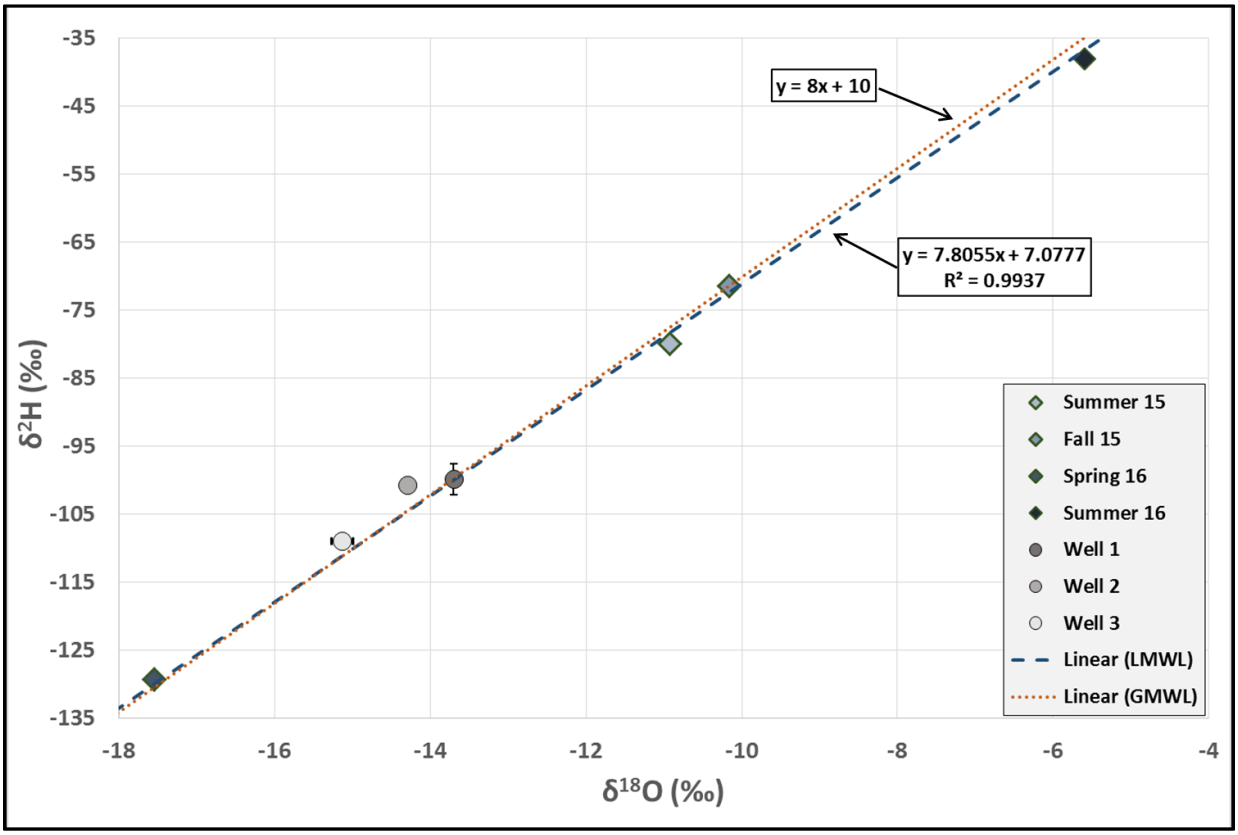


Figure 6.7: Overview graph depicting weighted mean precipitation and mean groundwater at each vegetation site. Well 1, 2, 3 (shaded circles) correspond to the unconfined groundwater at Site 1, 2, and 3. Shaded diamonds show the spread of weighted precipitation based on spring, summer, and fall seasons. Both the local meteoric water line (LMWL) and the global (GMWL) are shown for reference.

6.6 Results of Phreatophyte Water Use

Results of the phreatophyte water use study are displayed within a single graph for each site. *S. vermiculatus* is shown in red. *E. nauseosa* is shown in blue. Each of the seasonal samplings follows in chronological order from 1 through 4. At each site, *E. nauseosa* (rabbitbrush) and *S. vermiculatus* (greasewood) were sampled in summer 2015, fall 2015, spring 2016, and summer 2016. In each of the sampling periods, three stem samples per plant were cut, frozen, cryogenically extracted, and analyzed for δ^2H, $\delta^{18}O$. The three stem samples per plant, per season, were averaged to give one point on the graph, though the isotope results were very similar (and error bars can't be seen at this scale). Similarly, the groundwater reference is an average derived from sampling through multiple seasons, but seasonal influence is not seen in groundwater isotope values. Soil water was sampled alongside each plant in the final seasonal sampling of summer 2016. These targeted shallow rooting zone depths of 15 and 25 cm. Soil water points appear as pink triangles in Figure 6.8, Figure 6.9, and Figure 6.10.

The GMWL is shown for reference in Figures 6.8, 6.9, and 6.10 as a faint, pink dashed line. The valley floor LMWL is shown in these figures as a black dashed line, though these MWLs aren't as important for analyzing plant water. In general, plant water and soil water will move below the MWL—that is, they will become more enriched in ^{18}O and will show greater $\delta^{18}O$ values as they undergo fractionation from evaporation (whereby ^{16}O, which is lighter isotopically than ^{18}O, will evaporate preferentially). That is why soil water samples, extracted from depths of 15 and 25 cm deep and subjected to evaporation, will show more positive $\delta^{18}O$ values than will groundwater.

6.6.1 Results for Site 1

The phreatophyte shrubs at Site 1 should have no difficulty reaching groundwater because the average depth to groundwater over the sampling period ranged from 1.7-2.2 m, a depth easily reached by *E. nauseosa* and *S. vermiculatus* taproots. *S. vermiculatus*, as seen by following the red line in Figure 6.8, appears to utilize greater near-surface rainwater and snowmelt than does *E. nauseosa* at Site 1. The *S. vermiculatus* appears to be transitioning from groundwater to precipitation water in summer 2015, and it continues to use near-surface soil water (precipitation) in fall 2015. In spring 2016 it is still utilizing near-surface soil water, but it also using a small amount of groundwater and transitioning into groundwater utilization by July 15, 2016. Because a higher-than-average amount of precipitation arrived early (May) in 2015, *S. vermiculatus* may have already been transitioning to rainwater use during the first sampling period and previous summer, on July 15, 2015. *E. nauseosa*, on the other hand, seems to employ the opposite strategy at Site 1. While *S. vermiculatus* shifts to rainwater utilization in the fall (October 15), *E. nauseosa* remains using groundwater. The only time *E. nauseosa* alters its strategy to utilize—at least in part—rainwater in the upper soil is in the spring (April 15, 2016).

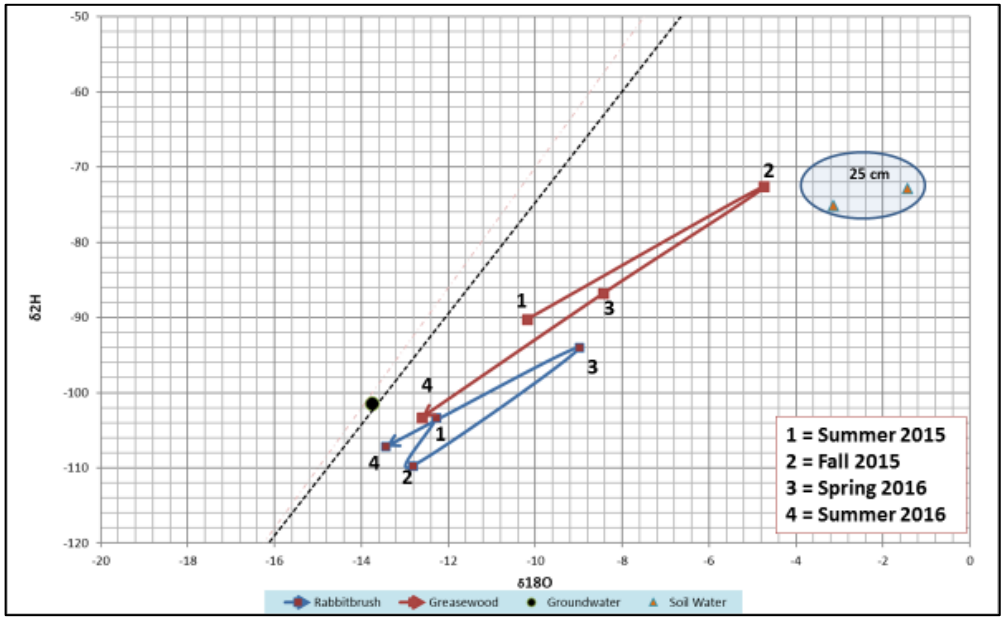


Figure 6.8: Facultative phreatophyte utilization of water through the seasons at Site 1. The red line shows seasonal variation in plant water extracted from *S. vermiculatus* and the blue line shows seasonal changes to water utilized by *E. nauseosa*. The circled triangles in the upper right show soil water signatures at shallow rooting depth. The black circle shows the groundwater signature, and since the depth to groundwater at Site 1 is shallow, the groundwater is easily accessed.

6.6.2 Results for Site 2

E. nauseosa and *S. vermiculatus* appear to follow similar water utilization strategies at Site 2, where the groundwater depth is 4.5 m, and where the soil profile is sandier than the other two sites because it is part of the Great Sand Dunes sand sheet. Both phreatophytes appear to switch (to some degree) to rainwater in the near-surface soil when large rain events cause significant wetting near the soil surface. Site 2 did not receive the same surplus of early spring rain in 2015 as did Site 1. However, in 2015 a significant amount of precipitation occurred in May. Both *E. nauseosa* and *S. vermiculatus* exhibit different isotopic signatures for summer 2015 and summer 2016 samplings. Both plants show more positive $\delta^{18}O$ and $\delta^{2}H$ values for summer 2015. This may be due to summer rains in 2015 and 2016 arriving at different times. Further evidence for this might be that both *E. nauseosa* and *S. vermiculatus* have very similar isotopic signatures for summer 2015 and spring 2016 (seasonal points 1 and 3). Seasonal points 1 and 3 for S. vermiculatus show a more positive $\delta^{2}H$ value than do the corresponding reference points for *E. nauseosa*. This indicates that *S. vermiculatus* is more heavily utilizing near-surface rainwater in its mix. By mid-October 2015 and mid-July 2016, both *E. nauseosa* and *S. vermiculatus* rely solely on groundwater.

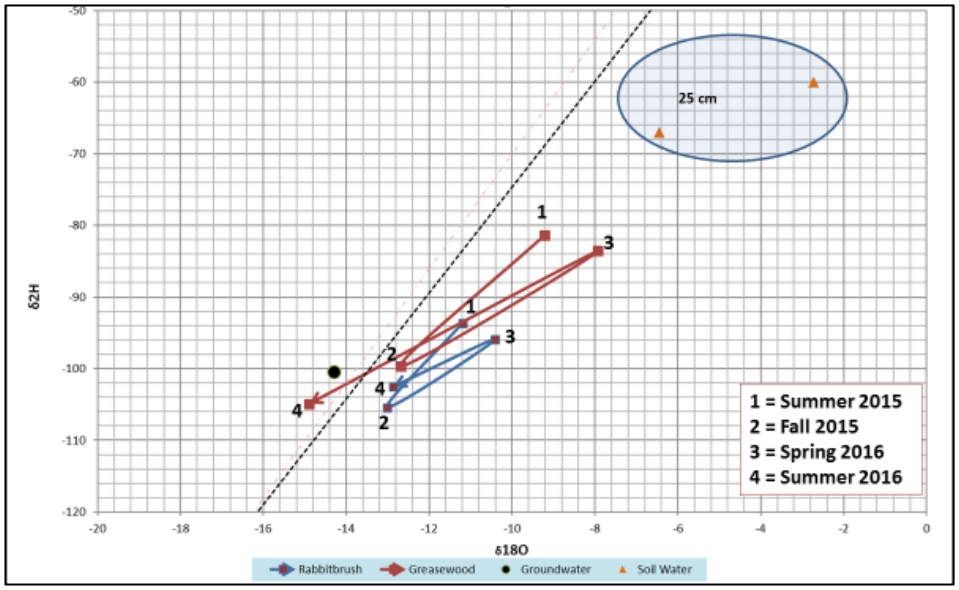


Figure 6.9: Site 2. *S. vermiculatus* (red arrow) returns to groundwater use in the autumn of 2015 (2) and summer 2016 (4). *E. nauseosa* in blue follows a similar pattern though it appears to utilize less soil water (circled triangles in upper right).

6.6.3 Results for Site 3

At Site 3, where the depth to groundwater is just over 6 m, it is likely that the *E. nauseosa* and *S. vermiculatus* plants would not be able to survive without accessing rainwater and near-surface snowmelt. The transition in isotopic signatures for *E. nauseosa* from spring to summer 2016 may indicate that in the spring of 2016, only a day after a blizzard, the *E. nauseosa* had access to snowmelt that underwent evaporative loss and fractionation before percolating into the soil. The *E. nauseosa*'s seasonal point for spring 2016 is a much greater distance to the right of the LMWL (more positive $\delta^{18}O$) than is the summer sample, taken three months later in the heat of July.

Both *E. nauseosa* and *S. vermiculatus* show their most negative $\delta^{2}H$ values during the cold, mid-April morning in 2016, a day after a blizzard. This is due to the isotopic signature of the snow versus the summer rain. It is notable that *E. nauseosa*'s spring 2016 sampling shows significant evaporative fractionation consistent with near-surface soil water. This suggests the plant's movement toward a more negative signature may reflect snowmelt on the valley floor, rather than a mixing of groundwater and near-surface soil water. *E. nauseosa* and *S. vermiculatus* at Site 3 do not appear to utilize groundwater throughout the 2015-2016 sampling periods.

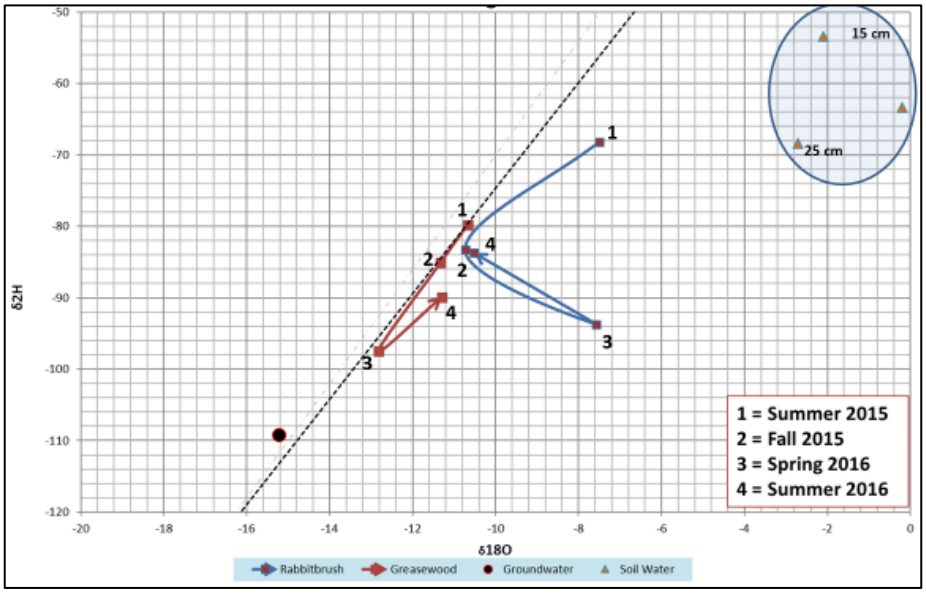


Figure 6.10: Site 3 has the greatest depth to groundwater, and the unconfined groundwater signature is shown in the lower left corner. *E. nauseosa* (blue line) and *S. vermiculatus* (red line) show changes to isotopic signatures seasonally but are still more than 2‰ away from the groundwater's $\delta^{18}O$. Note this graph's resolution does not allow for comparison to precipitation's weighted seasonal mean. Refer to Figure 6.7 for this.

6.7: Discussion and Conclusions

Most of the 200 mm/year precipitation in the San Luis Valley arrives in July, August, and the first half of September. Two tipping rain buckets with attached data loggers are located near Site 1—on the Alamosa Wildlife Refuge—and near Site 2—within the Great Sand Dunes National Park and Preserve. These demonstrate, as do most precipitation loggers placed only a few miles apart within the San Luis Valley, that precipitation is highly variable in time and place.

The data logger on the Alamosa Wildlife Refuge (Site 1) provided localized precipitation data from the end of 2015 through the sampling seasons of 2016. Before this time, non-automated measurements were taken from June 2015 and continued through November 2016. In 2015, unusually high rain was reported for May, but the largest single recorded rain event occurred on June 13 with 18 mm. The month of October had higher-than-average precipitation. In 2016, a blizzard and rain events in late April, followed by all-day rain events in early May, caused this month's precipitation to tower over the other months. April-May 2016 received more than three times as much precipitation as did July-August. This enormous spike in precipitation was localized to the central valley floor—it did not register as significantly further away at Great Sand Dunes National Park.

The data logger at Great Sand Dunes National Park and Preserver (near Site 2) shows annual variability on the total amount of precipitation but fairly consistently shows from 2010 to 2016 most precipitation arrives July through August. The notable exceptions to this pattern appear in 2010, when about as much precipitation fell in March and April as it did in July and August. Also, in 2015, an unusually high amount of precipitation arrived early in the year. Due to downpours during a single week in May, more precipitation arrived in the month of May than in July and August. This early precipitation in 2015 in the northeastern section of the San Luis Valley caused creeks to rise and overflow and localized flooding occurred. This flooding did not affect Site 2, but the early and heavy rains of 2015 are noted in the isotope analysis.

Distinct patterns of *E. nauseosa* and *S. vermiculatus* changes in water capture strategies can be seen between the different plot sites. The differences in strategy and timing are most apparent where groundwater is the most accessible (Site 1). Where groundwater is near to the surface, *E. nauseosa* relies on groundwater but *S. vermiculatus* survives on rain and near-surface soil moisture. Where the groundwater has dropped significantly over the last decade as at Site 3, where the water table dropped over 5 m and is currently 6 m to water, both *S. vermiculatus* and *E. nauseosa* rely exclusively on rain events. In the spring, where groundwater is too deep to be accessible, these plants utilize snowfall, which melts slowly during the sunny days and percolates into the ground where it is accessible to shallow roots. Relying exclusively on near-surface precipitation may limit the growth of these facultative phreatophytes—particularly *E. nauseosa*.

Neither *E. nauseosa* nor *S. vermiculatus* utilize any groundwater at Site 3, where there has been a 16 foot drop in groundwater levels over the past few decades and where water is currently 20 feet below ground. Lack of access to groundwater and limitations on soil moisture appear to be more of a constraint on *E. nauseosa* than *S. vermiculatus*. In dry years when rain is more scarce, the phreatophytes may experience a period of dormancy. On the sand sheet perimeter of Great Sand Dunes National Park and Preserve, moisture infiltrates very quickly and easily into the ground. At Site 2, *E. nauseosa* and *S. vermiculatus* exhibit the same seasonal utilization strategies. They mirror each other in their switching from near-surface rainwater to groundwater. This change may be induced by the arrival of rain. Although the facultative phreatophytes at Site 1 are a similar distance (about 1.3 m) apart, the soil is more compact and clay-rich. Infiltration of moisture is slower. Groundwater and soil moisture show a much higher TDS and salt content than at Site 2. Groundwater levels are highest at Site 1, and groundwater is easily accessible. However at Site 1, a different seasonal strategy for water utilization is employed by *E. nauseosa* and *S. vermiculatus*. *S. vermiculatus* shifts to near-surface rainwater in the late summer and fall while *E. nauseosa* uses only groundwater during this period.

Distinct patterns of water use and seasonal shifts are visible, and these species differences are most apparent where groundwater is most accessible. However, where the water table has dropped 6 m over the last decade, both *E. nauseosa* and *S. vermiculatus* survive only on near-surface snowmelt and rain. At Site 3, where there has been significant drawdown of the water table, shrub density is reduced by an order of magnitude, species diversity is lower, and the percentage of exposed, bare earth reaches 45%. The broader implications of this work point to a potential loss of biodiversity and wildlife habitat as well as a potential source of dust susceptible to wind storms when vegetation loses its ability to stabilize the soil. These may be important management considerations for shallow groundwater systems in arid environments dependent on snowmelt-driven recharge.

Chapter 7: Moisture Movement in the Soil

7.0 Summary

Electrical resistivity tomography experiments were conducted throughout the summer of 2014. A 5-meter transect with 25 metal electrodes was set up along an undisturbed area of a wildlife refuge away from irrigated land. The transect crossed phreatophyte shrubs and a 1.4 m section of bare soil. Electrical resistivity readings were taken every 15 minutes for several hours during and following rain events.

This study found most rain events in the San Luis Valley do not penetrate beyond 20-25 cm depth on the valley floor. These frequent but small rain events (typically < 1 mm) may be intercepted by vegetation canopies. Larger rain events (3-10 mm rainfall in < 3 hours) infiltrate more quickly to greater depths, and will be held longer in vegetated areas. Shrub roots appear to contribute to infiltration, especially in soils with clay content.

Movement of the zero flux plane (ZFP) is visible through the use of electrical resistivity tomography. Where the depth to water on the valley floor is < 2 m, soil moisture in the ZFP may either travel downward to join the water table and become recharge or travel upward and be released, either by transpiration or evaporation, as water vapour. As seen through time-lapse resistivity inversions along a vegetated transect, when the sun heats the valley floor, convection (and potentially advection) is greatest in unvegetated areas.

7.1 Chapter Questions, Aims, and Significance

This chapter examines diffuse recharge on the valley floor, away from areas reliant on mountain block recharge or surface water recharge. It focuses on soil moisture movement in the area between the zero flux plane and the near-surface unsaturated zone before looking more broadly at how resistivity techniques can help answer questions of recharge pathways on the valley floor and at the valley's margins. This chapter addresses the following questions:

- Can movement of the zero flux plane be visualized using electrical resistivity tomography?
- In areas with shallow water tables, how do rain events influence soil moisture on the valley floor? Does this differ between vegetated and non-vegetated areas?

To this end, the chapter aims to apply time-lapse, near-surface electrical resistivity in order to characterize soil moisture movement between vegetated and non-vegetated areas under different wetting and drying conditions.

7.2 Introduction

Recharge is generally defined as the downward flow of water reaching the water table and adding to water storage (Freeze and Cherry, 1979, Meinzer, 1923, Healy and Scanlon, 2018, Hogan et al., 2004, Hiscock, 2005) and is best understood by including an examination of the unsaturated zone (Stoertz et al., 1991). Water infiltration, movement, and retention change significantly between the unsaturated and saturated zones. Movement in the unsaturated zone is considered complex because there is an upward and downward movement of water, and the unsaturated zone faces complicating factors (such as hysteresis, air, and plant interactions). When not viewed from a microscopic lens, water movement into the soil may be described as a circular wetting front with horizontal and vertical movement. When the wetting front

reaches a deeper soil layer, the textural stratification determines how and at what rate water moves beyond this soil layer barrier. If the next soil layer is coarser, the air space and lower matric potential will cause a buildup of moisture. If the upper layer is loamy and the layer beneath is fine, the buildup of moisture will be due to lower hydraulic conductivity of the fine soil layer (Miyazaki, 2006).

The zero flux plane is defined as a horizontal plane within the unsaturated zone where the hydraulic gradient in the vertical direction (dH/dz) is 0 (Richards et al., 1956). Above the zero flux plane, water moves upward in response to evapotranspiration. Below the zero flux plane, water moves downward and may contribute to recharge (Healy and Scanlon, 2018). Early work in the San Luis Valley often had difficulty distinguishing transpiration and evaporation and noted discrepancies in methods of evapotranspiration (ET) measurements. A 1987 report notes where groundwater levels are shallow and depth to water < 1.25 m, evaporation from capillary rise through bare, unvegetated soil contributes a significant portion of ET measurements ascribed to *S. vermiculatus* and *E. nauseosa* shrubs (Charles et al., 1987).

7.3 Methods

This chapter relies on electrical resistivity techniques to examine moisture movement and recharge pathways through soil on the valley floor. At the plot scale, near-surface electrical resistivity tomography (ERT) data were collected in time-lapse series to measure soil moisture movement between vegetated and non-vegetated transect sections under different wetting and drying conditions. A GeoTom resistivity meter and switching unit took measurements between metal electrodes in a transect to calculate subsurface apparent resistivity, which was then inverted using the Res2Dinv software to provide a best-fit model resistivity contour plot.

The GeoTom measures voltage (V) and current (I) to calculate electrical resistance (R) through Ohm's law:

$$R = V/I \quad \text{[Eq. 7.1]}$$

Apparent resistivity (pa) is calculated using the equation:

$$pa = kR \quad \text{[Eq. 7.2]}$$

where k is a geometric constant determined by the metal electrodes along the transect (Loke, 2000).

Modeled contour plots of actual (though relative) resistivity values are created through an inversion software as a best-fit model. Electrical resistivity is inversely related to electrical conductivity. Since water is more conductive than dry soil, wet soil will show lower electrical resistivity in Ohm-m. ERT has been used to visualize water movement within stone walls and rock caves (Mol and Viles, 2011, Sass and Viles, 2010) to establish aquifer boundaries (Doetsch et al., 2012) and to identify stratification of saline water within an aquifer, as with salt water intrusion (Mills et al., 1988) or through Cl tracer tests (Singha and Gorelick, 2005). Larger ERT transects that penetrate to greater depths are also able to distinguish different rock layers, and the airborne version, called time-domain electromagnetic survey (TEM) have been used by the USGS to map subsurface layers of the San Luis Valley (Grauch and Ruleman, 2013). The electrical resistivity data of the western border of Great Sand Dunes National Park and Preserve were provided by the NPS. Wider, aerial TEM survey data with final data treatment were provided by the geophysics team at the USGS in Colorado.

Soil profiles were taken immediately adjacent to the resistivity plot transect (once resistivity testing was completed) to a depth of 0.5 m and 1 km away to a depth of 2.5 m. The deeper soil profile was taken at an opportunistic location in similar soil and provides a chemistry and water table reference, since sampling reached beneath the saturated zone.

Laboratory work was conducted in the School of Geography and the Environment, University of Oxford. Soil samples were weighed wet and weighed after 48 hours of oven drying. Particle size analysis was conducted on a Malvern Laser Particle Sizer (Mastersizer 2000) and analyzed through Gradistat software. Dry soil samples were eluted with deionized water, shaken, degassed, and allowed to sit overnight before they were filtered through a coarse filter and a 0.2 um filter for analysis on the Dionex 500 ion chromatography machine.

7.4 Experimental Design at Study Site

Throughout July, August, and September of 2014, electrical resistivity experiments were conducted at a protected study site in the Alamosa Wildlife Refuge (shown previously in Figure 5.2), adjacent to a fenced study plot (Site 1, pictured previously in Chapter 6) used in the previous chapter's plant-water study. The metal electrodes, numbered 1 through 25, were spaced 0.2 m apart in a transect totaling 5 m in length. Figure 7.1 (b) shows the numbered electrodes passing through vegetated and non-vegetated areas. Figure 7.1 (a, c) shows the theoretical and the actual 2-D plot generated from the electrical resistivity measurements. A transducer placed in an unconfined aquifer borehole located ~20 m away from the transect provided continuous depth to water measurements during the period of ERT testing. Depth to water table ranged from 1.5 m to 1.7 m during this study. Depth to water table was 1.7 m during the experiment whose results were selected for this chapter. This depth of 1.7 m is approximately twice the depth covered by the ERT. Although depth of the ERT coverage changed slightly based on the type of array run (e.g. Wenner or dipole-dipole) and the number of rows determined to give reliable results, the depth is constrained by the length of the transect and does not reach the saturated zone. This study was designed to analyze water movement in the unsaturated zone, in the shallow area between the subsurface at ~2 cm depth to just above the water table. Site 1 was chosen for ERT experiments because of its shallow water table, its typical soil, and its appropriate distance from surface water interference.

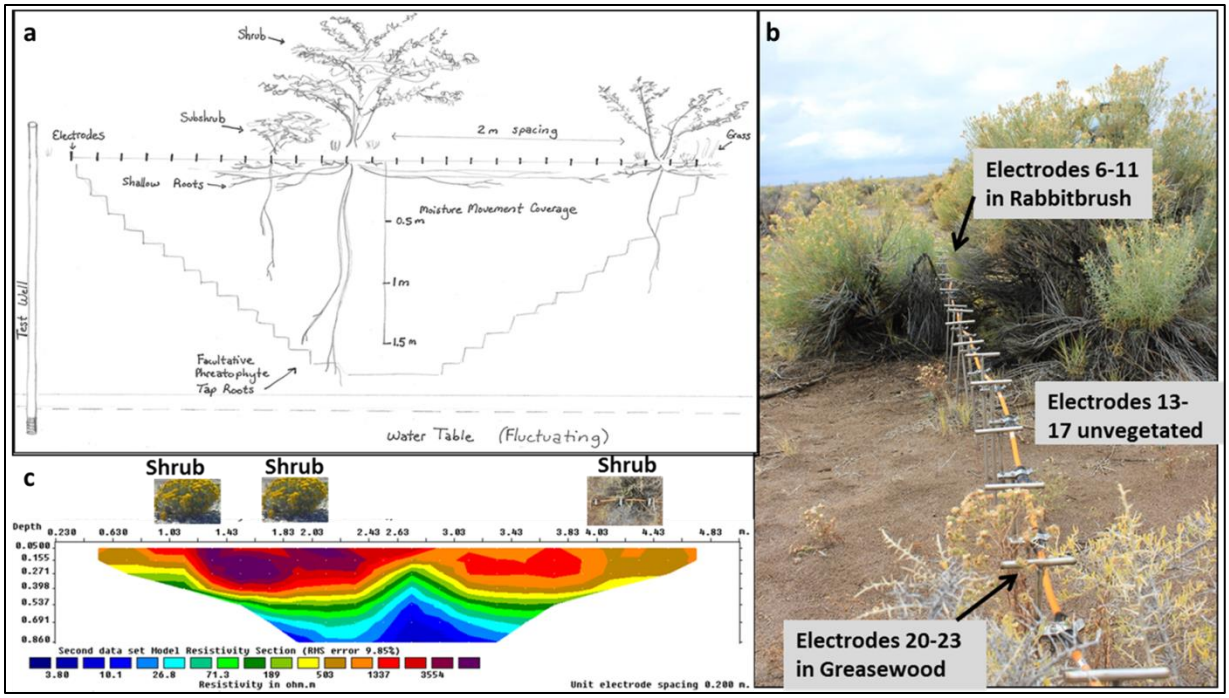


Figure 7.1: (a) a theoretical schematic showing 2-D area of resistivity coverage with plant shrubs and a fluctuating water table (b) photo of the electrode line shows areas passing through vegetation and areas across bare earth (c) an inverted resistivity plot showing distance, depth, and ohm-m resistivity values.

Once the transect was erected and baseline measurements were taken, the transect remained undisturbed for days. It was possible to disconnect the GeoTom machine from the transect, and this was done in order to leave the transect in as undisturbed a state as possible. Once the GeoTom was reconnected, and periodically throughout the testing day, "coupling" tests were performed to verify the reliability of each electrode's readings. Time-lapse readings for dipole-dipole and Wenner arrays were taken alternately in 15 minute increments over several hours.

In order to examine how soil moisture movement differs between vegetated and non-vegetated areas, the ERT transect was erected along a pathway that traveled through two *E. nauseosa* and one *S. vermiculatus* plants as shown in Figure 7.1 (b). Resistivity readings therefore included vegetated and non-vegetated regions. Experiments fell into "wetting" and "drying" categories to either capture time-lapse resistivity readings of water movement through the soil as it rained and for a time period following the rain, or to

capture time-lapse readings a few hours after a rain event and for a day or two thereafter (depending on the size of the rain event) in order to record how soil moisture moves during the process of capillary rise and evaporation. Because the experiment site was chosen for its shallow water table, it is considered the time-lapse readings and chemical profiling will provide insight into how rain events and groundwater fluctuations influence soil moisture on the valley floor. The best example of a wetting and a drying experiment are presented.

7.5 Results

7.4.1 Baseline ERT

Baseline ERT experiments were conducted over two days using transects set up adjacent to the three vegetation study plots (Site 1, Site 2, and Site 3 discussed in detail in Chapter 6). These consisted of resistivity readings in dry soil (it had not rained in over a week), and time-lapse resistivity readings after 1, 2, and 3 gallons of water had been poured in the center of the transects. In all cases there was a delay in water movement visualized by the inverted diagrams, and in all cases after 3 gallons had been poured in the center of the transect, the water had infiltrated the soil enough for visualization. While water movement appeared faster at Site 2 (on Great Sand Dunes National Park and Preserve), owing to greater porosity of the sandy soil, Site 1 was chosen for routine ERT experiments because of the following reasons:

1) Upward movement of water might be possible to visualize with a shallow depth to groundwater
2) The sandy loamy (with some clay) soil (including a higher Cl content) is more typical of the San Luis Valley floor

7.4.2 Soil Water Properties

There were two soil water profiles analyzed from the Alamosa Wildlife Refuge. The first, shown in Figure 7.2, is a soil pit at Site 1 adjacent to the transect. Once all resistivity measurements were complete, soil samples were extracted from this soil pit in 5 cm increments to a depth of 0.5 m. The soil at a depth < 20 cm was slightly alkaline with a pH 7.9. From the anion profiles of the soil samples (Figure 7.2) the Cl concentration is fairly consistent from 1-20 cm at between 1.8 mg/L and 2.6 mg/L. Cl increases with depth, with a concentration of 13.2 mg/L at 0.5 m. Fluoride and sulfate appear below depths of 20 cm, and sulfate reaches a concentration of 66.5 mg/L at a 0.5 m depth. Phosphate is only present near the surface at a depth < 25 m. Figure 7.2(a) shows this profile's particle size distribution as % soil type. The % clay content begins at 10 cm and increases to not more than 5-6%. At a depth of 20 cm, silt becomes the primary constituent, more so than % medium sand.

The second soil water profile, shown in Figure 7.3, was taken at an excavation site ~ 1 km away on land that, although now part of the wildlife refuge, was previously irrigated, fertilized, and farmed. The 2.5 meter profile extends beyond the saturated zone, which was reached at 1.7-1.8 m (marked with dashed line), and samples below the water line were measured and collected before the bulldozed pit filled with water. In contrast to nitrate results in Figure 7.2, Figure 7.3 shows elevated concentrations reaching 30 mg/L NO_3 at 20-30 cm depth. SO_4 and Cl peak at 50 cm at 25 mg/L and 13 mg/L respectively.

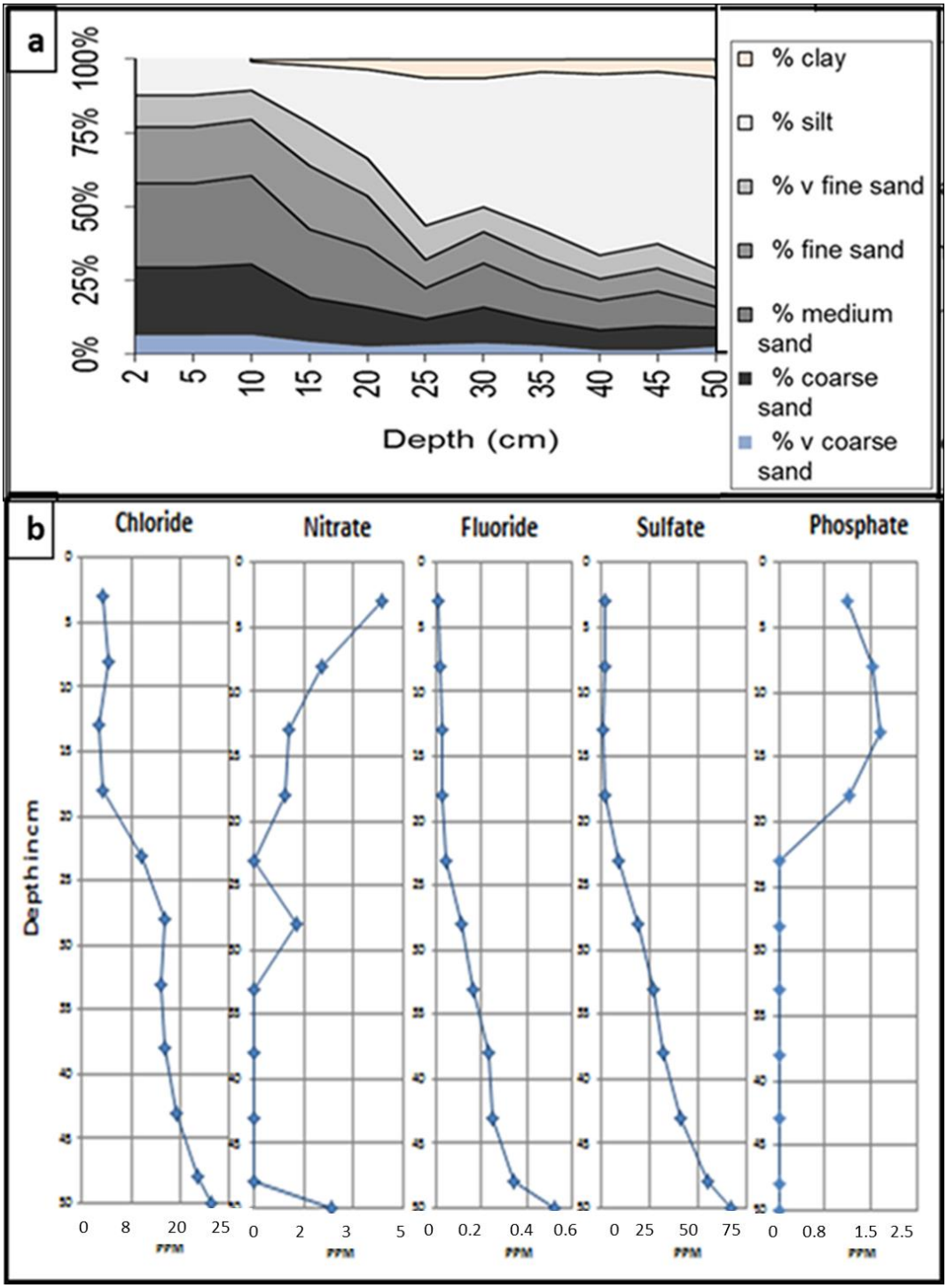


Figure7.2: Soil water profile 1 characteristics (a) Particle size analysis (b) Anion profile to 0.5 m.

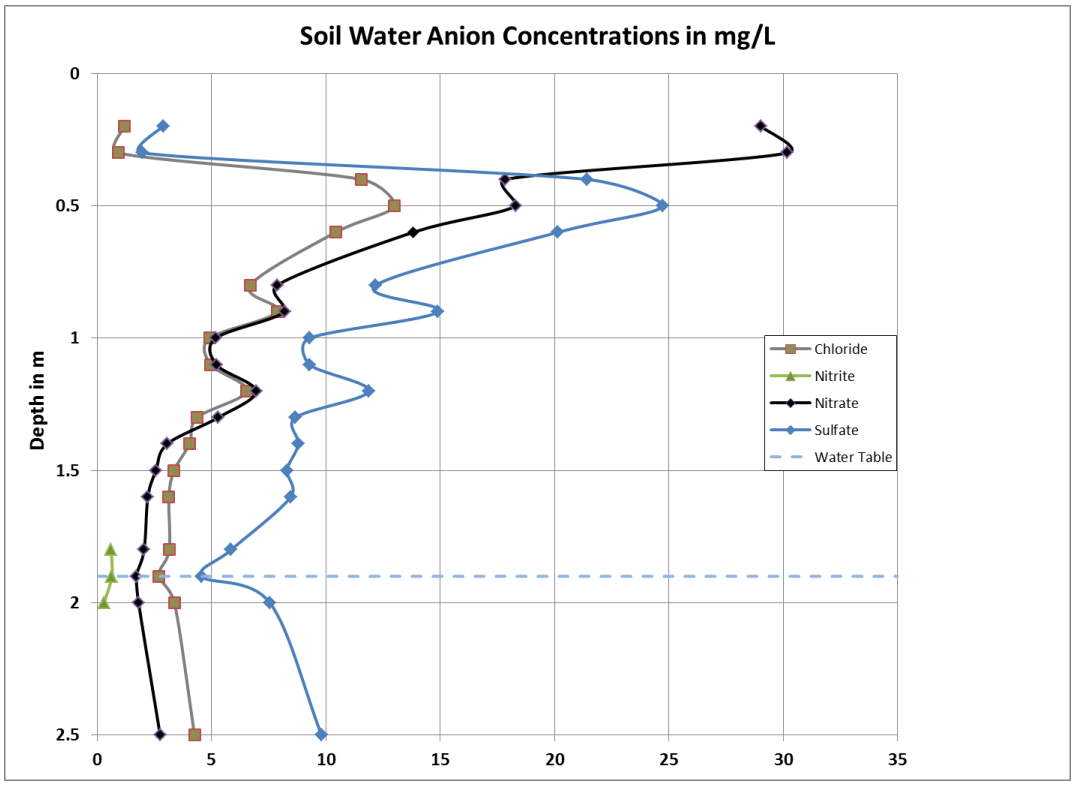


Figure 7.3: Soil water profile from a nearby soil pit in a previously farmed area. The dashed blue line represents the water table where soil was saturated and quickly filled in with water. Nitrate is shown as a black line.

7.4.3 Representative Electrical Resistivity Time-Lapse Results

To analyze, in a non-destructive manner, how water moves through the soil layers above the shallow aquifer, a series of "wetting" (through natural rain events) and "drying" (through evaporation in the hours and days after a heavy rain event) experiments were conducted in a protected area of the Alamosa Wildlife Refuge. All wetting and drying experiments were gathered over 21 days in the field season of resistivity testing in 2014. Supplemental data and baseline (artificial wetting) experiments were conducted in 2015 and 2016. Best or representative examples of the wetting and drying experiments are presented and discussed.

i. Wetting Experiments

The following example is selected from a 3.2 mm rain event that transpired over 35 minutes on the afternoon of September 21, 2014. Most of the rain events on the valley floor of the San Luis Valley are < 1 mm, and most of the smaller rain events do not reach the saturated zone. This 3.2 mm rain event was more substantial and thus more illustrative of what happens when rain infiltrates soil on the valley floor and adds recharge to the shallow aquifer. Figure 7.4 shows the interpreted resistivity contours in ohm-m values beginning shortly after the rain began, with measurements (subsequently inverted) every 15 minutes in descending order. The colour contours are arranged so that the blue end of the color scale is designated for soil with the greatest moisture content. Vegetated areas are shown at the top of the figure and are approximated between the 0.2 m-spaced electrodes. The transect coverage is 5 m across and 1 m deep. The unconfined aquifer was measured at 1.7 m below ground from a piezometer ~20 m away, but the zero-flux plane (ZFP) is understood to be the zone of saturated soil just above the measured water table depth, where soil moisture will fluctuate based on downward water movement toward the water table (and become recharge) or upward through capillary rise and evapotranspiration (and become water vapour).

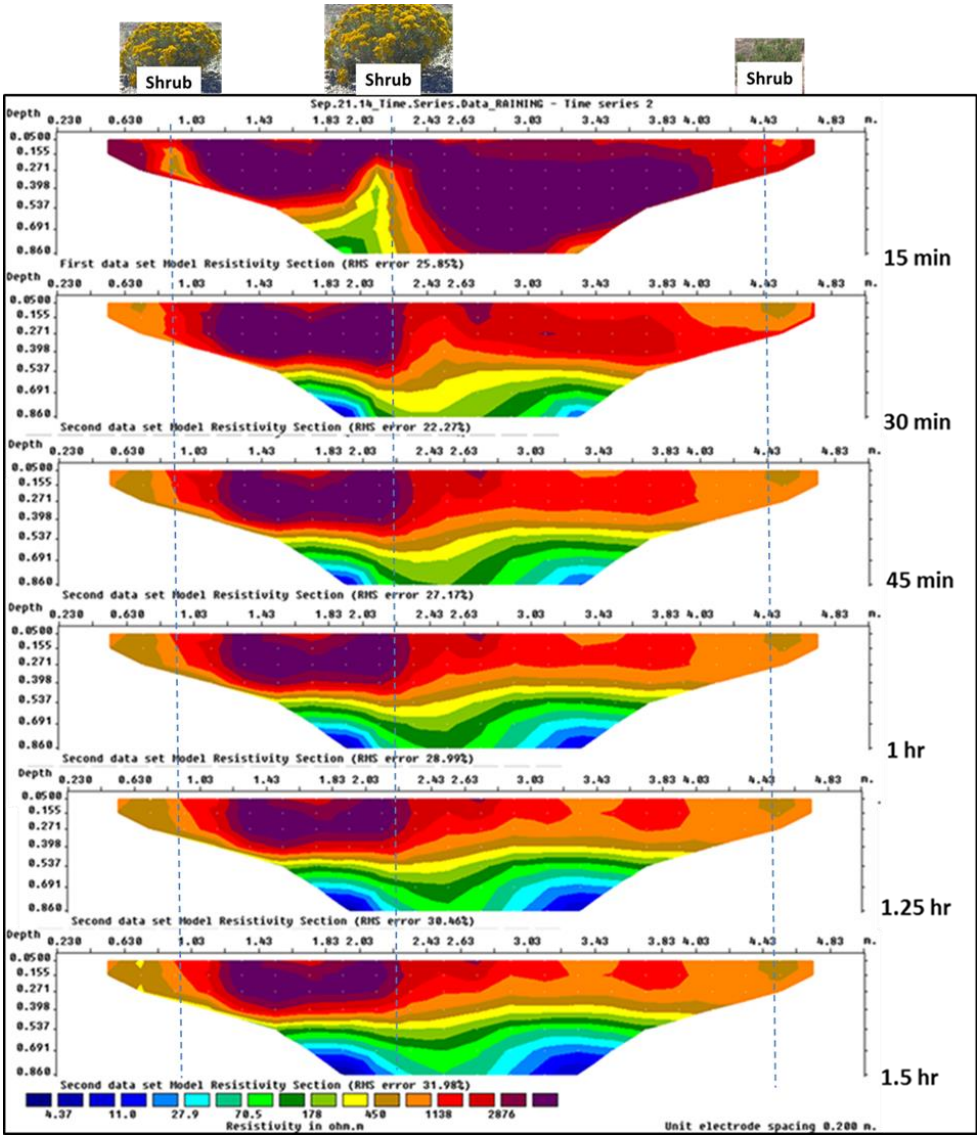


Figure 7.4: Interpreted resistivity contour of a Wenner time-lapse array during and immediately after a 3.2 mm rain event. Vegetated areas are approximated between 0.2 m-spaced electrodes. Transect is 5 m across and 1 m deep.

ii. Drying Experiments

Drying experiments were those conducted using the same transect and experimental setup in the hours and days following a rain event. Drying experiments maximized sun exposure, which was strongest in the unvegetated mid-section of the 5 m transect marked from electrode 12 to electrode 18. The following is an example of a drying experiment, and for consistency, it was selected from the same day as the wetting experiment. The results from the resistivity inversion are shown in Figure 7.5 and progress in 30 min increments from 1.5 hours to 4 hours following the 3.2 mm rain event. (Note that the resistivity scales in Figures 7.4 and 7.5 are slightly different due to batch processing of resistivity inversions.)

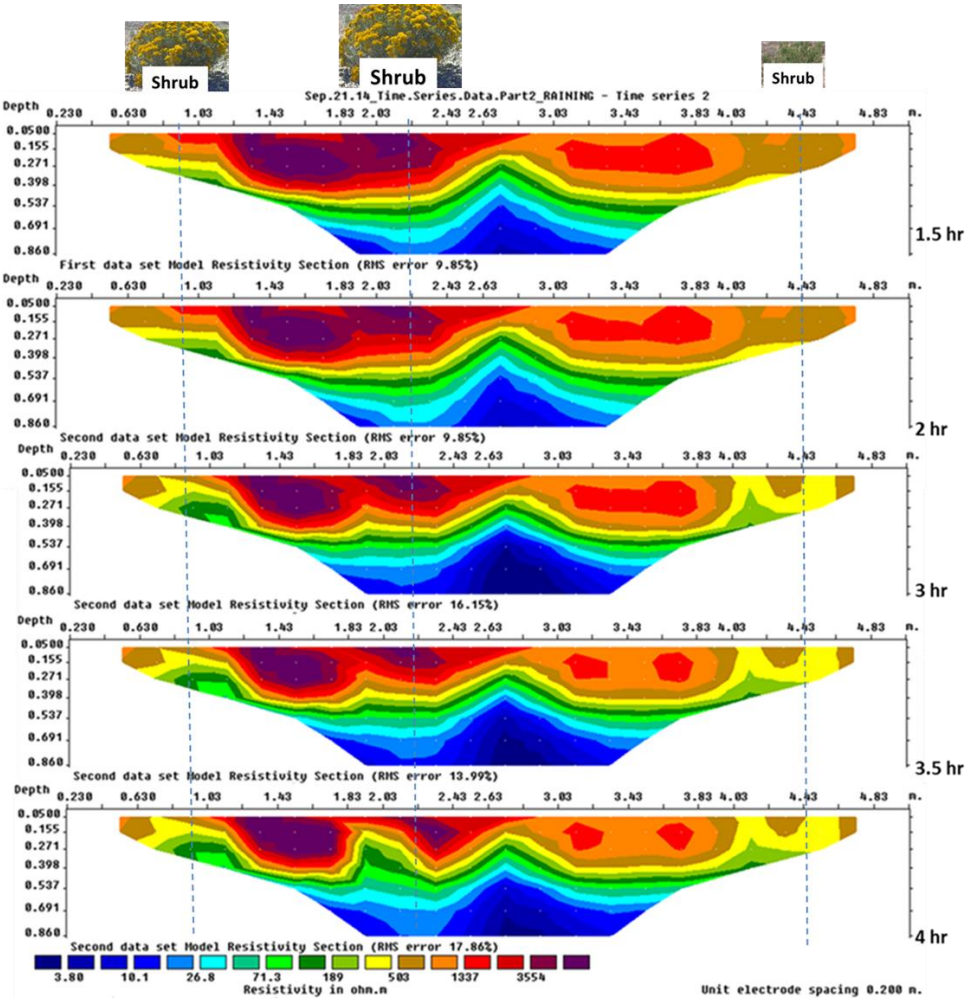


Figure 7.5: Interpreted resistivity values in batch inversions of a Wenner time-lapse array under drying conditions.

When figures from the selected experiments are stitched together, it is easier to see both downward and upward soil water movement during and after a rain event on the valley floor. The left column of Figure 7.6 shows inverted resistivity readings taken at 15 minutes and 30 minutes during the 3.2 mm rain event (which lasted 30 minutes). The right column of the figure shows inverted resistivity readings taken 1 hr and 3.5 hr after it stopped raining. (If comparing the two columns, note that higher ohm-m values are shown on the right-hand x axis, e.g. 3554, than on the left-hand x axis, e.g. 2876.) The sequence on the left shows black arrows indicating where water moves down—in the case of the vegetation at either edge of the transect, it appears that these shrubs, with minimal canopy coverage, assist water infiltration by providing stemflow pathways. White arrows indicate where water moves up, and in the case of the larger *E. nauseosa* shrub, the 15 minute reading may have captured transpiration. At 30 minutes into the heavy rain, some of the layers with greater soil moisture appear to move horizontally, as water may along soil stratifications. The white arrows indicate where soil moisture may have increased due to neighboring areas beyond the transect's coverage. The images on the right side of the figure present inverted resistivity readings once the rain has stopped and some time has passed. At 1.5 hours, water is more apparently moving upward. Electrode 11 through 18 are placed in bare earth, and this middle/right portion of the transect is a roughly 1.5 m long reading in unvegetated soil exposed to the greatest surface heating from the sun. The final contour plot labeled 4 hr shows upward water movement from the lower region nearly 1 m deep through the center and to the right, where the soil is unvegetated and, without canopy shading, is heated by the sun.

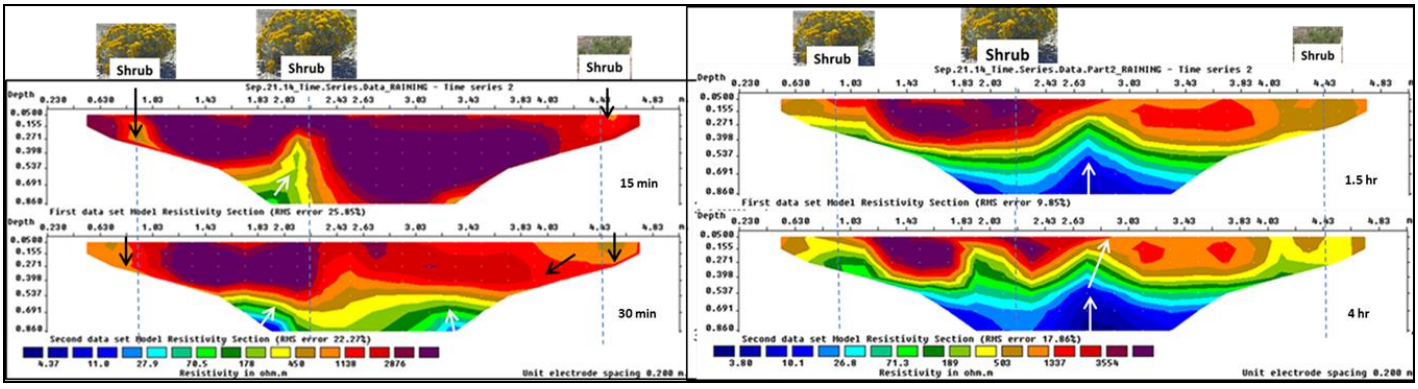


Figure 7.6: Combined resistivity inversions showing soil water movement during and following a 3.2 mm rain event.

7.6 Discussion

7.6.1 Discussion on the Plot Scale

As may be true for many instances of experiments designed in the field, in practice, the type and duration of the experiment was not something that could be controlled. Rain events were often unpredictable—or rather, they were predicted, and watched moving across the horizon, but a rain event 1 km away may not reach the transect at Site 1. Alternately, there were monsoonal downpours only 2 hours into a drying experiment. Because of this, and due to the dismissal of most resistivity experiments due to their abbreviated time-lapse, there were wetting and drying patterns that were recorded for short periods of time that could not be presented as a complete example. For plot scale resistivity readings aiming to capture evaporation, 15 min intervals may be too quick—30 min or 1 hour intervals may allow for better visualization of water movement, especially when considering the effects of capillary rise and evaporation in unvegetated areas. There were many days with no rain that turned into "drying experiments" days after a rain event.

Regarding the robustness of results, the GeoTom data processed through the Res2DInv software have a tendency toward high error rates (RMS error > 25% in Figure 7.5) when using a batch processing mode for time-lapse series, because it applies any removed outlier to all subsequent time-lapse calculations, thus increasing the error. The GeoTom results are more robust when processed individually, but then the issue of comparability arises since the resistivity in ohm-m value scale and color contour will change with every inversion. Additionally, it is understood that there is no straightforward way to equate resistivity in ohm-m with volumetric water content of soil—though, this has been correlated in several studies—but the modeled contour outputs are interpreted here as relative soil moisture values. While it is not thought below-ground plant biomass will significantly affect the resistivity readings (the resolution is not fine enough to visualize roots, for example), there is sufficient literature to suggest that very high salinity and

clay content do. The metal electrodes themselves may create a bias in that they protrude 2-5 cm into the ground and conduct heat during the day and provide a pathway for rain. Resistivity readings begin for an area below the electrodes, but this does not remove the potential bias. It was decided to limit the lower rows of resistivity readings for the purpose of achieving more reliable results. Electrical resistivity readings may vary slightly along heat gradients, though heat should be only a minor influence in clayey soils (Samouëlian et al., 2005).

When dealing with such a shallow unsaturated zone, where the water table is high and soil moisture flux can be visualized in the top meter, the presence of thermal gradients will have a strong influence on soil moisture movement (Hillel, 2006). These changing heat gradients, in addition to the hysteresis effect from wetting and re-wetting, may cause soil moisture to flow not in the direction of a water-content gradient but in a direction opposite.

Consistent with the bulk of literature on vegetation's influence on soil moisture, shrubs assist downward movement of soil water and shading protects soil moisture from evaporation (Kidron and Gutschick, 2013, Schwinning, 2001, Schwinning and Sala, 2004a, D'Odorico et al., 2007). When evaporation rates are high mid-day, they are the areas lacking vegetation that show the fastest drying and upward movement of water. This was observed repeatedly. To point out the obvious, the benefit of canopy shading disappears on cloudy, overcast days. Such days are rare in the San Luis Valley.

Soil profiles allow for insight into diffuse recharge processes on the valley floor. Both the 0.5 m and the 2.5 m profile suggest most of the moisture from rain events does not infiltrate beyond 20-25 cm. Phosphate appears only at < 25 cm soil depth from the 0.5 m soil profile. The 2.5 m soil profile could not be compared for phosphate. In the 2.5 m profile of nearby land that was previously farmed, NO_3, SO_4, and Cl all follow similar profiles and reach peak concentration at 0.5 m. The high concentrations of NO_2 and NO_3 seen in this plot are thought to be a result of past fertilizer application and flood irrigation.

7.6.2 Secondary Data from Wider Resistivity Surveys

The USGS conducted transient electromagnetic surveys along the western border of Great Sand Dunes National Park (GRSA) in 2006 (Fitterman and de Sozua Filho, 2009). In 2011, airborne magnetic and electromagnetic surveys of the San Luis Valley to map the shallow subsurface with the aim of marking the extent of the clay aquitards (Grauch and Ruleman, 2013, Ball et al., 2015). Figure 7.7 shows a generalized interpretation of resistivity data collected along a transect that spans the Great Sand Dunes boundary perimeter wells. Highlighted in this figure (blue dashed ellipses) are BP-3 and BP-7, whose water samples and rates of recharge were both discussed in Chapter 5. BP-7 was found to have the greatest rate of recharge, and its screen length spans 5-85 m deep. Figure 7.7 shows this well's extended (though simplified) sand layer. Also marked on this figure is a blue dashed line to show the 2335 m elevation of the area's ancestral Lake Alamosa, which is thought to have been responsible for much of the clay layers deposited in the valley. The water level from 1980 is also marked in light gray, and this shows that in 1980, BP-1, BP-2, BP-3, and potentially BP-4 were all submerged (had they then existed).

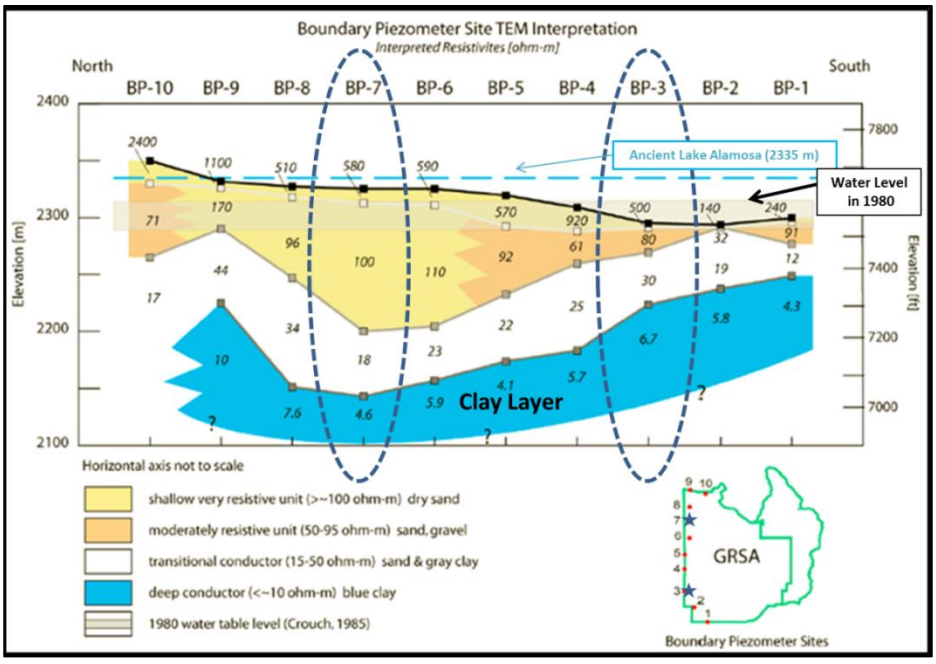


Figure 7.7: 2-D section plot along the western boundary of GRSA. Modified from Fitterman and de Souza Filho 2009.

7.7 Overall Conclusions

Most rain events in the San Luis Valley do not penetrate beyond 20-25 cm depth on the valley floor. These frequent but small rain events (typically < 1 mm) may be intercepted by vegetation canopies. Larger rain events (typically 3-10 mm rainfall in < 3 hours) infiltrate more quickly to greater depths, and will be held longer in vegetated areas. Shrub roots appear to contribute to infiltration, especially in soils with clay content. Perhaps more important is the benefit of shading and heat reduction. This is apparent when considering aridity and evaporation loss in unvegetated areas exposed to the summer sun.

There has been a considerable contribution of airborne ERT surveys (and Timed Electromagnetic readings) across the San Luis Valley to help map the underlying bedrock and near-surface lithological layers, concentrating on the valley's southern and eastern regions. Geophysical well logging at the valley's perimeters will be especially helpful in differentiating and understanding the complexities of lithological units and properties of multiple clay layers. These data, when combined with chemistry and isotope analysis, would further our understanding of site-specific flowpaths.

The chapters of this thesis may be thought of this way:

4: Atmospheric Source Water

5: Ground Water

6: Plant Water

7: Soil Water

As a whole, this work uses a "water-cycle" approach to investigate *Rain Events and Recharge Processes*. Before we arrive at the final conclusions, we will consider what these results actually mean, how they fit into a wider context, and why they may be important.

Chapter 8: Discussion of Results

- After contextualizing the study's findings in a wider context, are there important water and land management considerations for the San Luis Valley?
- What are the policy and management recommendations?
- What are the directions for further study?

This chapter rests on primary quantitative research conducted in the San Luis Valley, and the results and findings presented in Chapters 4-7, to inform a discussion on management considerations, policy and management recommendations, and directions for further study. This chapter also draws background and context from a review of the literature, and from qualitative research conducted in the San Luis Valley consisting of informal interviews, management meetings, and regional/industry tours.

8.1 Policy and Management Considerations

Residents of the San Luis Valley have much to be proud of when considering their substantial groundwater resources, their long history of water use for agriculture, the cultural preservation of living histories, the abundance of archeological sites of histories past, prehistoric hunting grounds that once also centered around water, the important migratory corridors provided by wild lands and wetlands, and the area's outstanding natural beauty.

The San Luis Valley is a remote, high-elevation desert. It does not have to contend with the varieties of pollution found in industrial and densely-settled areas. Its concerns for water pollution and water stress will not be the same as those of large cities like Denver and Los Angeles. Water tastes better from the San Luis Valley.

Still, those managing water in the San Luis Valley need to consider pollution, and issues relating to air and water quality need to be openly discussed and addressed. This is important for addressing the multiple, sometimes competing needs of water in the San Luis Valley, and it's also a matter of public health.

8.1.1 Rain Events and Dust Emissions

This thesis begins with atmospheric water, with water as vapour, from the time it condenses. When water vapour comes into contact with fine particulate matter, rain nuclei form around these particles and precipitation occurs. In this manner, rain events often 'draw out' fine particles from the atmosphere and fall to earth as wet deposition. This chapter includes a discussion on contaminants detected in rainfall.

Air pollution encompasses gaseous and particulate components. Fine atmospheric particulates may carry toxic and carcinogenic pollutants into human lungs. These can include SO_2, NOx, heavy metals such as arsenic, nickel, cadmium and mercury, and, though not regulated—pesticides, herbicides, and actinides. Air pollution episodes of poor air quality can extend over a large geographic area and last several days. These may be triggered by volcanic eruptions, smog, forest fires, strong winds and dust storms. While some pollutants are well studied and are routinely reported in air quality readings—such as general particulate matter size (e.g. PM <10 microns may be absorbed by the lungs, and PM <2.5 microns may enter the blood stream) or nutrients distributed by global movement of dust—this remains an area in which more information is needed. Radioactive elements, for example, have not been properly studied for their impacts on human health beyond limited exposure pathways. This will be especially important looking forward, since the EPA only offers guidelines for radioactive material ingested (2 L/day) rather than exposure to inhalation from sources in water droplets or water vapour.

By analyzing rainfall chemistry, this study found that for the years 2015, 2016, and 2017 (with limited coverage in 2017), the rain in the San Luis Valley showed a pattern of high acidity in the late summer. Acid rain may contribute to the mobilization of certain heavy metals, and it has been shown to damage trees. Since the San Luis Valley's soils are alkaline due to surrounding rock, it is thought that precipitation acidity is mitigated once it mixes with soil. Rain of pH < 5 is considered acid rain. The lowest pH found in rain falling on the Alamosa Wildlife Refuge in 2015 was pH 3.9 and the lowest in 2015 was pH 4.09. Figure 4.8 shows acid rain was common in summer monsoon months, and the degree of acidity does not correlate to rainfall size. For all three years, the period of greatest acidity found in rainfall occurred in the last week of July and first week of August.

When considering the source of acid rain, it may be important to consider three likely potential contributors to precipitation acidity, and to also consider these may offer some combination of contributions throughout the summer months.

1. Mining. Acid mine drainage in the abandoned mines of the San Juan Mountains. Acid mine drainage is a known issue in the Alamosa River due to past events at the Summitville mine, for instance. Mining activities that increase acidity also include cyanide application for currently operations mines, for instance those active mines in the Sangre de Cristo Mountains.
2. Combustion. There are unknown effects of intensive energy extraction in the Four Corners area. Other studies have considered the magnitude and extent of fossil fuel burning in the Four Corners area of the Southwest United States. To a lesser degree, forest fires may also play a role in altering rain pH.
3. Farming. Chemical vine kill has been used by San Luis Valley potato farmers from at least the 1940s. The timing of the sulfuric acid applications may coincide with the two week period of greatest acidity in the San Luis Valley.

While it is very likely San Luis Valley high-intensity agricultural practices have negative impacts on water quality both in the ground and in the air locally, it should also be considered that some of these same farming practices exist outside the valley in other dryland locations to the south and southwest. Nitrogen pollution—whether as nitrate, nitrite, or nitrous oxide—is, around the world, associated with farming practices, specifically N fertilizer applications. Studies have suggested N fertilizers contribute 10% nitrous oxide globally, directly contributing to climate change. N_2O emissions from agriculture may come directly from nitrification and denitrification of N inputs into the soil, or they may be indirect contributions from N volatilization, leaching, and runoff. Synthetic N fertilizer estimates for the San Luis Valley depend on crop and crop rotation. A recent study on greenhouse gas emissions in the San Luis Valley suggests 180 lbs/acre for small grains after potatoes, 80 lbs/acre for small grains after alfalfa, 220 lbs/acre for continuous small grains, 11 lbs/acre for alfalfa, and 185 lbs/acre for potatoes after small grains (Dubinsky and Karunanithi, 2016).

Most crop circles are, irrespective of crop, left bare over the winter and are sources for dust emission throughout the months of February and March when wind speeds in the San Luis Valley can reach 90 mph. The potato industry is a foundational pillar in the San Luis Valley economy, and the valley has more than 20 large warehouses that process the potatoes and distribute them across the country. Other cash crops include barley, most of which is processed and sold to Coors Brewing, and alfalfa, which is sold for cattle feed to farms in California, New Mexico, and China. One signature of potato farming is the intensive tilling and mechanical digging. Diggers sift through the bare earth and remove stones before the potatoes are planted. More digging will occur in late summer to early fall, when the potato tubers can be brought to the surface a couple weeks after the vine has been chemically or mechanically killed. Figure 8.1 shows the dust generated from the mechanical harvesting of the crop.



Figure 8.1: Potato harvesting during the San Luis Valley's annual Potato Festival.

Chemical desiccation is used in areas with short growing seasons. It allows the tuber to gain mass after the vine is killed and helps keep the skin from shrinking. This adds value to the cash crop. Chemical acid spraying has been done by the potato industry in the San Luis Valley from at least the 1940s (Binkley et al., 1948). The most common forms of chemical desiccant currently used in the SLV are a 93% sulfuric acid solution and a commercial version of diquat dibromide. Colorado State University's San Luis Valley Research Center conducted a study in 2005 and 2006 to test optimal timing of vine kill applications at 90, 100, 110, and 120 days after planting in mid-May. While the overall recommendation was to apply vine kill no later than 110 days after planting, owing to the short growing season and the timing of the first frost, optimization varies by potato variety (Essah, 2016). Some studies have suggested earlier vine kill application, at four weeks before harvest (Boydston et al., 2018). Alamosa's earliest first fall freeze on record was on August 9, 2009. The mean date of the first fall freeze is September 11 (NWS and NOAA, 2019). This study found the lowest rainfall pH between 2015 and 2017 occurred the last week of July and first week of August. Given that 93% sulfuric acid vine kill applications may be happening across a large area of the San Luis Valley beginning 90 days after planting and as late as two weeks before harvest, it may be that these applications contribute to rainfall acidity locally.

Of course, there may be other contributing factors to this observed acid rain pattern, and during the late summer, many of the monsoonal storms move through the Farmington, NM, and Four Corners area

before moving in a predominantly NE direction across the valley. Analysis using a Dionex for ion chromatography was insufficient to analyze anything other than NO_2, NO_3, and SO_4, and even in this, there was uncertainty (please refer back to Chapter 2 for further detail). More complex ions and organic pollutants from fertilizers, insecticides, herbicides, and pharmaceuticals (that may have provided more specific information) were not tested in rainfall. Hysplit back-trajectories were not done as part of this thesis's analysis, but could be done at a later time.

But what is interesting about the hypothesis that air pollution may be sourced within the San Luis Valley isn't the agricultural contribution to a lowered pH in and of itself. It's the idea that source moisture for precipitation may be influenced by, and furthermore, may be derived and recycled in the local environment. The case for moisture recycling is made in Chapter 5.

8.1.2 Toxic and Radiological Materials in the Air and in the Aquifer

There are many different types of toxic and radiological material that may be airborne, and these may be sourced from agricultural, industrial, mining, energy extraction, and power generation activities. While some of these materials are synthetic or produced, many others are naturally occurring. However, even with naturally occurring materials, human activities can increase the mobility and concentration. This section will discuss uranium as both a toxic and radiological material in the San Luis Valley, since not much attention has been drawn to this subject.

If we return to Chapter 4's findings and refer to Figure 4.8, we see the distribution of trace elements in San Luis Valley rain. While it is possible to ascribe dry deposition to snow contamination, as may happen with concentration spikes from dust-on-snow events, rain events on the valley floor that have been filtered through a 0.2 μm filter are classified as wet deposition. (Filter testing is discussed in Chapter 3, and the effects on snow are discussed in Chapter 4.) Lawrence et al. (2010) found As, Cu, Cd, Mo, Pb, and Zn in

dust-on-snow events near Silverton, Colorado, in the San Juan Mountains. They estimated the total winter/spring deposition flux to the SJM snowpack to range from 5 to 10 g m−2. They note dust deposition may occur at even higher concentrations in summer and that this dust deposition may be sourced from the Colorado Plateau and even as far as the Mohave Desert.

Chapter 4 demonstrates that rainfall on the valley floor routinely shows the presence of Cr, Cd, As, Pb, W, Mo, U, and Th. More than half the samples tested from 2015, 2016, and 2017 show the presence of uranium. In Figure 4.8 (b) we see that while certain elements such as U appear to be controlled by the size of the rain event, other elements such as Mo and W do not. In fact, Pb, As, U, Cr, and Cd all decrease in concentration as the size of the rain event increases until these elements may no longer be detected. While Mo and W have a higher LOD on the ICP-MS than do U and Th, the general trends displayed, with respect to increasing or decreasing with the size of the rain event are opposite, and this suggests that the source for U and U are different than the source for Mo and W.

As was discussed in Chapter 2, deposits of uranium were mined at the Pitch Mine (later Homestake) in Saguache County, and Th-REE deposits (with some U) were mined in the Crestone conglomerates of the Wet Mountains northeast of Great Sand Dunes. The American Southwest has seen a long history of poorly regulated and improperly cleaned uranium extraction sites all across Arizona, New Mexico, and Colorado. Most infamously, on the Navajo Reservation, where there are over 500 abandoned uranium mines (Hoover et al., 2017) and little recourse (Pasternak, 2011), since Native American-owned land is not protected under United States regulatory law.

Uranium is present in the earth's crust, and is found in mineral oxides such as uraninite and pitchblende (Pitch Mine), silicates such as zircon and coffinite, phosphates such as monazite and autunite, and vanadates like carnotite (Liesch et al., 2015). U compounds are mobilized in both acidic and in alkaline conditions. In water, uranium is usually found in its oxidized state. There are many controls on the solubility of uranium in water, and these include pH, Eh, and the presence of complexing agents.

Bicarbonate waters provide effective leaching and complexing agents for uranium, but even low amounts of phosphate, if present, causes $UO_2(HPO_4)_2$ to dominate carbonate species (Kraemer and Genereux, 1998).

It has been shown that the application of phosphate fertilizers in agricultural areas may increase uranium due to impurities concentrated in the phosphate fertilizer itself (Schnug and Haneklaus, 2015) or increase uranium mobility through the addition of phosphate, which may leach uranium from the soil, effectively increasing the concentrations of uranium found in water. This has been more heavily studied in nitrate, and nitrate contamination of shallow groundwater (often found in agricultural areas) is a primary mechanism by which secondary contamination of uranium may occur. NO_3 alters U solubility by oxidative dissolution of reduced U(VI) minerals, releasing U(VI) in water. Nolan and Weber found that in 78% of areas where U was found in groundwater above the EPA maximum contaminant level (MCL)—currently 30 μg/L but previously much lower—are correlated with nitrate pollution from agriculture (Nolan and Weber, 2015). They and others also point out that in agricultural areas irrigating with this U-enriched groundwater, uranium has been shown to accumulate in crops (Hakonson-Hayes et al., 2002, Jeambrun et al., 2012), though it should be noted that studies on uranium uptake in food crops are limited. As discussed in Chapter 2, early studies from the 1950s onward identified the agricultural area of present-day Sub-district 1 in the closed basin of the San Luis Valley as having a high degree of nitrate pollution from the application of N-fertilizers.

Under increasingly reducing conditions, uranium will precipitate out as an insoluble metal. There is usually then a deposit of uranium marking redox boundaries. Precipitation may be as uranitite, or if enough silica is present, coffinite. However, once in a reduced zone of the confined aquifer, there may be other mechanisms by which uranium is re-oxidized or mechanisms by which it remains in its oxidized (VI) state despite reducing conditions (Schumann et al., 2017). With a pH change, uranium may adsorb onto clay minerals or ferric oxyhydroxides (or Mn-oxyhydroxides). It may also sorb onto the organic components of peat.

To examine uranium, it is necessary to understand not only its occurrence, solubility and transport in the environment but also that of its 'daughter' or 'progeny' products, which include radium and radon. While there are many radionuclides of concern in drinking water, ^{238}U in µg/L, combined radium (^{226}Ra and ^{228}Ra) in pCi/L, and ^{222}Rn in pCi/L are the parameters initially screened for in routine testing in the United States. Figure 8.2 shows the decay chain of ^{238}U, which, if found in the natural environment, exists at over 99% abundance (as compared to ^{234}U and ^{235}U, for instance). Uranium is older than the age of the Earth, and it will outlive us. The decay chain shows the half-life of each radionuclide and the type of radiation it emits. After all of these reactions have taken place, the stable end product of ^{206}Pb is what remains.

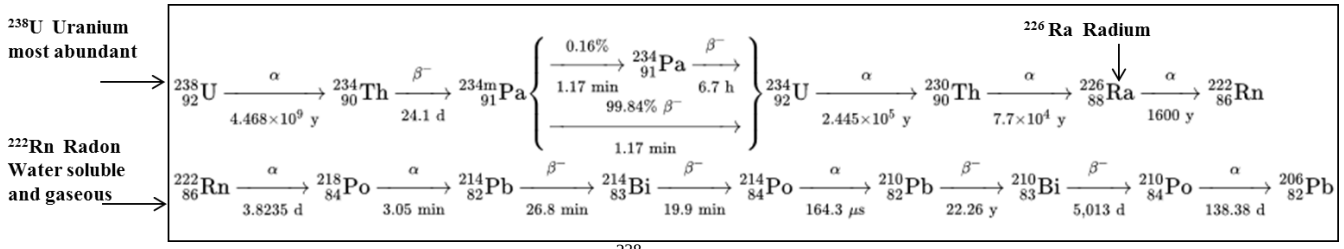


Figure 8.2: Uranium decay chain for ^{238}U showing decay products, half-lives, and radiation type. Modified from Wikipedia.

Radium may be released into water through dissolution of silicates and carbonates or through alpha-particle recoil (Kraemer and Genereux, 1998). Radium is also adsorbed onto clay minerals and Fe- and Mn-oxyhydroxides. When these dissolve in water, the radium is released (Szabo et al., 2012). Radon, on the other hand, is water-soluble and gaseous. Many people living in the American Southwest are familiar, to some degree, with mitigating radon gas in their homes associated with the underlying bedrock.

In groundwater, the radioactivity of ^{226}Ra and ^{222}Rn may far exceed that of its parent, ^{238}U (Osmond and Cowart, 2000). This is important to note. In places where radiation from Ra and Rn in drinking water is known to exist—such as in the San Luis Valley—home wells and sources of public drinking water should undergo Ra and Rn testing. Since radon is water-soluble and gaseous, and it is primarily through the

inhalation of U-series radionuclides that human health is placed at risk, it could be argued that public-use hot springs, pools, laundromats, and gyms with showers in the San Luis Valley should also meet these EPA guidelines for public health. The European Commission has estimated that 1000 Bq/L radon concentration dissolved in water discharged from a tap or a shower will on average increase the radon concentration by 100 Bq/m^3 of indoor air.

This study's rain chemistry findings suggest the source of U and Th is different than the source of Mo in rain events. It should be considered that contaminants in rainfall might arrive from outside the San Luis Valley or be internally generated, and the concentrations in air, dust, and rain may be from a combination of sources.

In the evaporite playas, uranium was concentrated in the valley's sump. Sampling of the San Luis Valley's playas in 2011 show a mean concentration of 240 μg/L of dissolved uranium, and a maximum concentration of 3.5 mg/L dissolved U (refer to Figure 5.8). It should be expected that dryland playas will have elevated concentrations of toxic metals and, if present in the groundwater, actinides. Sampling in a wetland playa will produce highly variable results in uranium concentrations, as demonstrated at the Boston Peak wetland 13 km north of Rocky Mountain National Park, where researchers found dissolved uranium concentrations in the range of 20-83 μg/L, maximum dissolved concentrations in sediment at 300 mg/L, and maximum dissolved concentrations in peat near the zone of groundwater seepage to be > 3 g/L (Schumann et al., 2017). One possibility for the aerosolization of heavy metals and actinides in the San Luis Valley is the drying of the valley's playas and the generation of dust particles in the air. This can be managed, to some extent, by the amount of water in the playas.

This study found uranium in the San Luis Valley groundwater in all layers of the aquifer but at greatest concentrations in the unconfined aquifer under agricultural areas of the closed basin. Initial analysis of water samples collected from agricultural pivot irrigation spray show uranium concentrations of up to 10 μg/L. Though agricultural activities are certainly not the source of geogenic contaminants, numerous

studies have shown that both significant groundwater abstraction and the application of nitrate and phosphate fertilizers can increase the amount of uranium dissolved in groundwater and used for agricultural irrigation.

From April through October, center pivot irrigators can be seen spraying water in slow rotations throughout the mornings, afternoons, and evenings. Figure 8.3 shows the extent of groundwater-irrigated pivot circles in the San Luis Valley, and the images depict the misting and the far-reaching spray of a typical center pivot irrigator. Some studies suggest bacteria and viruses have become aerosolized from spray irrigation (Courault et al., 2017, Dungan, 2012, Ayuso-Gabella et al., 2011). It is possible that major, minor, and trace elements dissolved (or suspended) in water droplets may also be transported in this manner.

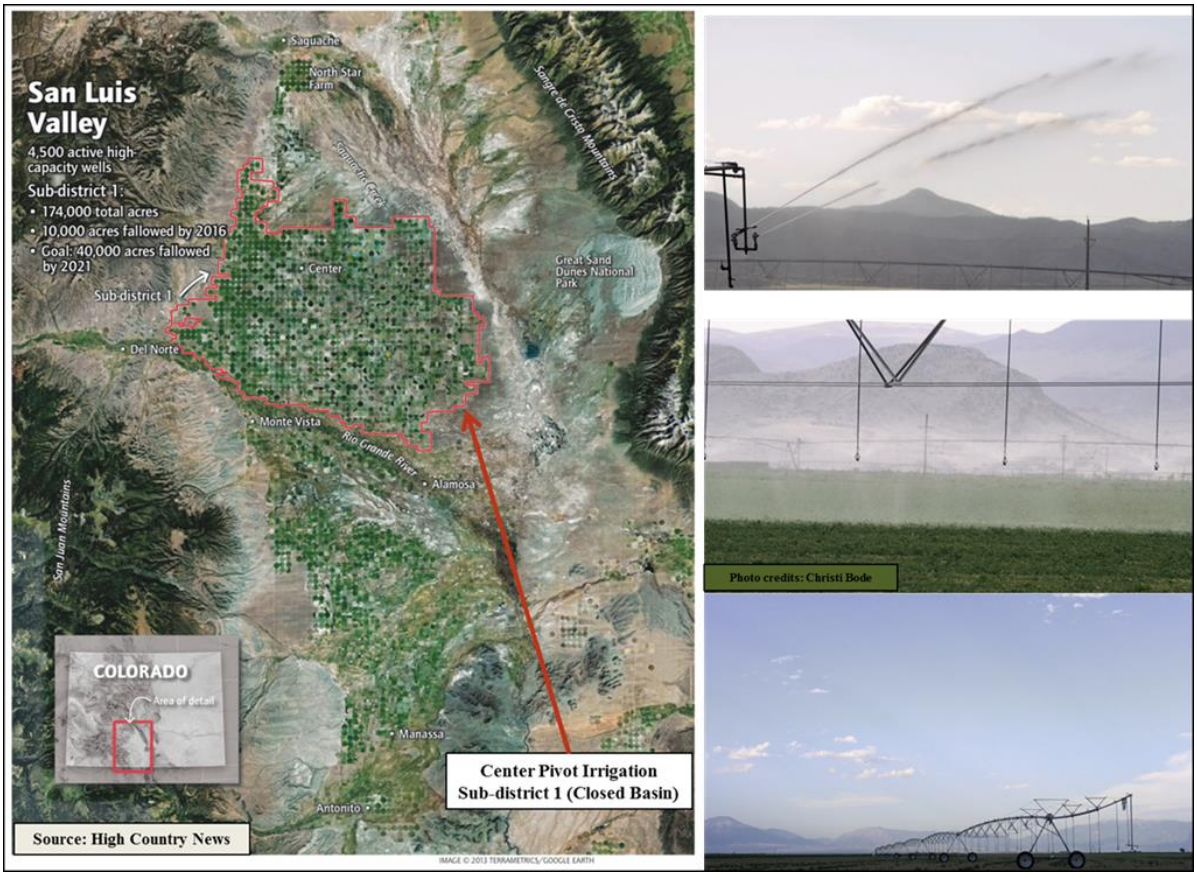


Figure 8.3: The extent of pivot irrigation in Sub-district 1 is seen via satellite imagery. Each center pivot is supplied by at least one groundwater well. Spraying generally occurs from April 1 to mid-October, and sprinklers can run at all hours.

8.1.3 Groundwater as Drinking Water

Presently, there are roughly 50,000 people who live across 6 counties in the San Luis Valley. All of the municipal and community drinking water systems utilize groundwater and serve fewer than 10,000 people. The city of Alamosa is the population center of the San Luis Valley. In the last decade, the city grew about 10%, and the public water utility now serves a population of 9,590. It is the only public water supplier to provide water treatment beyond chlorination. Most other public water supplier in the SLV serve rural communities of fewer than 1,000 people, and some public suppliers serve small communities of only 50. More than 1/3 of residents in the San Luis Valley rely on private wells to meet their household needs.

The city of Alamosa extracts water from 7 different wells across the city. Microbial contaminants in municipal systems are usually reported by the press because outbreaks affect many people in an immediate way. The 2008 *Salmonella typhimurium* outbreak in Alamosa was traced to poor municipal water storage and affected as many as 1,300 people with 124 laboratory-confirmed cases, 20 hospitalizations, and 1 death (Ailes et al., 2013). Over the long-term however, it can be the disinfectant biproducts, volatile organic compounds, synthetic organic chemicals, inorganic metals and radionuclides that prove more harmful and more difficult to analyze, report, and track.

The Environmental Protection Agency's (EPA) recommended level of maximum contamination for uranium (based on toxicity, not radiation) in the early 2000's was 20 μg/L, and many studies based exceedances on this mark. The EPA increased the maximum contaminant level to 30 μg/L in 2011. The World Health Organization (WHO) set a recommended maximum concentration for uranium at 2 μg/L in 2000, increased the limit provisionally in 2004 to 15 μg/L, and once again to 30 μg/L (P) in 2011. Such increases are usually not due to a reduced risk to the population but are economic and feasibility

considerations for water treatment facilities and water service providers. Aluminium is an example of an element the WHO made exceptions for based on the practicalities of water treatment plants using aluminium-based coagulants.

In many cases, regulatory bodies decrease maximum limits for drinking water as more research on human health impacts emerge. This was the case with arsenic. The WHO's 1983 guideline for As was 50 μg/L. This was reduced provisionally to 10 μg/L in 1993. One significant benefit of the EPA's adoption of the same lowered MCL for arsenic, is that requiring water treatment plant upgrades for those using water >10 μg/L As most likely lowers levels of many associated heavy metals, uranium, and associated radionuclides. The city of Alamosa upgraded its water treatment system in order to remove arsenic using a system of coagulation and filtration. Since doing so, the city's water quality improved sharply.

In the United States, radioactivity is measured in pCi. Most measure radioactivity in Becquerel (1 pCi = 0.037 Bq). In 2018 the WHO suggested drinking water limits of 0.5 Bq/L for gross alpha activity and 1 Bq/L for gross beta activity. If neither of these screening levels are exceeded, then the effective dose is below 0.1 mSv/yr, which is a measure the WHO and the European Commission have adopted in light of the way radiation affects the average human body drinking 2 L/day water. 1 Bq of radioactivity does not deliver the same dose of radiation. This will depend on the type of radiation and what human tissue or organ receives it. The "effective dose" or "dose equivalent" takes this into consideration. The US EPA has applied its effective dose of 4 mrem/yr to beta activity only.

The United States EPA regulates public and community drinking water provider compliance for radiation limits as follows: 4 mrem/yr for beta/photon emitters, 15 pCi/L (0.56 Bq/L) for gross alpha particle, 5 pCi/L (0.19 Bq/L) for combined radium, and 30 μg/L for uranium, though, it should again be noted that uranium's MCL is based primarily on its toxicity as a heavy metal and doesn't account for its radiological effects in the body. For all of these parameters, the EPA states the goal is zero. The EPA and the WHO explain, in their accompanying literature on how guidelines are set, that these maximum contaminant

levels address only the radiation that is directly ingested from drinking 2L/day water. Both agencies warn ingested radiation will almost always be a fraction of exposure compared to what is inhaled.

There have been several national studies on uranium in drinking water that have included the San Luis Valley (usually termed "Upper Rio Grande in Colorado"), but the sampling and wells are not consistent, and legal limits have changed over time. Szabo et al. (2012) examined occurrence of ^{226}Ra and ^{228}Ra in groundwater across the country, but samples analyzed for the San Luis Valley region don't reflect those public and community drinking water sources that resulted in 39 EPA violations for radionuclides.

Through the 2018 year end, there have been 39 radionuclide violations by community water providers and public drinking water suppliers in the San Luis Valley reported to the EPA. These MR exceedances for radionuclides in drinking water affect five different counties in the San Luis Valley. The three largest community water providers with reported radionuclide violations are the Baca Grande WSD serving a population of 1,520 near Great Sand Dunes, the Town of Monassa, serving 967 people in the southern part of the valley, and Costilla County WS serving 561 people in the southeastern part of the valley. The Baca Grande water services provider near Great Sand Dunes reported EPA radionuclide MR violations in 2007 for combined uranium, ^{226}Ra, and gross alpha excluding radon and uranium. State compliance was restored in 2008. The High Valley mobile home park in Alamosa (home to 85 people) has also reported EPA violations for radionuclides since 1995 for gross alpha excluding radon and uranium. These violations are outstanding, the situation is known, and the state of Colorado has granted intentional no-action status. The groundwater well providing the mobile home park with water is located off highway 17 just north of Road 5 South.

To the south—the town of Monassa also reported radionuclide MR violations for combined uranium and for gross alpha excluding radon and uranium in 2013, and although the situation is known, the violations (as of 2018) are outstanding. (State public notification is requested.) The Costilla County WS reported violations for combined radium (^{226}Ra and ^{228}Ra) and gross alpha excluding radon and uranium from

2016-2017. However its first reported violation for gross alpha excluding radon and uranium occurred from 1995-1996. In Conejos County, there are 18 reported radionuclide violations for the Guadalupe WA that serves a rural population of 40 people. These are repeated MR violations for gross alpha excluding radon and uranium, combined uranium, and combined radium. (State public notification has been received.)

More than 17,000 people living in the San Luis Valley rely on private household wells to meet their drinking water needs (Canaly, 2019). Since private well owners are not required to test their water's quality or to submit analysis to any county, state, or federal authority, the above records only highlight concerns with public water providers. Moreover, when a private well owner pays to have a complete water quality analysis done on their drinking water, the well owner is often unaware the water analysis will not cover all of those regulated items to which they may be exposed. The San Luis Valley water laboratory does not have access to an ICP-MS, nor does it have the ability to test for radon. Shipping a single water sample out of the valley for combined uranium, gross alpha, radon, and radium analysis may cost the well owner more than $4,500 (Sangre de Cristo Laboratories, 2019). For private well owners who are concerned about their water's quality, it is cheaper to purchase an in-home, multi-step reverse osmosis unit (~$200 plus installation) than it is to test the water.

Public water suppliers in the San Luis Valley may also find it difficult to pay for required and specialized testing. In general, and where possible, it is recommended public water suppliers take simple measures to provide some level of water treatment and offer education to the communities both on and off the water network about in-home water treatment.

8.1.4 100 Years of Land-use Changes to the Valley's Hydrology

While municipalities, industries, ranchers, state and federal agencies, private companies and private well owners all utilize groundwater from the San Luis Valley, the largest, the most significant user of groundwater is agriculture. Chapter 2 describes some of the land-use changes over the past 100 years as agricultural irrigation from surface water switched to irrigation from groundwater. Over the past century, there have been many alterations to the landscape which ultimately shifted the area's hydrology and recharge mechanisms. Stream flow diversions from mountain creeks, and the pumping of water off the Rio Grande for agricultural production changed the way mountain front recharge occurred near the San Juan Mountains , and the frequency with which the Rio Grande flooded and overflowed (providing recharge) was sharply reduced (Beauchaine, 2015). Once the Bureau of Reclamation's Closed Basin Project began pumping groundwater from the valley's unconfined aquifer in the closed basin and transferred this groundwater along an open canal to augment water delivery of the Rio Grande to downstream neighbors, this too significantly changed the area's hydrology.

Figure 8.4, which is taken from a USGS report, illustrates components of a water budget in the San Luis Valley developed as part of Colorado's Groundwater Decision Support Model, which separates hydrologic components into two categories: those prior to settlement and modern land-use changes, and those after modern development changed the landscape. The water budget used to describe the area's hydrology after modern development uses water estimates from the years 1970 to 2002. From these comparisons, mountain block recharge is estimated to have declined from 28% (pre-development) to 8%. Mountain front recharge is estimated to have declined from 41% (pre-development) to 12%. Evapotranspiration from native vegetation has significantly decreased and return-flow from surface water and groundwater irrigation is new (Bexfield and Anderholm, 2010).

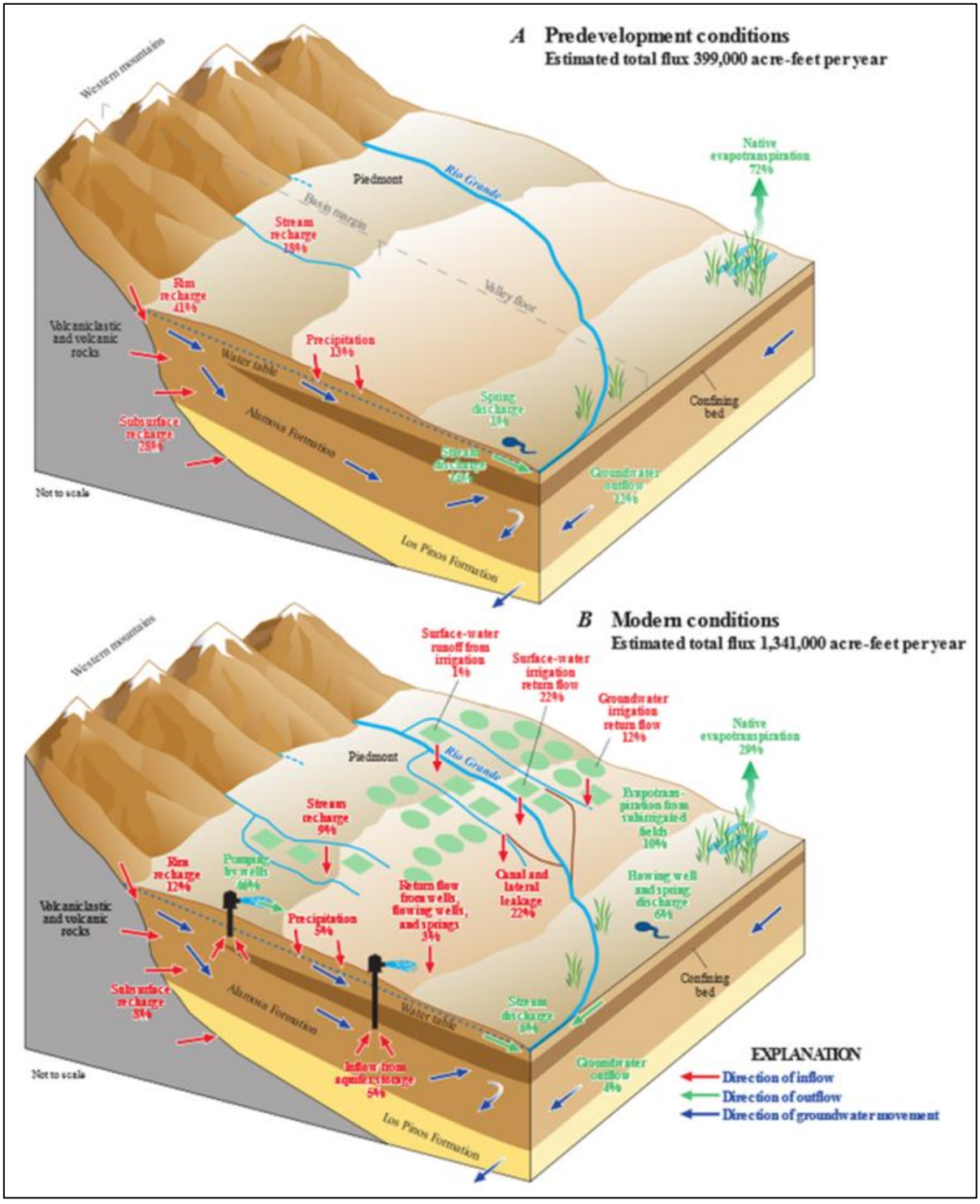


Figure 8.4: Hydrologic model created as part of Colorado's decision support includes a water budget for pre-development hydrology (A) and modern, post-development hydrology (B). Bexfield and Anderholm, 2010.

While it is difficult not to notice when individual wells go dry, or when an artesian well loses its artesian flow, it may be harder to visualize how the area's wetlands have diminished on a landscape scale. As noted in Chapter 2, when surveys of the San Luis Valley were conducted in the early 1900s, they detailed swamps, marshes, wetlands, and an extensive playa system (Siebenthal, 1910). Mishak Lake Complex in the northern region of the valley was fed by a series of springs sourced from San Juan snowmelt. Sanderson et al. modeled the natural hydrologic regime of these wetlands and found they would have often remained wet year-round, and for many years at a time (Sanderson et al., 2008). The playas in the closed basin sump used to be flushed with seasonal snowmelt as creeks overflowed (Valdez, 2016), and there is evidence from fish bones suggesting these playas used to be filled with water a few meters high (Lucero, 2016a). A recent study of wetlands across the San Luis Valley suggests this loss of wetland habitat continues today. Figure 8.5 from a study conducted by Wetland Dynamics found there has been a 50% reduction in wet acreage across the San Luis Valley since 1984 (Aloia and Nehring, 2019).

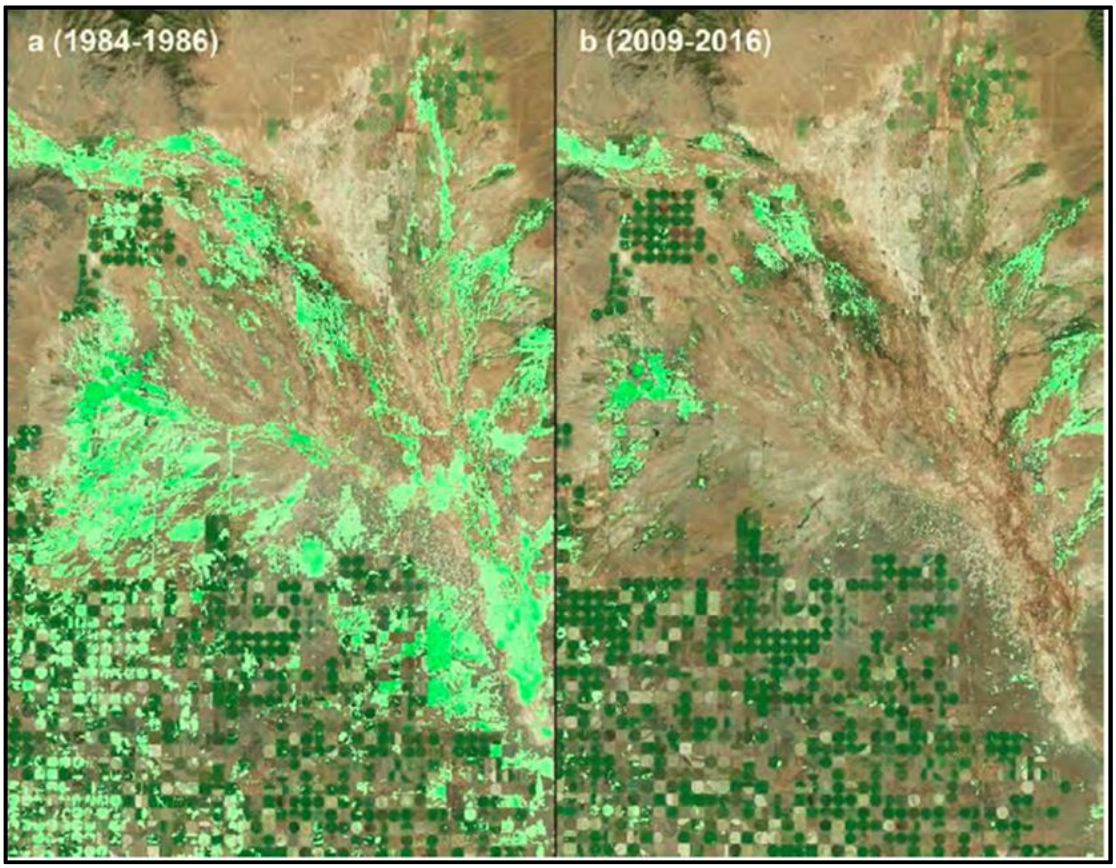


Figure 8.5: Analysis of remote sensing images twenty years apart. Wet acreage in light green. Aloia and Nehring, 2019.

Analysis in Chapter 5 suggests this landscape of extensive wetlands and playas may have provided a source for water recycling that lead to the severely depleted isotope signatures found in high-elevation snow of the past that is detected in old groundwater beneath the playas today.

Decades ago, and for good reason, water managers have been concerned about losing water through high rates of evapotranspiration in dryland areas with high water tables. But, from a management perspective, the cost of ET should be weighed against the cost of general capillary rise and evaporative loss that will happen when the sun heats bare soil on the valley floor. The benefits of shading, increased species diversity, and soil stabilization should also be weighed. How much dust is generated by driving over bare earth? What areas are susceptible to wind storms? Are dust emissions originating from areas of the valley that might also carry toxic and radiological material? Are these internally generated dust emissions deposited on snowpacks in the Sangre de Cristo or the San Juans mountains effectively reducing aquifer recharge to the San Luis Valley?

8.2 Policy and Management Recommendations

8.2.1 Mitigating Dust

- It is important to set aside water for wetlands and for instream-flow.
- Native vegetation may be viewed in a positive light with respect to stabilizing soils and providing ground shade.
- Providing incentives for farmers to plant cover crops over the winter will reduce the amount of bare earth exposed to wind storms in the early spring.
- Reducing internally-generated dust will improve public health and help keep snowpack frozen longer.
- Creating a network to monitor and mitigate dust generated from beyond the SLV is also beneficial for the entire SW region of the United States.

8.2.2 Sustainable Groundwater Management

- The San Luis Valley will need to consider the water needs of multiple users, from different sectors, as the area grows and expands. In what ways do western water laws limit the kinds of activities the area can sustain? How does the area plan for future growth? How might the San Luis Valley diversify its economy?
- The area's economy is currently dependent on farming. The agricultural sector is the largest user of groundwater in the San Luis Valley. Sustainable groundwater management will require that difficult questions are posed to the farming community. For example, are some crops better than others? Generally, Americans want to support agriculture and the government will invest in food security. But are crops that are used for beer production or cattle feed in other countries as necessary as those used for human food more locally? What considerations are given to the virtual water a crop represents and whether or not this crop is exported? Are there ways to incentivize smarter forms of farming?
- Irrespective of individual water rights, an aquifer is, in many ways, a common resource. This means that how one user abstract or pollutes water impacts other users. In some countries, the use of fertilizers for agricultural production has been heavily taxed as an effective way to reduce overuse. In some places, a "polluter pays" principle has been applied to those who use fertilizers, herbicides, or pesticides for their own economic gain and who have harmed the common resource by degrading its quality. In the San Luis Valley, the focus has been on water quantity. More attention needs to be given to water quality.
- Managed aquifer recharge, if not done properly, may introduce toxic and radiological material into the aquifers. Colorado may want to consider California's guidelines for managed aquifer recharge.

- In addition to nitrate pollution and the naturally high levels of arsenic, drinking water concerns in parts of the San Luis Valley may also include F, Cd, Cr, Mo, W, Pb, and more difficult parameters to measure such as total uranium, gross alpha, radon and radium. Attention should be given to finding and developing low-cost methods of treating public drinking water with the aim of reducing concentrations of heavy metals and radionuclides.
- When considering low-cost water treatment options, careful consideration must be given to the controls on individual elements of concern. For example, the redox and pH controls on arsenic are opposite those of uranium. If water treatment only considers arsenic, it may inadvertently increase the concentrations of uranium.
- There are and will be challenges to the San Luis Valley's groundwater as cities in other parts of Colorado look to satisfy their water demand through inter-basin transfers. The San Luis Valley is advised to keep its water.
- Water managers must plan for climate change and adapt when possible.

8.3 Future Directions for Further Study

This author would like to conduct further research in the San Luis Valley. There are several research directions one could take. Here are just a few.

One study may be to understand better how weather systems work within the valley. Since the area is drone-friendly, the San Luis Valley might utilize the equipment, skillset, and data from invited drone operators testing applications for climate-related research.

For example, while it may have been assumed most of the dust-on-snow events in the San Juan Mountains originate as long-range emissions from the Colorado Plateau and beyond, it is important to ask where and how far dust emissions generated from within the SLV travel? In order to acquire more data, it

would be beneficial to expand the existing monitoring networks in the valley, at the valley's margins, and in locations just beyond the valley. These would include efforts to increase air quality collection sites as part of the IMPROVE network and expand the current network's testing parameters.

As a follow-on from this work, it would be a wonderful idea to establish an isotope monitoring station at high elevation in both the San Juan Mountains and the Sangre de Cristo Mountains. This may prove invaluable data for interpreting storm systems, sources of moisture, and recharge processes in the valley. While it is ill-advised to establish multiple isotope monitoring sites at discrete elevations in the San Juan Mountains, it is beneficial to design a study collecting precipitation isotope data at discreet elevations in the Sangre de Cristo Mountains. This is because there may be isotopic carry-over as air masses move over the leeward side of a mountain range. Collections along the windward side of a mountain range should better reflect fractionation linked to the adiabatic lapse rate.

Expanding the coverage of water quality testing in the San Luis Valley is important, and it's especially important to improve data coverage for the central and western parts of the closed basin.

It is important to further map aquifer boundaries. This may involve joint efforts between agencies and groups. The USGS is perhaps best positioned to carry out this research. Within the USGS, a closer partnership between the geology, geophysics, and geochemistry group and the water science hydrologygroundwater modeling group would prove most beneficial. Previously, the USGS conducted hydrological studies in the San Luis Valley, and these may serve as useful baselines through which we may observe how things such as land-use, groundwater pumping, and water quality have changed over time.

It would be useful to re-test areas of the aquifer system for residence time dating, and multiple tracers should be used. To test young water input, ^{3}H with ^{3}He is advised, but this should be done in conjunction with multiple longer-range tracers. It should not be overlooked that trace elements and radionuclides (e.g. ^{222}Rn) may be good tracers of groundwater origin, flowpaths, and age, and this information would serve

future research efforts. Further hydrological study should be conducted in order to better understand groundwater flowpaths along fissures, fractured rock, and fault lines along the eastern edge of the San Luis Valley.

Conclusions

What are the main pathways and rates of recharge in the San Luis Valley?

Using chemical and isotopic tracers, what is the water's source?

These overarching questions form the backbone of the dissertation, and each chapter builds on the previous to provide a complete picture of rain events and recharge processes. Together, chemical and isotopic tracers from >400 samples are used to follow water pathways from air mass condensation, points of recharge, water-rock interaction along flowpaths, and, for near-surface moisture, chemical and isotopic tracers and electrical resistivity tomography are used to examine water-plant interactions and soil moisture movement in the unsaturated zone. Below, each chapter's main questions, objectives, and conclusions are presented.

Chapter 4: Precipitation Chemistry and Isotopic Baselines of Meteoric Waters

- What can precipitation isotope and chemistry data reveal about the sources of meteoric water?
- Do the isotope values and local meteoric water lines created from precipitation collected on the valley floor and on the San Juan mountain passes differ significantly in terms of slope, y-intercept, or deuterium excess?

To this end, the chapter characterizes the chemical and isotopic signature of precipitation in the San Luis Valley and, using $\delta^{18}O$ and $\delta^{2}H$, develop a local meteoric water line.

This study uses basic chemistry, trace element analyses, and isotopic signatures from 117 precipitation samples collected over three years from the valley floor and from the mountain passes. This study establishes the first local meteoric water line (LMWL) for this area of the southern Rockies and notes δ^2H/ $\delta^{18}O$ differences in precipitation collected at mountain pass and valley floor elevations.

This chapter presented a weighted monthly LMWL for San Luis Valley floor.

San Luis Valley LMWL: $\delta D = 7.73\ \delta 18O + 5.8$ ($R^2 = 1$)

The high-elevation meteoric water line, derived from averaged snow events at Wolf Creek Summit Pass, more than 1,000 m higher in elevation than the valley floor, shows a much different slope and intercept.

High-elevation SLV LMWL: $\delta D = 7.82\ \delta 18O + 12.76$ ($R^2 = 1$)

Source moisture baselines originating from the Pacific Northwest versus the Southwest monsoons are identified, and isotopic signatures of an Arctic airmass blizzard in April 2016 register δ^2H -240.36, $\delta^{18}O$ -31.39. These LMWLs and the precipitation chemistry (particularly Cl^-) help establish source water, pathways, and rates of recharge explored further within this thesis. Chemical analysis demonstrates a repeating pattern of acid rainfall, with highest acidity falling the last week of July and first week of August. Heavy metal analysis of rainfall shows contaminants of health concern in rain, including Cr, Cd, As, Pd, W, and Mo, and more than half the rainfall analyzed over three years shows the presence of uranium (Lanzoni, 2017).

<u>Chapter 5: Pathways and Rates of Recharge in the San Luis Valley</u>

- What do isotopic and chemical analyses tell us about groundwater in the San Luis Valley?
- With a focus on the closed basin, what are the main pathways and rates of recharge in both the unconfined and confined aquifers?

- Is there any indication the rates and mechanisms of recharge have changed over time?

To this end, the chapter determines different pathways and rates of recharge in the San Luis Valley using chemical and isotopic tracers, hydrographs, and groundwater fluctuations.

Mountain block recharge, where infiltration occurs at high elevations in the San Juan Mountains (also potentially categorized as mountain front recharge) appears to contribute the most recharge to the upper confined aquifer in the San Luis Valley. Of those wells sampled below 274 m (with sampling biased toward the eastern region of the closed basin), the mean isotopic values lie closer to the valley-floor MWL, suggesting that recharge primarily occurs through infiltration at the base of the mountains, as mountain front recharge. Of wells sampled, the greatest rate of recharge comes from long-screen wells in the deep, unconfined aquifer layer at the base of the Sangre de Cristo Mountains. Confined aquifer recharge is primarily snowmelt-driven, with sources of moisture originating from the NW. In some cases, wells in the unconfined aquifer show isotopic values sharing more in common with warm, monsoon rains.

Old water from the upper confined aquifer sampled within a 25km^2 area of the valley's sump shows a 2.5‰ ^{18}O spread and sits significantly above the LMWL and high-elevation MWL. This water shows a mean d-xs of 17.6 ‰, which is nearly double the d-xs of the LMWL. This study presents a common and previously unconsidered mechanism by which recycled water from the valley floor condenses at high elevation—and infiltrates at high elevation—in the San Juan Mountains. This isotopically distinct source-water was a significant contributor to mountain block recharge in the past. This study argues that in addition to other human alterations to recharge pathways (such as dust-on-snow albedo changes to snowpack, etc.) 20th Century draining of playa wetlands and diverting of surface water have altered a source of precipitation and recharge mechanism not previously considered (Lanzoni and Darling, 2019).

Chapter 6: Phreatophyte Shrubs as Indicators of Groundwater in the San Luis Valley

- How does the area's dominant native vegetation (facultative phreatophytes *S. vermiculatus* and *E. nauseosa*) respond to a lowered water table?
- Are distinct patterns of water use and seasonal shifts between the phreatophytes visible?
- How might a lowering of the water table affect species richness and plant density?

To this end, the chapter analyzes stem water samples from the valley's two dominant facultative phreatophyte shrubs at three different study plots with increasing depth to groundwater in order to establish seasonal variation in their water use strategies.

Two native phreatophyte plants of the San Luis Valley, *E. nauseosa* and *S. vermiculatus*, show distinct patterns of water use and seasonal shifts depending on water availability. Differences between the species are most apparent where groundwater is most accessible. However, where the water table has dropped 6 m over the last decade, both *E. nauseosa* and *S. vermiculatus* survive only on near-surface snowmelt and rain. At Site 3, where there has been significant drawdown of the water table, shrub density is reduced by an order of magnitude, species diversity is lower, and the percentage of exposed, bare earth reaches 45%.

Chapter 7: Moisture Movement in the Soil

- Can movement of the zero flux plane be visualized using electrical resistivity tomography?
- In areas with shallow water tables, how do rain events influence soil moisture on the valley floor? Does this differ between vegetated and non-vegetated areas?

To this end, the chapter applies time-lapse, near-surface electrical resistivity in order to characterize soil moisture movement between vegetated and non-vegetated areas under different wetting and drying conditions.

Most rain events in the San Luis Valley are < 2 mm and, based on time-lapse resistivity inversions, do not appear to penetrate to a depth sufficient to reach the water table. Soil profiles indicate most precipitation on the valley floor does not penetrate more than 25 cm. Movement of the zero flux plane (ZFP) is visible through the use of electrical resistivity tomography. Where the depth to water on the valley floor is < 2 m, soil moisture in the ZFP may either travel downward to join the water table and become recharge or travel upward and be released, either by transpiration or evaporation, as water vapour. Time-lapse resistivity inversions along a vegetated transect suggest when the sun heats the valley floor, convection (and potentially advection) is greatest in unvegetated areas.

References

1984. H.R.2823: A bill to amend title I of the Reclamation Project Authorization Act of 1972 in order to provide for the establishment of the Russell Lakes Waterfowl Management Area as a replacement for the authorized Mishak National Wildlife Refuge, and for other purposes. *Law No: 98-570.* House - Interior and Insular Affairs; Merchant Marine and Fisheries. Senate - Environment and Public Works ed.

1986. H.R.3443 - A bill to designate the Closed Basin Conveyance Channel of the Closed Basin Division, San Luis Valley Project, Colorado as the Franklin Eddy Canal. *Law 99-416.*

2008. In the Matter of the Application for Water Rights of the United States of America in Alamosa and Saguache Counties. *Hon. O. John Kuenhold.* District Court, Water Division No. 3, Colorado.

2019. SLV Wetland and Wildlife talk at ASU next week. *Valley Courier*, April 18, 2019.

ACIEGO, S. M., RIEBE, C. S., HART, S. C., BLAKOWSKI, M. A., CAREY, C. J., AARONS, S. M., DOVE, N. C., BOTTHOFF, J. K., SIMS, K. W. & ARONSON, E. L. 2017. Dust outpaces bedrock in nutrient supply to montane forest ecosystems. *Nat Commun,* 8**,** 14800.

ACKER, J. G. & LEPTOUKH, G. 2007. Online Analysis Enhances Use of NASA Earth Science Data. *Eos, Trans. AGU,* 88**,** 14-17.

AILES, E., BUDGE, P., SHANKAR, M., COLLIER, S., BRINTON, W., CRONQUIST, A., CHEN, M., THORNTON, A., BEACH, M. & BRUNKARD, J. M. 2013. Economic and Health Impacts Associated with a Salmonella Typhimurium Drinking Water Outbreak: Alamosa, CO, 2008. *PLoS ONE,* 8.

ALIZAI, H. U. & HULBERT, L. C. 1970. Effects of Soil Texture on Evaporative Loss and Available Water in Semi-Arid Climates. *Soil Science,* 110**,** 328-332.

ALLISON, G. B. 1982. The relationship between 18O and deuterium in water in sand columns undergoing evaporation. *Journal of Hydrology,* 55**,** 163-169.

ALOIA, C. & NEHRING, J. 2019. San Luis Valley Wetland and Wildlife Conservation Assessment. 2 ed.: Wetland Dynamics, LLC.

ANDERHOLM, S. K. 1996. Water quality assessment of the Rio Grande Valley, Colorado, New Mexico, and Texas--Shallow groundwater quality of a land-use area in the San Luis Valley, south-central Colorado. *U.S. Geological Survey Water-Resources Investigations Report.* USGS.

ANDERSON, L. 2012. Rocky Mountain hydroclimate: Holocene variability and the role of insolation, ENSO, and the North American Monsoon. *Global and Planetary Change,* 92-93**,** 198-208.

ANDERSON, L., BERKELHAMMER, M. & MAST, M. A. 2016. Isotopes in North American Rocky Mountain Snowpack 1993–2014. *Quaternary Science Reviews,* 131**,** 262-273.

ANDREWS, J. N., GOLDBRUNNER, J. E., W.G. DARLING, W. G., HOOKER, P. J., WILSON, G. B., YOUNGMAN, M. J., EICHINGER, L., RAUERT, W. & STICHLER, W. 1985. A radiochemical, hydrochemical and dissolved gas study of groundwaters in the Molasse basin of Upper Austria. *Earth and Planetary Science Letters,* 73**,** 317-332.

ANNING, D. W., PAUL, A. P., MCKINNEY, T. S., HUNTINGTON, J. M., BEXFIELD, L. M. & THIROS, S. A. 2012. Predicted Nitrate and Arsenic Concentrations in Basin-Fill Aquifers of the Southwestern United States. *In:* USGS (ed.) *Scientific Investigations Report 2012–5065.* USGS.

AUSTIN, A. T. 2004. Water pulses and biogeochemical cycles in arid and semiarid ecosystems. *Oecologia,* 141**,** 221-235.

AUSTIN, A. T., YAHDJIAN, L., STARK, J. M., BELNAP, J., PORPORATO, A., NORTON, U., RAVETTA, D. A. & SCHAEFFER, S. M. 2004. Water pulses and biogeochemical cycles in arid and semiarid ecosystems. *Oecologia,* 141**,** 221-35.

AYUSO-GABELLA, N., PAGE, D., MASCIOPINTO, C., AHARONI, A., SALGOT, M. & WINTGENS, T. 2011. Quantifying the effect of Managed Aquifer Recharge on the microbiological human health risks of irrigating crops with recycled water. *Agricultural Water Management,* 99**,** 93-102.

BALL, L. B., BLOSS, B. R., BEDROSIAN, P. A., GRAUCH, V. J. S. & SMITH, B. D. 2015. Airborne electromagnetic and magnetic survey data of the Paradox and San Luis Valleys, Colorado.

BARBIER, N., COUTERON, P., LEFEVER, R., DEBLAUWE, V. & LEJEUNE, O. 2008. Spatial decoupling of facilitation and competition at the origin of gapped vegetation patterns. *Ecology,* 89**,** 1521-1531.

BARBIER, N., COUTERON, P., LEJOLY, J., DEBLAUWE, V. & LEJEUNE, O. 2006. Self-organized vegetation patterning as a fingerprint of climate and human impact on semi-arid ecosystems. *Journal of Ecology,* 94**,** 537-547.

BAUDENA, M. & PROVENZALE, A. 2008. Rainfall intermittency and vegetation feedbacks in drylands. *Hydrology and Earth System Sciences,* 12**,** 679-689.

BEAUCHAINE, S. 2015. *RE: Rio Grande flood frequency.*

BÈGUE, N., TULET, P., PELON, J., AOUIZERATS, B., BERGER, A. & SCHWARZENBOECK, A. 2015. Aerosol processing and CCN formation of an intense Saharan dust plume during the EUCAARI 2008 campaign. *Atmospheric Chemistry and Physics,* 15**,** 3497-3516.

BELSKY, A. J., MWONGA, S. M., AMUNDSON, R. G., DUXBURY, J. M., AND A. R. ALI 1993. Comparative effects of isolated trees on their undercanopy environments in high- and low-rainfall savannas. *Journal of Applied Ecology,* 30**,** 143-155.

BENJAMIN, L., KNOBEL, L. L., HALL, L. F., CECIL, L. D. & GREEN, J. R. 2004. Development of a Local Meteoric Water Line for Southeastern Idaho, Western Wyomning, and South-Central Montana. *Scientific Investigations Report 2004-5126.* Idaho Falls, Idaho: USGS.

BERSHAW, J., SAYLOR, J. E., GARZIONE, C. N., LEIER, A. & SUNDELL, K. E. 2016. Stable isotope variations (δ18O and δD) in modern waters across the Andean Plateau. *Geochimica et Cosmochimica Acta,* 194**,** 310-324.

BEXFIELD, L. M. & ANDERHOLM, S. K. 2010. Section 10: Conceptual understanding of groundwater quality of the basin-fill aquifer in the San Luis Valley, Colorado and New Mexico. *In:* THIROS, S. A., BEXFIELD, L. M., ANNING, D. W. & HUNTINGTON, J. M. (eds.) *Conceptual understanding and groundwater quality of selected basin-fill aquifers in the Southwestern United States: U.S. Geological Professional Paper 1781.* USGS.

BINKLEY, A. M., KUNKEL, R. & EDMUNDSON, W. S. 1948. The Effect of Chemical Vine Killers on Yield and Quality of Red McClure and Bliss Triumph Potatoes *American Potato Journal* 25

BLASCH, K. W. & BRYSON, J. R. 2007. Distinguishing sources of ground water recharge by using delta2H and delta18O. *Ground Water,* 45**,** 294-308.

BOYDSTON, R. A., NAVARRE, D. A., COLLINS, H. P. & CHAVES-CORDOBA, B. 2018. The Effect of Vine Kill Method on Vine Kill, Tuber Skinning Injury, Tuber Yield and Size Distribution, and Tuber Nutrients and Phytonutrients in Two Potato Cultivars Grown for Early Potato Production. *American Journal of Potato Research,* 95**,** 54-70.

BRADY, N. 1974. *The nature and properties of soils,* New York, Macmillan.

BRISTER, B. S. & GRIES, R. R. 1994. Tertiary stratigraphy and tectonic development of the Alamos basin (northern San Luis Basin), Rio Grande rift, south-central Colorado. *Geological Society of America*

CALDWELL, M. M., DAWSON, T. E. & RICHARDS, J. H. 1998. Hydraulic Lift: Consequences of Water Efflux from the Roots of Plants. *Oecologia,* 113**,** 151-161.

CALLAWAY, R. M. 2007. *Positive Interactions and Interdependence in Plant Communities,* Dordrecht, Spring.

CANALY, C. April 25, 2019 2019. *RE: Private household wells in the San Luis Valley.* Type to LANZONI, M.

CAPPA, C. D. 2003. Isotopic fractionation of water during evaporation. *Journal of Geophysical Research,* 108.

CARLING, G. T., FERNANDEZ, D. P. & JOHNSON, W. P. 2012. Dust-mediated loading of trace and major elements to Wasatch Mountain snowpack. *Sci Total Environ,* 432**,** 65-77.

CDWR 2004. Rio Grande decision support system phase 4 groundwater model documentation. Colorado Division of Water Resources.

CHABOUREAU, J.-P., RICHARD, E., PINTY, J.-P., FLAMANT, C., DI GIROLAMO, P., KIEMLE, C., BEHRENDT, A., CHEPFER, H., CHIRIACO, M. & WULFMEYER, V. 2011. Long-range transport of Saharan dust and its radiative impact on precipitation forecast: a case study during the Convective and Orographically-induced Precipitation Study (COPS). *Quarterly Journal of the Royal Meteorological Society,* 137**,** 236-251.

CHADWICK, H. W. A. P. D. D. 1965. Plant Succession on Dune Sands in Fremont County, Idaho. *Ecology,* 46**,** 766-780.

CHARLES, F. L., MORGAN, J. A. & BAUSCH, W. C. 1987. Evapotranspiration of Native Vegetation in the Closed Basin of the San Luis Valley, Colorado. Colorado State University: Colorado Water Resources Research Institute.

CHEN, J., KNIGHT, R. & ZEBKER, H. A. 2017. The Temporal and Spatial Variability of the Confined Aquifer Head and Storage Properties in the San Luis Valley, Colorado Inferred From Multiple InSAR Missions. *Water Resources Research,* 53**,** 9708-9720.

CHIMNER, R. A. & COOPER, D. J. 2004. Using stable oxygen isotopes to quantify the water source used for transpiration by native shrubs in the San Luis Valley, Colorado U.S.A. *Plant and Soil,* 260**,** 225-236.

CLARK, I. 2015a. *Groundwater Geochemistry and Isotopes,* Boca Raton, Florida, CRC Press, Taylor and Francis Group.

CLARK, I. D. 2015b. *Groundwater geochemistry and isotopes,* Boca Raton

London, CRC Press.

CLARK, I. D. & FRITZ, P. 1997. *Environmental isotopes in hydrogeology,* Boca Raton, CRC Press/Lewis Publishers.

COLLINS, S. L., SINSABAUGH, R. L., CRENSHAW, C., GREEN, L., PORRAS-ALFARO, A., STURSOVA, M. & ZEGLIN, L. H. 2008. Pulse dynamics and microbial processes in aridland ecosystems. *Journal of Ecology,* 96**,** 413-420.

COLLON, P., KUTSCHERA, W., LOOSLI, H. H., LEHMANN, R. E., PURTSCHERT, R., LOVE, A., SAMPSON, L., ANTHONY, D., COLE, D., DAVIDS, B., MORRISSEY, D. J., SHERILL, B. M., STEINER, M., PARDO, R. C. & PAUL, M. 2000. ^{81}Kr in the great Artesian Basin, Australia: a new method for dating very old groundwater. *Earth and Planetary Science Letters,* 182**,** 103-113.

COOK, P. G. & HERCZEG, A. L. 2000. *Environmental tracers in subsurface hydrology,* Boston; London, Kluwer Academic Publishers.

COOPER, D. J., SANDERSON, J. S., STANNARD, D. I. & GROENEVELD, D. P. 2006. Effects of long-term water table drawdown on evapotranspiration and vegetation in an arid region phreatophyte community. *Journal of Hydrology,* 325**,** 21-34.

COTTEN, C. 2017. *RE: District Engineer Groundwater Update.*

COURAULT, D., ALBERT, I., PERELLE, S., FRAISSE, A., RENAULT, P., SALEMKOUR, A. & AMATO, P. 2017. Assessment and risk modeling of airborne enteric viruses emitted from wastewater reused for irrigation. *Sci Total Environ,* 592**,** 512-526.

CRAIG, H. 1961. Isotopic variations in meteoric waters. *Science,* 133**,** 1702-1703.

CRAIG, H. & GORDON, L. I. 1965. Deuterium and oxygen-18 variations in the ocean and the marine atmosphere. *In:* TONGIORGI, E. (ed.) *Stable Isotopes in Oceanographic Studies and Paleotemperatures.* Pisa: CNR-Laboratorio di Geologia Nucleare.

CRAINE, J. M., TOWNE, E. G., TOLLESON, D. & NIPPERT, J. B. 2013. Precipitation timing and grazer performance in a tallgrass prairie. *Oikos,* 122**,** 191-198.

CROUVI, O., SCHEPANSKI, K., AMIT, R., GILLESPIE, A. R. & ENZEL, Y. 2012. Multiple dust sources in the Sahara Desert: The importance of sand dunes. *Geophysical Research Letters,* 39**,** n/a-n/a.

CSIKI, S. J. C. & MARTIN, C. W. 2013. Spatial Variability of Heavy-Metal Storage in the Floodplain of the Alamosa River, Colorado. *Physical Geography,* 29**,** 306-319.

CUTLER, N. & EKLUND, J. 2010. 2-D Electrical Resistivity Tomography: using the GeoTom device and associated software. Rock Breakdown Laboratory: University of Oxford.

D'ODORICO, P., CAYLOR, K., OKIN, G. S. & SCANLON, T. M. 2007. On soil moisture-vegetation feedbacks and their possible effects on the dynamics of dryland ecosystems. *Journal of Geophysical Research G: Biogeosciences,* 112.

DANSGAARD, W. 1953. The Abundance of 18O in Atmospheric Water and Water Vapour. *Tellus,* V.

DANSGAARD, W. 1964. Stable Isotopes in Precipitation. *Tellus,* XVI**,** 436-468.

DARLING, W. G., EDMUNDS, W. M., KINNIBURG, D. G. & KOTOUB, S. 1987. Sources of recharge to the Basal Nubian sandstone aquifer, Butana region, Sudan. *In:* IAEA (ed.) *Isotope Techniques in Water Resources Development.* Vienna: IAEA.

DAVIS ENGINEERING SERVICE, I., GEOLOGICAL SOLUTIONS, I. & HRS WATER CONSULTANTS, I. 2012. Rio Grande County Hydrogeologic Report. Del Norte, Colorado.

DAVIS ENGINEERING SERVICE, I. & PRINCIPIA MATHEMATICA, I. 2019. San Luis Valley Well and Water-Level Database. RGWCD.

DAWSON, T. E. 1993a. Hydraulic lift and water use by plants: implications for water balance, performance and plant-plant interactions. *Oecologia,* 95**,** 565-574.

DAWSON, T. E. 1993b. Water Sources of Plants as Determined from Xylem-Water Isotopic Composition: perspectives on plant competition, distribution and water relations. *In:* EHLERINGER, J. R., HALL, A. E. & FARQUHAR, G. D. (eds.) *Stable Isotopes and Plant Carbon/Water Relations.* San Diego, CA: Acadeic Press.

DE VRIES, J. J. & SIMMERS, I. 2002. Groundwater recharge: an overview of processes and challenges. *Hydrogeology Journal,* 10**,** 5-17.

DELGADO-BAQUERIZO, M., MAESTRE, F. T., GALLARDO, A., BOWKER, M. A., WALLENSTEIN, M. D., QUERO, J. L., OCHOA, V., GOZALO, B., GARCIA-GOMEZ, M., SOLIVERES, S., GARCIA-PALACIOS, P., BERDUGO, M., VALENCIA, E., ESCOLAR, C., ARREDONDO, T., BARRAZA-ZEPEDA, C., BRAN, D., CARREIRA, J. A., CHAIEB, M., CONCEICAO, A. A., DERAK, M., ELDRIDGE, D. J., ESCUDERO, A., ESPINOSA, C. I., GAITAN, J., GATICA, M. G., GOMEZ-GONZALEZ, S., GUZMAN, E., GUTIERREZ, J. R., FLORENTINO, A., HEPPER, E., HERNANDEZ, R. M., HUBER-SANNWALD, E., JANKJU, M., LIU, J., MAU, R. L., MIRITI, M., MONERRIS, J., NASERI, K., NOUMI, Z., POLO, V., PRINA, A., PUCHETA, E., RAMIREZ, E., RAMIREZ-COLLANTES, D. A., ROMAO, R., TIGHE, M., TORRES, D., TORRES-DIAZ, C., UNGAR, E. D., VAL, J., WAMITI, W., WANG, D. & ZAADY, E. 2013. Decoupling of soil nutrient cycles as a function of aridity in global drylands. *Nature,* 502**,** 672-6.

DEMPSTER, A. J. 1918. A new Method of Positive Ray Analysis. *Physical Review,* 11**,** 316-325.

DESIMONE, L. A., MCMAHON, P. B. & ROSEN, M. R. 2015. The quality of our Nation's waters: Water quality in principal aquifers of the United States, 1991-2010. *In:* USGS (ed.).

DOETSCH, J., LINDE, N., PESSOGNELLI, M., GREEN, A. G. & GUNTHER, T. 2012. Constraining 3-D electrical resistance tomography with GPR reflection data for improved aquifer characterization. *Journal of Applied Geophysics,* 78.

DRENTH, B., GRAUCH, V. J. S. & RODRIGUEZ, B. D. 2013. Geophysical constraints on Rio Grande rift structure in the central San Luis Basin, Colorado and New Mexico. *In:* HUDSON, M. R. & GRAUCH, V. J. S. (eds.) *New Perspectives on Rio Grande Rift Basins: From Tectonics to Groundwater, Geological Society of America Special Paper 494.* GSA.

DREVER, J. I. 1988. *The geochemistry of natural waters,* Englewood Cliffs, New Jersey, Prentice Hall.

DUBINSKY, J. & KARUNANITHI, A. T. 2016. Greenhouse Gas Accounting of Rural Agrarian Regions: The Case of San Luis Valley. *ACS Sustainable Chemistry & Engineering,* 5**,** 261-268.

DUNGAN, R. S. 2012. Use of a culture-independent approach to characterize aerosolized bacteria near an open-freestall dairy operation. *Environ Int,* 41**,** 8-14.

EARMAN, S., CAMPBELL, A. R., PHILLIPS, F. M. & NEWMAN, B. D. 2006. Isotopic exchange between snow and atmospheric water vapor: Estimation of the snowmelt component of groundwater recharge in the southwestern United States. *Journal of Geophysical Research,* 111.

EDMUNDS, W. M. 2008a. Groundwater in Africa--paleowater, climate change, and modern recharge. *In:* ADELANA, S. M. A., MACDONALD, A.M. (ed.) *Applied Groundwater Studies in Africa.* CRC / Balkema.

EDMUNDS, W. M. 2009. Palaeoclimate and groundwater evolution in Africa—implications for adaptation and management. *Hydrological Sciences Journal,* 54**,** 781-792.

EDMUNDS, W. M., DARLING, W. G., PURTSCHERT, R. & CORCHO ALVARADO, J. A. 2014. Noble gas, CFC and other geochemical evidence for the age and origin of the Bath thermal waters, UK. *Applied Geochemistry,* 40**,** 155-163.

EDMUNDS, W. M., DARLING, W.G., KINNIBURGH, D.G. 1987a. Estimation of aquifer recharge using geochemical techniques: final report of the Lower Atbara River Basin Project. British Geological Survey Rep.: British Geological Survey.

EDMUNDS, W. M., DARLING, W.G., KINNIBURGH, D.G. 1987b. Estimation of aquifer recharge using geochemical techniques: final report of the Lower Atbara River Basin Project. Wallingford, UK: British Geological Survey.

EDMUNDS, W. M., SHAND, P. (ed.) 2008b. *Natural Groundwater Quality,* Oxford, UK: Blackwell.

EHLERINGER, J. R., EVANS, R. D. & WILLIAMS, D. G. 1998. Assessing sensitivity to change in desert ecosystems - a stable isotope approach. *In:* GRIFFITHS, H. (ed.) *Stable Isotopes Integration of Biological, Ecological, and Geochemical Processes.* Oxford: BIOS Scientific Publ.

EHLERINGER, J. R. & OSMOND, C. B. 1989. Stable Isotopes. *In:* PEARCY, R. W., EHLERINGER, J. R., MOONEY, H. A. & RUNDEL, P. W. (eds.) *Plant physiological ecology: field methods and instrumentation.* Kluwer Academic Publishers.

EHLERINGER, J. R., PHILLIPS, S. L., SCHUSTER, W. S. F. & SANDQUIST, D. R. 1991. Differential utilization of summer rains by desert plants. *Oecologia,* 88**,** 430434.

EMERY, P. A. 1971a. Water Resources of the San Luis Valley. *In:* USGS (ed.). Pueblo, Colorado: USGS.

EMERY, P. A. 1971b. Water resources of the San Luis Valley, Colorado. Pueblo, Colorado: USGS.

EMERY, P. A., PATTEN, E. P. & MOORE, J. E. 1975. Analog model study of the hydrology of the San Luis Valley, south-central Colorado. *Colorado Water Conservation Board Ground-Water Circular.* Denver.

ENGLISH, N. B., DETTMAN, D. L. & WILLIAMS, D. G. 2010. A 26-year stable isotope record of humidity and El Niño-enhanced precipitation in the spines of saguaro cactus, Carnegiea gigantea. *Palaeogeography, Palaeoclimatology, Palaeoecology,* 293**,** 108-119.

FITTERMAN, D. V. & DE SOZUA FILHO, O. A. 2009. Transient electromagnetic soundings near Great Sand Dunes National Park and Preserve, San Luis Valley (2006 Field Season). *In:* USGS (ed.). Colorado.

FONTES, J. C. & FRITZ, P. 1975. Isotope Hydrology 1974: A Review of the IAEA Symposium on Isotope Techniques in Groundwater Hydrology. *International Journal of Applied Radiation and Isotopes,* 26**,** I--8.

FREEZE, R. A. & CHERRY, J. A. 1979. *Groundwater,* Englewood Cliffs, NJ, Prentice-Hall Inc.

FRIEDMAN, I., BENSON, C. & GLEASON, J. 1991. Isotopic Changes During Snow Metamorphism. *In:* TAYLOR, H. P., O'NEIL, J. R. & KAPLAN, I. R. (eds.) *Stable Isotope Geochemistry: A Tribute to Samuel Epstein.* San Antonio, TX: The Geochemical Society.

FRITZ, P. & FONTES, J. C. 1980. *Handbook of environmental isotope geochemistry. Vol. 1-2, The terrestrial environment,* Amsterdam; Oxford, Elsevier.

FROEHLICH, K., KRALIK, M., PAPESCH, W., RANK, D., SCHEIFINGER, H. & STICHLER, W. 2008. Deuterium excess in precipitation of Alpine regions - moisture recycling. *Isotopes Environ Health Stud,* 44**,** 61-70.

FROEND, R. & SOMMER, B. 2010. Phreatophytic vegetation response to climatic and abstraction-induced groundwater drawdown: Examples of long-term spatial and temporal variability in community response. *Ecological Engineering,* 36**,** 1191-1200.

GANSKOPP, D. C. 1986. Tolerances of Sagebrush, Rabbitbrush, and Greasewood to Elevated Water Tables. *Journal for Range Management,* 39**,** 334-337.

GAT, J. & GONFIANTINI, R. 1981. *Stable isotope hydrology : deuterium and oxygen-18 in the water cycle : a monograph prepared under the aegis of the IAEA/UNESCO Working Group on Nuclear Techniques in Hydrology of the International Hydro-logical Programme / scientific editors: J.R. Gat, R. Gonfiantini,* Vienna, International Atomic Energy Agency.

GAT, J. R. & ISSAR, A. 1974. Desert isotope hydrology: water sources of the Sinai Desert. *Geochimica et Cosmochimica Acta,* 38**,** 1117-1131.

GATES, J., BOHLKE, K. & EDMUNDS, W. M. 2008. Ecohydrological Factors Affecting Nitrate Concentrations in a Phreatic Desert Aquifer in Northwestern China. *Environmental Science and Technology,* 42**,** 3531-3537.

GAYE, C. B., EDMUNDS, W. M. 1996. Groundwater recharge estimation using chloride, stable isotopes and tritium profiles in the sands of northwestern Senegal. *Environmental Geology,* 27**,** 246-251.

GIAUQUE, W. F. & JOHNSTON, H. L. 1929a. An isotope of oxygen of mass 17 in the earth's atmosphere. *Nature* 831.

GIAUQUE, W. F. & JOHNSTON, H. L. 1929b. An isotope of oxygen, mass 17, in the earth's atmosphere *Journal of the American Chemical Society,* 51**,** 3528-3534.

GIAUQUE, W. F. & JOHNSTON, H. L. 1929c. An isotope of oxygen, mass 18. *Nature***,** 318.

GILAD, E., SHACHAK, M. & MERON, E. 2007. Dynamics and spatial organization of plant communities in water-limited systems. *Theoretical Population Biology,* 72**,** 214-230.

GONFIANTINI, R., CONRAD, G., FONTES, J. C., SAUZAY, G. & PAYNE, B. R. Etude Isotopique de la Nappe du Continental Intercalaire et de ses Relations avec les Autres Nappes du Sahara Septentrional. *In:* IAEA, ed. Isotope Techniques in Groundwater Hydrology, 1974 Vienna.

GONFIANTINI, R., GRATZIU, S. & TONGIORGI, E. 1965. Oxygen isotopic composition of water in leaves. *In:* IAEA (ed.) *Isotopes and Radiation in Soil-Plant Nutrition Studies.* Vienna, Austria: IAEA.

GONI, I. B., FELLMAN, E., EDMUNDS, W.M. 2001. Rainfall geochemistry in the Sahel region of northern Nigeria. *Atmospheric Environment,* 35**,** 4331-4339.

GOOSEFF, M. N., LYONS, W. B., MCKNIGHT, D. M., VAUGHN, B. H., FOUNTAIN, A. G. & DOWLING, C. 2006. A Stable Isotopic Investigation of a Polat Desert Hydrologic System, McMurdo Dry Valleys, Antarctica. *Arctic, Antarctic, and Alpine Research,* 38**,** 60-71.

GRAF, W. L. 1994. *Plutonium and the Rio Grande: Environmental Change and Contamination in the Nuclear Age* Oxford University Press.

GRAF, W. L. 1996. Transport and deposition of plutonium-contaminated sediments by fluvial processes, Los Alamos Canyon, New Mexico. *GSA Bulletin,* 108**,** 1342–1355.

GRAUCH, V. J. S., L. SKIPP, G., THOMAS, J., DAVIS, J. & BENSON, M. E. 2015. *Sample Descriptions and Geophysical Logs for Cored Well BP-3-USGS, Great Sand Dunes, National Park, Alamosa County, Colorado*.

GRAUCH, V. J. S. & RULEMAN, C. A. 2013. Identifying Buried Segments of Active Faults in the Northern Rio Grande Rift Using Aeromagnetic, LiDAR, and Gravity Data, South-Central Colorado, USA. *International Journal of Geophysics,* 2013**,** 1-26.

GROENEVELD, D. P. & CROWLEY, D. E. 1988. Root System Response to Flooding in Three Desert Shrub Species. *Functional Ecology,* 2**,** 491-497.

GRONING, M., VAN DUREN, M. & ANDREESCU, L. Metrological characteristics of the conventional measurement scales for hydrogen and oxygen stable isotope amount ratios: the δ-scales. *In:* FAJGELJ, A., BELLI, M. & SANSONE, U., eds. Combining and Reporting Analytical Results: The role of traceability and uncertainty for comparing analytical results, 6-8 March 2006 2006 Rome. Royal Society of Chemistry, 62-72.

GUNDERSON, T., BUHL, T., ROMERO, R. & SALAZAR, J. 1983. Radiological Survey Following Decontamination Activities Near the TA-45 Site. Los Alamos, NM: DOE.

GUSTAFSON, J. R. 2007. Snowmelt Water Isotope Fractionation in High Elevation Seasonal Snowpacks: Implications for Isotope Hydrograph Studies. [Accessed Dec, 2016].

HAKONSON-HAYES, A. C., FRESQUEZ, P. R. & WHICKER, F. W. 2002. Assessing potential risks from exposure to natural uranium in well water. *Journal of Environmental Radioactivity,* 59**,** 29–40.

HANNA, T. & HARMON, E. 1989. An overview of the historical, stratigraphic, and structural setting of the aquifer system of the San Luis Valley. *Water in the valley: Colorado Groundwater Association, 8th Annual Field Trip, Guidebook***,** 1-34.

HEALY, R. W. & SCANLON, B. R. 2018. *Estimating Groundwater Recharge,* Cambridge, Cambridge University Press.

HEARNE, G. A. & DEWEY, J. D. 1988. Hydrologic analysis of the Rio Grande Basin north of Embudo, New Mexico; Colorado and New Mexico. *Water-Resources Investigations Report.* - ed.

HEM, J. D. 1985. Water and Interpretation of the Chemical Characteristics of Natural Water. *U S Geological Survey Water-Supply Paper 2254.* Third Edition ed.

HILLEL, D. 2006. *Environmental Soil Physics*.

HISCOCK, K. 2005. *Hydrogeology: Principles and Practice,* Oxford, UK, Blackwell.

HOGAN, J. F., PHILIPS F. M., SCANLON B. R. (ed.) 2004. *Groundwater Recharge in a Desert Environment: the Southwestern United States,* Washington, D.C.: American Geophysical Union.

HOGAN, J. F., PHILLIPS, F. M. & SCANLON, B. R. (eds.) 2004. *Groundwater Recharge in a Desert Environment: the Southwestern United States,* Washington, D.C.: American Geophysical Union.

HOLMGREN, M. & SCHEFFER, M. 2010. Strong facilitation in mild environments: the stress gradient hypothesis revisited. *Journal of Ecology,* 98**,** 1269-1275.

HOOVER, J., GONZALES, M., SHUEY, C., BARNEY, Y. & LEWIS, J. 2017. Elevated Arsenic and Uranium Concentrations in Unregulated Water Sources on the Navajo Nation, USA. *Expo Health,* 9**,** 113-124.

HUNTLEY, D. 1976. Hydrogeology of Northern San Luis Valley. *In:* EPIS, R. C. & WEIMER, R. J. (eds.) *Studies in Colorado Field Geology: Colorado School of Mines Professional Contributions.* Golden, CO.

HUNTLEY, D. 1979. Ground-water recharge to the aquifers of northern San Luis Valley, Colorado: summary. *Geological Society of America Bulletin,* 90**,** 707-709.

IAEA 1974. *Isotope techniques in groundwater hydrology, 1974 : proceedings of a symposium organized by the International Atomic Energy Agency and held in Vienna, 11-15 March 1974,* Vienna, International Atomic Energy Agency.

JEAMBRUN, M., POURCELOT, L., MERCAT, C., BOULET, B., PELT, E., CHABAUX, F., CAGNAT, X. & GAUTHIER-LAFAYE, F. 2012. Potential sources affecting the activity concentrations of 238U, 235U, 232Th and some decay products in lettuce and wheat samples. *J Environ Monit,* 14**,** 2902-12.

KAPPEN, B., SANFORD, W. & SANDERSON, J. S. 2004. Ground and Surface Water Interaction in Ephemeral Wetlands, San Luis Valley, Colorado. *Hydrology Days* [Online].

KARYDIS, V. A., KUMAR, P., BARAHONA, D., SOKOLIK, N. & NENES, A. 2011. On the effect of dust particles on global cloud condensation nuclei and cloud droplet number. *Journal of Geophysical Research,* 116**,** 16.

KENDALL, C. & MCDONNELL, J. J. 1998. *Isotope tracers in catchment hydrology,* Oxford, Elsevier.

KIDRON, G. J. & GUTSCHICK, V. P. 2013. Soil moisture correlates with shrub-grass association in the chihuahuan desert. *Catena,* 107**,** 71-79.

KIRKHAM, R. M., LOVEKIN, J. R. & SARES, M. A. Sources of acidity and heavy metals in the Alamosa River basin outside of the Summitville mining area, Colorado. *In:* POSEY, H. H., PENDLETON, J. A. & VAN ZYL, D., eds. Proceedings: Summitville Forum 1995. Colorado Geological Survey 42-57.

KIZITO, F., DRAGILA, M. I., SENÈ, M., BROOKS, J. R., MEINZER, F. C., DIEDHIOU, I., DIOUF, M., LUFAFA, A., DICK, R. P., SELKER, J. & CUENCA, R. 2012. Hydraulic redistribution by two semi-arid shrub species: Implications for Sahelian agro-ecosystems. *Journal of Arid Environments,* 83**,** 69-77.

KÖHLER, C. H. Optical properties of mineral dust aerosol in the thermal infrared. AIP Conference Proceedings, 2017. 050001.

KRAEMER, T. F. & GENEREUX, D. P. 1998. Applications of Uranium- and Thorium-Series Radionuclides in Catchment Hydrology Studies. *In:* KENDALL, C. & MCDONNELL, J. J. (eds.) *Isotope Tracers in Catchment Hydrology.* Oxford: Elsevier.

KRAY, J. A., COOPER, D. J. & SANDERSON, J. S. 2012. Groundwater use by native plants in response to changes in precipitation in an intermountain basin. *Journal of Arid Environments,* 83**,** 25-34.

LANZONI, M. 2017. Air-Surface-Ground Water Cycling in an Agricultural Desert Valley of Southern Colorado. *American Geophysical Union Fall Meeting.* New Orleans, LA: AGU.

LANZONI, M. & DARLING, W. G. 2019. Changes to Snowmelt-driven Recharge in a High-elevation Desert Valley. *In:* IAEA (ed.) *IAEA International Symposium on Isotope Hydrology.* Vienna.

LANZONI, M., DARLING, W. G. & EDMUNDS, W. M. 2018. Groundwater in Sudan: An improved understanding of wadi-directed recharge. *Applied Geochemistry,* 99**,** 55-64.

LAWRENCE, C. R., PAINTER, T. H., LANDRY, C. C. & NEFF, J. C. 2010. Contemporary geochemical composition and flux of aeolian dust to the San Juan Mountains, Colorado, United States. *Journal of Geophysical Research,* 115.

LEE, C. H. 1912. An intensive study of the water resources of a part of Owens Valley, California. *Water Supply Paper.* - ed.: United States Geological Survey.

LEFEVER, R., BARBIER, N., COUTERON, P. & LEJEUNE, O. 2009. Deeply gapped vegetation patterns: on crown/root allometry, criticality and desertification. *J Theor Biol,* 261**,** 194-209.

LEONARD, G. J. & WATTS, K. R. 1988. Hydrogeology and simulated effects of ground-water development on an unconfined aquifer in the Closed Basin Division, San Luis Valley, Colorado. US Geological Survey.

LIESCH, T., HINRICHSEN, S. & GOLDSCHEIDER, N. 2015. Uranium in groundwater--Fertilizers versus geogenic sources. *Sci Total Environ,* 536**,** 981-995.

LINDSEY, D. A. 2010a. The Geologic Story of Colorado's Sangre de Cristo Range. *Circular 1349.* USGS.

LINDSEY, D. K. 2010b. The Geologic Story of Colorado's Sangre de Cristo Range. *In:* USGS (ed.). Reston, Virginia.

LIPMAN, P. W., STEVEN, T. A. & MEHNERT, H. H. 1970. Volcanic History of the San Juan Mountains, Colorado, as Indicated by Potassium-Argon Dating. *Geological Society of America Bulletin,* 81**,** 2329-2352.

LIU, H.-H. 2011. Impact of climate change on groundwater recharge in dry areas: An ecohydrology approach. *Journal of Hydrology,* 407**,** 175-183.

LIU, N. & GUAN, L. 2012. Linkages between woody plant proliferation dynamics and plant physiological traits in southwestern North America. *Journal of Plant Ecology,* 5**,** 407-416.

LOIK, M. E., BRESHEARS, D. D., LAUENROTH, W. K. & BELNAP, J. 2004. A multi-scale perspective of water pulses in dryland ecosystems: climatology and ecohydrology of the western USA. *Oecologia,* 141**,** 269-81.

LOKE, M. H. 2000. Electrical imaging surveys for environmental and engineering studies: a practical guide to 2-D and 3-D surveys.

LUCERO, J. 2016a. *RE: Natural history of wetland playas.*

LUCERO, J. Oct 15, 2016 2016b. *RE: Wetland playa chemistry study.* Type to LANZONI, M.

LUDWIG, J. A., WILCOX, B. P., BRESHEARS, D. D., TONGWAY, D. J. & IMESON, A. C. 2005. Vegetation patches and runoff-erosion as interacting ecohydrological processes in semiarid landscapes. *Ecology,* 86**,** 288-297.

MACHETTE, M. N. New evidence for ancient Lake Alamosa in the San Luis basin of Colorado. Geological Society of America, Denver Annual Meeting, 2004.

MACHETTE, M. N., MARCHETTI, D. W. & THOMPSON, R. A. 2007. Ancient Lake Alamosa and the Pliocene to middle Pleistocene evolution of the Rio Grande. *Machette, MN, Coates, M.-M., and Johnson, ML, eds***,** 7-9.

MACHETTE, M. N., THOMPSON, R. A., MARCHETTI, D. W. & SMITH, R. S. U. 2013. Evolution of ancient Lake Alamosa and integration of the Rio Grande during the Pliocene and Pleistocene. *Special Paper of the Geological Society of America.* Geological Society of America.

MAYO, A. L. 2010. Ambient well-bore mixing, aquifer cross-contamination, pumping stress, and water quality from long-screened wells: What is sampled and what is not? *Hydrogeology Journal,* 18**,** 823-837.

MAYO, A. L. & CHRISTIANSEN, D. W. 1994. Solute and isotopic evidence for vertical stratification of ground water flow regimes in the upper 4,000 feet of the San Luis Valley, Colorado. *Geological Society of America.* Denver, Colorado: Geol Soc Am Abstract with programs.

MAYO, A. L., DAVEY, A. & CHRISTIANSEN, D. 2007. Groundwater flow patterns in the San Luis Valley, Colorado, USA revisited: an evaluation of solute and isotopic data. *Hydrogeology Journal,* 15**,** 383-408.

MCCALPIN, J. P. 1996. General Geology of the Northern San Luis Valley, Colorado.

MCCALPIN, J. P. 2018. *RE: Unconfined aquifer depth.* Type to LANZONI, M.

MEINZER, O. E. 1923. Outline of groundwater hydrology with definitions. *U.S. Geological Survey Water Supply Paper 494.* U. S. Geological Survey.

MEINZER, O. E. 1927. Plants as indicators of ground water. *U.S. Geological Survey Water Supply Paper No. 577.* Washington, D. C.: U. S. Geological Survey.

MEIXNER, T., MANNING, A. H., STONESTROM, D. A., ALLEN, D. M., AJAMI, H., BLASCH, K. W., BROOKFIELD, A. E., CASTRO, C. L., CLARK, J. F., GOCHIS, D. J., FLINT, A. L., NEFF, K. L., NIRAULA, R., RODELL, M., SCANLON, B. R., SINGHA, K. & WALVOORD, M. A. 2016. Implications of projected climate change for groundwater recharge in the western United States. *Journal of Hydrology,* 534**,** 124-138.

MERLIVAT, L. 1978. Molecular diffusivities of H2 16O, HD 16O, and H2 18O in gases. *J. Chem. Phys.,* 69**,** 2864.

MERLIVAT, L. & JOUZEL, J. 1979. Global climatic interpretation of the deuterium-oxygen 18 relationship for precipitation. *Journal of Geophysical Research,* 84**,** 5029.

MILLER, K. A., MACDONNELL, L. J. & RHODES, S. L. 1993. Groundwater Rights in an Uncertain Environment: Theoretical Perspectives on the San Luis Valley. *Natural Resources Journal,* 32.

MILLS, T., HOEKSTRA, P., BLOHM, M. & EVANS, L. 1988. Time Domain Electromagnetic Soundings for Mapping Sea-Water Intrusion in Monterey County, California. *Ground Water,* 26**,** 71-782.

MIX, K., LOPES, V. L. & RAST, W. 2011. Environmental Drivers of Streamflow Change in the Upper Rio Grande. *Water Resources Management,* 26**,** 253-272.

MIX, K., LOPES, V. L. & RAST, W. 2014. A Systems Approach to Understanding the Evolution of the Agro-Social-Ecological System of the Upper Rio Grande-San Luis Valley, Colorado. *Water Resources Management,* 29**,** 233-251.

MIYAZAKI, T. 2006. *Water Flow in Soils,* Boca Raton, FL; London, Taylor and Francis.

MOL, L. & VILES, H. 2011. *Sandstone weathering, Electrical Resistivity Tomography, and the deterioration of San Rock Art in the Golden Gate Highlands National Park, South Africa.* DPhil DPhil, University of Oxford.

MORRIS, B. L., GEORGE DARLING, W., GOODDY, D. C., LITVAK, R. G., NEUMANN, I., NEMALTSEVA, E. J. & PODDUBNAIA, I. 2005. Assessing the extent of induced leakage to an urban aquifer using environmental tracers: an example from Bishkek, capital of Kyrgyzstan, Central Asia. *Hydrogeology Journal,* 14**,** 225-243.

MOSER, H. & STICHLER, W. 1980. Environmental Isotopes in Ice and Snow. *In:* FRITZ, P. & FONTES, J. C. (eds.) *Handbook of Environmental Isotope Geochemistry Vol. 1.* Netherlands.

MULLER, T., SCHLADITZ, A., KANDLER, K. & WIEDENSOHLER, A. 2011. Spectral particle absorption coefficients, single scattering albedos and imaginary parts of refractive indices from ground based in situ measurements at Cape Verde Island during SAMUM-2. *Tellus,* 63B**,** 573–588.

NASH, J. T. 1988. Geology and Geochemistry of the Pitch Uranium Mine Area, Saguache County, Colorado. United States Geological Survey.

NASH, J. T. 2010. Volcanogenic Uranium Deposits: Geology, Geochemical Processes, and Criteria for Resource Assessment. United States Geological Survey.

NAVAR, J. 1993. The causes of stemflow variation in three semi-arid growing species of northeastern Mexico. *Journal of Hydrology,* 145**,** 175-190.

NÁVAR, J. 2011. Stemflow variation in Mexico's northeastern forest communities: Its contribution to soil moisture content and aquifer recharge. *Journal of Hydrology,* 408**,** 35-42.

NEWMAN, B. D., OSENBRUCK, K., AESCHBACH-HERTIG, W., SOLOMON, D. K., COOK, P., ROZANSKI, K. & KIPFER, R. 2010. Dating of 'young' groundwaters using environmental tracers: advantages, applications, and research needs. *Isotopes Environ Health Stud,* 46**,** 259-78.

NOLAN, J. & WEBER, K. A. 2015. Natural Uranium Contamination in Major U.S. Aquifers Linked to Nitrate. *Environmental Science & Technology Letters,* 2**,** 215-220.

NOY-MEIR, I. 1973. Desert ecosystems: Environment and producers. *Annual Review of Ecology and Systematics,* 4**,** 25-51.

NWS & NOAA. 2019. *Climate Fall Freeze Data* [Online]. Available: https://www.weather.gov/pub/ClimateFallFreezeData [Accessed 4/23/19.

OSMOND, J. K. & COWART, J. B. 2000. U-Series Nuclides as Tracers in Groundwater Hydrology. *In:* COOK, P. G. & HERCZEG, A. L. (eds.) *Environmental Tracers in Subsurface Hydrology.* Kluwer Academic Publishers.

PADDOCK, W. A. 2001. Rio Grande Compact of 1938, The. *U. Denv. Water L. Rev.,* 5**,** 1.

PAINTER, T. H., BARRETT, A. P., LANDRY, C. C., NEFF, J. C., CASSIDY, M. P., LAWRENCE, C. R., MCBRIDE, K. E. & FARMER, G. L. 2007. Impact of disturbed desert soils on duration of mountain snow cover. *Geophysical Research Letters,* 34.

PAINTER, T. H., DEEMS, J. S., BELNAP, J., HAMLET, A. F., LANDRY, C. C. & UDALL, B. 2010. Response of Colorado River runoff to dust radiative forcing in snow. *Proceedings of the National Academy of Sciences,* 107**,** 17125-17130.

PAINTER, T. H., SKILES, S. M., DEEMS, J. S., BRANDT, W. T. & DOZIER, J. 2017. Variation in Rising Limb of Colorado River Snowmelt Runoff Hydrograph Controlled by Dust Radiative Forcing in Snow. *Geophysical Research Letters,* 45**,** 797-808.

PASTERNAK, J. 2011. *Yellow Dirt: A poisoned land and the betrayal of the Navajos,* New York, Free Press.

PELÁEZ, M., DIRZO, R., FERNANDES, G. W. & PEREA, R. 2019. Nurse plant size and biotic stress determine quantity and quality of plant facilitation in oak savannas. *Forest Ecology and Management,* 437**,** 435-442.

PENG, H., MAYER, B., HARRIS, S. & KROUSE, H. R. 2017. The influence of below-cloud secondary effects on the stable isotope composition of hydrogen and oxygen in precipitation at Calgary, Alberta, Canada. *Tellus B: Chemical and Physical Meteorology,* 59**,** 698-704.

PEÑUELAS, J., SARDANS, J., RIVAS-UBACH, A. & JANSSENS, I. A. 2012. The human-induced imbalance between C, N and P in Earth's life system. *Global Change Biology,* 18**,** 3-6.

PHILLIPS, F. M., BENTLEY, H. W., DAVIS, S. N., ELMORE, D. & SWANNICK, G. B. 1986. Chlorine-36 dating of very old groundwater. II Milk River aquifer, Alberta. *Water Resources Research,* 22**,** 2003-2016.

PHILLIPS, F. M., WALVOORD, M. A. & SMALL, E. E. 2004. Effects of Environmental Change on Groundwater Recharge in the Desert Southwest. *In:* HOGAN, J. F., PHILLIPS, F. M. & SCANLON, B. R. (eds.) *Groundwater Recharge in a Desert Environment: the Southwest United States.* AGU.

PLUMMER, L. N. & GLYNN, P. 2013. Radiocarbon dating in groundwater systems. *In:* IAEA (ed.) *Isotope methods for dating old groundwater.* Vienna: IAEA.

POWELL, W. J. & MUTZ, P. B. 1958. Groundwater Resources of the San Luis Valley. *In:* USGS (ed.). Washington, DC: USGS.

RADOSEVICH, G. E. & RUTZ, R. W. 1979. San Luis Valley Water Problems: a legal perspective. *Information Series Report No. 34.* Colorado State University, Fort Collins, CO: Colorado Water Resources Research Institute.

REEVES, J. A., KNIGHT, R., ZEBKER, H. A., KITANIDIS, P. K. & SCHREÜDER, W. A. 2014. Estimating temporal changes in hydraulic head using InSAR data in the San Luis Valley, Colorado. *Water Resources Research,* 50**,** 4459-4473.

REN, W., YAO, T. & XIE, S. 2017. Key drivers controlling the stable isotopes in precipitation on the leeward side of the central Himalayas. *Atmospheric Research,* 189**,** 134-140.

REYNOLDS, R. L., MUNSON, S. M., FERNANDEZ, D., GOLDSTEIN, H. L. & NEFF, J. C. 2016. Concentrations of mineral aerosol from desert to plains across the central Rocky Mountains, western United States. *Aeolian Research,* 23**,** 21-35.

RGWCD 2017. Rio Grande Water Conservation District prinmath online dataset. *In:* DISTRICT, R. G. W. C. (ed.).

RICHARDS, J. H. & CALDWELL, M. M. 1987. Hydraulic lift: Substantial nocturnal water transport between soil layers by Artemisia tridentata roots. *Oecologia,* 73**,** 486-489.

RICHARDS, L. A., GARDNER, W. R. & OGATA, G. 1956. Physical processes determining water loss from soil. *Soil Sci. Soc. Am. Proc..* 20**,** 310--314.

RIO GRANDE ROUNDTABLE 2014. Rio Grande Interbasin Roundtable Minutes, September 9. *Interbasin Compact Committee Basin Roundtables.* RGBR.

RIVERSIDE TECHNOLOGY, I., HRS & BOYLE 1998. Rio Grande Decision Support System Feasibility Study. Colorado Division of Water Resources: Colorado Water Conservation Board.

ROBINSON, M. & WARD, R. C. 2017. *Hydrology : principles and processes,* London, IWA Publishing.

ROBINSON, T. W. 1958. *Phreatophytes*, US Government Printing Office.

RODELL, M., FAMIGLIETTI, J. S., WIESE, D. N., REAGER, J. T., BEAUDOING, H. K., LANDERER, F. W. & LO, M. H. 2018. Emerging trends in global freshwater availability. *Nature*.

ROHDE, M. 2009. *The determination of groundwater recharge using chloride as a geochemical tracer in semi-arid Rajasthan, India.* M.Sc. , University of Oxford.

RULEMAN, C. A., HUDSON, A. M., THOMPSON, R. A., MIGGINS, D. P., PACES, J. B. & GOEHRING, B. M. 2019. Middle Pleistocene formation of the Rio Grande Gorge, San Luis Valley, south-central

Colorado and north-central New Mexico, USA: Process, timing, and downstream implications. *Quaternary Science Reviews,* 223**,** 105846.

RUPERT, M. G. & PLUMMER, L. N. 2004. Ground-Water Flow Direction, Water Quality, Recharge Sources, and Age, Great Sand Dunes National Monument, South-Central Colorado, 2000-2001. *Scientific Investigations Report 2004-5027.* Denver, CO: USGS.

SALTZ, D., SHACHAK, M., CALDWELL, M., PICKETT, S. T. A., DAWSON, J., TSOAR, H., YOM-TOV, Y., WELTZ, M., FARROW, R. 1999. The Study and Management of Dryland Population Systems. *In:* HOEKSTRA, T. W. A. S., M. (ed.) *Arid Lands Management: towards ecological sustainability.* Urbana and Chicago: University of Illinois Press.

SAMI, K., HUGHES, A.D. 1996. A comparison of recharge estimates to a fractured sedimentary aquifer in South Africa from a chloridemassbalance and an integrated surface-subsurface model. *Journal of Hydrology,* 179**,** 111–136.

SAMOUËLIAN, A., COUSIN, I., TABBAGH, A., BRUAND, A. & RICHARD, G. 2005. Electrical resistivity survey in soil science: a review. *Soil and Tillage Research,* 83**,** 173-193.

SANDERSON, J. 2006. *Hydrology and Conservation of Intermountain Wetlands.* PhD, Colorado State University.

SANDERSON, J. S., KOTLIAR, N. B., STEINGRAEBER, D. A. & BROWNE, C. 2008. Simulated natural hydrologic regime of an intermountain playa conservation site. *Wetlands,* 28**,** 363-377.

SANGRE DE CRISTO LABORATORIES. 2019. *RE: Discussion of water quality testing and private-well water.* Type to LANZONI, M.

SASS, O. & VILES, H. 2010. Wetting and drying of masonry walls: 2D-resistivity monitoring of driving rain experiments on historic stonework in Oxford, UK. *Journal of Applied Geophysics,* 70**,** 72-83.

SCANLON, B. R., KEESE, K. E., FLINT, A. L., FLINT, L. E., GAYE, C. B., EDMUNDS, W. M. & SIMMERS, I. 2006. Global synthesis of groundwater recharge in semiarid and arid regions. *Hydrological Processes,* 20**,** 3335-3370.

SCHLESINGER, W. H. 1990. Biological feedbacks in global desertification. *Science,* 247**,** 1043-1048.

SCHLOSSER, P., STUTE, M., SONNTAG, C. & MUNNICH, K. O. 1989. Tritiogenic ^{3}He in shallow groundwater. *Earth and Planetary Science Letters,* 94**,** 245-256.

SCHNUG, E. & HANEKLAUS, N. 2015. Uranium in phosphate fertilizers – review and outlook. *In:* B., M. & A., A. (eds.) *Uranium - Past and Future Challenges.* Springer.

SCHOLES, R. J. & ARCHER, S. R. 1997. Tree-grass interactions in savannas. *Annu. Rev. Ecol. Syst.,* 28**,** 517-544.

SCHULZE, E. D., CALDWELL, M. M., CANADELL, J., MOONEY, H. A., JACKSON, R. B., PARSON, D., SCHOLES, R. J., SALA, O. E. & TRIMBORN, P. 1998. Downward flux of water through roots (i.e. inverse hydraulic lift) in dry Kalahari sands. *Oecologia,* 115**,** 460-462.

SCHUMANN, R. R., ZIELINSKI, R. A., OTTON, J. K., PANTEA, M. P. & OREM, W. H. 2017. Uranium delivery and uptake in a montane wetland, north-central Colorado, USA. *Applied Geochemistry,* 78**,** 363-379.

SCHWINNING, S. & SALA, O. E. 2004a. Hierarchy of responses to resource pulses in arid and semi-arid ecosystems. *Oecologia,* 141**,** 211-20.

SCHWINNING, S. & SALA, O. E. 2004b. Hierarchy of responses to resource pulses in arid and semi-arid ecosystems. *Oecologia,* 141**,** 211-220.

SCHWINNING, S. A. J. R. E. 2001. Water use trade-offs and optimal adaptations to pulse-driven arid ecosystems. *Journal of Ecology,* 89**,** 464-480.

SHANTZ, H. L. & PIEMEISEL, R. L. 1940. Types of Vegetation in Escalante Valley, Utah, as Indicators of Soil Conditions. 72.

SIEBENTHAL, C. E. 1910. Geology and Water Resources of the San Luis Valley. *Water Supply Paper 240.* Denver, Colorado: United States Geological Survey.

SIMMERS, I. (ed.) 1997. *Recharge of Phreatic Aquifers in (Semi-) Arid Areas,* Rotterdam, Brookfield: A. A. Balkema.

SINGHA, K. & GORELICK, S. M. 2005. Saline tracer visualized with three-dimensional electrical resistivity tomography: Field-scale spatial moment analysis. *Water Resources Research,* 41**,** 1-17.

SKILES, S. M. 2014. *Dust and Black Carbon Radiative Forcing Controls on Snowmelt in the Colorado River Basin.* PhD, University of California Los Angeles.

SLVDRG. 2016. *Annual Comprehensive Economic Development Strategy (CEDS) And Progress Report* [Online]. http://www.slvdrg.org/ceds_historic.php. [Accessed 3/2019.

STOERTZ, M. W., ANDERSON, M. P. & BRADBURY, K. R. 1991. *Field investigations and numerical studies on groundwater recharge through unsaturated sand : a methodology applied to central Wisconsin,* Madison, WI, University of Wisconsin-Extension, Geological and Natural History Survey.

STOGNER, R. W. 2001. Nitrate Concentrations, 1936-99, and Pesticide Concentrations, 1990-99, in the Unconfined Aquifer in the San Luis Valley, Colorado. Albuquerque, NM: USGS.

STONE, A. E., LANZONI, M. & SMEDLEY, P. 2019. Groundwater Resources: Past, Present, and Future. *In:* DADSON, S., GARRICK, D., HUGHES, J., HALL, J., HOPE, R. & PENNING-ROWSELL, E. (eds.) *Water Science Policy and Management: The Global Challenge.* Wiley.

STONE, A. E. C. & EDMUNDS, W. M. 2016. Unsaturated zone hydrostratigraphies: A novel archive of past climates in dryland continental regions. *Earth-Science Reviews,* 157**,** 121-144.

STONE, A. E. C., EDMUNDS, W.M. 2012. Sand, salt and water in the Stampriet Basin, Namibia: Calculating unsaturated zone (Kalahari dunefield) recharge using the chloride mass balance approach. *Water SA* 38**,** 367-78.

SZABO, Z., DEPAUL, V. T., FISCHER, J. M., KRAEMER, T. F. & JACOBSEN, E. 2012. Occurrence and geochemistry of radium in water from principal drinking-water aquifer systems of the United States. *Applied Geochemistry,* 27**,** 729-752.

TAYLOR, H. E., ANTWEILER, R. C., ROTH, D. A., BRINTON, T. I., PEART, D. B. & HEALY, D. F. 2001. The occurrence and distribution of selected trace elements in the Upper Rio Grande and tributaries in Colorado and northern New Mexico. *Arch Environ Contam Toxicol,* 41**,** 410-26.

TAYLOR, R. G., SCANLON, B., DÖLL, P., RODELL, M., VAN BEEK, R., WADA, Y., LONGUEVERGNE, L., LEBLANC, M., FAMIGLIETTI, J. S., EDMUNDS, M., KONIKOW, L., GREEN, T. R., CHEN, J., TANIGUCHI, M., BIERKENS, M. F. P., MACDONALD, A., FAN, Y., MAXWELL, R. M., YECHIELI, Y., GURDAK, J. J., ALLEN, D. M., SHAMSUDDUHA, M., HISCOCK, K., YEH, P. J. F., HOLMAN, I. & TREIDEL, H. 2012. Ground water and climate change. *Nature Climate Change,* 3**,** 322-329.

TAYLOR, S. 2001. *Isotopic Evolution of a Seasonal Snowpack and its Melt.* PhD, Dartmouth College.

TEDELA, N. Apr 11, 2019 2019. *RE: Wetland playa chemistry study.* Type to LANZONI, M.

THIROS, S. A., PAUL, A. P., BEXFIELD, L. M. & ANNING, D. W. 2014. Water Quality in Basin-Fill Aquifers of the Southwestern United States: Arizona, California, Colorado, Nevada, New Mexico, and Utah, 1993–2009. *In:* USGS (ed.). Reston, VA: USGS.

THUROW, T. L., BLACKBURN, W. H., WARREN, S. D. & TAYLOR, C. A. 1987. Rainfall Interception by Midgrass, Shortgrass, and Live Oak Mottes. *Journal of Range Management,* 40**,** 455-460.

TIETJEN, B., ZEHE, E. & JELTSCH, F. 2009. Simulating plant water availability in dry lands under climate change: A generic model of two soil layers. *Water Resources Research,* 45.

TOPPER, R., SPRAY, K. L., BELLIS, W. H., HAMILTON, J. L. & BARKMANN, P. E. 2003. *Ground Water Atlas of Colorado,* Denver, CO.

UDALL, M. K. D., INTERIOR, U. S. C. H. C. O. & INSULAR, A. 1984. Amending title I of the Reclamation Project Authorization Act of 1972 in order to provide for the establishment of the Russell Lakes Waterfowl Management Area as a replacement for the authorized Mishak National Wildlife Refuge, and for other purposes. September 13, 1984. -- Ordered to be printed.

UREY, H. C., BRICKWEDDE, F. G. & MURPHY, G. M. 1932. A Hydrogen Isotope of Mass 2. *Physical Review,* 39**,** 164-165.

USBR 2003. Relocation of Salvage Wells Closed Basin Division San Luis Basin Project, Colorado. Albuquerque Area Office: United States Bureau of Reclamation.

VALDEZ, A. Oct 8, 2016 2016. *RE: Stream Channel Characteristics of the Distal End of Sand, Big Spring and Little Spring Creeks.* Type to LANZONI, M.

VALDEZ, A. 2017. A Geologic Tour of the San Luis Valley. Alamosa, Colorado: Adams State University.

WALVOORD, M. A., PHILLIPS, F. M., TYLER, S. W. & HARTSOUGH, P. C. 2002. Deep arid system hydrodynamics 2. Application to paleohydrologic reconstruction using vadose zone profiles from the northern Mojave Desert. *Water Resources Research,* 38**,** 27-1-27-12.

WANG, H., SHI, G., ZHU, J., CHEN, B., CHE, H. & ZHAO, T. 2013. Case study of longwave contribution to dust radiative effects over East Asia. *Chinese Science Bulletin,* 58**,** 3673-3681.

WANG, Y., SHAO, M. A., LIU, Z. & WARRINGTON, D. N. 2012. Regional spatial pattern of deep soil water content and its influencing factors. *Hydrological Sciences Journal,* 57**,** 265-281.

WARD, J. M. 1978. History and Geology of Homestake's Pitch Project, Saguache County, Colorado *American Institute of Mining Metallurgical and Petroleum Engineers.* Denver, CO.

WASHINGTON, R., BOUET, C., CAUTENET, G., MACKENZIE, E., ASHPOLE, I., ENGELSTAEDTER, S., LIZCANO, G., HENDERSON, G. M., SCHEPANSKI, K. & TEGEN, I. 2009. Dust as a tipping element: the Bodele Depression, Chad. *Proc Natl Acad Sci U S A,* 106**,** 20564-71.

WEGER, M., HEINOLD, B., ENGLER, C., SCHUMANN, U., SEIFERT, A., FÖßIG, R., VOIGT, C., BAARS, H., BLAHAK, U., BORRMANN, S., HOOSE, C., KAUFMANN, S., KRÄMER, M., SEIFERT, P., SENF, F., SCHNEIDER, J. & TEGEN, I. 2018. The impact of mineral dust on cloud formation during the Saharan dust event in April 2014 over Europe. *Atmospheric Chemistry and Physics,* 18**,** 17545-17572.

WELKER, J. M. 2012. ENSO effects on delta18O, delta2H and d-excess values in precipitation across the U.S. using a high-density, long-term network (USNIP). *Rapid Commun Mass Spectrom,* 26**,** 1893-8.

WHEELER, G. M. & HUMPHREYS, A. A. 1878. Report Upon United States Geographical Surveys West of the One Hundredth Meridian. Washington, D. C.: Washington Government Printing Office.

WILLIAMS, D. G. & EHLERINGER, J. R. 2000. Intra- and Interspecific Variation for Summer Precipitation Use in Pinyon-Juniper Woodlands. *Ecological Monographs,* 70**,** 517-537.

WILLIAMS, D. G., EVANS, R. D., WEST, J. & EHLERINGER, J. R. 2007. Applications of stable isotope measurements for early-warning detection of ecological change. *In:* DAWSON, T. E. & SIEGWOLF, R. (eds.) *Isotopes as tracers of ecological change.* Elsevier Academic Press.

WILLIAMS, M. D. 1992. *Characterization of the Unconfined Alluvial Aquifer System of the Northern San Luis Valley, CO Using GIS Data Management and Visualization Techniques.* MS, Colorado School of Mines.

WILSON, J. L. & GUAN, H. 2004. Mountain-Block Hydrology and Mountain-Front Recharge. *Groundwater recharge in a desert environment: The Southwestern United States***,** 113-137.

XIE, G., LAVIAN, I. L., BARNESS, G. & STEINBERGER, Y. 2001. Dynamics of Soil Nitrogen along a Topoclimatic Gradient in the Judean Desert. *Arid Land Research and Management,* 15**,** 135-146.

YAHDJIAN, L. A. O. E. S. 2010. Size of Precipitation Pulses Controls Nitrgen Transformation and Losses in an Arid Patagonian Ecosystem. *Ecosystems* 13**,** 575-585.

YUAN, F., KORAN, M. R. & VALDEZ, A. 2013. Late Glacial and Holocene record of climatic change in the southern Rocky Mountains from sediments in San Luis Lake, Colorado, USA. *Palaeogeography, Palaeoclimatology, Palaeoecology,* 392**,** 146-160.

ZHU, G., GUO, H., QIN, D., PAN, H., ZHANG, Y., JIA, W. & MA, X. 2019. Contribution of recycled moisture to precipitation in the monsoon marginal zone: Estimate based on stable isotope data. *Journal of Hydrology,* 569**,** 423-435.

Appendices

Appendix 1: Precipitation Isotope Data

Table 1.1. Isotope data for individual precipitation events used to create the event-based LMWL.

Valley Floor Precipitation	δD	δ18O	Event (mm)
Rain	-94.99	-13.35	18.00
Rain	-67.23	-8.89	1.70
Rain	-76.76	-9.08	4.70
Rain	-50.30	-7.19	3.95
Rain	-57.60	-8.28	1.25
Rain	-26.52	-2.83	0.80
Rain	-23.18	-1.84	0.80
Rain	-55.10	-7.32	2.35
Rain	-26.75	-3.04	1.25
Rain	-47.03	-6.46	3.00
Rain	-14.68	-1.53	1.18
Rain	2.51	0.63	0.62
Rain	0.43	0.31	1.03
Rain	-1.47	0.26	0.80
Rain	-135.35	-18.97	5.40
Rain	-127.30	-15.84	1.25
Rain	-108.61	-13.92	0.68
Rain	-52.60	-5.98	1.25
Rain	-28.43	-5.50	5.60
Rain	-36.89	-7.60	3.40
Rain	-82.61	-11.39	3.20
Rain	-27.68	-2.74	0.20
Rain	-66.27	-4.52	0.20
Rain	23.01	4.63	0.20
Rain	-15.26	-2.96	2.60
Rain	-7.16	-0.54	1.20
Rain	-25.45	-4.67	3.00
Rain	-54.86	-8.77	10.40
Rain	-25.83	-3.50	1.50
Rain	-53.57	-7.70	10.40
Rain	-46.91	-7.93	2.00
Rain	-77.92	-11.41	8.00
Rain	-39.71	-5.49	1.20

Valley Floor Precipitation	δD	δ18O	Event (mm)
Snow	-155.94	-21.47	9.40
Snow	-134.00	-18.15	12.70
Snow	-167.84	-22.09	6.10
Snow	-171.48	-22.11	5.33
Snow	-240.36	-31.39	12.95
Snow	-225.33	-29.68	10.16
Snow	-73.79	-11.56	4.06
Snow	-214.79	-28.47	13.46
Snow	-102.26	-14.83	9.00
Snow	-159.59	-21.71	1.02
Snow	-122.00	-17.40	2.30
Snow	-189.00	-25.20	5.25
Snow	-183.00	-24.80	1.70
Snow	-203.00	-27.60	0.50
Snow	-166.00	-22.90	1.00

Appendix 2: Rainfall pH

Table 2.1: Summary pH of San Luis Valley precipitation.

Monthly Weighted Mean of Rainfall pH			
		2015	2016
	Apr		6.35
	May		4.99
	Jun	5.25	4.95
	Jul	4.79	4.80
	Aug	4.80	4.57
	Sep	4.96	5.21
	Oct	5.50	5.41

Table 2.2: pH of San Luis Valley precipitation for 2015 and 2016.

2015 Precipitation				
Date	**mm**	**pH 1**	**pH 2**	**Mean pH**
6-Jun	0.5			6.3
13-Jun	4			7.1
13-Jun	18	4.8	4.9	4.9
16-Jun	1.7	5.9	5.9	5.9
28-Jun	4.7	4.8	4.8	4.8
1-Jul	2		5.2	5.2
2-Jul	1.1		4.6	4.6
3-Jul	0.15		5.5	5.5
6-Jul	3.95		4.7	4.7
7-Jul	1.25		4.9	4.9
14-Jul	0.8	5.3	5.0	5.2
15-Jul	0.8	5.9	5.7	5.8
18-Jul	1.83	4.9	4.8	4.8
19-Jul	0.5	6.1	6.1	6.1
20-Jul	0.75	4.6	4.4	4.5
20-Jul	1.6	4.5	4.4	4.4
20-Jul	1	4.6	4.5	4.5
24-Jul	1.25	4.1	3.8	4.0
2-Aug	3	4.4	4.0	4.2
7-Aug	1.18	4.8	4.3	4.5
26-Aug	1.8	5.9	5.5	5.7
26-Aug	0.4	5.9	5.5	5.7
31-Aug	0.62	5.1	4.7	4.9
2-Sep	1.03	5.1	4.6	4.8
2-Sep	0.8	4.6	4.1	4.3
22-Sep	5.4	5.3	5.2	5.2
22-Sep	1.25	5.3	4.9	5.1
22-Sep	4.6	4.7	4.4	4.5
23-Sep	0.68	5.1	4.8	4.9
30-Sep	1.25	5.9	5.7	5.8
4-Oct	5.6	5.7	5.4	5.5

2016 Precipitation		
Date	**mm**	**pH**
28-Apr	3.4	6.4
26-May	0.6	5.9
27-May	3.2	4.8
29-Jun	2.6	4.9
30-Jun	1.2	5.0
1-Jul	3	4.8
2-Jul	0.4	5.2
1-Aug	10.4	4.9
4-Aug	3.5	5.4
4-Aug	1.5	5.8
4-Aug	10.4	4.1
5-Aug	0.3	4.4
5-Aug	2	4.1
5-Aug	8	4.2
6-Aug	1.2	4.9
7-Aug	0.2	5.6
10-Aug	0.9	5.2
23-Aug	2.8	4.5
29-Aug	1.9	4.5
31-Aug	0.2	5.7
2-Sep	1.2	5.8
3-Sep	0.8	4.5
13-Sep	1	5.0
13-Sep	1.1	5.3
21-Sep	1.7	5.1
23-Sep	1.1	5.3
1-Oct	0.3	5.7
2-Oct	0.5	5.3

Appendix 3: Isotope Data for Groundwater by Aquifer Layer and Surface Water Exposed to Evaporation

Table 3.1. Summary isotope data by groundwater type.

GW Layer	δ^2H	$\delta^{18}O$	N
Mean Unconfined	-99.41	-13.71	23
Mean Upper Confined	-99.01	-14.32	48
Mean Lower Confined	-109.10	-14.91	12

Table 3.2. Isotope data for the unconfined aquifer.

GW Layer	δ^2H	$\delta^{18}O$	TDS (ppm)	Temp °C	pH
Unconfined GW (Eastern SLV)	-100.41	-14.29	208	13.1	6.98
Unconfined GW (Eastern SLV)	-101.61	-14.31	186	12.3	7.87
Unconfined GW (Eastern SLV)	-99.29	-13.79	79	12.2	8.22
Unconfined GW (Eastern SLV)	-98.15	-13.43	61	14.7	8.08
Unconfined GW (Eastern SLV)	-100.49	-13.40	58	15.5	7.78
Unconfined GW (Eastern SLV)	-98.37	-13.54	72	14.7	7.80
Unconfined GW (Eastern SLV)	-95.96	-14.11	71	14.8	7.85
Unconfined GW (Eastern SLV)	-95.78	-13.40	84	17.1	6.23
Unconfined GW (Eastern SLV)	-97.18	-14.31	84	17.1	6.23
Unconfined GW (Eastern SLV)	-95.84	-13.77	34	11.3	6.61
Unconfined GW (Eastern SLV)	-96.57	-13.53	40	10.9	6.42
Unconfined GW (Eastern SLV)	-84.38	-10.40	112	15.5	6.51
Unconfined GW (Eastern SLV)	-104.08	-13.39	77	12.9	7.37
Unconfined GW (Eastern SLV)	-105.88	-14.51	77	12.9	7.37
Unconfined GW (Eastern SLV)	-99.74	-13.42	96	12.4	6.95
Unconfined GW (Eastern SLV)	-101.27	-13.75	77	10.6	7.87
Unconfined GW (Eastern SLV)	-96.87	-13.67	62	13.2	7.63
Unconfined GW (Eastern SLV)	-95.80	-13.71	68	13.6	7.80
Unconfined GW (Eastern SLV)	-99.15	-13.52	64	15.6	7.17
Unconfined GW (Eastern SLV)	-101.46	-13.76	505	18.9	7.03
Unconfined GW (Eastern SLV)	-107.89	-14.81	280	12.7	7.05
Unconfined GW (Eastern SLV)	-104.72	-14.08	256	12.5	7.05
Unconfined GW (Eastern SLV)	-105.47	-14.50	380	11.3	7.42
Mean	**-99.41**	**-13.71**	**131.78**	**13.73**	**7.27**

Table 3.3. Isotope data for the upper confined groundwater layer.

GW Layer	δ^2H	$\delta^{18}O$	TDS (ppm)	Temp °C	pH
Upper Confined GW	-104.31	-14.83	223	17.3	7.82
Upper Confined GW	-100.38	-13.65	90	11.1	8.60
Upper Confined GW	-100.93	-14.29	146	13.6	7.94
Upper Confined GW	-98.82	-14.56	58	15.3	8.29
Upper Confined GW	-104.83	-14.84	220	22.9	8.68
Upper Confined GW	-103.29	-13.88	608	19	7.84
Upper Confined GW	-106.73	-14.08	123	14.6	9.26
Upper Confined GW	-93.31	-12.93	433	15.9	7.65
Upper Confined GW	-115.93	-16.01	327	13	7.92
Upper Confined GW	-110.90	-15.28	96	12.7	8.00
Upper Confined GW	-94.53	-12.83	184	11.7	8.44
Upper Confined GW	-105.20	-13.91	169	11.7	7.74
Upper Confined GW	-104.57	-15.14	83	16.7	8.79
Upper Confined GW	-88.27	-13.35	53	17.6	8.73
Upper Confined GW	-103.92	-15.23	49	18.9	8.67
Upper Confined GW	-100.74	-14.63	73	19.5	8.95
Upper Confined GW	-104.84	-15.33	96	19.9	8.88
Upper Confined GW	-97.13	-14.42	108	19.7	8.83
Upper Confined GW	-102.10	-14.86	102	19.1	8.91
Upper Confined GW	-103.29	-15.16	70	19.6	9.03
Upper Confined GW	-102.53	-14.88	139	17.5	8.74
Upper Confined GW	-89.23	-13.45	116	18.8	8.93
Upper Confined GW	-88.76	-13.42	60	20	9.09
Upper Confined GW	-88.58	-13.39	51	17.8	8.90
Upper Confined GW	-91.04	-13.53	63	17.6	8.97
Upper Confined GW	-104.31	-15.08	76	20.9	9.10
Upper Confined GW	-87.57	-13.27	53	18	8.81
Upper Confined GW	-93.69	-13.95	49	16.3	8.83
Upper Confined GW	-87.88	-13.21	51	19.6	8.81
Upper Confined GW	-102.65	-15.04	58	18.4	9.08
Upper Confined GW	-99.47	-14.56	81	22.1	9.18
Upper Confined GW	-96.45	-14.28	77	19.7	8.96
Upper Confined GW	-102.15	-14.78	110	24.6	9.30
Upper Confined GW	-94.41	-13.92	64	18.8	9.16
Upper Confined GW	-89.19	-13.41	53	16.3	8.94
Upper Confined GW	-88.17	-13.35	53	18.7	8.70
Upper Confined GW	-106.32	-15.58	71	20.4	9.08
Upper Confined GW	-104.95	-15.23	124	19.8	8.86
Upper Confined GW	-101.56	-14.58	70	11	8.53
Upper Confined GW	-95.52	-13.87	67	11.5	8.14
Upper Confined GW	-93.83	-13.87	45	13.3	8.61
Upper Confined GW	-98.26	-14.06	90	11.8	7.53
Upper Confined GW	-89.00	-13.22	42	14.2	8.71
Upper Confined GW	-90.62	-13.49	45	12.8	8.50
Upper Confined GW	-123.32	-17.38			
Upper Confined GW	-103.12	-14.99	61	14.2	8.00
Upper Confined GW	-96.68	-14.24	58	16.8	8.20
Upper Confined GW*	~~-97.92~~	~~-13.99~~	~~1291~~	~~20.4~~	~~7.98~~
Mean	**-99.01**	**-14.32**	**111.70**	**16.97**	**8.62**

*This sample was excluded from the mean because of its high methane content and contamination from a stock-tank.

Table 3.4. Isotope data for the lower confined groundwater layer.

GW Layer	δ^2H	$\delta^{18}O$	TDS (ppm)	Temp °C	pH
Lower Confined GW	-108.21	-14.42	106	14.1	7.85
Lower Confined GW	-102.07	-13.94	89	18	7.42
Lower Confined GW	-105.85	-14.62	130	13.2	7.52
Lower Confined GW	-104.53	-14.45	103	14.4	7.73
Lower Confined GW	-105.24	-14.49	108	13.6	7.82
Lower Confined GW	-120.05	-16.32	108	16.1	7.27
Lower Confined GW	-108.00	-14.54	73	15.8	8.24
Lower Confined GW	-102.76	-13.59	73	16.1	7.90
Lower Confined GW	-121.39	-16.43	122	16.3	8.40
Lower Confined GW	-105.31	-14.63		26	
Lower Confined GW (2016)**	-116.48	-16.81	271	32.8	8.15
Lower Confined GW (2015)**	-116.80	-16.30			
Mean	**-109.10**	**-14.91**	**118.30**	**17.85**	**7.83**

**These are samples taken from the same deep well in different years. Both years are given to show only slight variability in isotopic signatures. Their average is used to calculate the overall mean.

Table 3.5. Surface water isotope data for the evaporite playas and for the creeks on the eastern and western slopes of the valley.

Sangre de Cristo Creeks	δ^2H	$\delta^{18}O$
BSC (sep 2016)	-96.10	-12.88
LSC (Sep 2016)	-100.87	-13.79
Medano Cr (Jun 2016)	-102.94	-14.68
SC (2015)	-92.66	-13.60
SC (2015)	-93.01	-13.60
SC (2016)	-102.69	-14.93
Al Cr (2015)	-100.52	-14.20
Al Cr (2016)	-105.26	-15.24
C Cr (2016)	-105.00	-15.08
S Cr (2016)	-105.41	-15.17
P Cr (2016)	-101.17	-14.80
N Crestone Cr (2015)	-97.14	-14.26
San Juan Creeks	δ^2H	$\delta^{18}O$
WC (2015)	-94.15	-13.60
WC (2016)	-92.28	-13.57
WC (2017)	-99.20	-14.44
WCP W	-87.34	-12.99
RG (2017)	-104.95	-14.90
LG (2016)	-92.96	-13.58

Surface Playa Water	δ^2H	$\delta^{18}O$
Surface Playa 1	-51.98	-5.16
Surface Playa 2	-57.78	-4.78
Surface Playa 3	-65.38	-6.99
Surface Playa 4	-18.52	1.84
Surface Playa 5	-21.58	1.39
Surface Playa 6	-17.79	2.19

Appendix 4: Isotope Data used in Vegetation Study

Table 4.1. Summary plant isotope data by sampling season.

Site 1: *E. nauseosa* sampling times and isotope means					
Sampling Date	**Season**	**Mean δ^2H**	**Mean $\delta^{18}O$**	**Stdev δ^2H**	**Stdev $\delta^{18}O$**
15-Jul-15	Sum 15	-103.33	-12.27	7.23	1.09
15-Oct-15	Fall 15	-109.72	-12.82	2.74	0.42
15-Apr-16	Spr 16	-93.98	-8.99	4.72	1.16
15-Jul-16	Sum 16	-107.17	-13.44	0.63	0.13
Site 2: *E. nauseosa* sampling times and isotope means					
Sampling Date	**Season**	**Mean δ^2H**	**Mean $\delta^{18}O$**	**Stdev δ^2H**	**Stdev $\delta^{18}O$**
16-Jul-15	Sum 15	-93.65	-11.19	1.64	0.41
16-Oct-15	Fall 15	-105.42	-13.01	1.90	0.22
17-Apr-16	Spr 16	-95.94	-10.41	2.15	0.52
16-Jul-16	Sum 16	-102.53	-12.86	1.35	0.12
Site 3: *E. nauseosa* sampling times and isotope means					
Sampling Date	**Season**	**Mean δ^2H**	**Mean $\delta^{18}O$**	**Stdev δ^2H**	**Stdev $\delta^{18}O$**
16-Jul-15	Sum 15	-68.20	-7.50	5.23	1.15
16-Oct-15	Fall 15	-83.30	-10.73	1.08	0.33
17-Apr-16	Spr 16	-93.78	-7.57	0.27	0.20
16-Jul-16	Sum 16	-83.73	-10.52	0.74	0.13
Site 1: *S. vermiculatus* sampling times and isotope means					
Sampling Date	**Season**	**Mean δ^2H**	**Mean $\delta^{18}O$**	**Stdev δ^2H**	**Stdev $\delta^{18}O$**
15-Jul-15	Sum 15	-90.23	-10.18	3.65	0.55
15-Oct-15	Fall 15	-72.61	-4.75	2.57	0.36
15-Apr-16	Spr 16	-86.77	-8.43	2.55	0.31
15-Jul-16	Sum 16	-103.31	-12.61	2.04	0.51
Site 2: *S. vermiculatus* sampling times and isotope means					
Sampling Date	**Season**	**Mean δ^2H**	**Mean $\delta^{18}O$**	**Stdev δ^2H**	**Stdev $\delta^{18}O$**
16-Jul-15	Sum 15	-81.35	-9.22	1.25	0.53
16-Oct-15	Fall 15	-99.67	-12.68	2.67	0.39
17-Apr-16	Spr 16	-83.53	-7.92	0.84	0.36
16-Jul-16	Sum 16	-104.93	-14.89	0.85	0.57
Site 3: *S. vermiculatus* sampling times and isotope means					
Sampling Date	**Season**	**Mean δ^2H**	**Mean $\delta^{18}O$**	**Stdev δ^2H**	**Stdev $\delta^{18}O$**
16-Jul-15	Sum 15	-79.81	-10.67	1.77	1.04
16-Oct-15	Fall 15	-85.12	-11.33	1.47	0.03
17-Apr-16	Spr 16	-97.47	-12.82	0.95	0.33
16-Jul-16	Sum 16	-89.93	-11.29	1.45	0.27

Table 4.2. Summary data for unconfined groundwater at each of the three plant sampling sites.

GW	DTW (m)	Mean δ^2H	Mean $\delta^{18}O$	Stdev δ^2H	Stdev $\delta^{18}O$	TDS	Temp °C	pH
Site 1	**1.7-2.2**	-99.82	-13.70	2.31	0.09	510	16.4	6.9
Site 2	**4.5-4.6**	-100.63	-14.29	0.30	0.00	208	13.1	6.98
Site 3	**5.9-6.0**	-108.96	-15.13	0.28	0.14	280	12.7	7.05

Appendix 5: Summary Chemistry Data

Table 5.1. Summary chemistry by water type.

Metric by Water Group	MDL (Method Detection Limit)	Rain (2015--2017)	Creeks and Rive	Surface Playas at Sump*	Other Surface Playas (Mishak)	Closed Basin Canal (Pumped From Unconfined GW)	Unconfined Groundwater	Upper Confined Groundwater (Excluding Sump)	Upper Confined Groundwater at Sump	Lower Active Confined Groundwater
N (number in summary)		52	25 (6 ICP-MS)	25	5	2	30 (13 ICP-MS)	22 (16 ICP-MS)	32 (10 ICP-MS)	11
pH (Mean)		5.09	7.3	9.0	8.9	7.6	8.2	8.2	8.9	7.9
pH (Range)		3.98--7.09	6.9--7.7	7.5--10.0	7.9--9.8		5.6--8.1	7.7--9.3	8.7--9.3	7.3--8.4
TDS (Mean mg/L)		16.8	35	78,760	221	154	162.9	157.8	76.3	132.2
TDS (Range mg/L)		BD--267	14--68	650--432,258	91--457		34--523	42--608	51--139	73--271
Chloride (Mean mg/L)	0.02	0.44		34,812		9.04	9	3.1	0.9	2.3
Chloride (Range mg/L)	0.02	0.02--3.62		19--362,482		6--12	0.15--66.54	BD--24.3	0.3--8.2	0.4--13.2
Nitrate (Mean mg/L)	0.01	1.63		7.42		BD	3.8	0.86	0.1	1.4
Nitrate (Range mg/L)	0.01	0.18--4.28		BD--13.56		BD	BD--43.7	BD--7.68	BD--0.8	BD--2.89
Sulfate (Mean mg/L)	0.01	1.12		27,984		60.60	23.9	3.05	6.5	11.5
Sulfate (Range mg/L)	0.01	0.05--12.03		52.6--173,100		41--80	0.05--99.5	BD--24.6	2.9--9.4	4--37.6
Phosphate (Mean mg/L)	0.3	0.3		74		BD	0.2	0.4	BD	BD
Phosphate (Range mg/L)	0.3	BD--1.9		0.8--614		BD	BD--0.9	BD--1.8	BD	BD
Bicarbonate (Mean mg/L)	5	BD		2273	98		79	144	59	67
Bicarbonate (Range mg/L)	5	BD		331--6,540	60--267		2--365	28--470	15--156	30--170
Sodium (Mean mg/L)	0.04	0.55	3.6	31,964	76		24.7	51.21	39	23.8
Sodium (Range mg/L)	0.04	0.03--5.59	0.9--13.8	154--244,100	14--216		1.7--139	BD--168.6	21--76	8.5--109
Calcium (Mean mg/L)	0.1	0.8	12	76	15		22	10	12	16
Calcium (Range mg/L)	0.1	0.2--3.9	2.3--27.7	0.3--594	10--23		7.8--65.3	1.4--37	BD--28.5	5.1--23.7
Magnesium (Mean mg/L)	0.02	0.08	2.2	1456	5		5	1.82	0.03	1.76
Magnesium (Range mg/L)	0.02	BD--0.48	0.3--6.0	0.01--21,960	3--7		0.8--17	BD--5.99	BD--0.1	0.29--5.59
Ammonium (Mean mg/L)	0.01	0.9	0.01	-	BD		0.1	0.79	BD	BD
Ammonium (Range mg/L)	0.01	0.2--3.1	BD--0.04	-	BD--0.01		BD--1.8	BD--4.42	BD	BD
Potassium (Mean mg/L)	0.2	0.8	2	2093	27		5	3.8	BD	4.1
Potassium (Range mg/L)	0.2	0.05--5.0	0.5--9	18--18,780	5--62		0.4--11	0.4--8.2	BD--0.3	1.2--10.8
Dissolved Iron (Mean mg/L)	0.00001	0.0049	0.097	1.1	0.014	0.008	0.0088	0.2326	0.0024	0.0017
Dissolved Iron (Range mg/L)	0.00001	0.0002--0.0404	0.006--0.316	BD--9.2	0.005--0.027	0.008	BD--0.073	BD--1.37	0.0012--0.0054	BD--.0067
Total Recov. Iron (Mean mg/L	5	-	-	17.8	-	-	-	-	-	-
Total Recov. Iron (Range mg/	5	-	-	BD--135	-	-	-	-	-	-
Silica (Mean mg/L)	0.5	BD	-	67	-	-	19	20	32	29
Silica (Range mg/L)	0.5	BD	-	8.8--225	-	-	3.4--27.4	4.4--34.6	26.7--46.5	23.4--40.9

*raw data from Tedela, N, 2011.

BD = Below Detection

Table 5.2. Summary chemistry by water type.

Metric by Water Group	MDL (Method Detection Limit)	Rain (2015--2017)	Creeks and River	Evaporite Playas at Sump*	Other Surface Playas (Mishak)	Closed Basin Canal (Pumped From Unconfined GW)	Unconfined Groundwater	Upper Confined Groundwater (Excluding Sump)	Upper Confined Groundwater at Sump	Lower Active Confined Groundwater
N (number in summary)		52	25 (6 ICP-MS)	25	5	2	30 (13 ICP-MS)	22 (16 ICP-MS)	32 (10 ICP-MS)	11
Uranium (Mean µg/L)	0.001	0.01	0.14	238.2	0.8	1.45	4.6	0.67	0.2	0.7
Uranium (Range µg/L)	0.001	BD--0.1	BD--0.32	1.4--3,460.0	0.205--1.679	1.43--1.46	BD--11	BD--8.31	0.05--0.41	0.09--3.0
Thorium (Mean µg/L)	0.01	0.03	BD	4.4	BD	BD	BD	0.224	0.08	BD
Thorium (Range µg/L)	0.01	BD--0.2	BD	BD--56.4	BD	BD	BD	BD--1.57	BD--0.4	BD
Arsenic (Mean µg/L)	0.02	0.25	0.13	1,586	15	1.87	3.95	4.64	11.75	11.5
Arsenic (Range µg/L)	0.02	BD--1.26	BD--0.45	18--14,200	7.82--25.29	1.7--2.0	BD--15.2	BD--18.01	5.6--20.6	1.9--56.1
Fluoride (Mean mg/L)	0.1	0.04		33.7		0.61	0.4	1.1	0.9	1.02
Fluoride (Range mg/L)	0.1	BD--0.67		BD--149.7		0.56--0.66	0.04--1.56	0.1--5.4	0.3--2.3	0.1--8.0
Barium (Mean µg/L)	0.02	-	-	50.7	-	-	-	-	-	-
Barium (Range µg/L)	0.02	-	-	15.9--136	-	-	-	-	-	-
Beryllium (Mean µg/L)	0.05	-	-	2.4	-	-	-	-	-	-
Beryllium (Range µg/L)	0.05	-	-	BD--43	-	-	-	-	-	-
Cadmium (Mean µg/L)	0.001	0.0183	0.03	5.2	0.017	0.007	0.007	0.007	0.036	0.0062
Cadmium (Range µg/L)	0.001	BD--0.163	BD--0.12	0.05--38.5	0.005--0.061	.007--.008	BD--0.04	BD--0.037	0.029--0.052	BD--0.35
Chromium (Mean µg/L)	0.003	0.0423	0.3	255	0.22	0.34	0.9	1.34	1.6	0.83
Chromium (Range µg/L)	0.003	BD--0.481	0.005--1.14	0.6--2,050	0.097--0.423	0.33--0.35	0.02--10.1	0.02--10.06	BD--12.23	0.03--3.27
Cobalt (Mean µg/L)	0.002	0.125	2.7	4.6	0.1	0.06	0.05	0.026	BD	BD
Cobalt (Range µg/L)	0.002	BD--0.884	BD--9.12	0.1--57.2	0.059--0.181	0.06--0.07	BD--0.17	BD--0.111	BD	BD--0.0043
Copper (Mean µg/L)	0.004	1.57	5.5	181	0.609	0.96	0.54	0.811	0.15	0.19
Copper (Range µg/L)	0.004	0.14--7.37	0.4--24	10--1,030	0.355--1.306	0.45--1.5	0.05--1.1	0.037--5.515	0.06--0.43	0.03--0.33
Hafnium (Mean µg/L)	0.01	0.05	0.4		0.19	BD	0.12	0.14	0.21	0.02
Hafnium (Range µg/L)	0.01	0.04--0.06	0.05--0.64		0.06--0.69	BD	BD--0.64	BD--0.81	0.18--0.26	BD--0.07
Lead (Mean µg/L)	0.0006	0.157	0.16	3.7	0.063	0.04	0.04	0.309	0.017	0.13
Lead (Range µg/L)	0.0006	0.008--2.102	0.05--0.22	BD--50.7	0.1--0.19	0.03--0.05	0.004--0.15	0.004--1.296	0.012--0.027	0.01--1.16
Lithium (Mean mg/L)	0.005	-	-	0.6	-	-	-	-	-	-
Lithium (Range mg/L)	0.005	-	-	0.01--8.55	-	-	-	-	-	-
Manganese (Mean µg/L)	0.006	22.72	193	448	5.57	4.5	482	137.69	0.95	4.08
Manganese (Range µg/L)	0.006	0.72--143.29	0.5--570	1.5--3,400	0.98--14.53	4.5--4.6	0.13--2,268	0.13--1,452	0.2--2.1	0.03--20.93
Mercury (Mean µg/L)	0.13	BD	BD	-	BD	BD	BD	BD	BD	0.08
Mercury (Range µg/L)	0.13	BD	BD	-	BD	BD	BD	BD	BD	BD--0.76
Molybdenum (Mean µg/L)	0.01	0.067	0.19	1220	4.05	6.1	4	6.41	4.47	4.73
Molybdenum (Range µg/L)	0.01	BD--0.402	BD--0.7	12.8--4,390	1.95--7.02	6.0--6.2	0.52--24.39	0.72--24.39	1.2--15.8	0.63--36.45
Nickel (Mean µg/L)	0.006	0.29	2.4	15.2	0.61	0.17	0.52	0.524	0.03	0.21
Nickel (Range µg/L)	0.006	BD--1.74	BD--8.9	0.8--86.5	0.13--1.73	0.1--0.2	BD--3.16	0.025--2.11	BD--0.2	BD--1.67
Selenium (Mean µg/L)	0.1	-	-	441	-	-	-	-	0.3	-
Selenium (Range µg/L)	0.1	-	-	5--2,980	-	-	-	-	BD--0.5	-
Thalium (Mean µg/L)	0.004	0.0026	0.08	6.4	0.014	BD	0.017	0.011	0.02	0.004
Thalium (Range µg/L)	0.004	BD--0.0206	BD--0.18	BD--51	BD--0.07	BD	BD--0.08	BD--0.071	0.02	BD--0.033
Tungsten (Mean µg/L)	0.01	0.031	BD	-	2	1.05	0.48	3.906	1.79	10.02
Tungsten (Range µg/L)	0.01	BD--0.629	BD	-	0.43--4.03	1.05--1.06	BD--2.9	0.02--12.68	0.8--3.43	0.11--82.76
Vanadium (Mean µg/L)	0.003	0.4113	0.6	235.6	20.71	4.55	9.1	12.95	44.5	15.14
Vanadium (Range µg/L)	0.003	0.011--3.349	0.3--1.5	BD--1,260	6.13--43.84	4.53--4.57	0.02--72	0.014--71.96	17.46--75.83	7.11--32.94
Zinc (Mean µg/L)	0.02	16.92	0.58	56.39	6.27	3.51	4.2	32.76	0.69	2.89
Zinc (Range µg/L)	0.02	1.35--104.98	0.08--0.89	2.71--194	0.89--18.89	3.4--3.6	0.9--9.7	1.02--384.24	0.21--1.24	1.09--7.78
* ICP-MS raw data from Tedela, N., 2011.										
BD = Below Detection										